

DESIGN OF KALMAN FILTER BASED ATTITUDE DETERMINATION AND
CONTROL ALGORITHMS FOR A LEO SATELLITE

A THESIS SUBMITTED TO
THE GRADUATE SCHOOL OF NATURAL AND APPLIED SCIENCES
OF
MIDDLE EAST TECHNICAL UNIVERSITY

BY

GAMZE EFENDİOĞLU

IN PARTIAL FULFILLMENT OF THE REQUIREMENTS
FOR
THE DEGREE OF MASTER OF SCIENCE
IN
ELECTRICAL AND ELECTRONIC ENGINEERING

NOVEMBER 2019

Approval of the thesis:

**DESIGN OF KALMAN FILTER BASED ATTITUDE DETERMINATION
AND CONTROL ALGORITHMS FOR A LEO SATELLITE**

submitted by **GAMZE EFENDIOGLU** in partial fulfillment of the requirements
for the degree of **Master of Science** in **Electrical and Electronic Engineering**,
Middle East Technical University by,

Prof. Dr. Halil Kalıپçilar
Dean, Graduate School of **Natural and Applied Sciences** _____

Prof. Dr. İlkay Ulusoy
Head of the Department, **Electrical and Electronics Eng.** _____

Prof. Dr. Mehmet Kemal Leblebicioğlu
Supervisor, **Electrical and Electronics Eng., METU** _____

Examining Committee Members:

Prof. Dr. Ozan Tekinalp
Aerospace Eng., METU _____

Prof. Dr. Mehmet Kemal Leblebicioğlu
Electrical and Electronics Eng., METU _____

Assoc. Prof. Dr. Afşar Saranlı
Electrical and Electronics Eng., METU _____

Assist. Prof. Dr. Yakup Özkanç
Electrical and Electronics Eng., Hacettepe Uni. _____

Assist. Prof. Dr. Mustafa Mert Ankaralı
Electrical and Electronics Eng., METU _____

Date: 29.11.2019



I hereby declare that all information in this document has been obtained and presented in accordance with academic rules and ethical conduct. I also declare that, as required by these rules and conduct, I have fully cited and referenced all material and results that are not original to this work.

Name, Last name : Gamze Efendioğlu

Signature :

ABSTRACT

DESIGN OF KALMAN FILTER BASED ATTITUDE DETERMINATION AND CONTROL ALGORITHMS FOR A LEO SATELLITE

Efendioğlu, Gamze

Master of Science, Electrical and Electronic Engineering

Supervisor : Prof. Dr. Mehmet Kemal Leblebicioğlu

November 2019, 189 pages

The design of different attitude controllers by using reaction wheels and magnetic rods as torque sources and the design of a multi-sensor integrated navigation system are developed for a three-axis stabilized Earth-orbiting microsatellite and presented in this thesis. Firstly, the fundamental parameters relevant to satellite attitude determination are presented, such as attitude sensors and actuators, space environmental effects, coordinate frames, satellite dynamic/kinematic equations with control components. These parameters are also used to set satellite linear and nonlinear mathematical models. Reaction wheels and magnetic torque rods are used to generate the required control torque for the purpose of providing attitude control. The momentum dumping effects of magnetic rods are also implemented to mathematical models and controlled by the help of Earth Magnetic Field.

Kalman Filter based attitude estimations with PID, LQR and SMC controllers were designed to support satellite orientation with respect to a given reference attitude. In addition to these controllers, a feedback controller is also designed for stabilizing the satellite angular velocity after separating from launcher. Simulating

of multi-sensor navigation sensors, satellite mathematical model and controller models under various internal and external disturbances and measurement noises are carried out by means of MATLAB/Simulink software tool. The results obtained from the simulations with related approaches were compared and analyzed.

Keywords: Satellite Attitude and Control System, Kalman Filters, PID Controller, LQR Controller, Sliding Mode Controller.

ÖZ

ALÇAK YÖRÜNGELİ BİR UYDU İÇİN KALMAN FİLTRE TABANLI YÖNELİM BELİRLEME VE KONTROL ALGORİTMALARININ TASARIMI

Efendioğlu, Gamze

Yüksek Lisans, Elektrik ve Elektronik Mühendisliği

Tez Yöneticisi: Prof. Dr. Mehmet Kemal Leblebicioğlu

Kasım 2019, 189 sayfa

Bu tez raporunda, üç eksende durağan bir alçak yörunge mikro uydusu için tepki tekerleği ve manyetik tork çubukları kullanılarak geribeslemeli yönelim belirleme ve kontrol algoritmaları ile entegre edilmiş çoklu sensör navigasyon sisteminin tasarımı sunulmaktadır. Tezin ilk bölümlerinde, kontrolcü tasarımları için gerekli olan uydunun dinamik ve kinematik denklemleri, uzay ortamı, koordinat sistemleri ile iç/dış etkenlerden kaynaklanan bozucu kuvvetler sunulmuştur. Tezin devamında, yönelim belirleme ve kontrol komponentleri detaylı bir şekilde tanıtılmıştır. Tepki tekerleri ve manyetik tork çubukları yönelim kontrolünü sağlamak amacıyla gerekli tork üretimi için kullanılmıştır. Tork çubuklarının, tekerlerde fazladan biriken momentum miktarnı boşaltma özelliği de modellere eklenmiş ve bu durum Dünya'nın manyetik alan verisinden faydalananarak kontrol edilmiştir.

İç ve dış bozucu etkenler ile sensör gürültüleri de göz önüne alınarak Kalman filtre tabanlı tahmini navigasyon değerleri ile birlikte uydunun dinamik/kinematik denklemlerinden doğrusal ve doğrusal olmayan matematiksel modeller oluşturulmuştur. Oransal integral türevsel kontrolcü (PID), doğrusal ikinci

dereceden regülatör (LQR) ve kayan kipli kontrolcü (SMC) tasarımları ile uydunun referans verilen yönelimi gerçeklestirmesi sağlanmıştır. Uydunun fırlatıcıdan ayrıldıktan sonraki hızının kararlı hale getirilebilmesi amacıyla takla hareketini sökülmek için geri beslemeli kontrolcü tasarlanmıştır. Tüm model ve kontrolcüler MATLAB/ Simulink yazılım araçları kullanılarak tasarlanmış, elde edilen sistem sonuçları karşılaştırılıp analiz edilmiştir.

Anahtar Kelimeler: Uydu Yönetim ve Kontrol Sistemi, Kalman Filtreleri, Oransal Integral Türevsel Kontrolcü, Doğrusal İkinci Dereceden Regülatör, Kayan Kipli Kontrolcü.



To Mehmet EFENDİOĞLU

ACKNOWLEDGMENTS

There is no word to explain my thankfulness to my supervisor, Prof. Dr. Mehmet Kemal Leblebicioğlu, who shows me his great patience several times. He always understood all my excuses and guided me whenever I am stuck in the problems of this study.

I would also like to thank Prof. Dr. Ozan Tekinalp, who motivated me about studying on the aerospace applications and the precious lessons that I took from him during my graduate education.

I extend my deepest thanks to Berk Yurtagül and Onur Deveci for their helpful advises and motivation during my difficult times. I'm also feeling very lucky that I have insightful managers, Alp Bülent Burç Sürmeli, Abdurrahman Tunca Tunç, Hasan Şimşek and Güray Yıldız. They always provide great motivation to me in every aspects of my academic life besides my business life.

I am very grateful to have my co-workers Özgür Baskın, Hüseyin Yılmaztekin, Ali Can Batur, Eren Bostancı and Emine Topdaş for their patience during the peak times of this study.

Finally, my special thanks go to my other half, Mehmet Efendioğlu for his endless love and my parents who are always teaching me about how to be a merciful person throughout my life.

TABLE OF CONTENTS

ABSTRACT	v
ÖZ	vii
ACKNOWLEDGMENTS	x
TABLE OF CONTENTS	xi
LIST OF TABLES	xvi
LIST OF FIGURES	xviii
LIST OF ABBREVIATIONS	xxii
1. INTRODUCTION	1
CHAPTERS	
1.1. Introduction	1
1.2. Literature Review	2
1.3. Microsatellites	4
1.3.1. The Selected Microsatellite.....	4
1.4. Problem Statements.....	6
1.5. Publication from This Thesis	7
1.6. The Thesis Organization	7
2. SATELLITE ATTITUDE DYNAMICS and KINEMATICS	9
2.1. Introduction	9
2.2. Coordinate Frames	10
2.2.1. Earth Centered Inertial Frame (ECI).....	10
2.2.2. Earth Centered Earth Fixed Frame (ECEF)	11
2.2.3. Local Orbit Frame (LLA).....	12

2.2.4. Body Frame	13
2.3. Satellite Kinematic Equations	14
2.3.1. Satellite Kinematic Equations with Direction Cosine Matrix.....	14
2.3.2. Satellite Kinematic Equations with Quaternions	17
2.4. Satellite Dynamic Equations	21
2.4.1. The Torque and Angular Momentum of Satellite	25
2.4.1.1. Satellite Inertia Matrix	26
2.4.1.2. Satellite Angular Velocity	27
2.4.2. The Torque and Angular Momentum of Actuators.....	29
2.4.2.1. The Control Torque of Reaction Wheels	30
2.4.2.2. The Control Torque of Magnetic Torque Rods.....	35
2.4.3. Disturbance Torques	38
2.4.3.1. Gravity Gradient Disturbance Torque.....	38
2.4.3.2. Solar Radiation Disturbance Torque	40
2.4.3.3. Aerodynamics Disturbance Torque.....	43
2.4.3.4. Magnetic Dipole Moment Disturbance Torque	45
2.5. Satellite Sensor Measurements	46
2.5.1. Sun Sensor Measurements	47
2.5.2. Magnetometer Measurements	48
2.5.3. Star Tracker Measurements	49
2.5.4. Fiber Optic Gyroscope Measurements.....	51
2.5.5. GPS Sensor Measurements	52
2.6. Summary	53
3. SPACE ENVIRONMENT MODEL.....	55

3.1. Introduction	55
3.2. Julian Date Model	55
3.3. Orbit Propagation Model.....	56
3.3.1. Kepler Parameters	56
3.3.2. Two Lines of Elements Data (TLE).....	58
3.3.3. Orbit Perturbations	61
3.3.4. Earth Gravitational Perturbations.....	62
3.4. Earth Magnetic Field Model	64
3.5. Sun Position Model.....	65
3.6. Summary	67
4. SATELLITE ATTITUDE MODEL.....	69
4.1. Introduction	69
4.2. Satellite Nonlinear Attitude Control Model.....	69
4.2.1. Nonlinear State Space Definition in Discrete Time	70
4.2.2. Nonlinear Sensor Measurement Model in Discrete Time	73
4.2.2.1. Nonlinear Model of Fiber Optic Gyroscopes.....	75
4.2.2.2. Nonlinear Model of Star Trackers.....	76
4.2.2.3. Nonlinear Model of Magnetometers	76
4.2.2.4. Nonlinear Model of Sun Sensors	77
4.2.2.5. Nonlinear Model of GPS Receiver Sensor.....	78
4.2.2.6. Nonlinear Model of Sensor Measurement Matrix	79
4.3. Satellite Linear Attitude Control Model	81
4.3.1. Linearization of Nonlinear Model Equations.....	83
4.3.1.1. Linearization of Satellite Nonlinear Attitude Model	84

4.3.1.2. Linearization of Satellite Nonlinear Sensor Measurement Model	87
4.3.1.3. Linear Satellite State Space Models.....	92
4.4. Controllability of Satellite Model	95
4.5. Stability of Satellite Model	96
4.6. Satellite Attitude Estimation with Kalman Filters	98
4.6.1. Kalman Filter Algorithm.....	99
4.7. Summary	104
5. SATELLITE ATTITUDE CONTROL	105
5.1. Introduction	105
5.2. Detumbling Control	107
5.3. Desaturation Control	110
5.4. PID Control	111
5.4.1. PD Controller for Satellite	111
5.4.2. PID Controller for Reaction Wheels DC Motor	114
5.5. LQR Control	120
5.6. Sliding Mode Control (SMC)	122
5.7. Summary	126
6. RESULTS and DISCUSSIONS	127
6.1. Introduction	127
6.2. The Results of Detumbling Control	127
6.3. The Results of Desaturation Control.....	132
6.4. The Results of PID Control.....	138
6.5. The Results of LQR Control	149
6.6. The Results of Sliding Mode Control	156

6.7. Summary	162
7. CONCLUSION.....	165
7.1. Summary	165
7.2. Conclusion	165
7.3. Future Works.....	167
REFERENCES.....	169
APPENDICES	
A. The Properties of Quaternions	178
B. Transfer Functions	181
C. MATLAB / Simulink Functions and Model Files	185
D. MATLAB / Simulink Model Blocks	186

LIST OF TABLES

TABLES

Table 1-1 The Fundamental Flying Laptop Microsatellite Characteristics	4
Table 2-1 The Characteristics of Satellite Actuators [9, 17].....	30
Table 2-2 Performance Parameters of Reaction Wheels (RWs).....	31
Table 2-3 Power Performance Parameters of Reaction Wheels (RWs).....	32
Table 2-4 Performance Parameters of Magnetic Torque Rods (MTRs)	36
Table 2-5 The Characteristics of Satellite Sensors [9, 17].....	47
Table 2-6 Performance Parameters of Fiber Optic Gyroscopes.....	52
Table 3-1 The Properties of Keplerian Orbits (Circular and Elliptic Orbits)	57
Table 3-2 TLE Data Set For Orbital Parameters [20]	59
Table 3-3 Orbital Parameters Obtained From TLE Data	59
Table 3-4 The Useful Orbital Parameters of Satellite.....	59
Table 4-1 The Equations of Kalman Filter Algorithm.....	100
Table 4-2 The Simulation Parameters of State Estimation (Case-1)	101
Table 4-3 The Simulation Parameters of State Estimator (Case-2)	103
Table 5-1 Reaction Wheel - DC Motor Parameters	117
Table 5-2 PID Controller Parameters of Inner Loop	119
Table 5-3 PID Controller Parameters of Outer Loop.....	119
Table 6-1 The Simulation Parameters of Detumbling Phase (Case-2)	128
Table 6-2 The Simulation Parameters of Desaturation Phase (Case-1).....	132
Table 6-3 The Simulation Parameters of Desaturation Phase (Case-4).....	136
Table 6-4 The Simulation Parameters of PID Controller (Case-1).....	139
Table 6-5 The Simulation Results of PID Controller for Case-1	141
Table 6-6 The Simulation Results of PID Controller for Case-2	143
Table 6-7 The Simulation Results of PID Controller for Case-3	145
Table 6-8 The Simulation Results of PID Controller for Case-4	147
Table 6-9 The Simulation Parameters of LQR Controller (Case-1)	149
Table 6-10 The Eigenvalues of Linearized Plant Model	150

Table 6-11 The Simulation Results of LQR Controller for Case-1	152
Table 6-12 The Simulation Results of LQR Controller for Case-2	154
Table 6-13 The Simulation Parameters of SM Controller (Case-1)	156
Table 6-14 The Simulation Results of SMC Controller for Case-1	158
Table 6-15 The Simulation Results of SMC Controller for Case-2.....	159
Table 6-16 The Simulation Results of SMC Controller for Case-2.....	161
Table 7-1 Useful MATLAB Functions	185



LIST OF FIGURES

FIGURES

Figure 1-1 The FLP Platform Setup [17]	5
Figure 2-1 Earth Centered Inertial Frame (ECI) [9]	10
Figure 2-2 Earth Centered Earth Fixed Frame (ECEF) [9].....	11
Figure 2-3 Local Orbit Frame wrt. ECEF and NED Frames [63].....	12
Figure 2-4 (a) Body Frame (b) FLP Microsatellite Body Frame [14, 17]	13
Figure 2-5 Satellite Rotation Around Z-Axis, Y-Axis, X-Axis Respectively [19]....	16
Figure 2-6 The Location of Reaction Wheels (Tetrahedron Configuration) [9, 17]..	31
Figure 2-7 Tetrahedron Configuration Diagram of RWs [48].....	33
Figure 2-8 The Electrical Representation of Reaction Wheels [9, 17]	33
Figure 2-9 Magnetic Torque Rods [9, 17]	35
Figure 2-10 The Location of Magnetic Torque Rods [9, 17].....	36
Figure 2-11 Distribution Torque Model Blocks	46
Figure 2-12 Sun Sensors [9].....	48
Figure 2-13 Location of Sun Sensor Units [9, 17]	48
Figure 2-14 Magnetometer Located in The Selected Satellite [9,17]	49
Figure 2-15 The Orientation of Magnetometers [9, 17].....	49
Figure 2-16 Star Tracker System Baffle and Camera Head Unit [9, 17]	50
Figure 2-17 The Location of Star Trackers [9, 17]	50
Figure 2-18 Fiber Optic Gyroscopes [9, 17]	51
Figure 2-19 The Location of Fiber Optic Gyroscopes [9, 17]	51
Figure 2-20 Phoenix (MG5001) GPS Receiver Board [39].....	53
Figure 2-21 The Location of GPS Antenna [9, 17].....	53
Figure 3-1 Kepler Orbital Parameters [19]	56
Figure 3-2 Orbit Propagator and Perturbation Model	63
Figure 3-3 Orbit Propagator Model.....	63

Figure 3-4 Sun Position Vector Illustration [57]	65
Figure 4-1 Sensor Measurements with Noise Effects	73
Figure 4-2 The Diagram of Kalman Filter Algorithm	100
Figure 4-3 LKF Output For Satellite Angular Velocity of PID (Case-1)	102
Figure 4-4 EKF Output For Satellite Angular Velocity of PID (Case-1)	102
Figure 4-5 Euler Angler Response of PID (Case-1)	102
Figure 4-6 LKF Output For Satellite Angular Velocity of PID (Case-2)	103
Figure 4-7 EKF Output For Satellite Angular Velocity of PID (Case-2)	103
Figure 4-8 Euler Angler Response of PID (Case-2)	104
Figure 5-1 Satellite Attitude Control Loop [46]	106
Figure 5-2 The Geometric Definition of Local Magnetic Field (B) [72].....	109
Figure 5-3 Satellite Attitude Control with Momentum Dumping.....	110
Figure 5-4 The Data Diagram of RW DC Motor.....	115
Figure 5-5 Cascade PID Controller General Diagram [85]	115
Figure 5-6 Inner and Outer Loop of Cascade PI Controllers for RW-DC motors...	116
Figure 5-7 The Open Loop Pole-Zero Map of Reaction Wheel DC Motor.....	117
Figure 5-8 Reaction Wheels Model Block Diagram.....	118
Figure 5-9 The Simulink Diagram of RW – DC Motors	118
Figure 5-10 The Step Response of Inner Controller Loop.....	119
Figure 5-11 The Step Response of Outer Controller Loop	120
Figure 5-12 LQR Controller Diagram of Satellite Linear Attitude Model	122
Figure 6-1 MTR Torque Command in Detumbling Phase (Case-1).....	128
Figure 6-2 Satellite Angular Velocity in Detumbling Phase (Case-1).....	129
Figure 6-3 MTR Torque Command in Detumbling Phase (Case-2).....	129
Figure 6-4 Satellite Angular Velocity in Detumbling Phase (Case-2).....	130
Figure 6-5 MTR Torque Command in Detumbling Phase (Case-3).....	130
Figure 6-6 Satellite Angular Velocity in Detumbling Phase (Case-3).....	131
Figure 6-7 MTR Torque Command in Detumbling Phase (Case-4).....	131
Figure 6-8 Satellite Angular Velocity in Detumbling Phase (Case-4).....	132
Figure 6-9 MTR Torque in Desaturation Phase of Satellite PID (Case-1)	133

Figure 6-10 RW Angular Momentum Desaturation of PID (Case-1).....	133
Figure 6-11 MTR Torque in Desaturation Phase of PID (Case-2)	134
Figure 6-12 RW Angular Momentum Desaturation of PID (Case-2).....	134
Figure 6-13 MTR Torque in Desaturation Phase of SMC (Case-3)	135
Figure 6-14 RW Angular Momentum Desaturation of PID (Case-3).....	135
Figure 6-15 MTR Torque in Desaturation Phase of SMC (Case-4)	136
Figure 6-16 RW Angular Momentum Desaturation of SMC (Case-4).....	137
Figure 6-17 MTR Torque in Desaturation Phase of LQR (Case-5).....	137
Figure 6-18 RW Angular Momentum Desaturation of LQR (Case-5)	138
Figure 6-19 RW Commanded Torque (PID / Case-1)	140
Figure 6-20 RW Angular Velocities (PID/Case-1).....	140
Figure 6-21 Satellite Euler Angles (PID/Case-1).....	141
Figure 6-22 Satellite Angular Velocities (PID/Case-1)	141
Figure 6-23 RW Commanded Torque (PID/Case-2)	142
Figure 6-24 RW Angular Velocities (PID/Case-2).....	142
Figure 6-25 Satellite Euler Angles (PID/Case-2).....	143
Figure 6-26 Satellite Angular Velocities (PID/Case-2)	143
Figure 6-27 RW Commanded Torque (PID/Case-3)	144
Figure 6-28 RW Angular Velocities (PID/Case-3).....	144
Figure 6-29 Satellite Euler Angles (PID/Case-3).....	145
Figure 6-30 Satellite Angular Velocities (PID/Case-3)	145
Figure 6-31 RW Commanded Torque (PID/Case-4)	146
Figure 6-32 RW Angular Velocities (PID/Case-4)	146
Figure 6-33 Satellite Euler Angles (PID/Case-4).....	147
Figure 6-34 Satellite Angular Velocities (PID/Case-4)	147
Figure 6-35 RW Power Consumption for a Non-Failure Case (PID)	148
Figure 6-36 RW Power Consumption for a RW Failure Case (PID).....	148
Figure 6-37 The Calculation of Electrical and Mechanical Power Consmp.....	149
Figure 6-38 RW Commanded Torque (LQR/Case-1).....	151
Figure 6-39 RW Angular Velocities (LQR/Case-1)	151

Figure 6-40 Satellite Euler Angles (LQR/Case-1)	152
Figure 6-41 Satellite Angular Velocities (LQR/Case-1).....	152
Figure 6-42 RW Commanded Torque (LQR/Case-2).....	153
Figure 6-43 RW Angular Velocities (LQR/Case-2)	153
Figure 6-44 Satellite Euler Angles (LQR/Case-2)	154
Figure 6-45 Satellite Angular Velocities (LQR/Case-1).....	154
Figure 6-46 RW Power Consumption for a Non-Failure Case (LQR)	155
Figure 6-47 RW Power Consumption for a RW Failure Case (LQR)	155
Figure 6-48 Torque Command of SMC with Chattering Problem (Case-1).....	156
Figure 6-49 RW Angular Velocity of SMC with Chattering Problem (Case-1).....	157
Figure 6-50 Satellite Ang. Vel. of SMC with Chattering Problem (Case-1)	157
Figure 6-51 Euler Angles of SMC with Chattering Problem (Case-1).....	157
Figure 6-52 Torque Command of SMC without Chattering Problem (Case-2).....	158
Figure 6-53 Euler Angles of SMC without Chattering Problem (Case-2).....	159
Figure 6-54 Torque Command of SMC without Chattering Problem (Case-3).....	160
Figure 6-55 Euler Angles of SMC without Chattering Problem (Case-3).....	160
Figure 6-56 Torque Command of SMC without Chattering Problem (Case-4).....	161
Figure 6-57 Euler Angles of SMC without Chattering Problem (Case-4).....	161
Figure 6-58 RW Power Consumption for a Non-Failure Case (SMC).....	162
Figure 6-59 RW Power Consumption for a RW Failure Case (SMC).....	162
Figure 8-1 B-dot Controller Design for Satellite Detumbling	186
Figure 8-2 PID Controller Design with Desaturation for Satellite Attitude	187
Figure 8-3 LQR Controller Design with Desaturation for Satellite Attitude.....	188
Figure 8-4 SMC Controller Design with Desaturation for Satellite Attitude	189

LIST OF ABBREVIATIONS

ABBREVIATIONS

Abbreviation	Definition
ECEF	Earth Centered Earth Fixed Frame Axes
ECI	Earth Centered Inertial Frame Axes
NED	Satellite Local Navigation Frame Axes
LLA	Latitude Longitude Altitude
FLP	Flying Laptop Microsatellite
LEO	Low Earth Orbit Satellite
EKF	Extended Kalman Filter
UKF	Unscented Kalman Filter
GPS	Globally Positioning System
DCM	Direction Cosine Matrix
IGRF2000	International Geomagnetic Reference Field
TLE	Two Lines of Data Set
NORAD	The North American Aerospace Defense Command
IEEE	Institute of Electrical and Electronics Engineers
WGS84	World Geodetic System - 1984
PID	Proportional Integral Derivative
LQR	Linear Quadratic Regulator
SMC	Sliding Mode Controller

CHAPTER 1

INTRODUCTION

1.1. Introduction

This thesis focuses on the issues of designing and developing satellite navigation and attitude control system integrating the Kalman filter based controller algorithms by utilizing the basic parameters of a microsatellite called Flying Laptop (FLP). The primary objective of this thesis is to model different attitude controllers with reaction wheels using as a momentum generator and magnetic torque rods using as both torque generator and redundant momentum damper in order to obtain higher degree of pointing accuracy for an Earth pointing microsatellite inserted in LEO orbit.

The selected microsatellite is designed by the Stuttgart University and launched in 2017 [17]. It is a Low Earth Orbit (LEO) satellite stabilized for its every three axes, and its orbit is a sun-synchronous orbit. The mission altitude is between 500 km and 900 km, it can be assumed that is the mean of these altitudes, $h = 700$ km. It has a rectangular shape with dimensions of 60 cm x 70 cm x 80 cm [9, 17].

The attitude determination and control subsystem of the selected satellite is composed of sun sensors, magnetometers, star trackers, gyroscopes and GPS receivers as satellite sensors. On the other hand, reaction wheels and magnetic torque rods are accepted as attitude actuators. This thesis gives also nonlinear and linear mathematical models which belong to these sensors and actuators, and describes how to combine each of them into an attitude Kalman Filter estimator with a Gauss-Newton method.

The Kalman filter is the estimation method to compound the processing of multi-sensors navigation and satellite attitude determination. Kalman filter based navigation algorithms are designed for both having an accurate estimation algorithm and solving time synchronization problems. Extended Kalman Filter (EKF) submits the satisfied estimation results for nonlinear systems wherever the first and second order Taylor series linearization approximates nonlinear motion characteristics [1, 2, 4]. The satellite orientation concerning a reference frame is determined by means of attitude determination process [18]. Furthermore, satellite sensors provide some useful data which helps to determine the location in space. Attitude determination process is in cooperation with control process in order to maintain the expected satellite orientation.

Four reaction wheels accommodated in tetrahedron configuration with three magnetic torque rods are used in control systems and their effects on satellite attitude are analyzed by PID, LQR and SMC controller methods [2].

Controllers receive the estimated measurements from sensors, then generate the appropriate control commands according to given reference attitude and transmit this command to actuators in order to provide the expected orientation to a satellite.

1.2. Literature Review

In this thesis, the satellite is a sun-synchronous and three-axis stabilized. A three-axis stabilized satellite generally use thrusters or reaction wheels for attitude control including attitude maneuvers, since the Earth's magnetic field is too weak to use magnetic torque rods for the same functions [4, 48]. For a three-axis stabilized system, six possible directions (roll, pitch, yaw directions and their negatives) are available for attitude maneuvering.

In the past decade, Earth observation satellites such as CubeSat 12U ATISE have been improved from relatively low resolution at about 5 meters to high resolution at

about 0.5 meters that can produce useful imagery products [59, 66, 67]. In addition to detumbling, AAUSAT-II satellite uses both torque rods and momentum wheels to manage controller problems for slew maneuvering [73].

Gravity gradient stabilization has been used for microsatellites to provide a low cost attitude control and a good pointing accuracy. In the study of [65], this stabilization is also provided with thrusters.

The linearization of nonlinear models [76, 51, 54] and applying the obtained linear controllers such as Linear Quadratic Regulators are commonly handled in several academic studies in order to facilitate the calculations of complex system equations [3, 46, 71, 73]. Linear Quadratic Regulator (LQR) generally focuses on finding out a suitable input from the initial state of a linear model to the final state of it in order to minimize cost function [83]. Although input signal is recoverable from full state feedback, gain values and gain matrix are not commonly estimated. In this case, a Riccati equation can be accepted as a solution [1, 4, 6].

There are lots of different Lyapunov based controller techniques besides LQR such as Sliding Mode Controller [52, 75] and PID controller [68, 73, 82] used to design a reliable attitude determination and control system for a microsatellite. Another simple controller called as B-dot controller is suggested to bring a satellite in a stable state using magnetic torque rods in detumbling phase such as DTU-Sat [54].

Finding a set of gains is the main task of attitude controller design for linear models, and the gain values are valid only around the equilibrium points. Multi-variable controllers such as PID controllers can be compound with the gain scheduling method to be able to apply founded gain values to the nonlinear models [5, 8, 45].

In literature, there are lots of studies on Kalman filter based attitude estimation algorithms. Some of them are focusing on the linear model designs [6, 7], but mostly on the nonlinear and complex aerospace applications. Kalman Filters combine the different sensor data and produce more accurate attitude solution [45, 59].

The basic form of Kalman filter can be generalized to the Extended Kalman Filter (EKF). In recent researches, the more enhanced Kalman Filter type is generally utilized called Unscented Kalman Filter (UKF) and it is very beneficial especially for poor initial filter conditions [1].

1.3. Microsatellites

The term "microsatellite" is usually applied to the name of an artificial satellite with a wet mass between 10 kg and 100 kg. However, this is not an official convention, and sometimes those terms can refer to satellites larger than this weight range, or smaller than this. The selected satellite for this study can be classified as a microsatellite.

1.3.1. The Selected Microsatellite

The selected microsatellite is called FLP microsatellite. Its orbit is designed as a kind of sun-synchronous orbit, and it has a circular shape. In the following table, the most important attitude properties of the selected satellite are listed (Table 1-1):

Table 1-1 The Fundamental Flying Laptop Microsatellite Characteristics

FLP Microsatellite Characteristics	
Dimensions	60 × 70 × 80 cm
Mass	117 kg
Desired Orbit	Circular and Polar Orbit
Orbit Altitude	~ 700 km
Attitude Control	Three Axis Stabilized
Solar Panels	3 Solar Panels (2 deployable)

The primary payload is a Multi-Spectral Imaging Camera (MICS), and the auxiliary payload is a Panoramic Camera (PAMCAM) used to obtain a more comprehensive overview of the observed area on the Earth surface.

This microsatellite consists of five fundamental subsystems are specified hereafter:

- ✓ **Data Handling Subsystem:** This subsystem collects some useful data (telemtries, images, etc.) from satellite payloads and sends this data to ground stations throughout a communication subsystem. The collected data can be recorded for later transmission.
- ✓ **Power Subsystem:** This subsystem provides the necessary power to the satellite in order to maintain its mission throughout its lifetime. It can change the states of power lines of platform and payload equipment as open or closed state and manages the battery charging/discharging control.
- ✓ **Attitude Control Subsystem:** The microsatellite is a three-axis stabilized by the help of avionic sensors (star trackers, magnetometers, gyros and GPS) and actuators (reaction wheels and magnetic torque rods). There is no propulsion subsystem in the selected satellite. The focusing point is to design three different attitude control systems as main controllers with an integration of multi-sensors for this thesis.

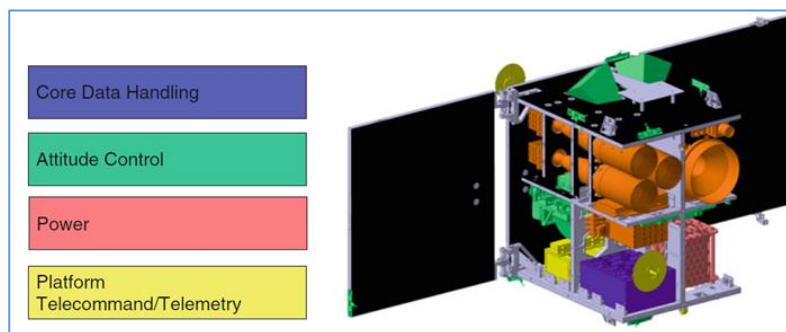


Figure 1-1 The FLP Platform Setup [17]

- ✓ **Telemetry Tracking and Control Subsystem:** This subsystem consists of a transceiver and omnidirectional antennas to be ensure there is a communication link between satellite and ground stations. The uplink and

downlink frequencies are 2.0 GHz and 2.3 GHz respectively for the selected satellite.

- ✓ **Thermal Control Subsystem (TCS):** This subsystem keeps the satellite platform and equipment temperature within the specified ranges. The satellite is mainly covered with multi-layer insulations to decrease the heat changes between satellite and space environment. The other element is radiator which transmits the heat from satellite to space.

1.4. Problem Statements

In this study, the main concern is to be able to control a microsatellite attitude and its orientation by changing the angular magnitudes of its rotational axes with multi-sensor navigation approach. In order to perform these actions, it is required to pay attention to time constraints and model accuracies. The detailed models of satellite sensors and actuators must be designed and simulated in an appropriate medium. The accuracy level of a satellite attitude determination can be affected negatively due to sensor measurement noises. In order to have a sensitive model, sensor noises and disturbance torques arising from internal and external parameters shall be taken into consideration and removed from the system.

The torques generated from actuators is required to be controlled. Because of this reason, the main goal is to advance system controllers such as PD, LQR and SMC controllers which provide states control and help to track orbit trajectory under environmental disturbance torques.

Satellite attitude dynamic and kinematic equations with their mathematical models shall be derived using Euler angles in a quaternion vector form and coordinate frame transformations. These equations are linearized under stable state conditions. After implementing linearization steps, both linear and nonlinear state space equations are obtained with their matrix representations to prepare system properties.

The satellite and its orbit properties shall be modelled to localize its angular velocity and position according to Earth Reference Frames. Notably, the detailed model of reaction wheels and magnetic coils, which are the most essential model items, is appropriately made to be able to represent the control torques.

All models of navigation processor with Kalman filters were visualized with graphics and compared the results in terms of some critical parameters such as the accuracy, efficiency and robustness.

1.5. Publication from This Thesis

The publication of “Design of Attitude Control with Kalman Filter for a LEO Microsatellite” was presented in a national conference called TOK2019 with the supervisor of this thesis.

1.6. The Thesis Organization

This thesis consists of seven different chapters, and all these chapters have a close relationship in terms of their contents. These chapters are organized, as mentioned below:

- ✓ In this chapter, there is an introduction for the navigation and attitude control of microsatellites. The selected microsatellite is specified with its subsystems and fundamental properties which are frequently mentioned for the following chapters.
- ✓ Chapter-2 mentions about the non-linear mathematical modelling of the attitude dynamics and kinematics of a microsatellite and their relevant state space definitions with its measurement equations.

- ✓ Chapter-3 includes mathematical modelling of space environment and its adverse effects on satellite attitude.
- ✓ Chapter-4 proposes nonlinear and linear state-space models to control the satellite attitude.
- ✓ Chapter-5 focuses on controller types (B-dot, PID, LQR and SMC) which are put into use in different phases during a satellite life such as Detumbling Phase and Tracking (Nominal) Phase.
- ✓ Chapter-6 discusses the results obtained from controller outputs given detailed information in the previous chapter.
- ✓ Chapter-7 summarizes the conclusions of all analyses performed in this study. Besides, this chapter provides some recommendations for future research to enhance and improve navigation processors and main controllers.

All models relative to attitude sensors, actuators, navigation solutions and controllers are designed and simulated with the most commonly used tools, MATLAB and Simulink in R2018b version.

CHAPTER 2

SATELLITE ATTITUDE DYNAMICS and KINEMATICS

2.1. Introduction

The knowledge of satellite attitude dynamics and kinematics are mandatory to control and stabilize its attitude. Attitude control process provides the satellite control and its orbit orientation in space. Attitude maneuver process supplies to reorient a satellite from one attitude to another by changing its angles between its rotational axes specified in different coordinate frames. Attitude stabilization process ensures to maintain the existing satellite attitude concerning the external reference frames.

Firstly, coordinate frames and transformations between them are handled as an introduction of a satellite attitude dynamics. Secondly, attitude representation methods are defined, and then the dynamic and kinematic equations of motions are clarified for a non-spinning satellite. The effects of rotating elements involved in the satellite such as reaction wheels are also incorporated into these equations.

The first problem is to find the angular momentum vectors of satellite and reaction wheels. The satellite is an Earth imaging satellite and its classification is termed as Low Earth Orbit. Because of this situation, the gravity gradient moment shall be taken into account to find out the total moments of a satellite. The dynamic equations of a satellite are obtained with Euler angles, and then state-space equations are acquired using Newton-Euler method for an attitude control simulation.

Assuming that the Local Navigation Frame and satellite Body Frame are coincident at the stable position and this assumption can be used as a starting point of the

simulation before applying any maneuvers to the satellite. If there are any disturbance torque sources in the space environment, the satellite starts to move on its orbit and orient its body according to these torques applied on it.

2.2. Coordinate Frames

Coordinate frames are used to clarify the position of a point relating to other specified reference frames for three-axis attitude stabilized system. Satellite attitude for any reference frame can be defined using Euler angles with direction cosine matrices or quaternion vectors, which are the different representation form of coordinate frames and attitude transformations.

2.2.1. Earth Centered Inertial Frame (ECI)

ECI Frame is located at the center of Earth mass and oriented with respect to the Earth's spin axis and stars. The X-axis (X_I) points towards the vernal equinox, Z-axis (Z_I) extends through the North Pole. Y-axis (Y_I) is the orthogonal complement of this frame, and it is in the equatorial plane together with X-axis.

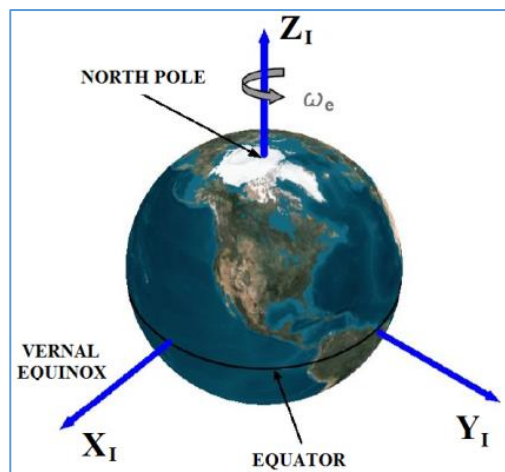


Figure 2-1 Earth Centered Inertial Frame (ECI) [9]

ECI Frame is fixed in space, and it means that it has not any rotations and movements. On the other hand, this frame is not an ideal inertial frame since Earth turns in its orbit and around the Sun.

2.2.2. Earth Centered Earth Fixed Frame (ECEF)

ECEF Frame origin is located at the Earth mass center. X-axis (X_E) points to the intersection of equatorial plane and the Greenwich reference meridian which defines zero degrees longitude. Z-axis (Z_E) points to the North Pole, and it also aligned with the satellite spin axis (rotation axis).

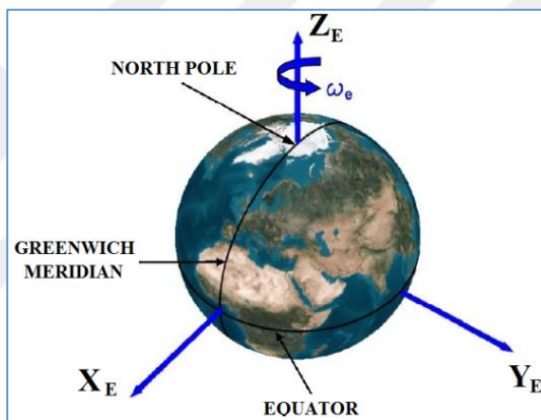


Figure 2-2 Earth Centered Earth Fixed Frame (ECEF) [9]

In order to find out the transformations between ECI and ECEF Frames, assuming that the centers and Z axes (Z_I, Z_E) are coincident. X (X_I, X_E) and Y (Y_I, Y_E) axes are also overlapped at time t_0 , then this frame rotates around Z axis at the specified time interval ($\Delta t = t - t_0$) with a constant Earth angular velocity (w_{IE}). The rotation matrix (C_{ECI}^{ECEF}) using the transformation from ECI to ECEF Frame is:

$$C_{ECI}^{ECEF} = \begin{bmatrix} \cos(w_{IE}(\Delta t)) & \sin(w_{IE}(\Delta t)) & 0 \\ -\sin(w_{IE}(\Delta t)) & \cos(w_{IE}(\Delta t)) & 0 \\ 0 & 0 & 1 \end{bmatrix} \quad (2.1)$$

This frame rotates one revolution in each sidereal day around Z-axis relative to ECI Frame with a constant angular velocity ($w_{IE} = 7.292115 \times 10^{-5}$ rad/s) [54].

The matrix C_{ECEF}^{ECI} providing the transformation in the opposite direction is equal to the transpose of previous matrix ($[C_{ECI}^{ECEF}]^T$):

$$C_{ECEF}^{ECI} = [C_{ECI}^{ECEF}]^T = \begin{bmatrix} \cos(w_{IE}(\Delta t)) & -\sin(w_{IE}(\Delta t)) & 0 \\ \sin(w_{IE}(\Delta t)) & \cos(w_{IE}(\Delta t)) & 0 \\ 0 & 0 & 1 \end{bmatrix} \quad (2.2)$$

2.2.3. Local Orbit Frame (LLA)

Local Orbit Frame known as geodetic latitude, longitude, altitude (LLA) coordinate frame is located at the satellite center. These values are required to determine satellite orientation with respect to the WGS84 standard [63]:

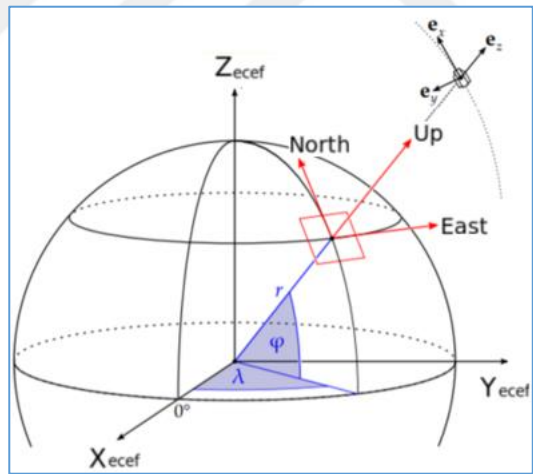


Figure 2-3 Local Orbit Frame wrt. ECEF and NED Frames [63]

The latitude angle (L_B) is between the equatorial plane and the normal to Earth surface. It is positive for the northern hemisphere and negative for the southern hemisphere (R is the norm of a satellite position vector in ECEF):

$$R = \sqrt{(R_x^{ECEF})^2 + (R_y^{ECEF})^2 + (R_z^{ECEF})^2} \quad (2.3)$$

$$L_B = \arcsin\left(\frac{R_z^{ECEF}}{R}\right) \quad (2.4)$$

The longitude angle (λ_B) is between the Greenwich meridian and satellite. It is counted positively towards the East and negatively towards the West.

$$\lambda_B = \arctan\left(\frac{R_y^{ECEF}}{R_x^{ECEF}}\right) \quad (2.5)$$

The altitude (h) is an approximation of the difference between the satellite and the reference surface measured normal to the geoid ($R_{Earth} \cong 6378 \text{ km}$):

$$h = R - R_{Earth} \quad (2.6)$$

2.2.4. Body Frame

The origin of Body Frame locates at satellite mass center, and this frame moves with satellite body. Rotations around X-Y-Z axes of orbit frame are denoted as roll, pitch and yaw axis respectively [54]:

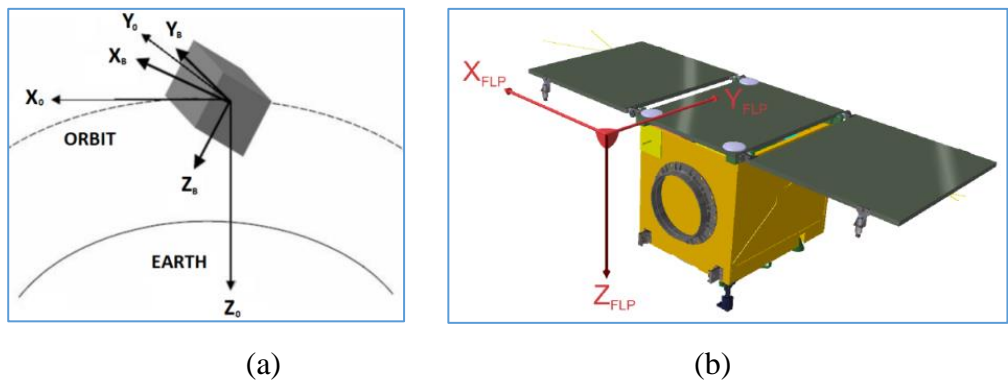


Figure 2-4 (a) Body Frame (b) FLP Microsatellite Body Frame [14, 17]

In the case of Euler angles have zero degrees in roll, pitch and yaw axes, Z-axis (Z_B) points the nadir direction; X (X_B) and Y (Y_B) axes coincide with the orbit reference frame axes at a stable position. The satellite can rotate all around its orthogonal axes of its Body Frame under some undesirable disturbance torques applied on it.

2.3. Satellite Kinematic Equations

Before explaining some important satellite dynamic and kinematic equations, it is mandatory to define what the rigid body is. It means that there are no moving elements inside a body. The selected satellite cannot be assumed as a rigid body since the rotating elements such as reaction wheels exist inside it. On the other hand, this assumption provides to have a better understanding of dynamic equations and the relationships between them. The most effective methods to exemplify attitude kinematic equations are Direction Cosine Matrix (DCM) and quaternion vectors.

2.3.1. Satellite Kinematic Equations with Direction Cosine Matrix

The major three-axis attitude transformation is based upon direction cosine matrix and it can be specified in terms of Euler angles. So long as all the matrix transformations are performed in the same reference frame, it is not crucial whether the reference frame is inertial or rotating with the orbit.

Direction cosine matrices [$C_{ORBIT}^{BODY} = C_O^B$] have the critical property of mapping vectors from a reference frame to Body Frame. This matrix is also a proper orthogonal matrix, as shown below:

$$[V]_B = [C_O^B][V]_O \quad (2.7)$$

$$[V]_B = \begin{bmatrix} X_B \\ Y_B \\ Z_B \end{bmatrix} = \begin{bmatrix} C_{11} & C_{12} & C_{13} \\ C_{21} & C_{22} & C_{23} \\ C_{31} & C_{32} & C_{33} \end{bmatrix} \begin{bmatrix} X_O \\ Y_O \\ Z_O \end{bmatrix} \quad (2.8)$$

The inverse of a DCM is equal to the transposition of the same matrix:

$$[C_o^B]^{-1} = [C_o^B]^T \Rightarrow [V]_o = [C_o^B]^T [V]_B \quad (2.9)$$

Euler Angle Rotation: Euler angles describe the satellite attitude of Body Frame with respect to Local Orbit Frame. These angles are defined at successive angular rotations around body axes. There are two types of rotational arrangements [15]:

- ✓ Successive rotations around each of three different axes are shown like:
 $X \rightarrow Y \rightarrow Z, X \rightarrow Z \rightarrow Y, Y \rightarrow X \rightarrow Z, Y \rightarrow Z \rightarrow X, Z \rightarrow X \rightarrow Y, Z \rightarrow Y \rightarrow X.$
- ✓ First and third rotations around the same axis and the second rotation around one of two remaining axes are shown like the following (In this type of sequence, singularities occur at zero and $\pm 180^\circ$ degrees for second rotation angles; at $\pm 90^\circ$ degrees for non-repeated axis sequences [66]):
 $X \rightarrow Y \rightarrow X, X \rightarrow Z \rightarrow X, Y \rightarrow X \rightarrow Y, Y \rightarrow Z \rightarrow Y, Z \rightarrow X \rightarrow Z, Z \rightarrow Y \rightarrow Z.$

Euler roll angle (Φ) is a rotation around X body axis (X_B), pitch angle (θ) is a rotation around Y body axis (Y_B), and yaw angle (ψ) is a rotation around Z body axis (Z_B). $[X_B \ Y_B \ Z_B]$ vector represents satellite Body Frame in space.

In this study, the attitude transformation order is selected as $Z \rightarrow Y \rightarrow X$ Euler angular rotation (Aerospace Euler Sequence). It means that this rotation is the transformation ($\psi \rightarrow \theta \rightarrow \Phi$) around Z, Y_1 and X_2 axis respectively. The transformation from Orbit Frame $[X_O \ Y_O \ Z_O]$ to Body Frame $[X_B \ Y_B \ Z_B]$ is provided with the following action items (It is assumed that $[X_B \ Y_B \ Z_B]$ is $[X_3 \ Y_3 \ Z_3]$ here):

- 1) Yaw Axis Rotation: First angular rotation about Z axis with ψ angle

$$\begin{bmatrix} X_1 \\ Y_1 \\ Z_1 \end{bmatrix} = \begin{bmatrix} \cos(\psi) & \sin(\psi) & 0 \\ -\sin(\psi) & \cos(\psi) & 0 \\ 0 & 0 & 1 \end{bmatrix} \begin{bmatrix} X_O \\ Y_O \\ Z_O \end{bmatrix} = [C_Z] \begin{bmatrix} X_O \\ Y_O \\ Z_O \end{bmatrix} \quad (2.10)$$

2) Pitch Axis Rotation: Second angular rotation about Y_1 axis with θ angle

$$\begin{bmatrix} X_2 \\ Y_2 \\ Z_2 \end{bmatrix} = \begin{bmatrix} \cos(\theta) & 0 & -\sin(\theta) \\ 0 & 1 & 0 \\ \sin(\theta) & 0 & \cos(\theta) \end{bmatrix} \begin{bmatrix} X_1 \\ Y_1 \\ Z_1 \end{bmatrix} = [C_Y] \begin{bmatrix} X_1 \\ Y_1 \\ Z_1 \end{bmatrix} \quad (2.11)$$

3) Roll Axis Rotation: Third angular rotation about X_2 axis with ϕ angle

$$\begin{bmatrix} X_B \\ Y_B \\ Z_B \end{bmatrix} = \begin{bmatrix} X_3 \\ Y_3 \\ Z_3 \end{bmatrix} = \begin{bmatrix} 1 & 0 & 0 \\ 0 & \cos(\phi) & \sin(\phi) \\ 0 & -\sin(\phi) & \cos(\phi) \end{bmatrix} \cdot \begin{bmatrix} X_2 \\ Y_2 \\ Z_2 \end{bmatrix} = [C_X] \begin{bmatrix} X_2 \\ Y_2 \\ Z_2 \end{bmatrix} \quad (2.12)$$

These angular rotations with the given order are illustrated in the following figure:

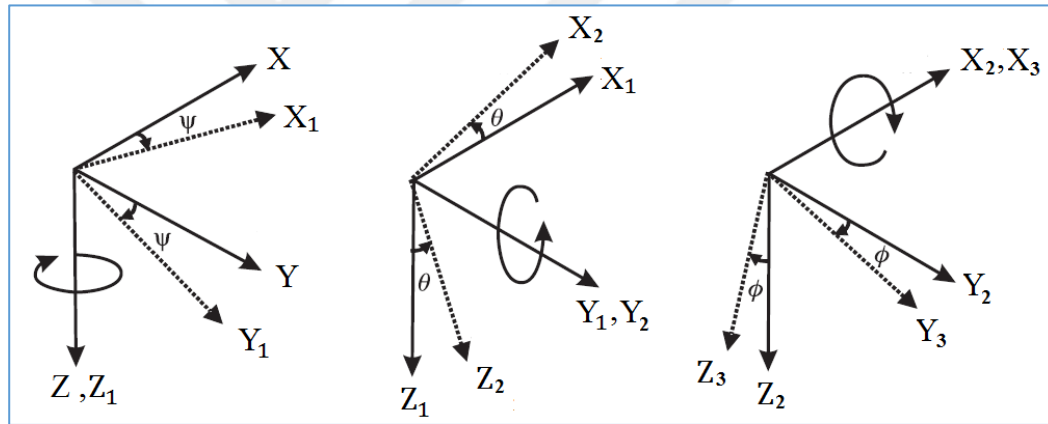


Figure 2-5 Satellite Rotation Around Z-Axis, Y-Axis, X-Axis Respectively [19]

The transformation from Orbit Frame directly to Body Frame is provided with the multiplication of the transformation matrices, respectively:

$$\begin{bmatrix} X_B \\ Y_B \\ Z_B \end{bmatrix} = [C_X] \begin{bmatrix} X_2 \\ Y_2 \\ Z_2 \end{bmatrix} = [C_X] [C_Y] \begin{bmatrix} X_1 \\ Y_1 \\ Z_1 \end{bmatrix} = [C_X] [C_Y] [C_Z] \begin{bmatrix} X_O \\ Y_O \\ Z_O \end{bmatrix} = [C_{ZYX}] \begin{bmatrix} X_O \\ Y_O \\ Z_O \end{bmatrix} \quad (2.13)$$

$$[C_O^B] = [C_{ZYX}] = [C_X] [C_Y] [C_Z] \quad (2.14)$$

After multiplying these matrices, it is obtained the following matrix (c denotes cosine function, and s denotes sinus function here):

$$[C_O^B] = \begin{bmatrix} c(\theta) c(\psi) & c(\theta) s(\psi) & -s(\theta) \\ -c(\phi) s(\psi) + s(\phi) s(\theta) c(\psi) & c(\phi) c(\psi) + s(\phi) s(\theta) s(\psi) & s(\phi) c(\theta) \\ s(\phi) s(\psi) + c(\phi) s(\theta) c(\psi) & -\sin(\phi) c(\psi) + c(\phi) s(\theta) s(\psi) & c(\phi) c(\theta) \end{bmatrix} \quad (2.15)$$

The trigonometric functions in this matrix have singularity problems, especially for large Euler angles. For example, these equations become singular as roll, pitch and yaw angles (ψ, θ, ϕ) approach to 90° degrees. Because of this drawback, the transformation can be obtained based on more effective kinematic expressions called quaternion vectors. The reverse transformation for roll, pitch and yaw angles is:

$$\Psi_{OB} = \text{atan2} ([C_O^B]_{12}, [C_O^B]_{11}) \quad (2.16)$$

$$\Theta_{OB} = -\text{asin} ([C_O^B]_{13}) \quad (2.17)$$

$$\Phi_{OB} = \text{atan2} ([C_O^B]_{23}, [C_O^B]_{33}) \quad (2.18)$$

2.3.2. Satellite Kinematic Equations with Quaternions

One approach to eliminate singularity problems of Euler angles is to implement quaternion vector that has the capability of quicker computations than direction cosine matrices, being computationally efficient in comparison with Euler angles and having less integration steps.

If the rotation angle of an axis is known, the related quaternion vector notation can be expressed using the following equations (Φ, θ, ψ are roll, pitch and yaw angles here) [47]:

$$q_x = \cos\left(\frac{\Phi}{2}\right) + i \sin\left(\frac{\Phi}{2}\right) \quad (2.19)$$

$$q_y = \cos\left(\frac{\theta}{2}\right) + j \sin\left(\frac{\theta}{2}\right) \quad (2.20)$$

$$q_z = \cos\left(\frac{\psi}{2}\right) + k \sin\left(\frac{\psi}{2}\right) \quad (2.21)$$

Defining q notation as the rotation product of q_x , q_y and q_z is:

$$q = q_z \ q_y \ q_x = q_1 i + q_2 j + q_3 k + q_4 \quad (2.22)$$

The last element (q_4) of quaternion vector represents the scalar part and the first three elements ($q_v = q_1 i + q_2 j + q_3 k$) represent the vector part [11, 47] :

$$q = q_1 i + q_2 j + q_3 k + q_4 = q_v + q_4 \quad (2.23)$$

The transformation from Euler angles to quaternion vector is calculated like in the following definition:

$$\begin{bmatrix} q_1 \\ q_2 \\ q_3 \\ q_4 \end{bmatrix} = \begin{bmatrix} \sin\left(\frac{\Phi}{2}\right) \cos\left(\frac{\theta}{2}\right) \cos\left(\frac{\psi}{2}\right) - \sin\left(\frac{\theta}{2}\right) \cos\left(\frac{\Phi}{2}\right) \sin\left(\frac{\psi}{2}\right) \\ \cos\left(\frac{\Phi}{2}\right) \sin\left(\frac{\theta}{2}\right) \cos\left(\frac{\psi}{2}\right) + \sin\left(\frac{\Phi}{2}\right) \cos\left(\frac{\theta}{2}\right) \sin\left(\frac{\psi}{2}\right) \\ \cos\left(\frac{\Phi}{2}\right) \cos\left(\frac{\theta}{2}\right) \sin\left(\frac{\psi}{2}\right) - \sin\left(\frac{\Phi}{2}\right) \sin\left(\frac{\theta}{2}\right) \cos\left(\frac{\psi}{2}\right) \\ \cos\left(\frac{\Phi}{2}\right) \cos\left(\frac{\theta}{2}\right) \cos\left(\frac{\psi}{2}\right) + \sin\left(\frac{\Phi}{2}\right) \sin\left(\frac{\theta}{2}\right) \sin\left(\frac{\psi}{2}\right) \end{bmatrix} \quad (2.24)$$

The DCM can be expressed in terms of quaternion vectors using the following way, $[C(q)]_O^B$ is the representation of DCM matrix in quaternion vector form:

$$[C_o^B] = [C(q)]_o^B = \left(q_4^2 - [q_v]^2 \right) I + 2[q_v][q_v]^T - 2q_4[\Omega(q_v)] \quad (2.25)$$

$$[\Omega(q_v)] = \begin{bmatrix} 0 & -q_3 & q_2 \\ q_3 & 0 & -q_1 \\ -q_2 & q_1 & 0 \end{bmatrix} \quad (2.26)$$

$$[C(q)]_o^B = \begin{bmatrix} (q_1^2 + q_4^2 - q_2^2 - q_3^2) & 2(q_1q_2 + q_3q_4) & 2(q_1q_3 - q_2q_4) \\ 2(q_1q_2 - q_3q_4) & (q_4^2 - q_1^2 + q_2^2 - q_3^2) & 2(q_2q_3 + q_1q_4) \\ 2(q_1q_3 + q_2q_4) & 2(q_2q_3 - q_1q_4) & (q_4^2 - q_1^2 - q_2^2 + q_3^2) \end{bmatrix} \quad (2.27)$$

The different quaternion definition for $[C(q)]_o^B$:

$$[C(q)]_o^B = \begin{bmatrix} 1 - 2(q_2^2 + q_3^2) & 2(q_1q_2 + q_3q_4) & 2(q_1q_3 - q_2q_4) \\ 2(q_1q_2 - q_3q_4) & 1 - 2(q_1^2 + q_3^2) & 2(q_2q_3 + q_1q_4) \\ 2(q_1q_3 + q_2q_4) & 2(q_2q_3 - q_1q_4) & 1 - 2(q_1^2 + q_2^2) \end{bmatrix} \quad (2.28)$$

$[C(q)]_o^B$ matrix can be defined with respect to the following column definitions:

$$[C(q)]_o^B = \begin{bmatrix} C(q)_{11} & C(q)_{12} & C(q)_{13} \\ C(q)_{21} & C(q)_{22} & C(q)_{23} \\ C(q)_{31} & C(q)_{32} & C(q)_{33} \end{bmatrix} = [C(q)_1 \quad C(q)_2 \quad C(q)_3] \quad (2.29)$$

The new matrix definition allows expressing quaternion vectors in terms of DCM elements. Firstly, it is assumed that scalar quaternion element (q_4) has the maximum value and the other quaternion elements can be formulated line by line [3, 19]:

$$q_4 = \frac{1}{2} \sqrt{1 + C(q)_{11} + C(q)_{22} + C(q)_{33}} \quad (2.30)$$

$$q_1 = \frac{1}{4} \frac{(C(q)_{23} - C(q)_{32})}{q_4} \quad (2.31)$$

$$q_2 = \frac{1}{4} \frac{(\mathcal{C}(q)_{31} - \mathcal{C}(q)_{13})}{q_4} \quad (2.32)$$

$$q_3 = \frac{1}{4} \frac{(\mathcal{C}(q)_{12} - \mathcal{C}(q)_{21})}{q_4} \quad (2.33)$$

The time derivation of quaternion vector representing attitude kinematic equation is also hereafter [11]:

$$\dot{q} = \frac{1}{2} [\Omega(w_{OB}^B)] q \quad (2.34)$$

$$\Omega(w_{OB}^B) = \begin{bmatrix} 0 & w_{OB_3}^B & -w_{OB_2}^B & w_{OB_1}^B \\ -w_{OB_3}^B & 0 & w_{OB_1}^B & w_{OB_2}^B \\ w_{OB_2}^B & -w_{OB_1}^B & 0 & w_{OB_3}^B \\ -w_{OB_1}^B & -w_{OB_2}^B & -w_{OB_3}^B & 0 \end{bmatrix} \quad (2.35)$$

The satellite velocity vector (w_{OB}^B) can be rewritten using the second column of DCM matrix ($\mathcal{C}(q)_2$) and the definition of ($w_{IO}^O = [0 \ -w_0 \ 0]^T$):

$$w_{OB}^B = w_{IB}^B - [\mathcal{C}(q)]_O^B \cdot w_{IO}^O \quad (2.36)$$

$$w_{OB}^B = w_{IB}^B - [\mathcal{C}(q)]_O^B \begin{bmatrix} 0 \\ -w_0 \\ 0 \end{bmatrix} = \begin{bmatrix} w_{IB_1}^B + \mathcal{C}(q)_{12} w_0 \\ w_{IB_2}^B + \mathcal{C}(q)_{22} w_0 \\ w_{IB_3}^B + \mathcal{C}(q)_{32} w_0 \end{bmatrix} \quad (2.37)$$

$$w_{OB}^B = \begin{bmatrix} w_{OB_1}^B \\ w_{OB_2}^B \\ w_{OB_3}^B \end{bmatrix} = \begin{bmatrix} w_{IB_1}^B + 2(q_1 q_2 + q_3 q_4) w_0 \\ w_{IB_2}^B + (q_4^2 - q_1^2 + q_2^2 - q_3^2) w_0 \\ w_{IB_3}^B + 2(q_2 q_3 - q_1 q_4) w_0 \end{bmatrix} \quad (2.38)$$

The new representation for skew symmetric matrix of satellite angular velocity ($\Omega(w_{OB}^B)$) according to angular velocity again, but defined with respect to ECI frame (w_{IB}^B) is depicted here:

$$\Omega(w_{OB}^B) = \begin{bmatrix} 0 & w_{IB_3}^B + C(q)_{32}w_0 & -w_{IB_2}^B - C(q)_{22}w_0 & w_{IB_1}^B + C(q)_{12}w_0 \\ -w_{IB_3}^B - C(q)_{32}w_0 & 0 & w_{IB_1}^B + C(q)_{12}w_0 & w_{IB_2}^B + C(q)_{22}w_0 \\ w_{IB_2}^B + C(q)_{22}w_0 & -w_{IB_1}^B - C(q)_{12}w_0 & 0 & w_{IB_3}^B + C(q)_{32}w_0 \\ -w_{IB_1}^B - C(q)_{12}w_0 & -w_{IB_2}^B - C(q)_{22}w_0 & -w_{IB_3}^B - C(q)_{32}w_0 & 0 \end{bmatrix} \quad (2.39)$$

2.4. Satellite Dynamic Equations

Attitude dynamics are modelled mainly to be able to predict the rotational motion and orientation of a satellite. The equations of attitude dynamics represented satellite orbit and position are used to provide position propagations based on the predictions of satellite orbit [1, 2, 15].

Satellite motion is specified with the following parameters [66]:

- ✓ Position and speed vectors describe the translational motion and they are the subject of orbit analysis and space navigation.
- ✓ Attitude angle and attitude rate vectors describe the rotational motion of satellite body and they are the subject of attitude analysis and dynamics.

The external torque applied on a satellite is divided into two parts; control torques and disturbance torques. The internal torque is generated by some internal effects such as propulsion tank sloshing, deployable appendages, etc. In this study, all internal torque sources are neglected and not included in dynamic equations.

The total external torque (M_T) is acting on the satellite comprised of both control torques (M_C) and the torques generating by different disturbing environmental

effects (M_D). In respect of this description, total torque can be defined with the following equation [10, 12, 14]:

$$M_T = M_C + M_D \quad (2.40)$$

The most efficient disturbance torque values are gravity gradient and magnetic field torques for the satellite altitude placed around 700 km. In conclusion, total disturbance torque is about the order of 10^{-5} Nm and detailed explanations are given in the related chapter (refer to 2.4.3 Disturbance Torques):

$$M_D = M_{GG} + M_{AERO} + M_{SR} + M_{MAG} \quad (2.41)$$

Satellite dynamic and kinematic equations are derived through Newton - Euler formulation. According to this formulation, the time derivative of satellite angular momentum (H_I) depends on the total external torque (called also angular moment) acting on satellite in inertial reference frame [10, 13]:

$$M_T = \frac{d\vec{H}_I}{dt} \quad (2.42)$$

The vector quantity of M_T is also defined in Body Frame like as follows:

$$M_T = \frac{d\vec{H}_I}{dt} = \frac{d\vec{H}_B}{dt} + \vec{w}_{IB}^B \times \vec{H}_B \quad (2.43)$$

The equation of satellite angular momentum in Body Frame is ($H_B = I_S w_{IB}^B$) and therefore a new definition of dynamic equation labeled as (2.43) can be represented like the following equation:

$$M_T = I_S \dot{w}_{IB}^B + (w_{IB}^B \times I_S w_{IB}^B) \quad (2.44)$$

The more compact form of the above equation for each satellite axes can be written using a skew-symmetric matrix definition ($\Omega(w_{IB}^B)$) of satellite angular velocity:

$$M_T = I_S \dot{w}_{IB}^B + \Omega(w_{IB}^B) I_S w_{IB}^B \quad (2.45)$$

$$\Omega(w_{IB}^B) = \begin{bmatrix} 0 & -w_{IB_3}^B & w_{IB_2}^B \\ w_{IB_3}^B & 0 & -w_{IB_1}^B \\ -w_{IB_2}^B & w_{IB_1}^B & 0 \end{bmatrix} \quad (2.46)$$

Case-1: Torque generators are only reaction wheels

The total angular momentum (H_B) can be extended by including both satellite angular momentum (H_S^B) and the angular momentum belongs to momentum exchange devices such as reaction wheels (H_{RW}^B). In this case, the new formulation of satellite dynamic equation is [15, 51]:

$$H_B = H_S^B + H_{RW}^B \quad (2.47)$$

The angular moment definition of reaction wheels (M_C^{RW}) is:

$$M_C^{RW} = \dot{H}_{RW}^B + (w_{IB}^B \times H_{RW}^B) \quad (2.48)$$

The angular moment definition is written with the help of the following definitions:

$$M_D = \frac{d}{dt}(H_S^B + H_{RW}^B) + w_{IB}^B \times (H_S^B + H_{RW}^B) \quad (2.49)$$

$$M_D = (\dot{H}_S^B + w_{IB}^B \times H_S^B) + (\dot{H}_{RW}^B + w_{IB}^B \times H_{RW}^B) \quad (2.50)$$

If the derivative of satellite angular moment is written like ($H_S^B = I_S w_{IB}^B$), disturbance moment equation will be:

$$M_D = I_S \dot{w}_{IB}^B + (w_{IB}^B \times I_S w_{IB}^B) + \dot{H}_{RW}^B + (w_{IB}^B \times H_{RW}^B) \quad (2.51)$$

The more compact form of the last equation can be written using skew-symmetric matrix definitions ($\Omega(w_{IB}^B)$, $\Omega(H_{RW}^B)$):

$$M_D = I_S \dot{w}_{IB}^B + \Omega(w_{IB}^B) I_S w_{IB}^B + \dot{H}_{RW}^B + \Omega(w_{IB}^B) H_{RW}^B \quad (2.52)$$

$$M_D - \dot{H}_{RW,B} = I_S \dot{w}_{IB}^B + \Omega(w_{IB}^B) I_S w_{IB}^B - \Omega(H_{RW}^B) w_{IB}^B \quad (2.53)$$

These non-linear torque equations with respect to each frame axes are:

$$M_{D_1} - \dot{H}_{RW_1}^B = I_{S_x} \dot{w}_{IB_1}^B + (I_{S_z} - I_{S_y}) w_{IB_2}^B w_{IB_3}^B - w_{IB_3}^B H_{RW_2}^B + w_{IB_2}^B H_{RW_3}^B \quad (2.54)$$

$$M_{D_2} - \dot{H}_{RW_2}^B = I_{S_y} \dot{w}_{IB_2}^B + (I_{S_x} - I_{S_z}) w_{IB_1}^B w_{IB_3}^B + w_{IB_3}^B H_{RW_1}^B - w_{IB_1}^B H_{RW_3}^B \quad (2.55)$$

$$M_{D_3} - \dot{H}_{RW_3}^B = I_{S_z} \dot{w}_{IB_3}^B + (I_{S_y} - I_{S_x}) w_{IB_1}^B w_{IB_2}^B - w_{IB_2}^B H_{RW_1}^B + w_{IB_1}^B H_{RW_2}^B \quad (2.56)$$

The time derivatives of angular velocity can be defined using the last equation:

$$\dot{w}_{IB}^B = I_S^{-1} [M_D - \dot{H}_{RW}^B - w_{IB}^B \times (I_S w_{IB}^B + H_{RW}^B)] \quad (2.57)$$

$$\dot{w}_{IB}^B = I_S^{-1} [M_D - \dot{H}_{RW}^B - \Omega(w_{IB}^B) I_S w_{IB}^B - \Omega(w_{IB}^B) H_{RW}^B] \quad (2.58)$$

$$\dot{w}_{IB}^B = I_S^{-1} [M_D - \dot{H}_{RW}^B - \Omega(w_{IB}^B) I_S w_{IB}^B + \Omega(H_{RW}^B) w_{IB}^B] \quad (2.59)$$

Case-2: Torque generators are only magnetic torque rods

If only magnetic torque rods are included in a satellite system as torque generators, total external torque and the time derivative of satellite angular velocity are defined with the following equations. In this case, there is no rotating element in satellite

body and therefore the entire angular momentum is not included the momentum generated by reaction wheels [54]:

$$M_T = M_C^{MTR} + M_D = I_S \dot{w}_{IB}^B + \Omega(w_{IB}^B) I_S w_{IB}^B \quad (2.60)$$

$$\dot{w}_{IB}^B = I_S^{-1} [M_C^{MTR} + M_D - \Omega(w_{IB}^B) I_S w_{IB}^B] \quad (2.61)$$

Case-3: Torque generators are both magnetic torque rods and reaction wheels

The dynamic equations are specified with the following equations in the case of using both torque rods and momentum wheels as torque generators:

$$M_T = M_C^{MTR} + M_C^{RW} + M_D = I_S \dot{w}_{IB}^B + \Omega(w_{IB}^B) I_S w_{IB}^B \quad (2.62)$$

$$\dot{w}_{IB}^B = I_S^{-1} [M_C^{MTR} + M_D - \dot{H}_{RW}^B - w_{IB}^B \times (I_S w_{IB}^B + H_{RW}^B)] \quad (2.63)$$

2.4.1. The Torque and Angular Momentum of Satellite

The external torques cause to accelerate the satellite proportionally to this torques in a stationary state, resulting in an increasing angular velocity. Conversely, if satellite body initially spins about an axis perpendicular to the applied torque, then it moves with a constant angular velocity proportional to this torque [66].

The selected satellite is assumed as a rigid body composed of m particles at the beginning of calculations, and it is moving relative to inertial frame. Assuming that there is no angular motion of this rigid body center, the angular momentum equation is hereafter (I_S is satellite inertial moment matrix):

$$H_{S,B} = I_S w_{IB}^B \quad (2.64)$$

Assuming that satellite Body axes are the principal axes of inertia and the general definition of satellite torque (angular moment) equation is:

$$M_{S,B} = \frac{dH_S^B}{dt} + (w_{IB}^B \times H_S^B) \quad (2.65)$$

$$M_{S,B} = I_S \dot{w}_{IB}^B + (w_{IB}^B \times I_S w_{IB}^B) = I_S \dot{w}_{IB}^B + \Omega(w_{IB}^B) I_S w_{IB}^B \quad (2.66)$$

2.4.1.1. Satellite Inertia Matrix

Inertia matrix represents the physical characteristic of a satellite, and each element of this matrix can be specified as below [11, 12]:

$$I_S = \begin{bmatrix} I_{S_{xx}} & -I_{S_{xy}} & -I_{S_{xz}} \\ -I_{S_{yx}} & I_{S_{yy}} & -I_{S_{yz}} \\ -I_{S_{zx}} & -I_{S_{zy}} & I_{S_{zz}} \end{bmatrix} \quad (2.67)$$

The inertia matrix of the selected satellite is approximated like that [9]:

$$I_S = \begin{bmatrix} 7.066197 & 0.471470 & 0.129597 \\ 0.471470 & 6.950219 & 0.209866 \\ 0.129597 & 0.209866 & 8.555828 \end{bmatrix} \quad (2.68)$$

The diagonal terms of satellite inertia matrix are known as the principal moments of inertia, and the corresponding axes are called principal axes of inertia. If Body Frame axes intersect the principal axes of inertia, satellite inertia matrix can be reduced to a diagonal matrix [12]:

$$I_S = \begin{bmatrix} 7.066197 & 0 & 0 \\ 0 & 6.950219 & 0 \\ 0 & 0 & 8.555828 \end{bmatrix} \rightarrow \begin{array}{l} I_{S_{xx}} = I_{S_x} = 7.066197 \\ I_{S_{yy}} = I_{S_y} = 6.950219 \\ I_{S_{zz}} = I_{S_z} = 8.555828 \end{array} \quad (2.69)$$

2.4.1.2. Satellite Angular Velocity

The satellite angular velocity vector defined in Body Frame can be oriented with respect to both Orbit and ECI Frame. The satellite angular velocity vector of Body Frame with respect to ECI Frame expressing in Body Frame ($\overrightarrow{w_{IB}^B}$) is defined in the following form:

$$\overrightarrow{w_{IB}^B} = \overrightarrow{w_{IO}^B} + \overrightarrow{w_{OB}^B} \rightarrow \overrightarrow{w_{OB}^B} = \overrightarrow{w_{IB}^B} - \overrightarrow{w_{IO}^B} \quad (2.70)$$

The mean motion of satellite is (w_0):

$$R = R_E + h = (6378.1370 + 700) \text{ km} \quad (2.71)$$

$$w_0 = \sqrt{\frac{\mu}{R^3}} \cong 0.0011 \text{ Hz} \cong 0.0069 \text{ rad/s} \quad (2.72)$$

- ✓ M is the Earth mass ($M = 5.9742 \times 10^{24} \text{ kg}$),
- ✓ G is the universal gravitational constant ($G = 6.6720 \times 10^{-11} \text{ Nm}^2/\text{kg}^2$),
- ✓ μ is the Earth gravitational constant
($\mu = M \cdot G = 3.986004418 \times 10^9 \text{ Nm}^2/\text{kg} - \text{m}^3/\text{s}^2$).

The satellite angular velocity of Local Navigation Frame with respect to ECI Frame expressing in Local Navigation Frame ($w_{IO}^0 = [0, -w_0, 0]^T$) can be defined by using satellite orbital mean motion (w_0). For small angle approximations, the satellite angular velocity of Orbit Frame with respect to ECI Frame (w_{IO}^B) [15]:

$$w_{IO}^B = [C_O^B] w_{IO}^0 = \begin{bmatrix} 1 & \psi & -\theta \\ -\psi & 1 & \phi \\ \theta & -\phi & 1 \end{bmatrix} \begin{bmatrix} 0 \\ -w_0 \\ 0 \end{bmatrix} = \begin{bmatrix} -\psi w_0 \\ -w_0 \\ \phi w_0 \end{bmatrix} \quad (2.73)$$

The same rotational motion ($Z_B \rightarrow Y_{B1} \rightarrow X_{B2}$) can be used for generating the angular velocity vector ($w_{OB}^B = [w_{OB_x}^B, w_{OB_y}^B, w_{OB_z}^B]^T$) from Orbit Frame to Body Frame. The time derivatives of rotation angles ($\dot{\psi}, \dot{\theta}, \dot{\phi}$) represent satellite angular velocities around Z_B, Y_{B1}, X_{B2} axis respectively.

The angular velocity around Z_B axis ($w_{OB_z}^B$) is subject to three successive angular transformations:

- ✓ First angular transformation is around Z_B axis (ψ angle),
- ✓ Second angular transformation is around Y_{B1} axis (θ angle),
- ✓ Third angular transformation is around X_{B2} axis (ϕ angle).

The angular velocity around Y_{B1} axis ($w_{OB_y}^B$) is subject to two successive angular transformations:

- ✓ First angular transformation is around Y_{B1} axis (θ angle),
- ✓ Second angular transformation is around X_{B2} axis (ϕ angle).

The angular velocity around X_{B2} axis ($w_{OB_x}^B$) is subject to only one attitude transformation that is around X_{B2} axis (ϕ angle). These transformations can be represented as a matrix form:

$$\begin{bmatrix} w_{OB_x}^B \\ w_{OB_y}^B \\ w_{OB_z}^B \end{bmatrix} = [C_X][C_Y][C_Z] \begin{bmatrix} 0 \\ 0 \\ \dot{\psi} \end{bmatrix} + [C_X][C_Y] \begin{bmatrix} 0 \\ \dot{\theta} \\ 0 \end{bmatrix} + [C_X] \begin{bmatrix} \dot{\phi} \\ 0 \\ 0 \end{bmatrix} \quad (2.74)$$

After performing matrix multiplications specified in the previous equation is:

$$\begin{bmatrix} w_{OB_x}^B \\ w_{OB_y}^B \\ w_{OB_z}^B \end{bmatrix} = \begin{bmatrix} 1 & 0 & -\sin(\theta) \\ 0 & \cos(\phi) & \cos(\theta)\sin(\phi) \\ 0 & -\sin(\phi) & \cos(\theta)\cos(\phi) \end{bmatrix} \begin{bmatrix} \dot{\phi} \\ \dot{\theta} \\ \dot{\psi} \end{bmatrix} \quad (2.75)$$

These equations are solved in terms of the derivative of Euler angular velocities:

$$w_{OB_x}^B = \dot{\phi} - \dot{\psi} \sin(\theta) \quad (2.76)$$

$$w_{OB_y}^B = \dot{\theta} \cos(\phi) + \dot{\psi} \cos(\theta) \sin(\phi) \quad (2.77)$$

$$w_{OB_z}^B = \dot{\psi} \cos(\theta) \cos(\phi) - \dot{\theta} \sin(\phi) \quad (2.78)$$

Satellite angular rate can be specified directly with the angular velocity vector in Orbit Frame ($w_{OB_x}^B = \dot{\phi}$, $w_{OB_y}^B = \dot{\theta}$, $w_{OB_z}^B = \dot{\psi}$) supposed that using small angle approximation ($\theta \approx \phi \approx 0^\circ$). Angular rate is controlled and stabilized with B-dot controller law in detumbling phase.

These equations can also have singularity problem like as direct cosine matrices have. Because of this reason, a special order of rotation ($Z \rightarrow Y \rightarrow X$) can be chosen to transform body frame to any reference frame in space. Through this assumption, nonlinear equation can be linearized and expressed in terms of Euler angles. In this study, the linearization process is applied using Taylor series expansion and indicated with system states including satellite angular velocity, quaternion vector and wheel angular momentum.

2.4.2. The Torque and Angular Momentum of Actuators

Two different kind of actuators such as reaction wheels as a momentum exchange device and magnetic torque rods as an auxiliary device to unload the saturated momentum on reaction wheels are located in the selected satellite. The rods can also carried out the same function of reaction wheels whenever they are not available. The actuator characteristics of the selected satellite are listed hereafter:

Table 2-1 The Characteristics of Satellite Actuators [9, 17]

	Reaction Wheels	Magnetic Torque Rods
Quantity	4 RWs	3 MTRs
Sampling Time (T_s)	0.1 s (10 Hz)	0.1 s (10 Hz)

2.4.2.1. The Control Torque of Reaction Wheels

A reaction wheel applies a control torque to satellite resulting in the changes of its angular momentum. The rotating elements in a satellite such as reaction wheels have their angular momentum, and it is a part of the momentum of an entire system in Euler's moment equations. When a torque acts on a satellite along one axis, the wheel reacts to this torque, absorbing it and maintaining its attitude. In these situations, the spin rate of wheels is able to maintain a constant attitude by increasing or decreasing it. When a reaction wheel rotates one way and its rotation speed changes, satellite rotates proportionately the opposite way in response to external torques imposed on it to ensure the conservation of angular moment [66].

It is not desirable to operate a reaction wheel at near saturation speeds. When wheel speed is outside of its saturation limit (operational limit), a momentum exchange device such as magnetic rods can be used to restore the wheel speed to its nominal operating value.

Reaction wheels are used along all three axes and generally, there is one additional wheel along the non-orthogonal axis to provide the redundancy. There are four reaction wheels located in a tetrahedron configuration and known as a fundamental actuator in the selected satellite. Assuming that all reaction wheels have the same specifications such as mass, inertia and the distances from the satellite center, their substantial performance parameters are listed hereafter:

Table 2-2 Performance Parameters of Reaction Wheels (RWs)

Performance Parameters	The Values of Reaction Wheels
Angular Momentum (H_{RW}^B)	$H_{RW,B} = I_{RW} \cdot w_{RW,B}^B = \pm 0.12 \text{ Nms (max.)}$
Operation Speed Range (w_{RW})	$\pm 2800 \text{ rpm } (\sim 293.215 \text{ rad/s})$
Angular Moment (M_{RW})	$\pm 5 \text{ mNm (at +2800 rpm)}$ $\pm 0.015 \text{ Nm (max.)}$
Inertial Moment (I_{RW})	$5 \times 10^{-4} \text{ kgm}^2$
Speed Limit	$< 3000 \text{ rpm}$

The advantage of tetrahedral configuration is that the wheel assembly can provide twice as much of maximum torque on rotation axis. The rotation axis of each reaction wheel is aligned to the Y-axis in Body Frame to optimize this configuration for the target pointing maneuver.

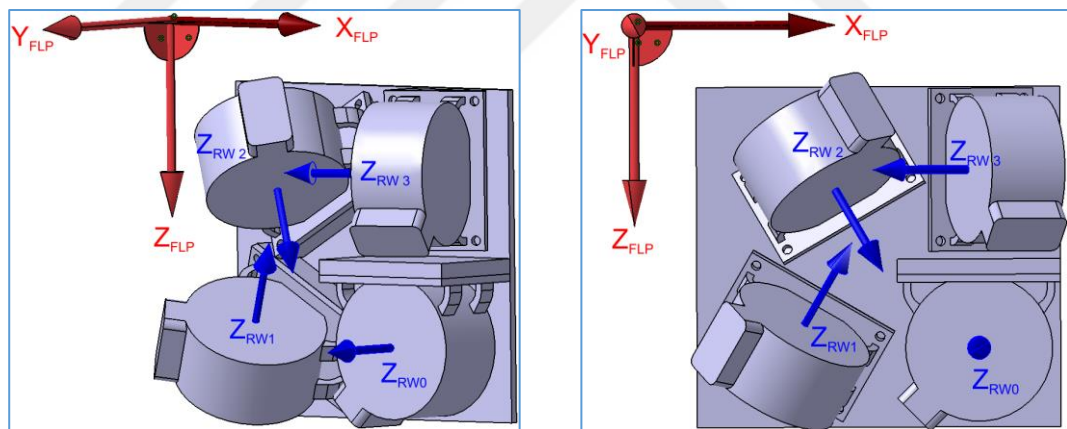


Figure 2-6 The Location of Reaction Wheels (Tetrahedron Configuration) [9, 17]

The orientation matrix is required to resolve control allocation problem between the Euler angles and reaction wheels. This matrix for reaction wheels comprises of four column vectors which represent the distribution of reaction wheel torques to each satellite rotation axis. The distribution matrix which has three rows and several

columns equal to the number of reaction wheels in the satellite. The power performance properties of reaction wheels are defined below:

Table 2-3 Power Performance Parameters of Reaction Wheels (RWs)

Power Performance Parameters	The Values of Reaction Wheels
Steady-state (at nominal speed)	< 2 W
Max. torque (at nominal speed)	< 4 W
Supply voltage	0.5 V – 20 V ($V_{max} = 20$ V) Nominal voltage = 5 ± 0.25 V
Input current	(20 V line) < 0.20 A ($I_{max} = 0.20$ A) (5 V line) < 0.12 A ($I_{min} = 0.12$ A)

The given distribution matrix of the layout configuration of reaction wheels is [17]:

$$C_{RW}^{BODY} = \begin{bmatrix} 0 & 0.4741 & 0.4741 & -0.9482 \\ -0.9999 & 0.3333 & 0.3333 & 0.3333 \\ 0 & -0.8165 & 0.8165 & 0 \end{bmatrix} \quad (2.79)$$

One of the possible distribution matrices for tetrahedral configuration to deliver the command torque in an equal way can be selected such as the following matrix [48]:

$$C_{RW}^{BODY} = \begin{bmatrix} \sqrt{3}/3 & -\sqrt{3}/3 & -\sqrt{3}/3 & \sqrt{3}/3 \\ \sqrt{3}/3 & -\sqrt{3}/3 & \sqrt{3}/3 & -\sqrt{3}/3 \\ \sqrt{3}/3 & \sqrt{3}/3 & -\sqrt{3}/3 & -\sqrt{3}/3 \end{bmatrix} \quad (2.80)$$

The distribution matrix for each row is satisfied in the following equations. If all four wheels provide equal torque, the total moments in satellite body frame are equal to zero value with respect to these equations [48]:

$$C_{RW}^{BODY} = \begin{bmatrix} C_{RW_X} \\ C_{RW_Y} \\ C_{RW_Z} \end{bmatrix} = \begin{bmatrix} C_{11} & C_{12} & C_{13} & C_{14} \\ C_{21} & C_{22} & C_{23} & C_{24} \\ C_{31} & C_{32} & C_{33} & C_{34} \end{bmatrix} = [C_1 \quad C_2 \quad C_3 \quad C_4] \quad (2.81)$$

$$C_{i1} + C_{i2} + C_{i3} + C_{i4} = 0 ; \quad i = 1, 2, 3 \quad (2.82)$$

Each column vector of a distribution matrix has the following properties:

$$\sqrt{(C_{1j})^2 + (C_{2j})^2 + (C_{3j})^2} = 1 ; \quad j = 1, 2, 3, 4 \quad (2.83)$$

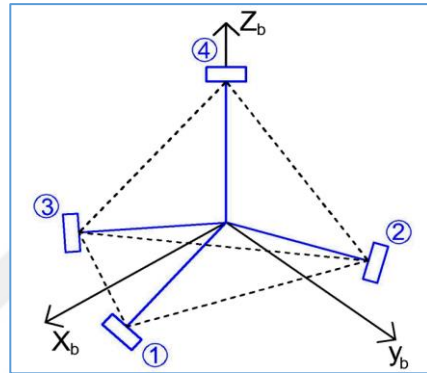


Figure 2-7 Tetrahedron Configuration Diagram of RWs [48]

The distribution of satellite angular momentum (H_{RW}^B) from satellite body to each reaction wheel (H_{RW}) can be defined with the inverse of distribution matrix (C_{RW}^{BODY}):

$$H_{RW} = [C_{RW}^{BODY}]^{-1} H_{RW}^B \quad (2.84)$$

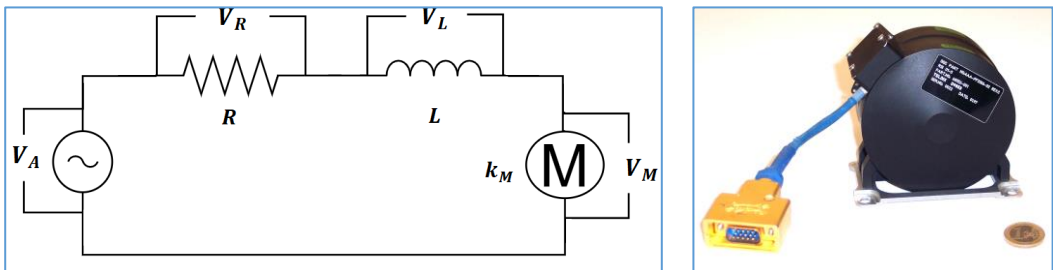


Figure 2-8 The Electrical Representation of Reaction Wheels [9, 17]

In order to make a system more reliable, brushless DC motors are chosen as actuators. Each motor consists of an electrical part and a mechanical part. The

electrical part of a motor can be modelled using Kirchhoff's Voltage Law like as the Figure 2-8 [47].

The source voltage (V_A) is the sum of resistance voltage (V_R), inductance voltage (V_L) and back electromotive force voltage (V_M). The detailed definition of source voltage is declared such as the following equation (R is the resistance, L is the inductance, i is the current and k_M is the back electromotive force coefficient):

$$V_A(t) = V_R(t) + V_L(t) + V_M(t) \quad (2.85)$$

$$V_A(t) = R i(t) + L \frac{di(t)}{dt} + k_M w_{RW}(t) \quad (2.86)$$

The mechanical part of the motor can be modelled by using torque definition. " k_t " is the motor torque coefficient [Nms/A], " b " is the viscous friction coefficient [Nms/rad] and therefore, " $b w_{RW}$ " represents the negative torque component in the following equation:

$$M_M = k_t i = I_{RW} \dot{w}_{RW} + b w_{RW} \quad (2.87)$$

The total angular momentum of reaction wheels (H_{RW}) are equal to the sum of each reaction wheels' angular momentum ($w_{RW} = [w_{RW1}, w_{RW2}, w_{RW3}, w_{RW4}]^T$):

$$H_{RW} = I_{RW} \cdot w_{RW}; \quad I_{RW} = I_{RW_x} = I_{RW_y} = I_{RW_z} \quad (2.88)$$

The reaction wheel torque has the same magnitude but it is in the opposite direction of the torque produced from satellite rotation in the scope of energy conservation principle. The rate change of total angular momentum from wheels is equal to the opposite direction of satellite control moment:

$$M_C^{RW} = \dot{H}_{RW}^B + (w_{IB}^B \times H_{RW}^B) = \begin{bmatrix} \dot{H}_{RW_x}^B + H_{RW_z}^B w_{IB_y}^B - H_{RW_y}^B w_{IB_z}^B \\ \dot{H}_{RW_y}^B + H_{RW_x}^B w_{IB_z}^B - H_{RW_z}^B w_{IB_x}^B \\ \dot{H}_{RW_z}^B + H_{RW_y}^B w_{IB_x}^B - H_{RW_x}^B w_{IB_y}^B \end{bmatrix} \quad (2.89)$$

2.4.2.2. The Control Torque of Magnetic Torque Rods

It is common to take advantage of Earth magnetic field as a magnetic control torque to counter the effects of disturbance torques. Magnetic control systems are relatively lightweight and cheaper than momentum control systems. However, they also have some disadvantages such as power constraints and dependability of magnetic field configuration. Three coils generate a magnetic moment on each satellite axis and create a torque interfering with Earth's magnetic field to align satellite to the desired attitude [66].

Magnetic torque rods are generally used to dump the accumulated momentum on reaction wheels and to create control torque interacting with Earth's magnetic field for small attitude maneuvers. Besides these fields of usages, torque rods are also used for detumbling to decrease initial satellite angular velocity after deployment phase, momentum/nutation dumping and precise orientation [79]. In this study, the effects of detumbling and desaturation controllers are investigated in the following sections with their simulation results.



Figure 2-9 Magnetic Torque Rods [9, 17]

In most applications, at least three number of torque rods are preferred to produce magnetic moment on the orthogonal axes of satellite Body Frame [49]. The torque rods in the selected satellite are produced by ZARM-Technik, and they are also used as control torque generators besides reaction wheels in Figure 2-9.

The performance parameters of ZARM-Technik torque rods are listed here:

Table 2-4 Performance Parameters of Magnetic Torque Rods (MTRs)

Performance Parameters	MTRs Values
Magnetic dipole moment (m^B)	$\pm 6 \text{ Am}^2$ (max.)
Supply current	95 mA
Supply voltage	$\pm 5.0 \text{ V}$
Power consumption (P)	$P = 0.5 \text{ W}$
Current (I)	$I = 95 \text{ mA}$
Number of turns (N)	$N = 2$
Dia (D) / Radius (R) / Length (L)	$D = 14.5 \text{ mm} / R = 7.25 \text{ mm} / L = 325 \text{ mm}$

Each magnetic rod (MTR0, MTR1, MTR2) is assigned to one of satellite body axes:

- ✓ MTR-0 is aligned with X-Axis (X_B) of satellite Body Frame
- ✓ MTR-1 is aligned with Y-Axis (Y_B) of satellite Body Frame
- ✓ MTR-2 is aligned with Z-Axis (Z_B) of satellite Body Frame

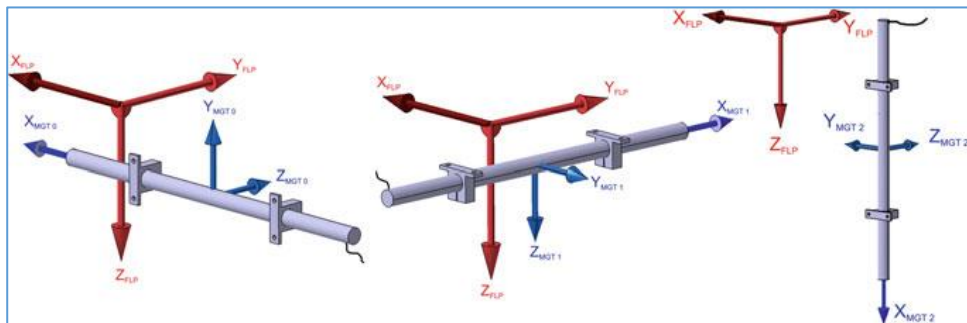


Figure 2-10 The Location of Magnetic Torque Rods [9, 17]

The current applied to magnetic rods creates a magnetic dipole moment (m^B) along the main axis of the unit (in a direction perpendicular to the plane of the rods), and results in a control torque in Earth magnetic flux. The product of dipole moment and Earth' magnetic field vector gives magnetic control torque value (M_C^{MTR}) given by the following equation [52]:

$$\vec{M}_C^{MTR} = m^B \times \vec{B}_{meas}^B \quad (2.90)$$

$$M_C^{MTR} = \Omega(m^B) B_{meas}^B = \Omega(-B_{meas}^B) m^B \quad (2.91)$$

$$M_C^{MTR} = \begin{bmatrix} 0 & B_{meas,z}^B & -B_{meas,y}^B \\ -B_{meas,z}^B & 0 & B_{meas,x}^B \\ B_{meas,y}^B & -B_{meas,x}^B & 0 \end{bmatrix} \begin{bmatrix} m_x^B \\ m_y^B \\ m_z^B \end{bmatrix} \quad (2.92)$$

- ✓ m^B is the magnetic dipole moment generated from torque rods,
- ✓ \vec{B}_{meas}^B is the measured Earth magnetic field vector in satellite Body Frame,
- ✓ M_C^{MTR} is the calculated magnetic control moment in satellite Body Frame.

The control torque only acts perpendicular to torque rods [74]:

$$M_C^{MTR} = \frac{m^B \times B_{meas}^B}{|B_{meas}^B|} \times B_{meas}^B = \frac{1}{|B_{meas}^B|} \Omega(m^B)^T \Omega(m^B)^T m^B \quad (2.93)$$

Magnetic dipole moment ($m^B = [m_x^B, m_y^B, m_z^B]^T$) is computed by the number of turns in wire coil (N), the current passing through the coils (I) and the coils cross area ($A = \pi r^2$):

$$m^B = N I A = \begin{bmatrix} N_x I_x A_x \\ N_y I_y A_y \\ N_z I_z A_z \end{bmatrix} \quad (2.94)$$

2.4.3. Disturbance Torques

Disturbance torques are space environmental torques, and never eliminated. Because of this reason, they must be controlled by satellite attitude controllers. The environmental disturbance torques derive from environmental conditions, varies with time in a sinusoidal manner throughout an orbit such as [11, 12, 13, 66]:

- ✓ Gravity Gradient Disturbance Torques (M_{GG}),
- ✓ Solar Radiation Disturbance Torques (M_{SR}),
- ✓ Aerodynamics Disturbance Torques (M_{AERO}),
- ✓ Magnetic Dipole Moment Disturbance Torques (M_{MAG}).

The most significant disturbance torques are magnetic field and gravity gradient torques around the altitude of the selected satellite. The total disturbance torque in satellite Body Frame is defined hereafter (M_{Ext}^B):

$$M_{Ext}^B = M_{GG}^B + M_{SR}^B + M_{AERO}^B + M_{MAG}^B \quad (2.95)$$

2.4.3.1. Gravity Gradient Disturbance Torque

The satellite is subject to gravitational torque because of the variations in Earth's gravitational force over the satellite body. If the satellite mass distribution is not uniform, the force arising from Earth gravity is also distributed unevenly on a satellite. General expressions for gravity gradient torque have been calculated for both spherical and non-spherical Earth models.

For most applications, spherical mass distribution of Earth is sufficient to calculate this torque value [12]:

$$M_{GG} = \frac{3\mu}{R^3} [R \times (I_S R)] \quad (2.96)$$

- ✓ M_{GG} is the gravity gradient torque,
- ✓ R is the distance between the Earth center and satellite geometric center,
- ✓ μ is the Earth gravitational constant,
- ✓ I_S is the satellite moment of inertia matrix.

The satellite geometric center and mass center are represented by different points in satellite Body Frame. Ignoring this difference, it is possible to calculate the gravity gradient torque only by using the distance between the Earth center and the geometric center of the selected satellite.

The torque magnitude is one of the largest torque sources. Therefore, it must be taken into account as an input torque value for the controller design. This torque can also be expressed in the dyadic form (R_3 represents the last column of the DCM matrix ($[C(q)]_O^B$) and $\Omega(R_3)$ is the skew-symmetric matrix) [14]:

$$M_{GG} = 3 w_0^2 (\vec{R}_3 \times I_S \vec{R}_3) = 3 w_0^2 \Omega(R_3) I_S R_3 \quad (2.97)$$

Finally, gravity gradient torque can be written as follows:

$$R_3 = \begin{bmatrix} C(q)_{13} \\ C(q)_{23} \\ C(q)_{33} \end{bmatrix} = \begin{bmatrix} 2(q_1 q_3 - q_2 q_4) \\ 2(q_2 q_3 + q_1 q_4) \\ 1 - 2(q_1^2 + q_2^2) \end{bmatrix}; \quad w_0 = \sqrt{\mu/R^3} \quad (2.98)$$

$$M_{GG}^B = 3w_0^2 \begin{bmatrix} 0 & -C(q)_{33} & C(q)_{23} \\ C(q)_{33} & 0 & -C(q)_{13} \\ -C(q)_{23} & C(q)_{13} & 0 \end{bmatrix} \begin{bmatrix} I_{S_x} & 0 & 0 \\ 0 & I_{S_y} & 0 \\ 0 & 0 & I_{S_z} \end{bmatrix} \begin{bmatrix} C(q)_{13} \\ C(q)_{23} \\ C(q)_{33} \end{bmatrix} \quad (2.99)$$

$$M_{GG}^B = 3w_0^2 \begin{bmatrix} (I_{S_z} - I_{S_y}) C(q)_{23} C(q)_{33} \\ (I_{S_x} - I_{S_z}) C(q)_{33} C(q)_{13} \\ (I_{S_y} - I_{S_x}) C(q)_{13} C(q)_{23} \end{bmatrix} \quad (2.100)$$

$$M_{GG}^B = 6w_0^2 \begin{bmatrix} (I_{S_z} - I_{S_y})(q_2 q_3 + q_1 q_4)(1 - 2(q_1^2 + q_2^2)) \\ (I_{S_x} - I_{S_z})(q_1 q_3 - q_2 q_4)(1 - 2(q_1^2 + q_2^2)) \\ 2(I_{S_y} - I_{S_x})(q_1 q_3 - q_2 q_4)(q_2 q_3 + q_1 q_4) \end{bmatrix} \quad (2.101)$$

The last equation can be reduced using small angle approximations (θ is assumed that the maximum deviation from its rotation axis):

$$M_{GG}^B = \frac{3}{2} w_0^2 |I_{S_z} - I_{S_y}| \sin(2\theta) = 3 w_0^2 |I_{S_z} - I_{S_y}| \sin(\theta) \cos(\theta) \quad (2.102)$$

The model is carried out by using long-term equations, and the other approaches can be performed as part of the future works. Generally, the effect level of this disturbance torque on the selected satellite is in the order of 10^{-5} Nm.

2.4.3.2. Solar Radiation Disturbance Torque

Solar radiation (incident radiation) on a satellite's surface generates disturbance torque around the center of satellite mass and this torque value is independent of satellite position and velocity. The applied torque on satellite is always perpendicular to the line of sun light affected by the following factors [11, 12]:

- ✓ The intensity of Sun incident radiation,
- ✓ The geometry of satellite surface,
- ✓ The optical properties of satellite surface,
- ✓ The Sun vector orientation with respect to satellite.

Direct solar radiation is one of the dominated disturbance sources above ~ 1000 km as disturbance torque. The torque produced by the solar wind is generally negligible, and therefore it is not a part of the torque calculations in this study.

In general situations, a satellite configuration can be approximated as a collection of geometrical shapes such as nearly spherical or rectangular. In this thesis, it can be assumed that the satellite is a rectangular shape with dimensions of 60 x 70 x 80 cm. It is commonly supposed that solar radiation pressure can be calculated as if the satellite absorbs all photons without considering its orientation with respect to the Sun. In that case, incident angles can be ignored in these calculations:

$$\vec{M}_{SR} = \vec{F}_{SR} \times \Delta \vec{R}; \Delta \vec{R} = \Delta X \vec{i} + \Delta Y \vec{j} + \Delta Z \vec{k} \quad (2.103)$$

$$\vec{M}_{SR}^B = C_r \frac{k I_{SR} A_s}{c} \left(\frac{A_u}{R} \right)^2 \left(\frac{\vec{R}}{R} \right) \quad (2.104)$$

- ✓ $\Delta \vec{R}$ is the distance vector between the center of solar radiation pressure and the center of satellite mass for each axis,
- ✓ \vec{F}_{SR} is the solar radiation pressure force,
- ✓ C_r is the radiation pressure coefficient ($C_r \cong 1.0$),
- ✓ k is the illumination (reflectance) factor:
 - In Eclipse Phase $\rightarrow k = 0$,
 - In Illuminated Phase $\rightarrow 0 < k < 1$,
- ✓ I_{SR} is the mean solar flux or solar constant ($I_s \cong 1358 \text{ W/m}^2$),
- ✓ A_s is the effective surface area normal to Sun vector ($A_s = [A_x, A_y, A_z]^T$),
- ✓ A_u is the astronomical unit ($A_u \cong 1.49597870 \times 10^{11} \text{ m}$),
- ✓ c is the speed of light ($c \cong 300000 \text{ m/s}$),
- ✓ R_{sat} is the geocentric distance of satellite ($R_{sat} \cong 6378 + 700 \text{ km}$),
- ✓ R_{sun} is the geocentric distance of the Sun,
 $(R_{sun} = 149.597.870.700 \text{ m} \cong 149.600.000 \text{ km})$ [23],
- ✓ \vec{R} is the Sun position vector relative to satellite ($\vec{R} = \vec{R}_{sat} - \vec{R}_{sun}$),
- ✓ R is the distance from Sun to satellite ($R = \|R_{sat} - R_{sun}\| \text{ m}$).

For the selected satellite;

- ✓ +X plane is a rectangle with the dimensions of $A_X = (60 \times 80) \text{ cm}^2$,
- ✓ +Y plane is a rectangle with the dimensions of $A_Y = (70 \times 80) \text{ cm}^2$,
- ✓ +Z plane is a rectangle with the dimensions of $A_Z = (60 \times 70) \text{ cm}^2$.

The solar disturbance torque equation can be rearranged taking into account all the surface areas like in the following [16]:

$$\vec{M}_{SR,X}^B = C_r \frac{k I_{SR} A_X}{c} \left(\frac{A_U}{R} \right)^2 \left(\frac{\vec{R}_X}{R} \right) \quad (2.105)$$

$$\vec{M}_{SR,Y}^B = C_r \frac{k I_{SR} A_Y}{c} \left(\frac{A_U}{R} \right)^2 \left(\frac{\vec{R}_Y}{R} \right) \quad (2.106)$$

$$\vec{M}_{SR,Z}^B = C_r \frac{k I_{SR} A_Z}{c} \left(\frac{A_U}{R} \right)^2 \left(\frac{\vec{R}_Z}{R} \right) \quad (2.107)$$

The sun position vector with respect to a satellite is provided by the Sun position model designed as a space environment model and explained in the following chapter. The worst condition is that all the surfaces placed on the three different satellite axes are directly exposed to Sun radiation. In that case, total solar radiation disturbance torque can be expressed as shown below:

$$\vec{M}_{SR}^B = \vec{M}_{SR,X}^B + \vec{M}_{SR,Y}^B + \vec{M}_{SR,Z}^B \quad (2.108)$$

For enhancing the calculations using geometrical details, it can be assumed that the center of solar radiation pressure for each satellite surface is the center of the related surface area [22]. It means that the distance from the satellite mass center is 40 cm for +Z plane ($\Delta Z = 0.40 \text{ m}$), 35 cm for +X plane ($\Delta X = 0.35 \text{ m}$) and 30 cm for +Y

plane ($\Delta Y = 0.30 \text{ m}$). These distances are precisely proportional to the half of satellite dimensions (i is the Sun incidence angle):

$$M_{SR} = \frac{I_s}{c} A_s (1 + k) \cos(i) \quad (2.109)$$

The most challenging part is to find out Sun incidence angle (φ, γ), and Ephemeris model can be used to express it for rectangular shaped satellite:

$$\varphi = \arctan(R_Y/R_X) \text{ and } \gamma = \arcsin(R_Z) \quad (2.110)$$

$$M_{SR,X}^B = \frac{I_s}{c} A_X (1 + k) \cos(\varphi) \Delta X \quad (2.111)$$

$$M_{SR,Y}^B = \frac{I_s}{c} A_Y (1 + k) \sin(\varphi) \Delta Y \quad (2.112)$$

$$M_{SR,Z}^B = \frac{I_s}{c} A_Z (1 + k) \sin(\gamma) \Delta Z \quad (2.113)$$

The first approach is accepted to make these calculations more manageable, and the second method can be applied as part of future works in order to compare the differences between the two models. Generally speaking, the magnitude of this disturbance torque is the level of 10^{-6} Nm .

2.4.3.3. Aerodynamics Disturbance Torque

The interaction of upper atmosphere with the satellite surface results in the disturbance torques around the satellite mass center. This torque is one of the least dominant disturbance torques for Earth-orbiting satellites. Atmospheric drag may be an important disturbance effect when the satellite altitude descends into Earth's atmosphere [19]. The aerodynamic torque equation can be formulated, such as the following equations [11, 12]:

$$\vec{M}_{AERO} = \vec{F}_{AERO} \times \Delta \vec{R}; \quad \Delta \vec{R} = \Delta X \vec{i} + \Delta Y \vec{j} + \Delta Z \vec{k} \quad (2.114)$$

$$\vec{F}_{AERO}^B = \frac{1}{2} A_s \rho C_D \vec{V}^2 \quad (2.115)$$

- ✓ \vec{F}_{AERO}^B is the aerodynamic drag vector in satellite Body Frame,
- ✓ A_s is the effective surface area ($A_s = [A_X \ A_Y \ A_Z]^T = [0.48; \ 0.56; \ 0.42]^T$),
- ✓ ρ is the atmospheric density at low solar activity ($\rho = 3.58 \times 10^{-15} \text{ kg/m}^3$),
- ✓ C_D is the aerodynamic drag coefficient ($1 < C_D < 2$),
- ✓ V is the satellite velocity vector ($V = V_0 - w_e \cdot r$).

The second term of the velocity equation which includes Earth rotational velocity can be negligible, and orbital velocity is equal to the satellite velocity ($V = V_0$).

The aerodynamic disturbance torque equation can be rearranged considering all the diagonal distances of these surface areas like in the following ($\Delta X = 0.35 \text{ m}$, $\Delta Y = 0.30 \text{ m}$, $\Delta Z = 0.40 \text{ m}$):

$$\vec{M}_{AERO,X}^B = \frac{1}{2} (A_X \rho C_D \vec{V}^2) \Delta X \quad (2.116)$$

$$\vec{M}_{AERO,Y}^B = \frac{1}{2} (A_Y \rho C_D \vec{V}^2) \Delta Y \quad (2.117)$$

$$\vec{M}_{AERO,Z}^B = \frac{1}{2} (A_Z \rho C_D \vec{V}^2) \Delta Z \quad (2.118)$$

The total aerodynamic disturbance torque can be expressed as shown below:

$$\vec{M}_{AERO}^B = \vec{M}_{AERO,X}^B + \vec{M}_{AERO,Y}^B + \vec{M}_{AERO,Z}^B \quad (2.119)$$

Generally, the magnitude of this disturbance torque level is about 10^{-7} Nm depending on the altitude of selected satellite ($\sim 700 \text{ km}$).

2.4.3.4. Magnetic Dipole Moment Disturbance Torque

The interaction between the residual magnetic field of a satellite with Earth magnetic field can result in magnetic field disturbance torque. There are several diverse electronic components being used in a satellite and they are different from each other in the sense of electronic characteristics [71]. Satellites are generally designed of selective materials to decrease the negative effect of this disturbance torque. The magnetic torque equation can be written like as:

$$\vec{M}_{MAG}^B = m \times \vec{B}^B = \Omega(-B^B) m = -\Omega(B^B) m \quad (2.120)$$

- ✓ m is the satellite residual magnetic dipole ($m = 1 \text{ Amp m}^2$),
- ✓ \vec{B}^B is the local magnetic field vector in satellite Body Frame:
 - $\vec{B}^B = 2.M/\vec{R}^3$ for points above the poles,
 - $\vec{B}^B = M/\vec{R}^3$ for points above the equator,
- ✓ M_{MAG} is the Earth magnetic moment ($M_{MAG} = 7.96 \times 10^{15} \text{ Tesla m}^3$),
- ✓ R is the orbit radius ($R = R_E + h = 6378 + 700 \text{ km}$).

For creating the worst case, the equation for points above the poles can be handled. The Earth magnetic field vector is provided by Earth Magnetic Field model described in the following chapter. The total magnetic disturbance torque is calculated by the following equation:

$$\vec{M}_{MAG}^B = \vec{M}_{MAG,X}^B + \vec{M}_{MAG,Y}^B + \vec{M}_{MAG,Z}^B \quad (2.121)$$

In general, the magnitude of this disturbance torque is about the order of 10^{-5} Nm and cannot be ignored in terms of simulations. In conclusion, the most efficient disturbance torques is gravity gradient and magnetic field disturbance torques for the satellite altitude around 700 km.

The total disturbance torque is the level of 10^{-5} Nm.

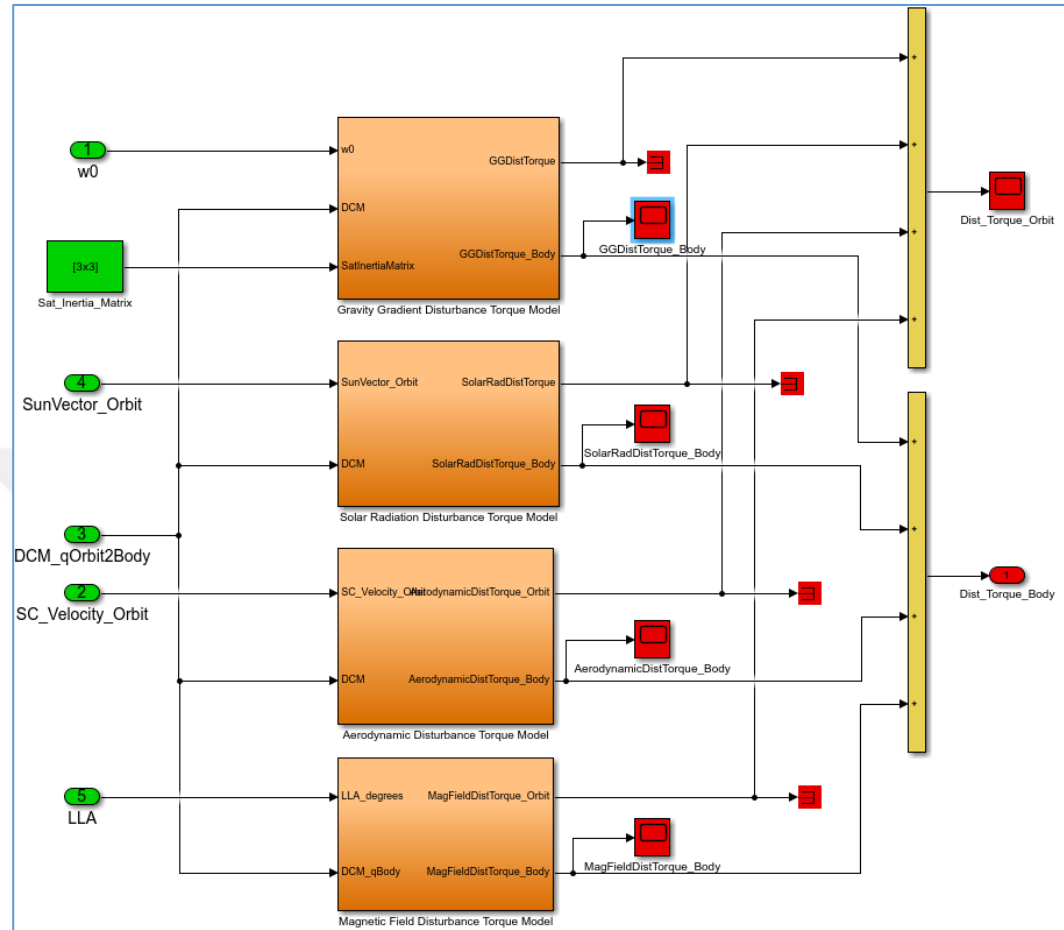


Figure 2-11 Distribution Torque Model Blocks

2.5. Satellite Sensor Measurements

The attitude control requirements are based on three-axis stabilized satellite system with high pointing accuracy capabilities provided by fine pointing sensors such as star trackers and gyroscopes (or in a different form like as IMU sensors).

The sensor characteristics of the selected satellite are listed in the following table:

Table 2-5 The Characteristics of Satellite Sensors [9, 17]

	MGM	STR	GPS	SS	FOG
Output	Magnetic Field Vector	Quaternion Vector	Position Velocity	Sun Position	Angular Rate
Dimension	(3×1)	(4×1)	(3×1)	(3×1)	(3×1)
Quantity	2 MGM	2 STR	3 GPS	8 SS	4 FOG
Accuracy	5 nT	5 arc sec	10 m 0.1 m/s	50 mA	2×10^{-6} deg/s
Control Rate	1.5, 3, 6 Hz	5 Hz	1 Hz	10 Hz	10 Hz

These sensors are modelled to provide the measured values which are necessary to calculate the error inputs sent to attitude controller design.

2.5.1. Sun Sensor Measurements

Sun sensors determine satellite attitude enabling the coarse Sun direction vector. Two different types of sun sensors, analog and digital sun sensors, are employed to provide Sun position vector to orient solar panels toward the Sun. Analog sun sensors can provide sufficient accuracy for many specific tasks. These types of sensors are based on silicon solar cells, and its output current is proportional to the cosine function of incident angle [12].

At least two analog and single sun sensors are necessary to measure sun incident angle in a defined plane. By orienting two sensors perpendicular to each other, the direction of Sun can be fully determined [66]. The sensors located in the selected satellite consist of GaAs solar cells manufactured by Azur Space and depicted below. The solar cells included in sun sensors generate voltages (about 2.5V) in the illuminated phase:

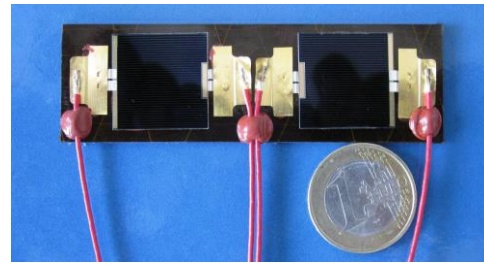


Figure 2-12 Sun Sensors [9]

Eight piece of sun sensors are located in satellite and used to obtain the complete 4π FOV instead of 2π FOV maximizing the exposed Sun light time [59]. Four number of sun sensors (SuS0, SuS1, SuS2 and SuS3) are mounted at the edges of the satellite structure. Two of sun sensors (SuS4 and SuS5) are mounted on each solar panel, and the remaining two sensors (SuS6 and SuS7) are located in the solar panel directions.

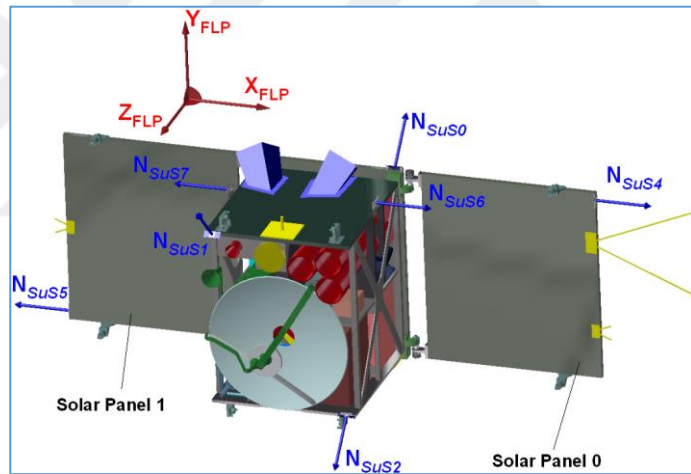


Figure 2-13 Location of Sun Sensor Units [9, 17]

2.5.2. Magnetometer Measurements

Magnetometers measure local magnetic field direction and magnitude vector which is a combination of both Earth magnetic field and any magnetic field generated by different sources. In a typical case, these measurements are used to estimate the torque applied by magnetic torque rods in all three satellite axes. The satellite is

equipped with two orthogonally arranged magnetometers (anisotropic magneto-resistive sensors) manufactured by ZARM-Technik with the measurement range of $\pm 200\mu\text{Tesla}$:



Figure 2-14 Magnetometer Located in The Selected Satellite [9,17]

The magnetometers are generally located on the satellite payload module, not very close to magnetic torque rods. Because of the generated magnetic field, magnetic torque rods can cause the saturation of measurements. The orientation of both sensors with respect to the satellite coordinates is depicted below:

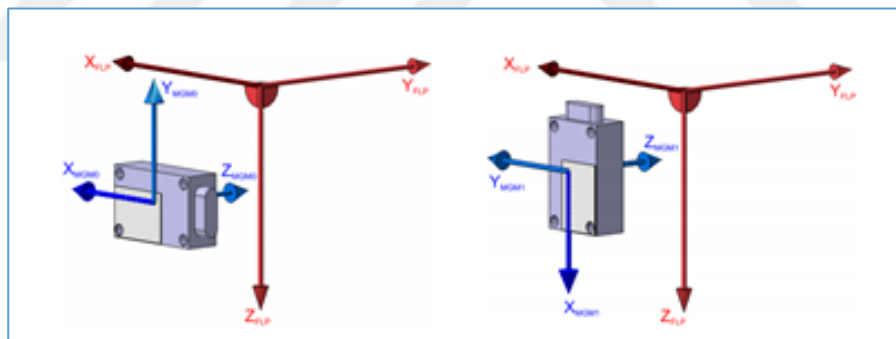


Figure 2-15 The Orientation of Magnetometers [9, 17]

2.5.3. Star Tracker Measurements

Star trackers identify the viewed star pattern and measure the satellite orientation relative to Earth inertial reference frame in an accurate manner [66]. Star trackers with sufficient operational field of view use the star light intensity and reduce the number of attitude sensors required for fine attitude knowledge providing quaternion

vectors [43, 44, 59]. The star tracker model is the micro-Advances Stellar Compass (μ ASC) consisting of a processing unit, camera head units and baffles shown in the following figures [42]:

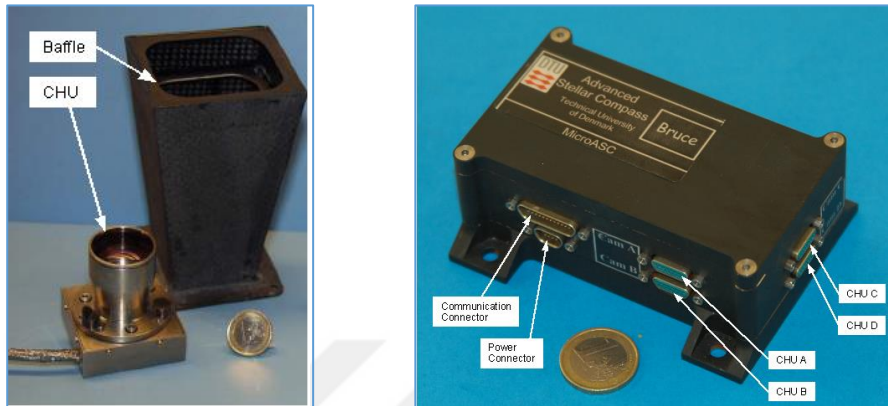


Figure 2-16 Star Tracker System Baffle and Camera Head Unit [9, 17]

During the operational phase, the processing unit creates a digital image every 0.5 seconds and this image is adjusted for bright objects. Star light sensitivity, star detection threshold, the number of stars in the sensor field of view and the sky coverage are fundamental elements to define a star tracker performance. The camera head units are located on the satellite body so that simultaneous blinding or occultation effect arising from the space objects (Earth, Moon, Sun and the other satellites, etc.) is avoided. The location of each sensor is shown in Figure 2-17.

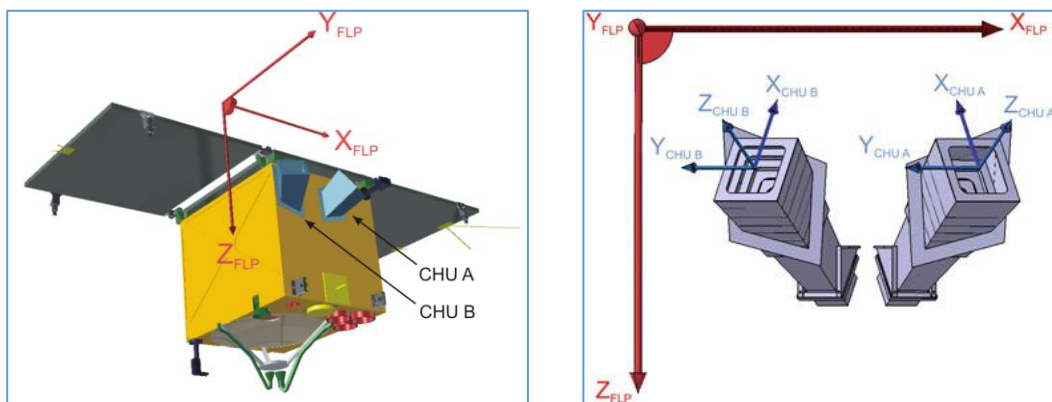


Figure 2-17 The Location of Star Trackers [9, 17]

2.5.4. Fiber Optic Gyroscope Measurements

There are two types of optical gyroscopes (ring laser, fiber optic gyroscopes) using interferometer or interferometric method properties of electromagnetic radiation to sense the rotation and angular motion of satellite [35]. In this satellite, fiber optic gyroscope is a type of Commercial Fiber Optic Rate Sensor (LITEF C-FORS):



Figure 2-18 Fiber Optic Gyroscopes [9, 17]

In general, gyroscopes are not located in the neighbourhood of magnetometers. Four gyroscopes are assembled in a tetrahedron configuration to avoid single sensor failures. The measurement axis of each gyroscope is also aligned to the rotation axis of the related reaction wheels and each sensor measurements are obtained around its Z-axis as shown below [17, 36]:

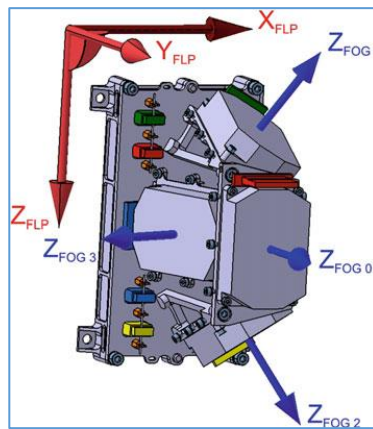


Figure 2-19 The Location of Fiber Optic Gyroscopes [9, 17]

The angular velocity data is estimated as long as at least three of gyroscopes have valid data. Based on this situation, there are three different sensor combinations such as $\{\vec{Z}_{FOG0}, \vec{Z}_{FOG1}, \vec{Z}_{FOG2}\}$, $\{\vec{Z}_{FOG0}, \vec{Z}_{FOG2}, \vec{Z}_{FOG3}\}$ and $\{\vec{Z}_{FOG1}, \vec{Z}_{FOG2}, \vec{Z}_{FOG3}\}$. The sensor measurement noise sources such as fixed bias (g-independent bias), g-dependent bias, scale factor error, misalignment error, angular random walk, rate random walk and rate ramp error are taken into consideration in a gyroscope model [33, 60]. The performance parameters and error specifications are specified below:

Table 2-6 Performance Parameters of Fiber Optic Gyroscopes

Performance Parameters	Fiber Optic Gyroscopes
Rate Bias	1575.42 Hz ($\leq 2^\circ/\text{h} (1\sigma)$)
Angular Random Walk	17 dB ($\leq 0.15^\circ/\sqrt{\text{h}}$)
Scale Factor Error	$\leq 1000 \text{ ppm} (1\sigma), \leq 0.2^\circ \% (1\sigma)$
Misalignment Error	$\pm 5 \text{ mrad (max)}$
Measurement range	$\pm 1000^\circ/\text{s}$

2.5.5. GPS Sensor Measurements

Satellite navigation information such as position, velocity and time are provided by GPS receivers for the development of orbit determination system. After measuring the distance of at least four GPS satellites, satellite position and time can be computed, and then GPS receivers can determine velocity and track information [37, 38].

Phoenix GPS receivers comprise of three independent receiver parts, each part is connected to separate antennas and two cascaded low noise amplifiers, which reduce the required antenna gain [40]:

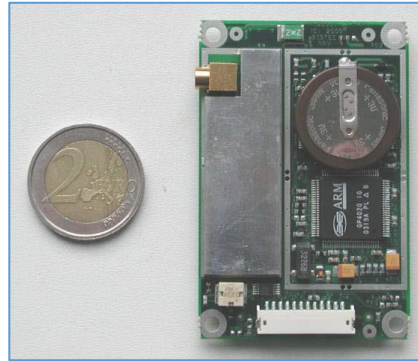


Figure 2-20 Phoenix (MG5001) GPS Receiver Board [39]

GPS antennas are located on the middle solar panel of satellite, and its direction is opposite to the payload module. This specification also provides the optimum reception of signals from GPS satellites.

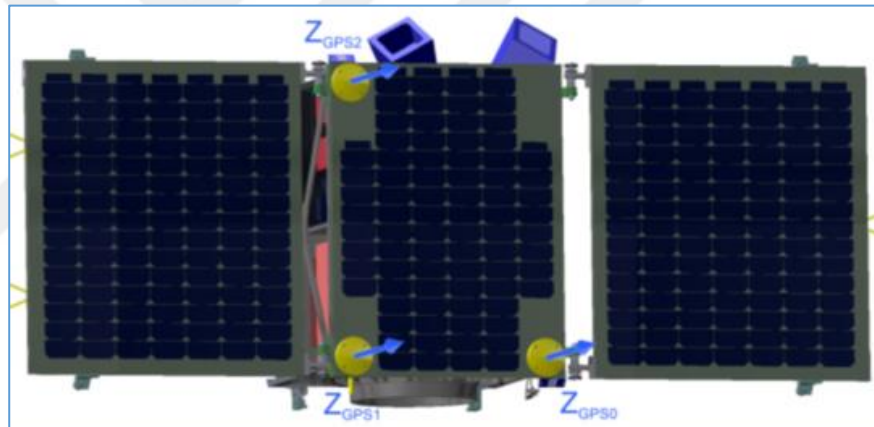


Figure 2-21 The Location of GPS Antenna [9, 17]

2.6. Summary

This chapter clarifies the coordinate frame transformations representing with Euler angles and quaternion vectors as attitude parameterization. The most important attitude representations such as inertia matrix, angular velocity and angular momentum are also located in this chapter. The internal and external torque sources applied on the selected satellite are classified and expressed with details. Satellite dynamic and kinematic equations are clarified using all these information.

Besides, sun sensors, magnetometers, GPS receivers, fiber optic gyroscopes and star trackers are defined as satellite attitude sensors. On the other hand, reaction wheels and magnetic torque rods are specified as satellite actuators.



CHAPTER 3

SPACE ENVIRONMENT MODEL

3.1. Introduction

Modelling of space environment is an essential part of attitude determination in order to develop and verify various attitude control algorithms in a correct manner.

The outputs from space environment model including Earth Magnetic Field Model and Sun Position Model together with satellite dynamic-kinematic model are used as inputs for attitude sensors. The torque outputs of actuators are also used for satellite attitude determination and control systems.

3.2. Julian Date Model

Due to precession and nutation of Earth spin axis, ECI Frames have to be specified at some epoch time. The commonly used ECI Frames is J2000 Frame. This frame uses the mean equator and equinox of Universal Time Coordinated (UTC) January 1, 2000 [16, 49].

$$\begin{aligned} JD = & 367(year) - \text{floor} \left[\frac{7}{4} \left(year + \text{floor} \left(\frac{month + 9}{12} \right) \right) \right] \\ & + \text{floor} \left[275 \left(\frac{month}{9} \right) \right] + day + 1721013.5 \\ & + \frac{1}{24} \left(\frac{1}{60} \left(\frac{second}{60} + minute \right) + hour \right) \end{aligned} \quad (3.1)$$

The Julian Date (JD) can be converted to Modified Julian Date (MJD) using the following equations [3, 4]:

$$JD_{2000} = JD - 2451545 \quad (3.2)$$

$$MJD = JD - 2400000.5 \quad (3.3)$$

3.3. Orbit Propagation Model

3.3.1. Kepler Parameters

The satellite orbits are specified using Kepler parameters which indicate the orientation of an orbital ellipse and satellite position in this ellipse. These parameters are visualized with the following figures [10, 11, 13]:

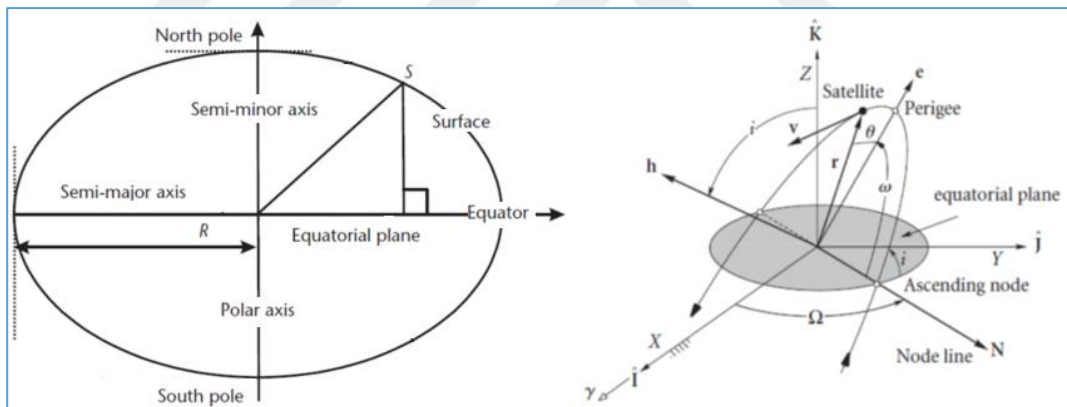


Figure 3-1 Kepler Orbital Parameters [19]

Kepler parameters are listed as follows:

- ✓ i = Inclination,
- ✓ Ω = Right Ascension of Ascending Node,
- ✓ ω = Argument of Perigee,
- ✓ e = Eccentricity,

- ✓ a = Semi-major Axis,
- ✓ M = Mean Anomaly,
- ✓ n = Mean Motion ($n = \sqrt{\mu_E/a^3}$).

The first four elements (i , Ω , ω , e) determine the orbital plane orientation in space. On the other hand, mean motion (n) and mean anomaly (M) define the satellite position in its orbit. The basic properties of Keplerian orbits for circular and elliptical orbits are listed below:

Table 3-1 The Properties of Keplerian Orbits (Circular and Elliptic Orbits)

Orbits	Eccentricity	The Radius	Energy
Circular Orbits	$e = 0$	$r = p = \frac{h^2}{\mu} = \frac{[r \cdot v \cdot \cos(\beta)]^2}{\mu}$	$E = -\frac{\mu^2}{2h^2} < 0$
Elliptic Orbits	$0 < e < 1$	$r_a = p/(1+e)$ $r_b = p/(1-e)$	$E = -\frac{\mu}{2a} < 0$

The angle between orbital plane and equatorial plane is called inclination. By convention, orbit period (T) is a number between the amount of time to complete one revolution around Earth.

Mean motion is the mean angular velocity and mean anomaly gives the direction of satellite motion at perigee and apogee points. There is a close relationship between mean anomaly (M), eccentric anomaly (E) and true anomaly (v):

$$\cos(v) = \frac{\cos(E) - e}{1 - e \cos(E)} ; \sin(v) = \frac{\sqrt{1 - e^2} \sin(E)}{1 - e \cos(E)} \quad (3.4)$$

$$\tan\left(\frac{v}{2}\right) = \sqrt{\frac{1+e}{1-e}} \tan\left(\frac{E}{2}\right) \quad (3.5)$$

The relationship between mean and eccentric anomaly can be denoted by:

$$E(t) = M(t) + e \sin(E(t)) \quad (3.6)$$

The changes of mean anomaly are defined with an iteration equation:

$$M(t_0 + t) = M(t_0) + nt \rightarrow M_{i+1} = M_i + nt \quad (3.7)$$

In order to calculate the mean anomaly changing with time $M(t)$, time equation is expressed in a discrete form and then propagated for each discrete point:

$$E_{i+1} = M_i + e \sin(E_i) \quad (3.8)$$

$$E_{i+1} = E_i + \frac{M_i + e \sin(E_i) - E_i}{1 - e \cos(E_i)} \quad (3.9)$$

3.3.2. Two Lines of Elements Data (TLE)

TLE data is a set of two lines including orbital elements which describe an Earth-orbiting satellite position (r) and velocity (v). In this study, the NORAD TLE data of FLP microsatellite is modified and taken as an input argument for the calculations of orbit propagator model.

The orbit information becomes available in the time frame of days after launch. NORAD supplies the satellite tracking information in the form of TLE data set and this data can be used as an input for orbit propagator model. There are two lines in TLE Data Set shown in the following table:

Table 3-2 TLE Data Set For Orbital Parameters [20]

Line	TLE Data Set (FLP)
1	42831U 17042G 19164.90037843 +.00000129 +00000-0 +18434-4 0 9993
2	42831 097.5659 058.0490 0015745 077.4852 282.8127 14.91002723104220

This table includes the orbital parameters obtained from the second line of TLE data:

Table 3-3 Orbital Parameters Obtained From TLE Data

Orbital Parameters	Abb.	Value	Value
Inclination	i	097.5659 (deg)	1.7028462 rad
Right Ascension of Ascending Node	Ω	612.9 (deg)	10.697123 rad
Eccentricity	e	0.015745	--
Argument of Perigee	ω	077.4852 (deg)	1.3523718 rad
Mean Anomaly	M	282.8127 (deg)	4.936013 rad
Mean Motion	n	14.910027 (rev/day)	0.00108 rad/s

The following table shows the useful orbital parameters obtained from TLE data:

Table 3-4 The Useful Orbital Parameters of Satellite

Orbital Parameters	Abb.	Value	Dimension
Perigee	r_p	591.0	km
Apogee	r_a	612.9	km
Period	T	96.6	minutes
Semi Major Axis	a	6991.4	km

The satellite semi-major axis is found by using the mean motion definition (n) [50]:

$$n \frac{2\pi}{86400} = n \left[\frac{\text{rad}}{\text{s}} \right] \rightarrow 14.910027 \frac{2\pi}{86400} \cong 0.00108 \frac{\text{rad}}{\text{s}} \quad (3.10)$$

$$n = \sqrt{\frac{\mu}{a^3}} \rightarrow a = \frac{\mu^{\frac{1}{3}}}{n^{\frac{2}{3}}} = \frac{(3.986004418 \times 10^{14})^{\frac{1}{3}}}{(0.00108)^{\frac{2}{3}}} \cong 6991.4 \text{ km} \quad (3.11)$$

The magnitude of the moving satellite position (r) is represented with Kepler parameters such as semi-latus rectum (p) and true anomaly (v):

$$r = \frac{p}{1 + e \cos(v)} = \frac{a(1 - e^2)}{1 + e \cos(v)} \quad (3.12)$$

The transformations from Keplerian parameters to Cartesian position (R^O) and velocity vector (V^O) in orbital plane are specified hereafter:

$$R^O = \begin{bmatrix} R_x^{ORBIT} \\ R_y^{ORBIT} \\ R_z^{ORBIT} \end{bmatrix} = \begin{bmatrix} r \cos(v) \\ r \sin(v) \\ 0 \end{bmatrix} = a \begin{bmatrix} \cos(E) - e \\ \sqrt{1 - e^2} \sin(E) \\ 0 \end{bmatrix} \quad (3.13)$$

$$V^O = \begin{bmatrix} V_x^{ORBIT} \\ V_y^{ORBIT} \\ V_z^{ORBIT} \end{bmatrix} = \begin{bmatrix} -\sqrt{\mu/p} \sin(v) \\ \sqrt{\mu/p} (e + \cos(v)) \\ 0 \end{bmatrix} = \frac{a^2 n}{r} \begin{bmatrix} -\sin(E) \\ \sqrt{1 - e^2} \cos(E) \\ 0 \end{bmatrix} \quad (3.14)$$

The position and velocity vectors are also defined in ECI Frame (R^{ECI} , V^{ECI}) [49]:

$$R^{ECI} = [R][R^O]; V^{ECI} = [R][V^O] \quad (3.15)$$

$$[R] = \begin{bmatrix} c\Omega c\omega - s\Omega s\omega ci & -c\Omega s\omega - s\Omega c\omega ci & s\Omega si \\ s\Omega c\omega + c\Omega s\omega ci & -s\Omega s\omega + c\Omega c\omega ci & -c\Omega si \\ s\omega si & c\omega si & ci \end{bmatrix} \quad (3.16)$$

These definitions can be defined with the following alternative equations:

$$[R^{ECI}] = ([C_Z(\Omega)]^T [C_X(i)]^T [C_Z(\omega)]^T) [R^O] \quad (3.17)$$

$$[V^{ECI}] = ([C_Z(-\Omega)] . [C_X(-i)] . [C_Z(-\omega)]) [V^O] \quad (3.18)$$

The position and velocity vectors can be defined in ECEF Frame (R^{ECEF} , V^{ECEF}) with the following matrix multiplications ($w_{IE} = 7.292115 \times 10^{-5}$ rad/s):

$$[R^{ECEF}] = ([C_Z(-\Omega + w_{IE})] [C_X(-i)] [C_Z(-\omega)]) [R^O] \quad (3.19)$$

$$[V^{ECEF}] = ([C_Z(-\Omega + w_{IE})] [C_X(-i)] [C_Z(-\omega)]) [V^O] \quad (3.20)$$

3.3.3. Orbit Perturbations

Orbit perturbations result in small deviations of the satellite orbital motion. There are various perturbing sources applied on satellite in space as listed below:

- ✓ Earth gravity harmonics,
- ✓ Earth tides effect,
- ✓ Sun and Moon gravitational effect,
- ✓ Solar radiation pressure,
- ✓ Atmospheric drag.

Atmospheric drag and solar radiation pressure effects are disturbance torque sources. In terms of the other perturbations, the adverse effects caused by Earth gravity harmonics are only taken into consideration.

3.3.4. Earth Gravitational Perturbations

Earth gravity harmonics represent the mathematical expansion of the deviations from a perfect sphere shape. In ordinary situations, the second terms of zonal ($J_2 = 0.00108263$) and tesseral gravity harmonics (J_{22}) are encountered in computations [49]. The J_2 term (flattening factor) is related to Earth equatorial oblateness, which is the eccentricity depending on the difference between polar and equatorial radius. This effect can be represented by the rate of argument of perigee ($\dot{\omega}$), right ascension of the ascending node ($\dot{\Omega}$), and the correction of orbit mean motion (\bar{n}):

$$\dot{\Omega} = -\frac{3}{2} \frac{J_2 R_E^2}{p^2} \bar{n} \cos(i) \quad (3.21)$$

$$\dot{\omega} = \frac{3}{2} \frac{J_2 R_E^2}{a_0^2 (1 - e^2)^2} \bar{n} \left(2 - \frac{5}{2} \sin^2(i) \right) \quad (3.22)$$

$$\bar{n} = \sqrt{\frac{\mu}{a_0^3}} \left(1 + \frac{3}{2} \frac{J_2 R_E^2}{p^2} \left(1 - \frac{3}{2} \sin^2(i) \right) \sqrt[2]{1 - e^2} \right) \quad (3.23)$$

The J_{22} term is related to the ellipticity of Earth equatorial plane, and its effects appear on geosynchronous orbits. Because of this reason, it is not evaluated as a part of the perturbation computations. The position and velocity vectors can be defined with integrating these perturbation terms in ECEF Frame:

$$[R^{ECEF}] = [C_Z(-(\Omega + \dot{\Omega}t) + w_{IE})] [C_X(-i)] [C_Z(-(\omega + \dot{\omega}t))] [R^0] \quad (3.24)$$

$$[V^{ECEF}] = [C_Z(-(\Omega + \dot{\Omega}t) + w_{IE})] [C_X(-i)] [C_Z(-(\omega + \dot{\omega}t))] [V^0] \quad (3.25)$$

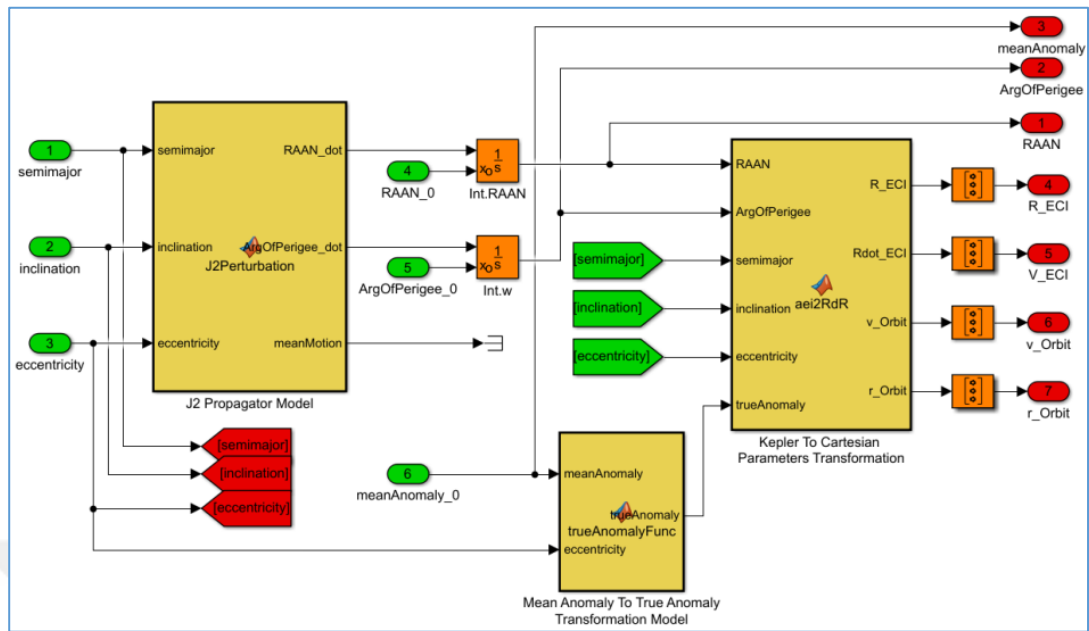


Figure 3-2 Orbit Propagator and Perturbation Model

The orbit propagator model placed in the previous figure is:

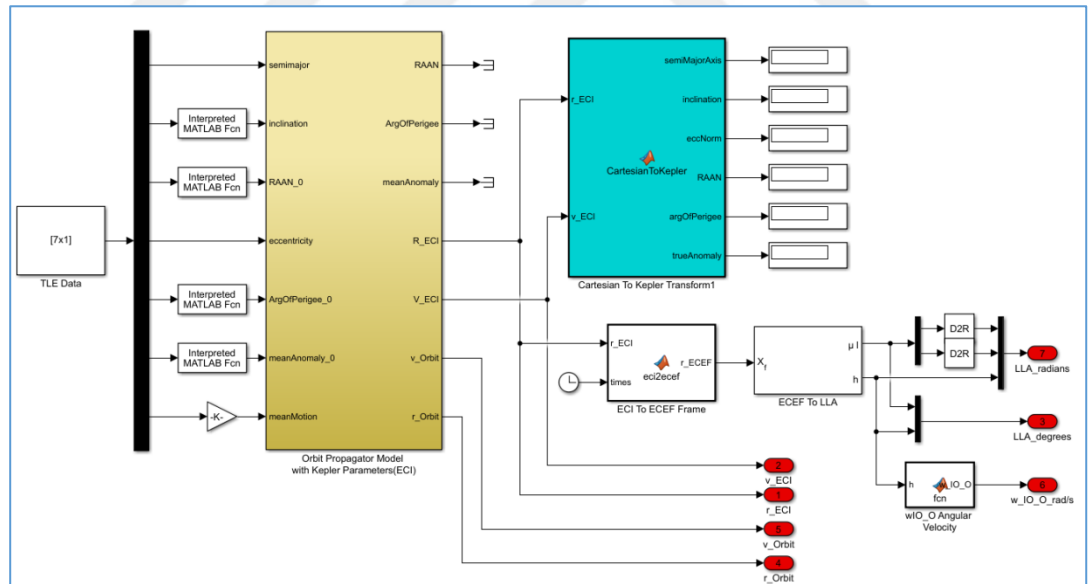


Figure 3-3 Orbit Propagator Model

3.4. Earth Magnetic Field Model

External references such as the Sun, other specific stars and Earth magnetic field direction can be used to determine the orientation and attitude of a satellite.

The magnetic field model uses an International Geomagnetic Reference Field (IGRF2015) standard model comprising a set of spherical harmonic coefficients and is updated by the International Association of Geomagnetism and Aeronomy every five years. This model as a truncated series expansion of a geomagnetic function (V) is defined taking the first 10 harmonics [53, 54, 58, 62]:

$$V = a \sum_{n=1}^N \sum_{m=0}^n \left(\frac{a}{r}\right)^{n+1} (g_n^m \cos(m\lambda) + h_n^m \sin(m\lambda)) P_n^m \cos(\theta) \quad (3.26)$$

- ✓ a is the mean radius of Earth,
- ✓ r is the distance from Earth centre,
- ✓ λ is the longitude angle from Greenwich to eastward,
- ✓ θ is the colatitude angle defined as 90° minus the latitude,
- ✓ g_n^m and h_n^m are spherical harmonic coefficients of degree n and order m ,
- ✓ N is the maximal spherical harmonical degree of the series expansion,
- ✓ $P_n^m \cos(\theta)$ is the Schmidt quasi-normalised associated Legendre functions of degree n and order m ($n \geq 1$ and $m \leq n$).

Although the strength of magnetic field is relatively stable over time, some alterations in the ionosphere region deflect the surface magnetic fields of Earth. In most cases, this field can be considered constant and not changes with time.

In this study, 12th generation IGRF model (IGRF-12) is implemented to the system model for satellite location defined with latitude, longitude and altitude values [1, 2].

An orbit propagator model supplies the satellite latitude, longitude and altitude information to IGRF model. The magnitude of this field is about 10^{-5} Tesla.

3.5. Sun Position Model

Determining the relative position of the Sun from the Earth involves a series of calculations at any time of year, assuming that the Sun is in an ecliptic orbit around the Earth [56]. The angles describing the solar position vector are shown in the following figure [57]:

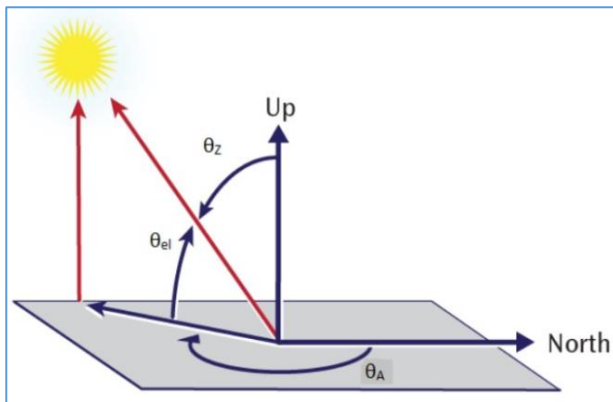


Figure 3-4 Sun Position Vector Illustration [57]

- ✓ θ_Z is the solar zenith angle,
- ✓ θ_A is the solar azimuth angle,
- ✓ θ_{EL} is the solar elevation angle ($90^\circ - \theta_Z$).

The report of [55] presents an algorithm in order to calculate the solar zenith and azimuth angles with uncertainties of ± 0.0003 degrees.

The eccentric anomaly (E) from mean anomaly (M) and eccentricity (e) for very near circular orbits shown in the below [54, 56]:

$$E = M + e \sin(M) (1.0 + e \cos(M)) \quad (3.27)$$

The distance of Sun (R_{SUN}) and its true anomaly (v_{SUN}) are:

$$R_{SUN,X} = R_{SUN} \cos(v_{SUN}) = a (\cos(E) - e) \quad (3.28)$$

$$R_{SUN,Y} = R_{SUN} \sin(v_{SUN}) = a (\sin(E) \sqrt{1 - e^2}) \quad (3.29)$$

$$R_{SUN} = \sqrt{(R_{SUN,X})^2 + (R_{SUN,Y})^2} \quad (3.30)$$

$$v_{SUN} = \text{atan2}\left(\frac{R_{SUN,X}}{R_{SUN,Y}}\right) \quad (3.31)$$

The Sun centric longitude angle (lon_{SUN}) is found from the argument at perihelion (ω_{SUN}) and the true anomaly (v_{SUN}):

$$lon_{SUN} = \omega_{SUN} + v_{SUN} \quad (3.32)$$

The Sun position vector ($X_{SUN}, Y_{SUN}, Z_{SUN}$) in a coordinate system in the ecliptic plane by using the trigonometric functions of the Sun longitude angle:

$$\begin{bmatrix} X_{SUN} \\ Y_{SUN} \\ Z_{SUN} \end{bmatrix} = \begin{bmatrix} R_{SUN} \cdot \cos(lon_{SUN}) \\ R_{SUN} \cdot \sin(lon_{SUN}) \\ 0 \end{bmatrix} \quad (3.33)$$

The same definition in the inertial geocentric coordinate system ($X_{SUN,E}, Y_{SUN,E}, Z_{SUN,E}$) is given by:

$$\begin{bmatrix} X_{SUN,E} \\ Y_{SUN,E} \\ Z_{SUN,E} \end{bmatrix} = \begin{bmatrix} X_{SUN} \\ Y_{SUN} \cdot \cos(e) \\ Y_{SUN} \cdot \sin(e) \end{bmatrix} \quad (3.34)$$

3.6. Summary

The space environment model designed in this chapter clarifies the propagation of satellite orbit concerning Keplerian motion equations and orbital perturbations. It is mandatory to simulate space environment which includes satellite trajectories.

This chapter also states the vector models of Earth magnetic field and Sun position which are used to generate the required inputs for attitude sensor calculations.



CHAPTER 4

SATELLITE ATTITUDE MODEL

4.1. Introduction

The state space definitions of both satellite nonlinear and linear attitude models are handled in this chapter. Besides, the controllability and Lyapunov based stability properties of the derived attitude equations are assessed under the following titles.

4.2. Satellite Nonlinear Attitude Control Model

The definition of nonlinear system and measurement models are expressed:

$$x_{k+1} = f(x_k, u_k, w_k, k) \quad (4.1)$$

$$\tilde{y}_k = h(x_k, v_k, k) \quad (4.2)$$

In this study, the state vector (x_k) is selected according to system dynamic characteristics. The values of satellite angular velocity (w_{IB}^B), quaternion vector (q) and reaction wheel angular momentum (H_{RW}^B) change dynamically as simulation time progressed:

$$x_k = [w_{IB}^B \quad q \quad H_{RW}^B]^T \quad (4.3)$$

In this study, u_k is the input function generating from control torques (M_C^{RW} , M_C^{MTR}) and disturbance torques (M_D) exerted on satellite. The component numbers of input vector are dependent on the torque generators integrated in satellite structure:

$$u_k = [M_C^{RW} \quad M_C^{MTR} \quad M_D]^T \quad (4.4)$$

4.2.1. Nonlinear State Space Definition in Discrete Time

The combined dynamic and kinematic equations give the general nonlinear model definition for satellite's angular motion. The nonlinear equation of satellite dynamics ($f_1(x_k, u_k)$) is shown with the equation of satellite angular moments and torque definitions when reaction wheels are used as torque generators [51]:

$$\dot{\bar{w}}_{IB_1}^B = I_{S_x}^{-1} \left((I_{S_y} - I_{S_z}) \bar{w}_{IB_2}^B \bar{w}_{IB_3}^B + \bar{w}_{IB_3}^B \bar{H}_{RW_2}^B - \bar{w}_{IB_2}^B \bar{H}_{RW_3}^B + \bar{M}_{C_1}^{RW} + \bar{M}_{D_1} \right) \quad (4.5)$$

$$\dot{\bar{w}}_{IB_2}^B = I_{S_y}^{-1} \left((I_{S_z} - I_{S_x}) \bar{w}_{IB_1}^B \bar{w}_{IB_3}^B + \bar{w}_{IB_1}^B \bar{H}_{RW_3}^B - \bar{w}_{IB_3}^B \bar{H}_{RW_1}^B + \bar{M}_{C_2}^{RW} + \bar{M}_{D_2} \right) \quad (4.6)$$

$$\dot{\bar{w}}_{IB_3}^B = I_{S_z}^{-1} \left((I_{S_x} - I_{S_y}) \bar{w}_{IB_1}^B \bar{w}_{IB_2}^B + \bar{w}_{IB_2}^B \bar{H}_{RW_1}^B - \bar{w}_{IB_1}^B \bar{H}_{RW_2}^B + \bar{M}_{C_3}^{RW} + \bar{M}_{D_3} \right) \quad (4.7)$$

If magnetic torque rods are using as torque generators, these dynamic equations are:

$$\dot{\bar{w}}_{IB_1}^B = I_{S_x}^{-1} \left((I_{S_y} - I_{S_z}) \bar{w}_{IB_2}^B \bar{w}_{IB_3}^B + \bar{M}_{C_1}^{MTR} + \bar{M}_{D_1} \right) \quad (4.8)$$

$$\dot{\bar{w}}_{IB_2}^B = I_{S_y}^{-1} \left((I_{S_z} - I_{S_x}) \bar{w}_{IB_1}^B \bar{w}_{IB_3}^B + \bar{M}_{C_2}^{MTR} + \bar{M}_{D_2} \right) \quad (4.9)$$

$$\dot{\bar{w}}_{IB_3}^B = I_{S_z}^{-1} \left((I_{S_x} - I_{S_y}) \bar{w}_{IB_1}^B \bar{w}_{IB_2}^B + \bar{M}_{C_3}^{RW} + \bar{M}_{D_3} \right) \quad (4.10)$$

The second nonlinear equation of satellite kinematics ($f_2(x_k, u_k)$) can be rewritten using the satellite velocity vector (w_{OB}^B) represented with the second column of DCM matrix ($C(q)_2$) and the angular velocity specified in Orbit Frame ($w_{IO}^O = [0 \quad -w_0 \quad 0]^T$) like in the following equation. Before resolving the second nonlinear equation, it is beneficial to recall this new angular velocity definition:

$$w_{OB}^B = w_{IB}^B - [C(q)]_O^B \cdot w_{IO}^O \quad (4.11)$$

$$w_{OB}^B = w_{IB}^B - [C(q)]_O^B \begin{bmatrix} 0 \\ -w_0 \\ 0 \end{bmatrix} = \begin{bmatrix} w_{IB_1}^B + C(q)_{12} w_0 \\ w_{IB_2}^B + C(q)_{22} w_0 \\ w_{IB_3}^B + C(q)_{32} w_0 \end{bmatrix} \quad (4.12)$$

$$w_{OB}^B = \begin{bmatrix} w_{OB_1}^B \\ w_{OB_2}^B \\ w_{OB_3}^B \end{bmatrix} = \begin{bmatrix} w_{IB_1}^B + 2(q_1 q_2 + q_3 q_4) w_0 \\ w_{IB_2}^B + (q_4^2 - q_1^2 + q_2^2 - q_3^2) w_0 \\ w_{IB_3}^B + 2(q_2 q_3 - q_1 q_4) w_0 \end{bmatrix} \quad (4.13)$$

The new representation for skew symmetric matrix ($\Omega(w_{OB}^B)$) according to the satellite angular velocity (w_{IB}^B) is:

$$\Omega(w_{OB}^B) = \begin{bmatrix} 0 & w_{IB_3}^B + C(q)_{32} w_0 & -w_{IB_2}^B - C(q)_{22} w_0 & w_{IB_1}^B + C(q)_{12} w_0 \\ -w_{IB_3}^B - C(q)_{32} w_0 & 0 & w_{IB_1}^B + C(q)_{12} w_0 & w_{IB_2}^B + C(q)_{22} w_0 \\ w_{IB_2}^B + C(q)_{22} w_0 & -w_{IB_1}^B - C(q)_{12} w_0 & 0 & w_{IB_3}^B + C(q)_{32} w_0 \\ -w_{IB_1}^B - C(q)_{12} w_0 & -w_{IB_2}^B - C(q)_{22} w_0 & -w_{IB_3}^B - C(q)_{32} w_0 & 0 \end{bmatrix} \quad (4.14)$$

The second nonlinear equation of satellite kinematics $f_2(x_k, u_k)$ is:

$$\dot{\bar{q}}_1 = \frac{1}{2} (\bar{q}_2 (\bar{w}_{IB_3}^B + C(q)_{32} w_0) - \bar{q}_3 (\bar{w}_{IB_2}^B + C(q)_{22} w_0) + \bar{q}_4 (\bar{w}_{IB_1}^B + C(q)_{12} w_0)) \quad (4.15)$$

$$\dot{\bar{q}}_2 = \frac{1}{2} (-\bar{q}_1 (\bar{w}_{IB_3}^B + C(q)_{32} w_0) + \bar{q}_3 (\bar{w}_{IB_1}^B + C(q)_{12} w_0) + \bar{q}_4 (\bar{w}_{IB_2}^B + C(q)_{22} w_0)) \quad (4.16)$$

$$\dot{\bar{q}}_3 = \frac{1}{2} (\bar{q}_1 (\bar{w}_{IB_2}^B + C(q)_{22} w_0) - \bar{q}_2 (\bar{w}_{IB_1}^B + C(q)_{12} w_0) + \bar{q}_4 (\bar{w}_{IB_3}^B + C(q)_{32} w_0)) \quad (4.17)$$

$$\dot{\bar{q}}_4 = \frac{1}{2} (-\bar{q}_1 (\bar{w}_{IB_1}^B + C(q)_{12} w_0) - \bar{q}_2 (\bar{w}_{IB_2}^B + C(q)_{22} w_0) - \bar{q}_3 (\bar{w}_{IB_3}^B + C(q)_{32} w_0)) \quad (4.18)$$

The third nonlinear equation of satellite kinematics $f_3(x_k, u_k)$ is:

$$\dot{H}_{RW}^B = -\bar{M}_C^{RW} \quad (4.19)$$

Case-1: Torque generators are only reaction wheels

The nonlinear dynamic and kinematic equations in the case of using reaction wheels as torque generators are given hereafter:

$$\begin{bmatrix} f_1(x_k, u_k) \\ f_2(x_k, u_k) \\ f_3(x_k, u_k) \end{bmatrix} = \begin{bmatrix} \dot{w}_{IB}^B \\ \dot{q} \\ \dot{H}_{RW}^B \end{bmatrix} = \begin{bmatrix} I_S^{-1} [M_D + M_C^{RW} - \Omega(w_{IB}^B) I_S w_{IB}^B - \Omega(w_{IB}^B) H_{RW}^B] \\ \frac{1}{2} \Omega(w_{OB}^B) q \\ -M_C^{RW} \end{bmatrix} \quad (4.20)$$

Case-2: Torque generators are only magnetic torque rods

The nonlinear dynamic and kinematic equations in the case of using torque rods as torque generators are presented below:

$$\begin{bmatrix} f_1(x_k, u_k) \\ f_2(x_k, u_k) \end{bmatrix} = \begin{bmatrix} \dot{w}_{IB}^B \\ \dot{q} \end{bmatrix} = \begin{bmatrix} I_S^{-1} [M_D + M_C^{MTR} - \Omega(w_{IB}^B) I_S w_{IB}^B] \\ \frac{1}{2} \Omega(w_{OB}^B) q \end{bmatrix} \quad (4.21)$$

Case-3: Torque generators are both magnetic torque rods and reaction wheels

The combined nonlinear dynamic and kinematic equations in the case of using both reaction wheels and magnetic torque rods are depicted here:

$$\begin{bmatrix} \dot{w}_{IB}^B \\ \dot{q} \\ \dot{H}_{RW}^B \end{bmatrix} = \begin{bmatrix} I_S^{-1} [M_D + M_C^{RW} + M_C^{MTR} - \Omega(w_{IB}^B) I_S w_{IB}^B - \Omega(w_{IB}^B) H_{RW}^B] \\ \frac{1}{2} \Omega(w_{OB}^B) q \\ -M_C^{RW} \end{bmatrix} \quad (4.22)$$

4.2.2. Nonlinear Sensor Measurement Model in Discrete Time

The matrix (H_k) defines the changes of measurement vectors with time and it is consisted of each sensor measurements. This matrix is commonly a function of satellite kinematics such as Euler angles or quaternion vectors and calculated for each iteration. The measurement equations of attitude sensors ($y_k = H_k x_k + v_k$) are defined with its noise vectors (v_k) with respect to system states. The measurement vector is configured as if all sensor measurements are available:

$$y_k = \begin{bmatrix} y_{GYRO,k} \\ y_{STR,k} \\ y_{MGM,k} \\ y_{SuS,k} \\ y_{GPS1,k} \\ y_{GPS2,k} \end{bmatrix} = \begin{bmatrix} w_{meas} \\ q_{meas} \\ B_{meas} \\ SV_{meas} \\ r_{meas} \\ v_{meas} \end{bmatrix} = \begin{bmatrix} H_{GYRO} \\ H_{STR} \\ H_{MGM} \\ H_{SuS} \\ H_{GPS1} \\ H_{GPS2} \end{bmatrix} x_k + \begin{bmatrix} v_{GYRO} \\ v_{STR} \\ v_{MGM} \\ v_{SuS} \\ v_{GPS1} \\ v_{GPS2} \end{bmatrix} \quad (4.23)$$

In a sensor model, the output measurements can be estimated around the satellite's position adding the effects of some noises generated by misalignment error (non-orthogonality error), measurement error, scale factor, and bias. These noise sources have a large negative contribution to total sensor measurement values and each sensor is modelled considering these noise signals [29].

The measured quantities of sensor outputs can be shown in the following diagram:

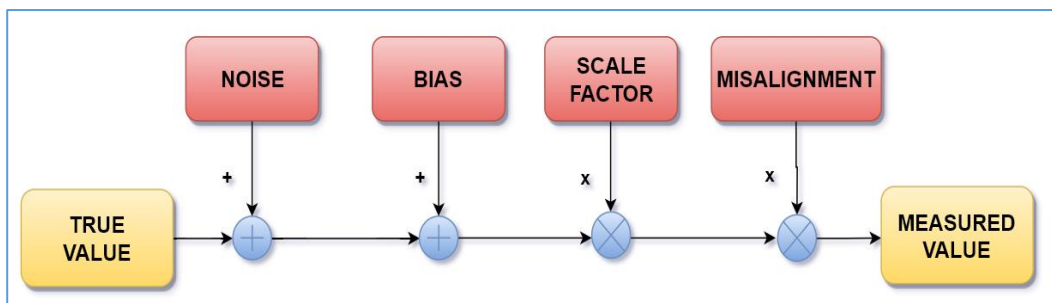


Figure 4-1 Sensor Measurements with Noise Effects

The general formula of sensor measurements is:

$$y_{meas} = y_{true} + (v_{SF} y_{true} + v_{MA} y_{true} + v_{BIAS}) \quad (4.24)$$

- ✓ v_{SF} is the error matrix representing scale factor,
- ✓ v_{MA} is the error matrix representing misalignment,
- ✓ v_{BIAS} is the sensor measurement bias error.

When a satellite goes into the eclipse phase, its attitude solution can be degraded and then it is required to propagate the solution incorporating the other sensor model data such as Star Tracker model [59].

Scale Factor Error (v_{SF}):

The ratio between the measured output value and the change in input value is called the scale factor. It also represents a linear approximation to sensor output error over a given full input range as a dimensionless quantity. It is stated as a percentage or the unit of parts per million. The combination of scale factor and misalignment error is generally inserted into the sensor models especially for gyroscopes.

Misalignment Error (v_{MA}):

Misalignment errors are derived from the angular difference between ideal and true axis vectors. Sensor axes are not located orthogonally in the satellite, therefore the measurement of these axes displacement is known as misalignment error. This error signal is modelled as random constant value and unitless quantity.

Bias Error (v_{BIAS}):

Fixed sensor bias error is known as the most critical error source and a constant value over a specified time and at a specified operating condition [64]. Bias stability

and instability are modelled as random constant value and random walk value respectively.

4.2.2.1. Nonlinear Model of Fiber Optic Gyroscopes

The error model equation of measured angular velocity for each gyroscope set can be expressed like the following [31, 32, 33, 34]. The measurement equations of magnetometers ($y_{GYRO,k}$) with its measurement matrix ($[H_{GYRO}]$) are defined:

$$w_{meas}^{BODY} = w_{IB}^B + (v_{SF} w_B + v_{MA} w_B + v_{BIAS} + v_{ARW} + v_{RRW} + v_{RR}) \quad (4.25)$$

$$y_{GYRO,k} = w_{meas}^{BODY} = w_{IB}^B + v_{GYRO} = [C_O^B]w_O + v_{GYRO} \quad (4.26)$$

$$y_{GYRO,k} = [H_{GYRO}]x_k + [R_{GYRO}]v_{GYRO} \quad (4.27)$$

- ✓ w_B and w_O are the true angular velocity vector in Body and Orbit Frame,
- ✓ w_{meas}^{BODY} is the measured angular velocity vector in satellite Body Frame,
- ✓ v_{RRW} is the rate random walk error,
- ✓ v_{ARW} is the angular random walk error,
- ✓ v_{RR} is the rate ramp error,
- ✓ v_{GYRO} is the measurement noise vector of gyroscopes represented with a band limited white noise signal and its noise power is denoted by sensor noise matrix (R_{GYRO}).

Rate random walk and angular random walk errors are generally represented by a zero mean Gaussian random noise signals with a variance calculated from Allan Variance Diagram [28, 29, 30, 59].

It is generally preferred to use a combination of star trackers and gyroscopes whenever the mission requires the highest accuracy in measurements.

4.2.2.2. Nonlinear Model of Star Trackers

Several conditions such as high radiation dose and different luminous objects adversely impact the performance of star trackers. Therefore, a Gaussian random noise with variance value is added to output measurements in the model.

The sensor model output is a form of quaternion vector to obtain the estimated satellite position. The input is a quaternion vector defined in satellite Body Frame delayed by multiplying its bias properties [66]. The measurement equations of star trackers ($y_{STR,k}$) with its measurement matrix ($[H_{STR}]$) are defined:

$$y_{STR,k} = q_{meas}^{BODY} = q^B + v_{STR} = [C_O^B]q_O + v_{STR} \quad (4.28)$$

$$y_{STR,k} = [H_{STR}]x_k + [R_{STR}]v_{STR} \quad (4.29)$$

- ✓ q_B and q_O is the true quaternion vectors in satellite Body and Orbit Frame,
- ✓ q_{meas}^{BODY} is the measured quaternion vector in satellite Body Frame,
- ✓ v_{STR} is the measurement noise vector of star trackers represented with a band limited white noise signal and its noise power is denoted by sensor noise matrix (R_{STR}).

4.2.2.3. Nonlinear Model of Magnetometers

In a magnetometer model, the direction and magnitude of magnetic field can be estimated around satellite's position adding the effects of some noises generated by scale factor and misalignment error. The IGRF model is used as a reference input for this sensor measurement.

Earth magnetic field strength which decreases with distance from Earth and residual satellite magnetic bias dominate total magnetic field measurement. The combined measurements of magnetometers integrated with amplifiers and low pass filters

provide accurate outputs by decreasing the unwanted sensor noises. The local magnetic field measurement of magnetometers is calculated with the following equation ($y_{MGM,k}$) [59]:

$$B_{meas}^{BODY} = B_B + (v_{SF}B_B + v_{MA}B_B + v_{BIAS}) = [C_O^B]B_O + v_{MGM} \quad (4.30)$$

$$y_{MGM,k} = B_{meas}^{BODY} = [H_{MGM}]x_k + [R_{MGM}]v_{MGM} \quad (4.31)$$

- ✓ B_B and B_O are the local magnetic field vectors in Body and Orbit Frame,
- ✓ B_{meas}^{BODY} is the measured magnetic field vector in Body Frame,
- ✓ v_{MGM} is the measurement noise vector of magnetometers represented with a band limited white noise signal and its noise power is denoted by sensor noise matrix (R_{MGM}).

The magnetometer bias (v_{BIAS}) is dependent on the sensor location in satellite. It also includes the magnetic field of satellite electronics and magnetic torque rods. Measurement noise, axes misalignment errors, the residual and saturation limits of magnetic moment shall be taken into consideration in the modelling phase of magnetic rods [66].

4.2.2.4. Nonlinear Model of Sun Sensors

The input signal is the incident angle of Sun position vector obtained from the measured currents for each axis. The output signal is a voltage, indicating whether the Sun is within the sensor's field of view or not. Although there are eight sun sensors in the actual satellite, only three brightest orthogonal sensors are selected to determine whether the satellite is in the eclipse phase or not. The measurement equations of sun sensors ($y_{Sus,k}$) with its measurement matrix ($[H_{Sus}]$) are defined:

$$SV_{meas}^{BODY} = [C_O^S]SV_O + v_{Sus} = SV_B + (v_{SF}SV_B + v_{MA}SV_B + v_{BIAS}) \quad (4.32)$$

$$y_{SUS,k} = SV_{meas}^{BODY} = [H_{SUS}]x_k + [R_{SUS}]v_{SUS} \quad (4.33)$$

- ✓ SV_B and SV_O are the Sun position vector in Body and Orbit Frame,
- ✓ SV_{meas}^{BODY} is the measured Sun position vector in Body Frame,
- ✓ v_{SUS} is the measurement noise vector of Sun sensors represented with a band limited white noise signal and its noise power is denoted by sensor noise matrix (R_{SUS}).

4.2.2.5. Nonlinear Model of GPS Receiver Sensor

The satellite ephemeris errors and ionospheric path delays are major error sources for GPS sensor models and they limit navigation accuracy to around 10 meters [39, 41]. Ionosphere error depends on the interaction between GPS signal and electrically charged ions and this error reduces signal speed and introduces measurement error. Satellite ephemeris error is derived from the difference between the expected and actual orbital position of a GPS satellite.

The error model equation of measured Cartesian position and velocity vectors from each GPS sensor can be expressed like the following [25, 26, 27]. The measurement equations of GPS receivers ($y_{GPS1,k}$) with its measurement matrices ($[H_{GPS1}]$) are defined hereafter:

$$r_{meas}^{BODY} = r_B + (v_{SF} r_B + v_{MA} r_B + v_{BIAS}) = [C_O^B]r_O + v_{GPS} \quad (4.34)$$

$$y_{GPS1,k} = r_{meas}^{BODY} = [H_{GPS1}]x_k + [R_{GPS}]v_{GPS} \quad (4.35)$$

- ✓ r_B and r_O are the true position vectors in Body and Orbit Frame,
- ✓ r_{meas}^{BODY} is the measured position vector in Body Frame,

- ✓ v_{GPS} is the measurement noise vector of GPS receivers represented with a band limited white noise signal and its noise power is denoted by sensor noise matrix (R_{GPS}).

The measurement equations of GPS receivers ($y_{GPS2,k}$) with its measurement matrices ($[H_{GPS2}]$) are defined here:

$$v_{meas}^{BODY} = v_B + (v_{SF} v_B + v_{SF} v_B + v_{BIAS}) = [C_O^B]v_O + v_{GPS} \quad (4.36)$$

$$y_{GPS1,k} = v_{meas}^{BODY} = [H_{GPS2}]x_k + [R_{GPS}]v_{GPS} \quad (4.37)$$

- ✓ v_B and v_O are the true velocity vectors in Body and Orbit Frame,
- ✓ v_{meas}^{BODY} is the measured velocity vector in Body Frame,
- ✓ v_{GPS} is the measurement noise vector of GPS receivers and its noise power is denoted by the sensor noise matrix (R_{GPS}).

4.2.2.6. Nonlinear Model of Sensor Measurement Matrix

For nonlinear measurement equations ($y_k = H_k x_k + D_k u_k$), assuming that there is no input value in y_k equation ($D_k = 0$). The transformation matrix written with respect to quaternion vector can be used to indicate the measured quantities in state space form ($C_O^B = \{[C_O^B]_x, [C_O^B]_y, [C_O^B]_z\}$):

$$[C_O^B]_x = \begin{bmatrix} q_1 & -q_2 & -q_3 & q_4 \\ q_2 & q_1 & q_4 & q_3 \\ q_3 & -q_4 & q_1 & -q_2 \end{bmatrix} \begin{bmatrix} q_1 \\ q_2 \\ q_3 \\ q_4 \end{bmatrix} = [H_1]q \quad (4.38)$$

$$[C_O^B]_y = \begin{bmatrix} q_2 & q_1 & -q_4 & -q_3 \\ -q_1 & q_2 & -q_3 & q_4 \\ q_4 & q_3 & q_2 & q_1 \end{bmatrix} \begin{bmatrix} q_1 \\ q_2 \\ q_3 \\ q_4 \end{bmatrix} = [H_2]q \quad (4.39)$$

$$[C_O^B]_y = \begin{bmatrix} q_3 & q_4 & q_1 & q_2 \\ -q_4 & q_3 & q_2 & -q_1 \\ -q_1 & -q_2 & q_3 & q_4 \end{bmatrix} \begin{bmatrix} q_1 \\ q_2 \\ q_3 \\ q_4 \end{bmatrix} = [H_3]q \quad (4.40)$$

The nonlinear measurement matrix definition in terms of each measurement in Orbit Frame such as B_O , SV_O , r_O and v_O , when reaction wheels are torque generators:

$$H_k \Delta x_k = \begin{bmatrix} w_{meas} \\ q_{meas} \\ B_{meas} \\ SV_{meas} \\ r_{meas} \\ v_{meas} \end{bmatrix} = \begin{bmatrix} [H_{GYRO}^{non}]_{3x3} & 0_{3x4} & 0_{3x3} \\ 0_{4x3} & [H_{STR}^{non}]_{4x4} & 0_{4x3} \\ 0_{3x3} & [H_{MGM}^{non}]_{3x4} & 0_{3x3} \\ 0_{3x3} & [H_{SuS}^{non}]_{3x4} & 0_{3x3} \\ 0_{3x3} & [H_{GPS1}^{non}]_{3x4} & 0_{3x3} \\ 0_{3x3} & [H_{GPS2}^{non}]_{3x4} & 0_{3x3} \end{bmatrix} \begin{bmatrix} \Delta w_{IB}^B \\ \Delta q \\ \Delta H_{RW}^B \end{bmatrix} \quad (4.41)$$

$$H_k = \begin{bmatrix} [H_{GYRO}^{non} = I]_{3x3} & [0]_{3x4} & [0]_{3x3} \\ [0]_{4x3} & [H_{STR}^{non} = I]_{4x4} & [0]_{4x3} \\ [0]_{3x3} & \begin{bmatrix} H_{MGM,1}^{non} = B_O^T \cdot H_1 \\ H_{MGM,2}^{non} = B_O^T \cdot H_2 \\ H_{MGM,3}^{non} = B_O^T \cdot H_3 \end{bmatrix}_{3x4} & [0]_{3x3} \\ [0]_{3x3} & \begin{bmatrix} H_{SuS,1}^{non} = SV_O^T \cdot H_1 \\ H_{SuS,2}^{non} = SV_O^T \cdot H_2 \\ H_{SuS,3}^{non} = SV_O^T \cdot H_3 \end{bmatrix}_{3x4} & [0]_{3x3} \\ [0]_{3x3} & \begin{bmatrix} H_{GPS1,1}^{non} = r_O^T \cdot H_1 \\ H_{GPS1,2}^{non} = r_O^T \cdot H_2 \\ H_{GPS1,3}^{non} = r_O^T \cdot H_3 \end{bmatrix}_{3x4} & [0]_{3x3} \\ [0]_{3x3} & \begin{bmatrix} H_{GPS2,1}^{non} = v_O^T \cdot H_1 \\ H_{GPS2,2}^{non} = v_O^T \cdot H_2 \\ H_{GPS2,3}^{non} = v_O^T \cdot H_3 \end{bmatrix}_{3x4} & [0]_{3x3} \end{bmatrix} \begin{bmatrix} \Delta w_{IB_1}^B \\ \Delta w_{IB_2}^B \\ \Delta w_{IB_3}^B \\ \Delta q_1 \\ \Delta q_2 \\ \Delta q_3 \\ \Delta q_4 \\ \Delta H_{RW_1}^B \\ \Delta H_{RW_2}^B \\ \Delta H_{RW_3}^B \end{bmatrix} \quad (4.42)$$

When torque rods are using as torque generators, the nonlinear measurement matrix will be shown here:

$$H_k \Delta x_k = \begin{bmatrix} w_{meas} \\ q_{meas} \\ B_{meas} \\ SV_{meas} \\ r_{meas} \\ v_{meas} \end{bmatrix} = \begin{bmatrix} [H_{GYRO}^{non}]_{3x3} & 0_{3x4} \\ 0_{4x3} & [H_{STR}^{non}]_{4x4} \\ 0_{3x3} & [H_{MGM}^{non}]_{3x4} \\ 0_{3x3} & [H_{SuS}^{non}]_{3x4} \\ 0_{3x3} & [H_{GPS1}^{non}]_{3x4} \\ 0_{3x3} & [H_{GPS2}^{non}]_{3x4} \end{bmatrix} \begin{bmatrix} \Delta w_{IB}^B \\ \Delta q \end{bmatrix} \quad (4.43)$$

4.3. Satellite Linear Attitude Control Model

The linear function in a discrete-time case in terms of state (x_k), input (u_k), and system noise vector (w_k) definitions are given hereafter:

$$\dot{x}_k = x_{k+1} = f(x_k, u_k, w_k, k) = A_k x_k + B_k u_k + G_k w_k ; w_k \sim N(0, Q_k) \quad (4.44)$$

The measurement vector (y_k) is a set of system measurements which are the functions of state vectors and measurement noise vector (v_k):

$$y_k = h(x_k, v_k, k) = H_k x_k + D_k u_k + v_k ; v_k \sim N(0, R_k) \quad (4.45)$$

Q_k and R_k are system and measurement covariance matrices respectively. The covariance between the zero mean Gaussian white noise distribution vectors w_k and v_k is zero value and there is no correlation between these noise vectors:

$$E\{w_k v_j^T\} = 0 \quad (4.46)$$

Case-1: Torque generators are only reaction wheels

The state space definition is written with the following representation (x_k^{RW} is state vector and u_k^{RW} is input vector for this configuration) in the case of reaction wheels are used as torque generators [8, 16, 51]:

$$\dot{x}_k = x_{k+1}^{RW} = A_k x_k^{RW} + B_k u_k^{RW} + G_k w_k^{RW}; w_k^{RW} \sim N(0, Q_k) \quad (4.47)$$

$$\dot{x}_k = \begin{bmatrix} \dot{w}_{IB}^B \\ \dot{q} \\ \dot{H}_{RW}^B \end{bmatrix} = A_k \begin{bmatrix} w_{IB}^B \\ q \\ H_{RW}^B \end{bmatrix} + B_k \begin{bmatrix} M_C^{RW} \\ M_D \end{bmatrix} + Q_k \begin{bmatrix} M_C^{RW} \\ M_D \end{bmatrix} \quad (4.48)$$

Case-2: Torque generators are only magnetic torque rods

The state space definition for this case is written like the following representation (x_k^{MTR} is state vector and u_k^{MTR} is input vector for this configuration):

$$\dot{x}_k = x_{k+1}^{MTR} = A_k x_k^{MTR} + B_k u_k^{MTR} + G_k w_k^{MTR}; w_k^{MTR} \sim N(0, Q_k) \quad (4.49)$$

$$\dot{x}_k = \begin{bmatrix} \dot{w}_{IB}^B \\ \dot{q} \end{bmatrix} = A_k \begin{bmatrix} \dot{w}_{IB}^B \\ \dot{q} \end{bmatrix} + B_k \begin{bmatrix} M_C^{MTR} \\ M_D \end{bmatrix} + Q_k \begin{bmatrix} M_C^{MTR} \\ M_D \end{bmatrix} \quad (4.50)$$

Case-3: Torque generators are both magnetic torque rods and reaction wheels

The state space definition of the nonlinear equations specified above is written with the following representation (x_k^{RW+MTR} is state vector and u_k^{RW+MTR} is input vector for this configuration):

$$\dot{x}_k = x_{k+1}^{RW+MTR} = A_k x_k^{RW+MTR} + B_k u_k^{RW+MTR} + G_k w_k^{RW+MTR} \quad (4.51)$$

$$\dot{x}_k = \begin{bmatrix} \dot{w}_{IB}^B \\ \dot{q} \\ \dot{H}_{RW}^B \end{bmatrix} = A_k \begin{bmatrix} w_{IB}^B \\ q \\ H_{RW}^B \end{bmatrix} + B_k \begin{bmatrix} M_C^{RW} \\ M_C^{MTR} \\ M_D \end{bmatrix} + Q_k \begin{bmatrix} M_C^{RW} \\ M_C^{MTR} \\ M_D \end{bmatrix} \quad (4.52)$$

In this study, the simulation results are based on this model configuration.

4.3.1. Linearization of Nonlinear Model Equations

Nonlinear satellite equations can be linearized using the steady-state satellite conditions. In practice, the values of system (w_k) and measurement (v_k) noise vectors are not to be involved into the linearization computations:

$$\dot{x}_k = x_{k+1} = f(x_k, u_k, k) = A_k x_k + B_k u_k \quad (4.53)$$

$$y_k = h(x_k, u_k, k) = H_k x_k + D_k u_k \quad (4.54)$$

In order to obtain a linear model around a specific set of constant values called operating or equilibrium points (\bar{x}_k, \bar{u}_k), the small deviations from these points ($\Delta x_k, \Delta y_k, \Delta u_k$) are introduced like the following:

$$\Delta x_k = x_k - \bar{x}_k \rightarrow x_k = \Delta x_k + \bar{x}_k \rightarrow \dot{x}_k = \Delta \dot{x}_k + \dot{\bar{x}}_k \quad (4.55)$$

$$\Delta y_k = y_k - \bar{y}_k \rightarrow y_k = \Delta y_k + \bar{y}_k \quad (4.56)$$

$$\Delta u_k = u_k - \bar{u}_k \rightarrow u_k = \Delta u_k + \bar{u}_k \quad (4.57)$$

The first order of Taylor series expansion can be applied to first nonlinear scalar equations by reducing the higher order components [51]:

$$\Delta \dot{x}_k + \dot{\bar{x}}_k = f(\bar{x}_k, \bar{u}_k, k) + \left. \frac{\partial f(\bar{x}_k, \bar{u}_k, k)}{\partial x_k} \right|_{\bar{x}_k} \Delta x_k + \left. \frac{\partial f(\bar{x}_k, \bar{u}_k, k)}{\partial u_k} \right|_{\bar{u}_k} \Delta u_k + \dots \quad (4.58)$$

$$\Delta y_k + \bar{y}_k = h(\bar{x}_k, \bar{u}_k, k) + \left. \frac{\partial h(\bar{x}_k, \bar{u}_k, k)}{\partial x_k} \right|_{\bar{x}_k} \Delta x_k + \left. \frac{\partial h(\bar{x}_k, \bar{u}_k, k)}{\partial u_k} \right|_{\bar{u}_k} \Delta u_k + \dots \quad (4.59)$$

Considering the definitions of $\dot{\bar{x}}_k = f(\bar{x}_k, \bar{u}_k, k)$ and $\bar{y}_k = h(\bar{x}_k, \bar{u}_k, k)$, state-space model is defined with the following equations by truncating to the first order

of Taylor series. The Jacobian definitions of A_k , B_k , H_k and D_k matrices are calculated by taking partial derivatives with respect to states and inputs around operating points:

$$\Delta \dot{x}_k = A_k \Delta x_k + B_k \Delta u_k = \left. \frac{\partial f(\bar{x}_k, \bar{u}_k, k)}{\partial x_k} \right|_{\bar{x}_k} \Delta x_k + \left. \frac{\partial f(\bar{x}_k, \bar{u}_k, k)}{\partial u_k} \right|_{\bar{u}_k} \Delta u_k \quad (4.60)$$

$$\Delta y_k = H_k \Delta x_k + D_k \Delta u_k = \left. \frac{\partial h(\bar{x}_k, \bar{u}_k, k)}{\partial x_k} \right|_{\bar{x}_k} \Delta x_k + \left. \frac{\partial h(\bar{x}_k, \bar{u}_k, k)}{\partial u_k} \right|_{\bar{u}_k} \Delta u_k \quad (4.61)$$

$$A_k = \begin{bmatrix} \frac{\partial f_1}{\partial x_1} & \frac{\partial f_1}{\partial x_2} & \cdots & \frac{\partial f_1}{\partial x_m} \\ \frac{\partial f_2}{\partial x_1} & \frac{\partial f_2}{\partial x_2} & \cdots & \frac{\partial f_2}{\partial x_m} \\ \vdots & \vdots & \ddots & \vdots \\ \frac{\partial f_n}{\partial x_1} & \frac{\partial f_n}{\partial x_2} & \cdots & \frac{\partial f_n}{\partial x_m} \end{bmatrix}; \quad B_k = \begin{bmatrix} \frac{\partial f_1}{\partial u_1} & \frac{\partial f_1}{\partial u_2} & \cdots & \frac{\partial f_1}{\partial u_m} \\ \frac{\partial f_2}{\partial u_1} & \frac{\partial f_2}{\partial u_2} & \cdots & \frac{\partial f_2}{\partial u_m} \\ \vdots & \vdots & \ddots & \vdots \\ \frac{\partial f_n}{\partial u_1} & \frac{\partial f_n}{\partial u_2} & \cdots & \frac{\partial f_n}{\partial u_m} \end{bmatrix} \quad (4.62)$$

$$H_k = \begin{bmatrix} \frac{\partial h_1}{\partial x_1} & \frac{\partial h_1}{\partial x_2} & \cdots & \frac{\partial h_1}{\partial x_m} \\ \frac{\partial h_2}{\partial x_1} & \frac{\partial h_2}{\partial x_2} & \cdots & \frac{\partial h_2}{\partial x_m} \\ \vdots & \vdots & \ddots & \vdots \\ \frac{\partial h_n}{\partial x_1} & \frac{\partial h_n}{\partial x_2} & \cdots & \frac{\partial h_n}{\partial x_m} \end{bmatrix}; \quad D_k = \begin{bmatrix} \frac{\partial h_1}{\partial u_1} & \frac{\partial h_1}{\partial u_2} & \cdots & \frac{\partial h_1}{\partial u_m} \\ \frac{\partial h_2}{\partial u_1} & \frac{\partial h_2}{\partial u_2} & \cdots & \frac{\partial h_2}{\partial u_m} \\ \vdots & \vdots & \ddots & \vdots \\ \frac{\partial h_n}{\partial u_1} & \frac{\partial h_n}{\partial u_2} & \cdots & \frac{\partial h_n}{\partial u_m} \end{bmatrix} \quad (4.63)$$

4.3.1.1. Linearization of Satellite Nonlinear Attitude Model

A mathematical model of satellite attitude is separated into two sections. The first one describes the behaviour under the effects of external forces, and the second one defines the relation between Body Frame and Local Navigation Frame. Linearization process is applied for the case of using both RWs and MTRs as actuators here. However, this process can be adjusted in compliance with different actuator

configurations. The derivative of nonlinear dynamic equation with respect to state vector ($A_k x_k$):

$$\Delta \dot{x}_k = A_k \Delta x_k + B_k \Delta u_k \rightarrow \dot{x} = A_k x_k + B_k u_k \quad (4.64)$$

$$A_k x_k = \begin{bmatrix} \frac{\partial f_1(\bar{x}_k, \bar{u}_k)}{\partial \bar{w}_{IB}^B} & \frac{\partial f_1(\bar{x}_k, \bar{u}_k)}{\partial \bar{q}} & \frac{\partial f_1(\bar{x}_k, \bar{u}_k)}{\partial \bar{H}_{RW}^B} \\ \frac{\partial f_2(\bar{x}_k, \bar{u}_k)}{\partial \bar{w}_{IB}^B} & \frac{\partial f_2(\bar{x}_k, \bar{u}_k)}{\partial \bar{q}} & \frac{\partial f_2(\bar{x}_k, \bar{u}_k)}{\partial \bar{H}_{RW}^B} \\ \frac{\partial f_3(\bar{x}_k, \bar{u}_k)}{\partial \bar{w}_{IB}^B} & \frac{\partial f_3(\bar{x}_k, \bar{u}_k)}{\partial \bar{q}} & \frac{\partial f_3(\bar{x}_k, \bar{u}_k)}{\partial \bar{H}_{RW}^B} \end{bmatrix} \begin{bmatrix} w_{IB}^B \\ q \\ H_{RW}^B \end{bmatrix} \quad (4.65)$$

$$A_k x_k = \begin{bmatrix} \frac{\partial \dot{w}_{IB}^B}{\partial \bar{w}_{IB}^B} & \frac{\partial \dot{w}_{IB}^B}{\partial \bar{q}} & \frac{\partial \dot{w}_{IB}^B}{\partial \bar{H}_{RW}^B} \\ \frac{\partial \dot{q}}{\partial \bar{w}_{IB}^B} & \frac{\partial \dot{q}}{\partial \bar{q}} & \frac{\partial \dot{q}}{\partial \bar{H}_{RW}^B} \\ \frac{\partial \dot{H}_{RW}^B}{\partial \bar{w}_{IB}^B} & \frac{\partial \dot{H}_{RW}^B}{\partial \bar{q}} & \frac{\partial \dot{H}_{RW}^B}{\partial \bar{H}_{RW}^B} \end{bmatrix} \begin{bmatrix} w_{IB}^B \\ q \\ H_{RW}^B \end{bmatrix} \quad (4.66)$$

$$\frac{\partial \dot{w}_{IB}^B}{\partial \bar{w}_{IB}^B} = \begin{bmatrix} 0 & \frac{(I_{S_y} - I_{S_z})\bar{w}_{IB_3}^B - \bar{H}_{RW_3}^B}{I_{S_x}} & \frac{(I_{S_y} - I_{S_z})\bar{w}_{IB_2}^B + \bar{H}_{RW_2}^B}{I_{S_x}} \\ \frac{(I_{S_z} - I_{S_x})\bar{w}_{IB_3}^B + \bar{H}_{RW_3}^B}{I_{S_y}} & 0 & \frac{(I_{S_z} - I_{S_x})\bar{w}_{IB_1}^B - \bar{H}_{RW_1}^B}{I_{S_y}} \\ \frac{(I_{S_x} - I_{S_y})\bar{w}_{IB_2}^B - \bar{H}_{RW_2}^B}{I_{S_z}} & \frac{(I_{S_x} - I_{S_y})\bar{w}_{IB_1}^B + \bar{H}_{RW_1}^B}{I_{S_z}} & 0 \end{bmatrix} \quad (4.67)$$

$$\frac{\partial \dot{w}_{IB}^B}{\partial \bar{q}} = [0]_{3x4} \quad (4.68)$$

$$\frac{\partial \dot{w}_{IB}^B}{\partial \bar{H}_{RW}^B} = \begin{bmatrix} 0 & \frac{\bar{w}_{IB_3}^B}{I_{S_x}} & -\frac{\bar{w}_{IB_2}^B}{I_{S_x}} \\ -\frac{\bar{w}_{IB_3}^B}{I_{S_y}} & 0 & \frac{\bar{w}_{IB_1}^B}{I_{S_y}} \\ \frac{\bar{w}_{IB_2}^B}{I_{S_z}} & -\frac{\bar{w}_{IB_1}^B}{I_{S_z}} & 0 \end{bmatrix} = -I_S^{-1} \Omega(\bar{w}_{IB}^B) \quad (4.69)$$

$$\frac{\partial \dot{\bar{q}}}{\partial \bar{w}_{IB}^B} = \frac{1}{2} \begin{bmatrix} \bar{q}_4 & -\bar{q}_3 & \bar{q}_2 \\ \bar{q}_3 & \bar{q}_4 & -\bar{q}_1 \\ -\bar{q}_2 & \bar{q}_1 & \bar{q}_4 \\ -\bar{q}_1 & -\bar{q}_2 & -\bar{q}_3 \end{bmatrix} \quad (4.70)$$

$$\frac{\partial \dot{\bar{q}}}{\partial \bar{q}} = \frac{1}{2} [\Omega(\bar{w}_{IB}^B)] + w_0 \begin{bmatrix} \bar{q}_1 \bar{q}_3 & \bar{q}_2 \bar{q}_3 & \frac{1+2\bar{q}_3^2}{2} & \bar{q}_3 \bar{q}_4 \\ \bar{q}_1 \bar{q}_4 & \bar{q}_2 \bar{q}_4 & \bar{q}_3 \bar{q}_4 & \frac{-(1+2\bar{q}_1^2)}{2} \\ \frac{-(1+2\bar{q}_1^2)}{2} & -\bar{q}_1 \bar{q}_2 & -\bar{q}_1 \bar{q}_3 & -\bar{q}_1 \bar{q}_4 \\ -\bar{q}_1 \bar{q}_2 & \frac{-(1+2\bar{q}_2^2)}{2} & -\bar{q}_2 \bar{q}_3 & -\bar{q}_2 \bar{q}_4 \end{bmatrix} \quad (4.71)$$

$$\frac{\partial \dot{\bar{q}}}{\partial \bar{H}_{RW}^B} = [0]_{4x3} \quad (4.72)$$

$$\frac{\partial \dot{\bar{H}}_{RW}^B}{\partial \bar{w}_{IB}^B} = \frac{\partial \dot{\bar{H}}_{RW}^B}{\partial \bar{H}_{RW}^B} = [0]_{3x3}; \quad \frac{\partial \dot{\bar{H}}_{RW}^B}{\partial \bar{q}} = [0]_{3x4} \quad (4.73)$$

The state space definition of nonlinear dynamic/kinematic equations with respect to input vector (u_k) is:

$$B_k u_k = \begin{bmatrix} \frac{\partial f_1(\bar{x}_k, \bar{u}_k)}{\partial \bar{M}_C^{RW}} & \frac{\partial f_1(\bar{x}_k, \bar{u}_k)}{\partial \bar{M}_C^{MTR}} & \frac{\partial f_1(\bar{x}_k, \bar{u}_k)}{\partial \bar{M}_D} \\ \frac{\partial f_2(\bar{x}_k, \bar{u}_k)}{\partial \bar{M}_C^{RW}} & \frac{\partial f_2(\bar{x}_k, \bar{u}_k)}{\partial \bar{M}_C^{MTR}} & \frac{\partial f_2(\bar{x}_k, \bar{u}_k)}{\partial \bar{M}_D} \\ \frac{\partial f_3(\bar{x}_k, \bar{u}_k)}{\partial \bar{M}_C^{RW}} & \frac{\partial f_3(\bar{x}_k, \bar{u}_k)}{\partial \bar{M}_C^{MTR}} & \frac{\partial f_3(\bar{x}_k, \bar{u}_k)}{\partial \bar{M}_D} \end{bmatrix} \begin{bmatrix} M_C^{RW} \\ M_C^{MTR} \\ M_D \end{bmatrix} \quad (4.74)$$

$$B_k u_k = \begin{bmatrix} \frac{\partial \dot{\bar{w}}_{IB}^B}{\partial \bar{M}_C^{RW}} & \frac{\partial \dot{\bar{w}}_{IB}^B}{\partial \bar{M}_C^{MTR}} & \frac{\partial \dot{\bar{w}}_{IB}^B}{\partial \bar{M}_D} \\ \frac{\partial \dot{\bar{q}}}{\partial \bar{M}_C^{RW}} & \frac{\partial \dot{\bar{q}}}{\partial \bar{M}_C^{MTR}} & \frac{\partial \dot{\bar{q}}}{\partial \bar{M}_D} \\ \frac{\partial \dot{\bar{H}}_{RW}^B}{\partial \bar{M}_C^{RW}} & \frac{\partial \dot{\bar{H}}_{RW}^B}{\partial \bar{M}_C^{MTR}} & \frac{\partial \dot{\bar{H}}_{RW}^B}{\partial \bar{M}_D} \end{bmatrix} \begin{bmatrix} M_C^{RW} \\ M_C^{MTR} \\ M_D \end{bmatrix} \quad (4.75)$$

$$\frac{\partial \dot{\bar{w}}_{IB}^B}{\partial \bar{M}_C^{RW}} = \frac{\partial \dot{\bar{w}}_{IB}^B}{\partial \bar{M}_C^{MTR}} = \frac{\partial \dot{\bar{w}}_{IB}^B}{\partial \bar{M}_D} = \begin{bmatrix} I_{S_x}^{-1} & 0 & 0 \\ 0 & I_{S_y}^{-1} & 0 \\ 0 & 0 & I_{S_z}^{-1} \end{bmatrix} = diag(I_S^{-1})_{3x3} \quad (4.76)$$

$$\frac{\partial \dot{\bar{q}}}{\partial \bar{M}_C^{RW}} = \frac{\partial \dot{\bar{q}}}{\partial \bar{M}_C^{MTR}} = \frac{\partial \dot{\bar{q}}}{\partial \bar{M}_D} = [0]_{4x3} \quad (4.77)$$

$$\frac{\partial \dot{\bar{H}}_{RW}^B}{\partial \bar{M}_C^{RW}} = \begin{bmatrix} -1 & 0 & 0 \\ 0 & -1 & 0 \\ 0 & 0 & -1 \end{bmatrix} = diag(-1)_{3x3} \quad (4.78)$$

$$\frac{\partial \dot{\bar{H}}_{RW}^B}{\partial \bar{M}_D} = \frac{\partial \dot{\bar{H}}_{RW}^B}{\partial \bar{M}_C^{MTR}} = [0]_{3x3} \quad (4.79)$$

The Jacobian matrix definition of input vector (B_k):

$$B_k u_k = \begin{bmatrix} diag(I_S^{-1})_{3x3} & diag(I_S^{-1})_{3x3} & diag(I_S^{-1})_{3x3} \\ [0]_{4x3} & [0]_{4x3} & [0]_{4x3} \\ diag(-1)_{3x3} & [0]_{3x3} & [0]_{3x3} \end{bmatrix} \begin{bmatrix} M_C^{RW} \\ M_C^{MTR} \\ M_D \end{bmatrix} \quad (4.80)$$

4.3.1.2. Linearization of Satellite Nonlinear Sensor Measurement Model

The matrix (H_k) defines the changes of measurement vectors with time and it is consisted of each sensor measurements. This matrix is commonly a function of satellite kinematics such as Euler angles or quaternion vectors and it is calculated for each iteration.

The measurement equations of attitude sensors ($y_k = H_k x_k + v_k$) are defined with its noise vectors (v_k) with respect to system states ($x_k = [w_{IB}^B, q, H_{RW}^B]^T$):

$$y_k = \begin{bmatrix} y_{GYRO,k} \\ y_{STR,k} \\ y_{MGM,k} \\ y_{SuS,k} \\ y_{GPS1,k} \\ y_{GPS2,k} \end{bmatrix} = \begin{bmatrix} w_{meas} \\ q_{meas} \\ B_{meas} \\ SV_{meas} \\ r_{meas} \\ v_{meas} \end{bmatrix} = \begin{bmatrix} H_{GYRO} \\ H_{STR} \\ H_{MGM} \\ H_{SuS} \\ H_{GPS1} \\ H_{GPS2} \end{bmatrix} \cdot x_k + \begin{bmatrix} v_{GYRO} \\ v_{STR} \\ v_{MGM} \\ v_{SuS} \\ v_{GPS1} \\ v_{GPS2} \end{bmatrix} \quad (4.81)$$

Linear Measurement Model of Fiber Optic Gyroscopes:

The measurement matrix for gyroscopes (H_{GYRO}) is constructed as follows:

$$\Delta y_{GYRO,k} = [H_{GYRO}] \Delta x_k = \frac{\partial H_{GYRO}}{\partial x_k} \Big|_{x_k=\bar{w}_{IB}^B} \Delta x_k \quad (4.82)$$

$$[H_{GYRO}] = \begin{bmatrix} H_{GYRO,1} \\ H_{GYRO,2} \\ H_{GYRO,3} \end{bmatrix} = \frac{\partial H_{GYRO}}{\partial x_k} \Big|_{x_k=\bar{w}_{IB}^B} = \frac{\partial w_B}{\partial x_k} \Big|_{x_k=\bar{w}_{IB}^B} = I_{3x3} \quad (4.83)$$

$$\Delta y_{GYRO,k} = [H_{GYRO,1} \quad H_{GYRO,2} \quad H_{GYRO,3} \quad 0_{3x4} \quad 0_{3x3}] \begin{bmatrix} \Delta w_{IB}^B \\ \Delta q \\ \Delta H_{RW}^B \end{bmatrix} \quad (4.84)$$

$$\Delta y_{GYRO,k} = [I_{3x3} \quad 0_{3x4} \quad 0_{3x3}] \begin{bmatrix} \Delta w_{IB}^B \\ \Delta q \\ \Delta H_{RW}^B \end{bmatrix} \quad (4.85)$$

Linear Measurement Model of Star Trackers:

The measurement matrix for star trackers ($[H_{STR}]$) is constructed as follows:

$$\Delta y_{STR,k} = [H_{STR}] \Delta x_k = \frac{\partial H_{STR}}{\partial x_k} \Big|_{x_k=\bar{q}} \Delta x_k \quad (4.86)$$

$$[H_{STR}] = \begin{bmatrix} H_{STR,1} \\ H_{STR,2} \\ H_{STR,3} \\ H_{STR,4} \end{bmatrix} = \frac{\partial H_{STR}}{\partial x_k} \Bigg|_{x_k=\bar{q}} = \frac{\partial q_B}{\partial x_k} \Bigg|_{x_k=\bar{q}} = I_{4 \times 4} \quad (4.87)$$

$$\Delta y_{STR,k} = [0_{4 \times 3} \quad H_{STR,1} \quad H_{STR,2} \quad H_{STR,3} \quad H_{STR,4} \quad 0_{4 \times 3}] \begin{bmatrix} \Delta w_{IB}^B \\ \Delta q \\ \Delta H_{RW}^B \end{bmatrix} \quad (4.88)$$

$$\Delta y_{STR,k} = [0_{4 \times 3} \quad I_{4 \times 4} \quad 0_{4 \times 3}] \begin{bmatrix} \Delta w_{IB}^B \\ \Delta q \\ \Delta H_{RW}^B \end{bmatrix} \quad (4.89)$$

Linear Measurement Model of Magnetometers:

If we define the derivative of transition matrix ($[C_O^B]$) with respect to state quaternion vector, the linearized measurement matrix can be written for sensor measurements obtained from Orbit Frame:

$$\frac{\partial [C_O^B]}{\partial x_k} \Bigg|_{x_k=\bar{q}_1} = 2 \begin{bmatrix} q_1 & q_2 & q_3 \\ q_2 & -q_1 & q_4 \\ q_3 & -q_4 & -q_1 \end{bmatrix} \quad (4.90)$$

$$\frac{\partial [C_O^B]}{\partial x_k} \Bigg|_{x_k=\bar{q}_2} = 2 \begin{bmatrix} -q_2 & q_1 & -q_4 \\ q_1 & q_2 & q_3 \\ q_4 & q_3 & -q_2 \end{bmatrix} \quad (4.91)$$

$$\frac{\partial [C_O^B]}{\partial x_k} \Bigg|_{x_k=\bar{q}_3} = 2 \begin{bmatrix} -q_3 & q_4 & q_1 \\ -q_4 & -q_3 & q_2 \\ q_1 & q_2 & q_3 \end{bmatrix} \quad (4.92)$$

$$\frac{\partial [C_O^B]}{\partial x_k} \Bigg|_{x_k=\bar{q}_4} = 2 \begin{bmatrix} q_4 & q_3 & -q_2 \\ -q_3 & q_4 & q_1 \\ q_2 & -q_1 & q_4 \end{bmatrix} \quad (4.93)$$

The measurement matrix of magnetometers ($[H_{MGM}]$) is constructed as follows:

$$\Delta y_{MGM,k} = [H_{MGM}] \Delta x_k = \frac{\partial H_{MGM}}{\partial x_k} \Big|_{x_k=\bar{q}} \Delta x_k \quad (4.94)$$

$$[H_{MGM}] = \begin{bmatrix} H_{MGM,1} \\ H_{MGM,2} \\ H_{MGM,3} \\ H_{MGM,4} \end{bmatrix} = \frac{\partial H_{MGM}}{\partial x_k} \Big|_{x_k=\bar{q}} = \frac{\partial [C_O^B]}{\partial x_k} \Big|_{x_k=\bar{q}} B_O \quad (4.95)$$

$$\Delta y_{MGM,k} = [0_{3x3} \quad H_{MGM,1} \quad H_{MGM,2} \quad H_{MGM,3} \quad H_{MGM,4} \quad 0_{3x3}] \begin{bmatrix} \Delta w_{IB}^B \\ \Delta q \\ \Delta H_{RW}^B \end{bmatrix} \quad (4.96)$$

Linear Measurement Model of Sun Sensors:

The measurement matrix for sun sensors ($[H_{Sus}]$) is extracted after applying linearization method to sun sensor measurement model:

$$\Delta y_{Sus,k} = [H_{Sus}] \Delta x_k = \frac{\partial H_{Sus}}{\partial x_k} \Big|_{x_k=\bar{q}} \Delta x_k \quad (4.97)$$

$$[H_{Sus}] = \begin{bmatrix} H_{Sus,1} \\ H_{Sus,2} \\ H_{Sus,3} \\ H_{Sus,4} \end{bmatrix} = \frac{\partial H_{Sus}}{\partial x_k} \Big|_{x_k=\bar{q}} = \frac{\partial [C_O^B]}{\partial x_k} \Big|_{x_k=\bar{q}} SV_O \quad (4.98)$$

$$\Delta y_{Sus,k} = [0_{3x3} \quad H_{Sus,1} \quad H_{Sus,2} \quad H_{Sus,3} \quad H_{Sus,4} \quad 0_{3x3}] \begin{bmatrix} \Delta w_{IB}^B \\ \Delta q \\ \Delta H_{RW}^B \end{bmatrix} \quad (4.99)$$

Linear Measurement Model of GPS Receiver Sensors:

The measurement matrices for GPS receivers ($[H_{GPS1}], [H_{GPS2}]$) in terms of position and velocity values ($r_{meas}^{BODY}, v_{meas}^{BODY}$) are constructed like the following:

$$\begin{bmatrix} \Delta y_{GPS1,k} \\ \Delta y_{GPS2,k} \end{bmatrix} = \begin{bmatrix} H_{GPS1} \\ H_{GPS2} \end{bmatrix} \Delta x_k \quad (4.100)$$

$$[H_{GPS1}] = \begin{bmatrix} H_{GPS1,1} \\ H_{GPS1,2} \\ H_{GPS1,3} \\ H_{GPS1,4} \end{bmatrix} = \frac{\partial H_{GPS1}}{\partial x_k} \Bigg|_{x_k=\bar{q}} = \frac{\partial [C_O^B]}{\partial x_k} \Bigg|_{x_k=\bar{q}} r_o \quad (4.101)$$

$$[H_{GPS2}] = \begin{bmatrix} H_{GPS2,1} \\ H_{GPS2,2} \\ H_{GPS2,3} \\ H_{GPS2,4} \end{bmatrix} = \frac{\partial H_{GPS2}}{\partial x_k} \Bigg|_{x_k=\bar{q}} = \frac{\partial [C_O^B]}{\partial x_k} \Bigg|_{x_k=\bar{q}} v_o \quad (4.102)$$

$$\Delta y_{GPS1,k} = [0_{3x3} \quad H_{GPS1,1} \quad H_{GPS1,2} \quad H_{GPS1,3} \quad H_{GPS1,4} \quad 0_{3x3}] \begin{bmatrix} \Delta w_{IB}^B \\ \Delta q \\ \Delta H_{RW}^B \end{bmatrix} \quad (4.103)$$

$$\Delta y_{GPS2,k} = [0_{3x3} \quad H_{GPS2,1} \quad H_{GPS2,2} \quad H_{GPS2,3} \quad H_{GPS2,4} \quad 0_{3x3}] \begin{bmatrix} \Delta w_{IB}^B \\ \Delta q \\ \Delta H_{RW}^B \end{bmatrix} \quad (4.104)$$

Assuming that all the sensor measurements are available, the state space definition of linearized measurement equations ($\Delta y_k = H_k \Delta x_k$) around the operating points ($\bar{x}_k = (\bar{w}_{IB}^B, \bar{q}, \bar{H}_{RW}^B)$) is represented hereafter:

$$H_k \Delta x_k = \begin{bmatrix} w_{meas} \\ q_{meas} \\ B_{meas} \\ SV_{meas} \\ r_{meas} \\ v_{meas} \end{bmatrix} = \begin{bmatrix} I_{3x3} & 0_{3x4} & 0_{3x3} \\ 0_{4x3} & I_{4x4} & 0_{4x3} \\ 0_{3x3} & [H_{MGM}]_{3x4} & 0_{3x3} \\ 0_{3x3} & [H_{SuS}]_{3x4} & 0_{3x3} \\ 0_{3x3} & [H_{GPS1}]_{3x4} & 0_{3x3} \\ 0_{3x3} & [H_{GPS2}]_{3x4} & 0_{3x3} \end{bmatrix} \begin{bmatrix} \Delta w_{IB}^B \\ \Delta q \\ \Delta H_{RW}^B \end{bmatrix} \quad (4.105)$$

4.3.1.3. Linear Satellite State Space Models

There are three different linear models that can be defined with respect to the selected actuator in a plant model. The linear state space definition with Jacobian matrices represents the case which is involving both RWs and MTRs as torque generators. The matrix definitions of linear model are (A_k , B_k , H_k , D_k):

$$A_k = \left[\begin{array}{ccc} Aw_k = \dot{w}_{IB}^B|_{\bar{x}_k}, & Aq_k = \dot{q}|_{\bar{x}_k}, & Ahrw_k = \dot{H}_{RW}^B|_{\bar{x}_k} \end{array} \right]$$

$$Aw_k =$$

$$\left[\begin{array}{ccc} 0 & \frac{(I_{S_y} - I_{S_z})\bar{w}_{IB_3}^B - \bar{H}_{RW_3}^B}{I_{S_x}} & \frac{(I_{S_y} - I_{S_z})\bar{w}_{IB_2}^B + \bar{H}_{RW_2}^B}{I_{S_x}} \\ \frac{(I_{S_z} - I_{S_x})\bar{w}_{IB_3}^B + \bar{H}_{RW_3}^B}{I_{S_y}} & 0 & \frac{(I_{S_z} - I_{S_x})\bar{w}_{IB_1}^B - \bar{H}_{RW_1}^B}{I_{S_y}} \\ \frac{(I_{S_x} - I_{S_y})\bar{w}_{IB_2}^B - \bar{H}_{RW_2}^B}{I_{S_z}} & \frac{(I_{S_x} - I_{S_y})\bar{w}_{IB_1}^B + \bar{H}_{RW_1}^B}{I_{S_z}} & 0 \\ \frac{1}{2}\bar{q}_4 & -\frac{1}{2}\bar{q}_3 & \frac{1}{2}\bar{q}_2 \\ \frac{1}{2}\bar{q}_3 & \frac{1}{2}\bar{q}_4 & -\frac{1}{2}\bar{q}_1 \\ -\frac{1}{2}\bar{q}_2 & \frac{1}{2}\bar{q}_1 & \frac{1}{2}\bar{q}_4 \\ -\frac{1}{2}\bar{q}_1 & -\frac{1}{2}\bar{q}_2 & -\frac{1}{2}\bar{q}_3 \\ 0 & 0 & 0 \\ 0 & 0 & 0 \\ 0 & 0 & 0 \end{array} \right]$$

$$Aq_k =$$

$$\left[\begin{array}{cccc} 0 & 0 & 0 & 0 \\ 0 & 0 & 0 & 0 \\ 0 & 0 & 0 & 0 \\ w_0\bar{q}_1\bar{q}_3 & \frac{\bar{w}_{IB_3}^B}{2} + w_0\bar{q}_2\bar{q}_3 & -\frac{\bar{w}_{IB_2}^B}{2} + \frac{w_0}{2}(1+2\bar{q}_3^2) & \frac{\bar{w}_{IB_1}^B}{2} + w_0\bar{q}_3\bar{q}_4 \\ -\frac{\bar{w}_{IB_3}^B}{2} + w_0\bar{q}_1\bar{q}_4 & w_0\bar{q}_2\bar{q}_4 & \frac{\bar{w}_{IB_1}^B}{2} + w_0\bar{q}_3\bar{q}_4 & \frac{\bar{w}_{IB_2}^B}{2} - \frac{w_0}{2}(1+2\bar{q}_1^2) \\ \frac{\bar{w}_{IB_2}^B}{2} - \frac{w_0}{2}(1+2\bar{q}_1^2) & -\frac{\bar{w}_{IB_1}^B}{2} - w_0\bar{q}_1\bar{q}_2 & -w_0\bar{q}_1\bar{q}_3 & \frac{\bar{w}_{IB_3}^B}{2} - w_0\bar{q}_1\bar{q}_4 \\ -\frac{\bar{w}_{IB_1}^B}{2} - w_0\bar{q}_1\bar{q}_2 & -\frac{\bar{w}_{IB_2}^B}{2} - \frac{w_0}{2}(1+2\bar{q}_2^2) & -\frac{\bar{w}_{IB_3}^B}{2} - w_0\bar{q}_2\bar{q}_3 & -w_0\bar{q}_2\bar{q}_4 \\ 0 & 0 & 0 & 0 \\ 0 & 0 & 0 & 0 \\ 0 & 0 & 0 & 0 \end{array} \right]$$

$$Ahrw_k = [0_{10 \times 3}]$$

$$B_k =$$

$$\begin{bmatrix} I_{S_x}^{-1} & 0 & 0 & I_{S_x}^{-1} & 0 & 0 & I_{S_x}^{-1} & 0 & 0 \\ 0 & I_{S_y}^{-1} & 0 & 0 & I_{S_y}^{-1} & 0 & 0 & I_{S_y}^{-1} & 0 \\ 0 & 0 & I_{S_z}^{-1} & 0 & 0 & I_{S_z}^{-1} & 0 & 0 & I_{S_z}^{-1} \\ 0 & 0 & 0 & 0 & 0 & 0 & 0 & 0 & 0 \\ 0 & 0 & 0 & 0 & 0 & 0 & 0 & 0 & 0 \\ 0 & 0 & 0 & 0 & 0 & 0 & 0 & 0 & 0 \\ 0 & 0 & 0 & 0 & 0 & 0 & 0 & 0 & 0 \\ -1 & 0 & 0 & 0 & 0 & 0 & 0 & 0 & 0 \\ 0 & -1 & 0 & 0 & 0 & 0 & 0 & 0 & 0 \\ 0 & 0 & -1 & 0 & 0 & 0 & 0 & 0 & 0 \end{bmatrix}$$

$$H_k =$$

$$D_k = 0$$

The selected operating points for state vectors are hereafter and these points are selected assuming that the satellite behaves like an inverted pendulum:

- $\checkmark \quad \bar{W}_{IB}^B = [\bar{w}_{IB_1}^B \quad \bar{w}_{IB_2}^B \quad \bar{w}_{IB_3}^B]^T = [0 \quad 0 \quad 0]^T,$
- $\checkmark \quad \bar{q} = [\bar{q}_1 \quad \bar{q}_2 \quad \bar{q}_3 \quad \bar{q}_4]^T = [0 \quad 0 \quad 0 \quad 1]^T,$
- $\checkmark \quad \bar{H}_{RW}^B = [\bar{H}_{RW_1}^B \quad \bar{H}_{RW_2}^B \quad \bar{H}_{RW_3}^B]^T = [0 \quad 0 \quad 0]^T.$

The matrices around the operating points of state vector ($\bar{A}_k = A_k|_{\bar{w}_{IB}^B, \bar{q}, \bar{H}_{RW}^B}$), input vector ($\bar{B}_k = B_k|_{\bar{w}_{IB}^B, \bar{q}, \bar{H}_{RW}^B}$) and measurement vector ($\bar{H}_k = H_k|_{\bar{w}_{IB}^B, \bar{q}, \bar{H}_{RW}^B}$) are hereafter:

$$\bar{A}_k =$$

$$\begin{bmatrix} 0 & 0 & 0 & 0 & 0 & 0 & 0 & 0 & 0 & 0 \\ 0 & 0 & 0 & 0 & 0 & 0 & 0 & 0 & 0 & 0 \\ 0 & 0 & 0 & 0 & 0 & 0 & 0 & 0 & 0 & 0 \\ 0.5 & 0 & 0 & 0 & 0 & 0.0033 & 0 & 0 & 0 & 0 \\ 0 & 0.5 & 0 & 0 & 0 & 0 & 0.010 & 0 & 0 & 0 \\ 0 & 0 & 0.5 & -0.0033 & 0 & 0 & 0 & 0 & 0 & 0 \\ 0 & 0 & 0 & 0 & -0.0033 & 0 & 0 & 0 & 0 & 0 \\ 0 & 0 & 0 & 0 & 0 & 0 & 0 & 0 & 0 & 0 \\ 0 & 0 & 0 & 0 & 0 & 0 & 0 & 0 & 0 & 0 \\ 0 & 0 & 0 & 0 & 0 & 0 & 0 & 0 & 0 & 0 \end{bmatrix} \quad (4.106)$$

$$\bar{B}_k =$$

$$\begin{bmatrix} 0.1415 & 0 & 0 & 0.1415 & 0 & 0 & 0.1415 & 0 & 0 \\ 0 & 0.1439 & 0 & 0 & 0.1439 & 0 & 0 & 0.1439 & 0 \\ 0 & 0 & 0.1169 & 0 & 0 & 0.1169 & 0 & 0 & 0.1169 \\ 0 & 0 & 0 & 0 & 0 & 0 & 0 & 0 & 0 \\ 0 & 0 & 0 & 0 & 0 & 0 & 0 & 0 & 0 \\ 0 & 0 & 0 & 0 & 0 & 0 & 0 & 0 & 0 \\ 0 & 0 & 0 & 0 & 0 & 0 & 0 & 0 & 0 \\ -1 & 0 & 0 & 0 & 0 & 0 & 0 & 0 & 0 \\ 0 & -1 & 0 & 0 & 0 & 0 & 0 & 0 & 0 \\ 0 & 0 & -1 & 0 & 0 & 0 & 0 & 0 & 0 \end{bmatrix} \quad (4.107)$$

$$H_k =$$

$$\begin{bmatrix} 1 & 0 & 0 & 0 & 0 & 0 & 0 & 0 & 0 & 0 \\ 0 & 1 & 0 & 0 & 0 & 0 & 0 & 0 & 0 & 0 \\ 0 & 0 & 1 & 0 & 0 & 0 & 0 & 0 & 0 & 0 \\ 0 & 0 & 0 & 1 & 0 & 0 & 0 & 0 & 0 & 0 \\ 0 & 0 & 0 & 0 & 1 & 0 & 0 & 0 & 0 & 0 \\ 0 & 0 & 0 & 0 & 0 & 1 & 0 & 0 & 0 & 0 \\ 0 & 0 & 0 & 0 & 0 & 0 & 1 & 0 & 0 & 0 \\ 0 & 0 & 0 & 0 & 0 & 0 & 0 & 0 & 0 & 0 \\ 0 & 0 & 0 & 2 \begin{bmatrix} 0 \\ B_{Oz} \\ -B_{Oy} \end{bmatrix} & 2 \begin{bmatrix} -B_{Oz} \\ 0 \\ B_{Ox} \end{bmatrix} & 2 \begin{bmatrix} B_{Oy} \\ -B_{Ox} \\ 0 \end{bmatrix} & 2 \begin{bmatrix} B_{Ox} \\ B_{Oy} \\ B_{Oz} \end{bmatrix} & 0 & 0 & 0 \\ 0 & 0 & 0 & 2 \begin{bmatrix} SV_{Oz} \\ -SV_{Oy} \end{bmatrix} & 2 \begin{bmatrix} -SV_{Oz} \\ 0 \\ SV_{Ox} \end{bmatrix} & 2 \begin{bmatrix} SV_{Oy} \\ -SV_{Ox} \\ 0 \end{bmatrix} & 2 \begin{bmatrix} SV_{Ox} \\ SV_{Oy} \\ SV_{Oz} \end{bmatrix} & 0 & 0 & 0 \\ 0 & 0 & 0 & 2 \begin{bmatrix} 0 \\ r_{Oz} \\ -r_{Oy} \end{bmatrix} & 2 \begin{bmatrix} -r_{Oz} \\ 0 \\ r_{Ox} \end{bmatrix} & 2 \begin{bmatrix} r_{Oy} \\ -r_{Ox} \\ 0 \end{bmatrix} & 2 \begin{bmatrix} r_{Ox} \\ r_{Oy} \\ r_{Oz} \end{bmatrix} & 0 & 0 & 0 \\ 0 & 0 & 0 & 2 \begin{bmatrix} 0 \\ v_{Oz} \\ -v_{Oy} \end{bmatrix} & 2 \begin{bmatrix} -v_{Oz} \\ 0 \\ v_{Ox} \end{bmatrix} & 2 \begin{bmatrix} v_{Oy} \\ -v_{Ox} \\ 0 \end{bmatrix} & 2 \begin{bmatrix} v_{Ox} \\ v_{Oy} \\ v_{Oz} \end{bmatrix} & 0 & 0 & 0 \end{bmatrix} \quad (4.108)$$

H_k matrix still shows a dynamic characterization and therefore some assumptions can be made for the dynamically changed elements such as $\{B_o, SV_o, r_o, v_o\}$. This matrix is directly taken as a unit matrix for linear optimal controller design (LQR) in this study. The damping ratio ξ and natural frequency ω_n can be taken as -1 and 0.0057 or 0.0033 respectively for the linearized system with respect to the results of MATLAB “damp()” function.

4.4. Controllability of Satellite Model

If every state vector is transferred from any initial state to any desired state in a finite time period, this system is named as completely controllable. n is the dimension of A matrix ($n = 10$) and Q_C ($Q_C = [B \ AB \ \dots \ A^{n-1}B]$) is the controllability matrix :

$$Q_C = [B \ AB \ A^2B \ A^3B \ A^4B \ A^5B \ A^6B] \quad (4.109)$$

The designed satellite model is completely controllable [70]:

- ✓ The first six rows are linearly independent,
- ✓ Q_C matrix has full row rank $\Rightarrow \text{rank}(Q_C) = 10 = n$.

The measurements of star trackers and gyroscopes are sufficient to identify every state, and then the system is completely observable. Q_o is the observability matrix ($Q_o = [H^T \ A^T H^T \ \dots \ (A^{n-1})^T H^T]$):

$$Q_o = [H^T \ A^T H^T \ (A^2)^T H^T \ (A^3)^T H^T \ (A^4)^T H^T \ (A^5)^T H^T \ (A^6)^T H^T] \quad (4.110)$$

The given satellite model is completely state observable [70]:

- ✓ The first seven columns are linearly independent,
- ✓ Q_o matrix has full row rank $\Rightarrow \text{rank}(Q_o) = 10 = n$.

In conclusion, it can be said that the system model is both observable and controllable according to the relevant theorems.

4.5. Stability of Satellite Model

For a linear system $\dot{x}(t) = Ax(t) + Bu(t)$ with the state-feedback controller $u(t) = -Kx(t)$ the closed loop system becomes:

$$\checkmark \quad \dot{x}(t) = (A - BK)x(t)$$

The linear closed-loop system is said to be stabilizable if all the eigenvalues of $(A - BK)$ matrix has strictly negative real parts. The definition of satellite kinetic energy is determined like as below [4, 52]:

$$E_{KIN} = \frac{1}{2} (w_{OB}^B)^T I_S w_{OB}^B \quad (4.111)$$

The satellite potential energy is comprised of the energy of gravity gradient (E_{GG}) and the energy of gyroscopic motion (E_{GYRO}):

$$E_{GG} = \frac{3}{2} (w_0)^2 \left([(C_O^B)_3]^T I_S [(C_O^B)_3] - I_{S_z} \right) \quad (4.112)$$

$$E_{GYRO} = \frac{1}{2} (w_0)^2 \left(I_{S_x} - [(C_O^B)_1]^T I_S [(C_O^B)_1] \right) \quad (4.113)$$

- ✓ $(C_O^B)_1 = [C_{11}, C_{21}, C_{31}]^T$ is the first column of transformation matrix,
- ✓ $(C_O^B)_3 = [C_{13}, C_{23}, C_{33}]^T$ is the third column of transformation matrix.

The total energy (E_{TOT}) that is the sum of kinetic (E_{KIN}) and potential energy (E_{POT}) defined above can be selected as Lyapunov candidate function ($V(x)$):

$$V(x) = E_{TOT} = E_{KIN} + E_{POT} = E_{KIN} + E_{GG} + E_{GYRO} \quad (4.114)$$

$$\begin{aligned}
V(x) &= \frac{1}{2} \cdot (w_{OB}^B)^T I_S w_{OB}^B \\
&+ \frac{3}{2} (w_0)^2 \cdot \left(I_{S_x}(C_{13})^2 + I_{S_y}(C_{23})^2 + I_{S_z}((C_{33})^2 - 1) \right) \\
&+ \frac{1}{2} (w_0)^2 \left(I_{S_x}(1 - (C_{11})^2) + I_{S_y}(C_{21})^2 + I_{S_z}(C_{31})^2 \right)
\end{aligned} \tag{4.115}$$

The new definition of Lyapunov function by considering the following statements about matrix elements is:

- ✓ $(C_{13})^2 + (C_{23})^2 + (C_{33})^2 = 1 \rightarrow (C_{33})^2 = 1 - (C_{13})^2 - (C_{23})^2$
- ✓ $(C_{11})^2 + (C_{21})^2 + (C_{31})^2 = 1 \rightarrow (C_{11})^2 = 1 - (C_{21})^2 - (C_{31})^2$

$$\begin{aligned}
V(x) &= \frac{1}{2} (w_{OB}^B)^T I_S w_{OB}^B \\
&+ \frac{3}{2} (w_0)^2 \left((I_{S_x} - I_{S_z})(C_{13})^2 + (I_{S_y} - I_{S_z})(C_{23})^2 \right) \\
&+ \frac{1}{2} (w_0)^2 \left((I_{S_x} - I_{S_y})(C_{21})^2 + (I_{S_x} - I_{S_z})(C_{31})^2 \right)
\end{aligned} \tag{4.116}$$

The state vector of $V(x)$ can be taken as $x = [w_{OB}^B, C_{13}, C_{23}, C_{21}, C_{31}]^T$. For stability theorem, assuming that ($x = 0$) is an equilibrium point for $\dot{x} = f(x)$ and $V(x)$ is a continuously differentiable function such that;

- ✓ $V(0) = 0 ; V(x) > 0$ in $D - \{0\} ; D \subset R^N$
- ✓ $\dot{V}(x) \leq 0$ in $D \rightarrow x = 0$ is stable
- ✓ $\dot{V}(x) < 0$ in $D - \{0\} \rightarrow x = 0$ is asymptotically stable

Satellite inertia moments must have the sequence of $I_{S_x} > I_{S_y} > I_{S_z}$ in order to meet the first requirement relating about the positive definition of Lyapunov candidate function ($V(x) > 0$). However, its sorting is $I_{S_z} > I_{S_x} > I_{S_y}$ in the selected satellite

and therefore the abovementioned limitation is not satisfied. The derivative of $V(x) = E_{TOT}$ is herein below with respect to [4] and [52, 75]:

$$\begin{aligned}\dot{V}(x) &= I_S w_{OB}^B + 3(w_0)^2 \left((I_{S_x} - I_{S_z}) C_{13} + (I_{S_y} - I_{S_z}) C_{23} \right) \\ &\quad + (w_0)^2 \left((I_{S_x} - I_{S_y}) C_{21} + (I_{S_x} - I_{S_z}) C_{31} \right)\end{aligned}\tag{4.117}$$

The compact form of the derivative function is hereafter [71, 75]:

$$\dot{V}(x) = (w_{OB}^B)^T M_{cmd}\tag{4.118}$$

This definition can be used to prove some attitude controllers are asymptotically stable such as PID and linear quadratic regulator. On the other hand, it is required to declare another Lyapunov function to show that sliding mode controller has also stable behavior:

$$V(q) = (q_v)^T q_v + (1 - q_4)^2\tag{4.119}$$

4.6. Satellite Attitude Estimation with Kalman Filters

The Kalman Filter is a Bayesian estimation algorithm and designed as an optimal state estimator. It is used when the variables of interest are measured indirectly and the system measurements are available from various sensors. Kalman filter is an iterative process that it predicts the system states such as position, velocity or attitude vectors together with instrument errors, such as accelerometer and gyro biases in a recursive way. It also updates the uncertainties in state estimates with the help of integrating a stream of latest measurements [52, 59].

In Kalman filter equations, the initial values of the state vectors and covariance matrix are generally set to constant values. The iteration process is maintained by

calculating the weighted average of the previous measurement values. The time variation of noise sources can be modelled using the white noise processing method. The samples taken at different times are uncorrelated for white noise signals and its variance is assumed to have zero-mean Gaussian distribution.

4.6.1. Kalman Filter Algorithm

Kalman filter algorithm uses measurement system models to maintain optimal state estimates. In the absence of new measurements, state uncertainties increase with time and state estimates go out of date, because of the unknown changes defined as system noise. Kalman filter algorithm consists of system and measurement propagation phases.

The system propagation phase: In this phase, state vector and system noise covariance matrix are predicted from the time of the last valid measurements. This phase consists of the following steps (the estimated state vector is \hat{x}_k and its propagation is \hat{x}_{k+1}^-):

1. Calculation of the transition matrix (Φ_k) which defines state vector changes with time and it is calculated every iteration,
2. Calculation of the system noise covariance matrix (Q_k) which defines the degree of correlation between errors of state estimates,
3. Propagation of the state vector estimation (\hat{x}_{k+1}^-) from \hat{x}_k^+ ,
4. Propagation of the error covariance matrix (P_{k+1}^-) from P_k^+ ,

Its diagonal terms are the variances of each state estimate and its off-diagonal terms are the correlations between errors of state estimates.

The measurement propagation phase: Measurement vector is iterated by updating state estimates to incorporate the measurement data weighted with the Kalman gain. Noise covariance matrix (R_k) is also iterated by updating error covariance matrix (P_k) to find the new values. The phase is including the steps listed below:

1. Calculation of measurement matrix (H_k),
2. Calculation of measurement noise covariance matrix (R_k) which its diagonal terms represent the variances of each measurement vector,
3. Calculation of Kalman gain matrix (K_k),
4. Updating of state vector estimate (\hat{x}_k^+) from \hat{x}_k^- ,
5. Updating of error covariance matrix (P_k^+) from P_k^- .

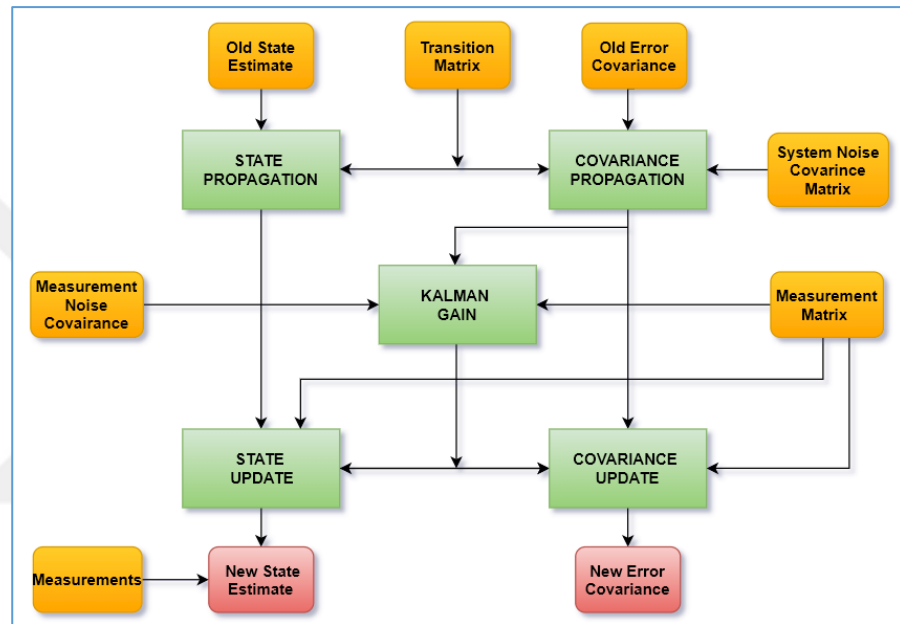


Figure 4-2 The Diagram of Kalman Filter Algorithm

The system responses and outputs of both linear and extended Kalman filters are illustrated in the following figures in the case of using gyroscopes and star trackers as attitude sensors for different process and noise covariance matrices. The Kalman filter basic equations are listed in the following table:

Table 4-1 The Equations of Kalman Filter Algorithm

Parameter	Definition
System Model	$\hat{x}_{k+1} = \Phi_k \cdot \hat{x}_k + \Gamma_k \cdot u_k + G_k \cdot w_k ; \quad w_k \sim N(0, Q_k)$

Parameter	Definition
Measurement Model	$\tilde{y}_k = H_k \cdot \hat{x}_k + v_k ; v_k \sim N(0, R_k)$
R_k	$E\{v_k \cdot v_j^T\} = R_k \cdot \delta_{kj} \rightarrow R_k = E\{v_k \cdot v_k^T\}; \text{when } k=j$
Q_k	$E\{w_k \cdot w_j^T\} = Q_k \cdot \delta_{kj} \rightarrow Q_k = E\{w_k \cdot w_k^T\}; \text{when } k=j$
Kalman Gain	$K_k = P_k^- \cdot H_k^T \cdot [H_k \cdot P_k^- \cdot H_k^T + R_k]^{-1}$
Update State Estimate (\hat{x}_k^+) Error Covariance (P_k^+)	$\hat{x}_k^+ = \hat{x}_k^- - K_k \cdot [\tilde{y}_k - H_k \cdot \hat{x}_k^-]$ $P_k^+ = [I - K_k \cdot H_k] \cdot P_k^-$ $P_k^+ = E\{(\hat{x}_k^+ - x_k) \cdot (\hat{x}_k^+ - x_k)^T\}$
Propagation State Estimate (\hat{x}_{k+1}^-) Error Covariance (P_{k+1}^-)	$\hat{x}_{k+1}^- = \Phi_k \cdot \hat{x}_k^+ + \Gamma_k \cdot u_k$ $P_{k+1}^- = \Phi_k \cdot P_k^+ \cdot \Phi_k^T + G_k \cdot Q_k \cdot G_k^T$ $P_{k+1}^- = E\{(\hat{x}_{k+1}^- - x_{k+1}) \cdot (\hat{x}_{k+1}^- - x_{k+1})^T\}$

The following test results are obtained from both Linear and Extended Kalman filter blocks placed in satellite model.

Case - 1: No RW Failure & PID Controller

Table 4-2 The Simulation Parameters of State Estimation (Case-1)

Parameters	Values
Initial satellite velocity	$w_0 = [0.1, 0.1, 0.1]$
Initial / Desired Euler Angles (Roll, Pitch, Yaw = $[\psi, \theta, \phi]$)	$[\psi_0, \theta_0, \phi_0] = [0, 0, 0]$ $[\psi_d, \theta_d, \phi_d] = [20, 10, 3]$
System Noise Covariance Matrix	$Q_k = 1 \times 10^{-7}$
Measurement Noise Covariance Matrix	$R_{gyro} = 1 \times 10^{-7}; R_{str} = 1 \times 10^{-7}$

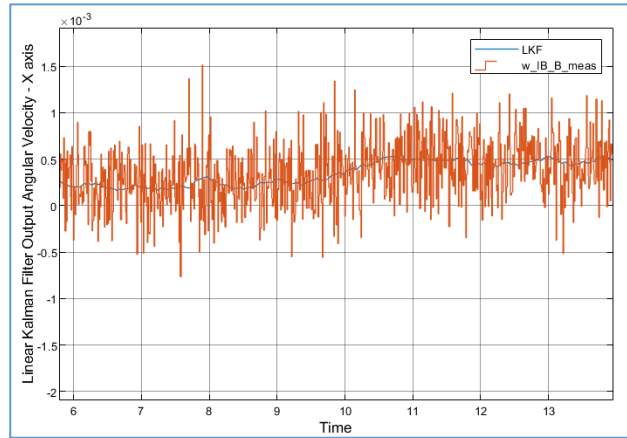


Figure 4-3 LKF Output For Satellite Angular Velocity of PID (Case-1)

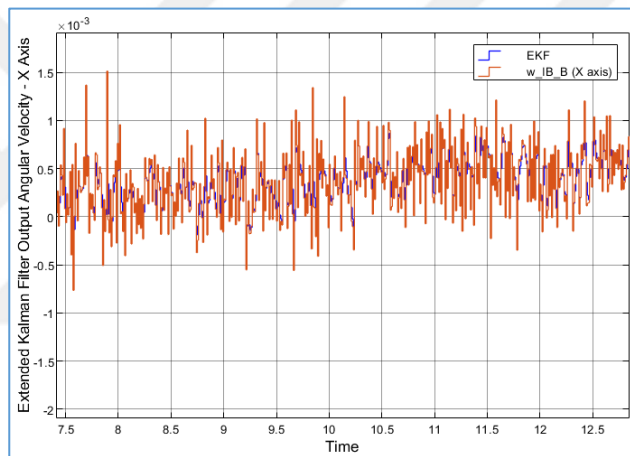


Figure 4-4 EKF Output For Satellite Angular Velocity of PID (Case-1)

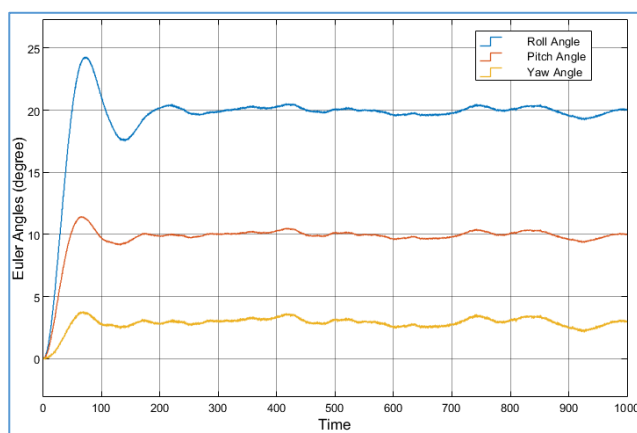


Figure 4-5 Euler Angler Response of PID (Case-1)

In the next case, the same simulation parameters are handled like listed in the Table 4-2, but using with different covariance matrices.

Case - 2: No RW Failure & PID Controller

Table 4-3 The Simulation Parameters of State Estimator (Case-2)

Parameters	Values
System Noise Covariance Matrix	$Q_k = 1 \times 10^{-10}$
Measurement Noise Covariance Matrix	$R_{gyro} = 1 \times 10^{-10}; R_{str} = 1 \times 10^{-10}$

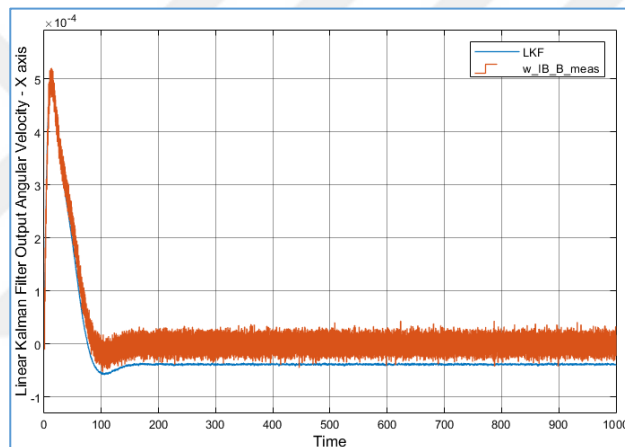


Figure 4-6 LKF Output For Satellite Angular Velocity of PID (Case-2)

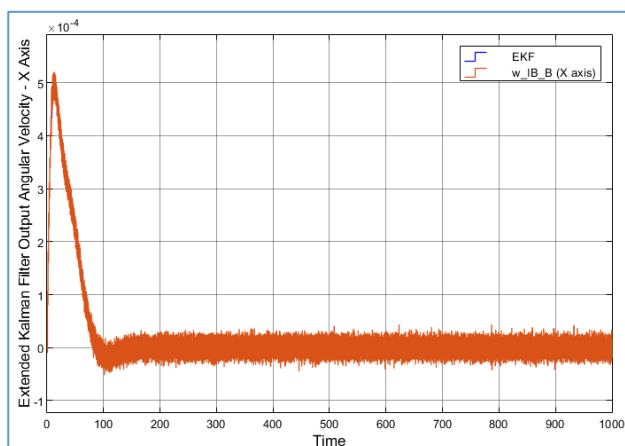


Figure 4-7 EKF Output For Satellite Angular Velocity of PID (Case-2)

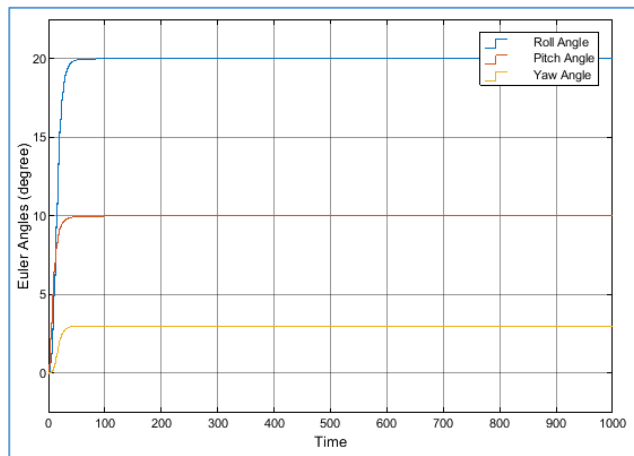


Figure 4-8 Euler Angles Response of PID (Case-2)

In conclusion, the estimated measurements taken from the outputs of Extended Kalman filter have higher accuracies than the results of Linear Kalman filter.

4.7. Summary

The implementation of linearization process on the nonlinear state-space equations was detailed in this chapter. Furthermore, Lyapunov based system stability, controllability and observability conceptions which are specific to the selected satellite were analyzed. Both Linear and Extended Kalman filters were also mentioned as a navigation solution for the usage of estimated sensor measurements.

CHAPTER 5

SATELLITE ATTITUDE CONTROL

5.1. Introduction

The most common sources of control torques for active control systems are propulsion subsystems with thrusters, magnetic torque rods and reaction wheels. Beyond these control torque sources, there is also environmental disturbance torques [3, 4, 5] effecting adversely on attitude control processing.

The controller design targets to provide stability and robustness to the modelled system, to reject the disturbances arising from environmental effects, to avoid actuator saturation and to perform attitude maneuvers by keeping the satellite pointed in the right direction [53, 54]. Most of the cases, all these targets cannot be achieved simultaneously. Therefore, it is mandatory to apply some optimization process on system controller design according to the matter in hand.

Control system output is the measurement to demonstrate the controller status and effectiveness. The controller design performance depends on stability, sensitivity, disturbance and noise rejection and robustness for system uncertainties. It stabilizes and orients the satellite in any direction relative to reference frames [21].

The fundamental concept of a closed loop control system relies on sensor measurements; the measured attitude and its comparison with the desired attitude drive controller process. The numerical differences between these two values result in error signals used to achieve the desired attitude and corrective control torques are generated by means of actuators in positive or negative axis relative to satellite body axes [66].

Attitude maneuvers are necessary to reorient the axes of attitude sensors to some special celestial objects in initial phase or after a failure. Maneuvering capabilities are also essential to give a new direction to the axes of payloads. This new direction can be the coordinates of ground targets sent with telecommands as reference coordinates from ground station to Earth imaging satellites.

Attitude control can be achieved by controlling the angular accelerations, which are internal torques and external torques (magnetic or reaction torques) exerted on the satellite. In common cases, the momentum and angular acceleration of wheels are transformed to satellite to meet the required opposite torque for attitude stability.

The primary task of attitude control is to stabilize the satellite attitude against external torque disturbances and it requires attitude maneuvers based on control torques throughout its lifetime. Because of this reason, control law equations applied in different ways are explained at the beginning of this section.

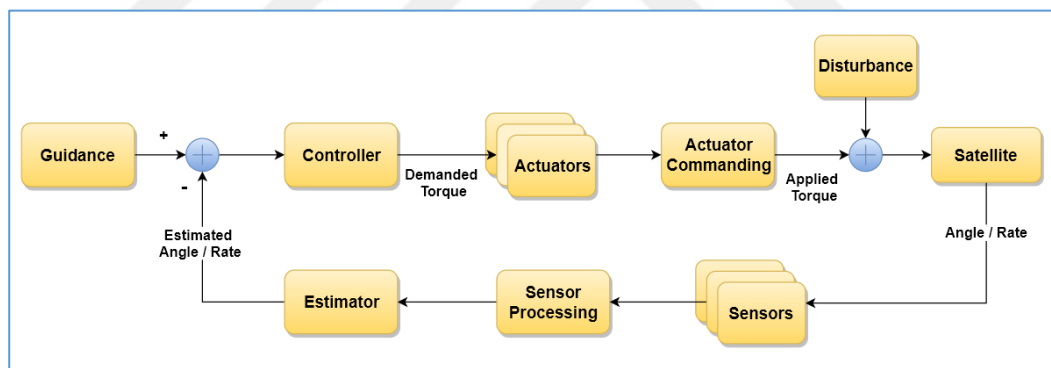


Figure 5-1 Satellite Attitude Control Loop [46]

In a satellite attitude controller system, the measurements obtained from system plant are observed continuously and compared with the desired position given as an initial step. The difference between the measured and desired position values is called as system error and used to generate control torque command [53, 66]. In general, system error is defined with Euler angles for small attitude maneuvers. On

the other hand, it can be written in quaternion vector form for large attitude maneuvers [1, 2].

Basically, a mathematical model of a satellite attitude control consists of an amplifier model as a controller gain, DC motor model for each reaction wheels and a plant model indicating motion equations [69].

In the first step, a mathematical model of a satellite with its actuators were developed using angular dynamic and kinematic equations in the previous sections. The controller is applied to deal with nonlinearities, unknown parameters and disturbance sources in these equations. The controller also receives the offset from the desired position in a quaternion vector form, and propagates the control torque command (M_{cmd}) as an output to system actuators.

A nonlinear satellite model is essential for the controller types of PID and sliding mode. On the other side, LQR controller is needed to operate together with the linearized form of a satellite nonlinear model.

5.2. Detumbling Control

The main purpose of detumbling controller called also B-dot controller is to slow down the initial rotational motion (E_{KIN}) of a satellite and to minimize the changes in its angular velocity to maintain stabilization in three axis. Magnetometer measurements are implemented by B-dot controller in order to fulfill these conditions after deployment [71, 72].

B-dot controller only responds to the changes in Earth magnetic field vector defined in Body Frame (B^B). Lyapunov candidate function can be taken as kinetic energy function as stated below [73, 75, 82]:

$$\dot{V} = \dot{E}_{KIN} = (w_{IB}^B)^T M_C^{MTR} \quad (5.1)$$

$$\dot{V} = \dot{E}_{KIN} = (w_{IB}^B)^T (m^B \times B^B) \quad (5.2)$$

$$\dot{V} = \dot{E}_{KIN} = -(w_{IB}^B)^T (B^B \times m^B) \quad (5.3)$$

Using the theorem of $A^T(B \times C) = C^T(A \times B)$, the last equation can be rewritten:

$$\dot{V} = \dot{E}_{KIN} = -(m^B)^T (w_{IB}^B \times B^B) < 0 \quad (5.4)$$

The last inequality can be resolved as stated below [79]:

$$m^B = K_{Bdot} (w_{IB}^B \times B^B) = \frac{K_{Bdot} (w_{IB}^B \times B^B)}{\|B^B\|} \quad (5.5)$$

- ✓ m^B is the magnetic control output moment,
- ✓ K_{Bdot} is a positive definite control gain,
 - If K_{Bdot} is too low → satellite angular velocity cannot be reduced,
 - If K_{Bdot} is too high → system is too sensitive and unstable,
- ✓ \dot{B}^B is the time derivative of measured local magnetic field and it represents the changes in this field.

K_{Bdot} gain has an important role to specify detumbling time, system stability and sensitivity. In the reference article of [79], the simulation results exhibit that the more controller gain is large, the more settling time is short. However, there are also possibilities to cause disturbances on controllers according to the bias moments in this case.

The changes in B-field vector are derived from both the satellite motions and Earth rotations. The time derivative of magnetic field vector (\dot{B}^B) is perpendicular to the vector of rotations and it cannot be directly measured from any sensors in the satellite. The controller is implemented by applying a magnetic torque in the

opposite direction of the rate of local magnetic field change with the following equations [54, 81]:

$$\dot{B}^B = \frac{dB^B}{dt} \Big|_{B^B} = \left(\frac{dB^B}{dt} \right) - w_{IB}^B \times B^B \approx -w_{IB}^B \times B \quad (5.6)$$

$$m^B = \frac{K_{Bdot}(w_{IB}^B \times B^B)}{\|B^B\|} = \frac{-K_{Bdot}\dot{B}^B}{\|B^B\|} \quad (5.7)$$

The geometric definition for B-field vector is illustrated hereafter:

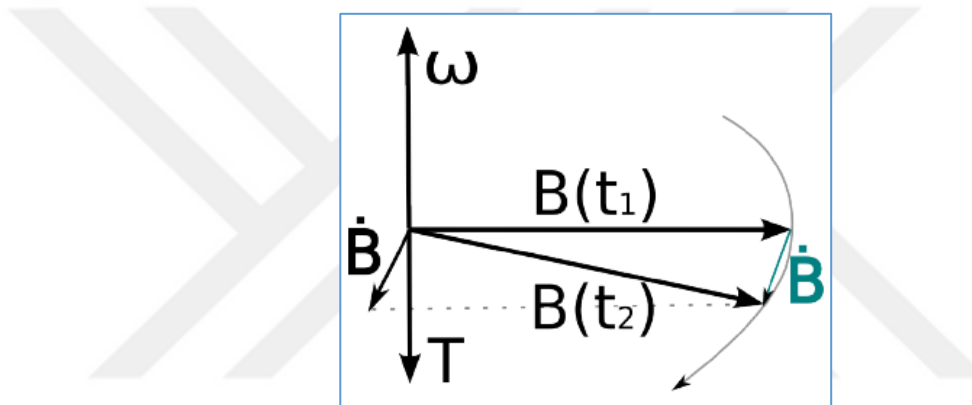


Figure 5-2 The Geometric Definition of Local Magnetic Field (B) [72]

The simulation time of detumbling controller is constrained with respect to the magnetic moment capacity of torque rods and it is in the range of $\mp 6.0 \text{ Am}^2$ for the selected satellite [81]. The control torque will be:

$$M_c^{MTR} = m^B \times B^B = \frac{-K_{Bdot}\dot{B}^B}{\|B^B\|} \times B^B \quad (5.8)$$

When B-dot controller is applied to torque rods, they generate magnetic dipole moment and magnetic torque in the opposite direction of local magnetic field vector. After performing a control command to a satellite system, its kinetic energy decreases over time and its angular velocity reaches up to zero for each axis [71, 72].

5.3. Desaturation Control

The disturbance torques arising from gravitational and aerodynamic effects lead to accumulate unwanted angular momentum on reaction wheels over time. This momentum must be desaturated by torque rods interacting with Earth magnetic field to apply an external torque in the reverse direction. After reaching their predefined saturation limit, reaction wheels are not be able to create the control torque which is necessary to orient the satellite to a desired attitude [73, 78]. In addition to this, the angular velocity of reaction wheels can be taken to an acceptable level (operating range) by the help of momentum dumping [66].

In some academic studies [80], both main attitude controller and desaturation controller are formulated in a single problem. However, the operation of momentum unloading is accomplished separately in this study as shown in the following diagram:

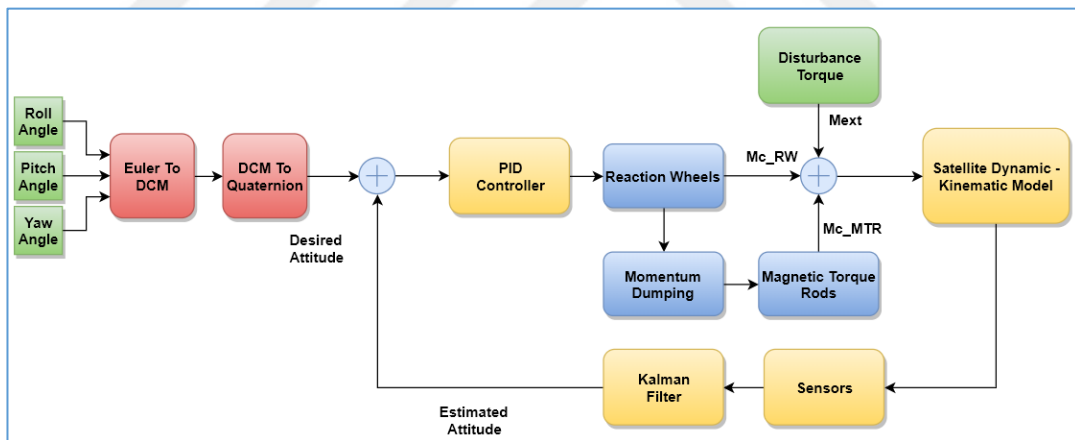


Figure 5-3 Satellite Attitude Control with Momentum Dumping

The magnetic torque depends on the angle between Earth magnetic field vector and angular momentum vector. It has the maximum value when these vectors are completely perpendicular to each other and it is equal to zero value when they are in the same direction. The dipole moment can be calculated as stated below (K is a constant controller gain here):

$$m^B = -\frac{K_{MD}}{\|B^B\|} (B^B \times \Delta H_{RW}^B) \quad (5.9)$$

$$\Delta H_{RW}^B = H_{RW,nom}^B - H_{RW,sim}^B \quad (5.10)$$

ΔH_{RW}^B is the bias error between the nominal ($H_{RW,nom}^B$) and simulated wheel angular momentum ($H_{RW,sim}^B$) and it must be kept at a minimum value. If error vector is parallel to B-field vector in Body Frame, it is not possible to unload the unnecessary angular momentum from wheels. If they are lying in an orthogonal plane, desaturation is performed entirely [73]. In this circumstance, the desaturation control torque is written like as follow:

$$M_C^{MTR} = m^B \times B^B = K_{MD} \frac{(\Delta H_{RW}^B \times B^B)}{\|B^B\|^2} \quad (5.11)$$

Momentum dumping maintains a stable attitude as long as the main controller shows a stable behavior. It can be proposed that the desaturation controller can be deactivated whenever redundant angular momentum is completely unloaded.

5.4. PID Control

5.4.1. PD Controller for Satellite

PD controller can be used to change the satellite orientation according to the desired reference values specified as roll, pitch and yaw angles. It is proportional to the position error and its derivative in a PD controller.

The selected satellite is a kind of light weight microsatellite and the elements of its inertia matrix have comparatively small values. Because of this reason, the following command torque equation (M_{cmd}) can be found by taking into account the stability

requirement of Lyapunov candidate function $\dot{V}(x) < 0$ which is mentioned in the section called “Stability of Satellite Model”:

$$M_{cmd} = -K_P q_{v,err} q_{err,4} - K_{PD} w_{IB}^B \quad (5.12)$$

$$\begin{bmatrix} M_{cmd,x} \\ M_{cmd,y} \\ M_{cmd,z} \end{bmatrix} = \begin{bmatrix} -K_{P,x} q_{err,1} q_{err,4} - K_{PD,x} w_{IB_x}^B \\ -K_{P,y} q_{err,2} q_{err,4} - K_{PD,y} w_{IB_y}^B \\ -K_{P,z} q_{err,3} q_{err,4} - K_{PD,z} w_{IB_z}^B \end{bmatrix} \quad (5.13)$$

- ✓ $q_{v,err}$ is the vector part of quaternion error ($q_{v,err} = [q_{err,1}; q_{err,2}; q_{err,3}]$),
- ✓ $q_{err,4}$ is the scalar part of quaternion error,
- ✓ K_P is the positive definite proportional gain constant,
- ✓ K_{PD} is the positive definite proportional and derivative gain constant.

Commanded torque can also be chosen one of the following equations. All these equations satisfy the asymptotically stability theorem [72]:

$$M_{cmd} = -K_P q_{v,err} q_{err,4} - K_{PD} w_{OB}^B \quad (5.14)$$

$$M_{cmd} = -K_P q_{v,err} q_{err,4} - K_{PD} \dot{q}_{err} \quad (5.15)$$

$$M_{cmd} = -K_P q_{v,err} - K_{PD} w_{IB}^B + I_S \dot{w}_{IB}^B + w_{IB}^B \times I_S w_{IB}^B \quad (5.16)$$

The gain matrices K_P and K_{PD} shall be selected to be compatible with asymptotically stable. Attitude error value demonstrates the required rotation for each satellite axes to arrive the commanded orientation. This error vector (q_{err}) is calculated by multiplying the reference quaternion (q_{ref}) and estimated quaternion vectors with its conjugate definition (q_{est}^*). If this kind of multiplication is considered as a transition from a current state to an expected state, it can be denoted by these equations:

$$q_{ref} = q_{est}^{ref} q_{est} \quad (5.17)$$

$$q_{ref} q_{est}^{-1} = (q_{est}^{ref} q_{est}) q_{est}^{-1} \rightarrow q_{ref} q_{est}^{-1} = q_{est}^{ref} \quad (5.18)$$

The inverse of a quaternion vector (q_{est}^{-1}) is equal to its conjugate equivalent (q_{est}^*). By means of this equality, a quaternion error vector can be accepted as the transition vector which is specified above ($q_{est}^{ref} \approx q_{err}$):

$$q_{est}^{-1} = \frac{q_{est}^*}{|q_{est}|^2} = q_{est}^* = [-q_{est,1}; -q_{est,2}; -q_{est,3}; q_{est,4}]^T \quad (5.19)$$

$$q_{err} = q_{ref} \otimes q_{est}^* = q_{est}^* \odot q_{ref} \quad (5.20)$$

$$q_{err} = \begin{bmatrix} q_{err,1} \\ q_{err,2} \\ q_{err,3} \\ q_{err,4} \end{bmatrix} = \begin{bmatrix} q_{ref,4} & q_{ref,3} & -q_{ref,2} & q_{ref,1} \\ -q_{ref,3} & q_{ref,4} & q_{ref,1} & q_{ref,2} \\ q_{ref,2} & -q_{ref,1} & q_{ref,4} & q_{ref,3} \\ -q_{ref,1} & -q_{ref,2} & -q_{ref,3} & q_{ref,4} \end{bmatrix} \begin{bmatrix} -q_{est,1} \\ -q_{est,2} \\ -q_{est,3} \\ q_{est,4} \end{bmatrix} \quad (5.21)$$

The following definition also gives the same results for an attitude error (q_{err}):

$$q_{err} = \begin{bmatrix} q_{err,1} \\ q_{err,2} \\ q_{err,3} \\ q_{err,4} \end{bmatrix} = \begin{bmatrix} q_{est,4} & q_{est,3} & -q_{est,2} & -q_{est,1} \\ -q_{est,3} & q_{est,4} & q_{est,1} & -q_{est,2} \\ q_{est,2} & -q_{est,1} & q_{est,4} & -q_{est,3} \\ q_{est,1} & q_{est,2} & q_{est,3} & q_{est,4} \end{bmatrix} \begin{bmatrix} q_{ref,1} \\ q_{ref,2} \\ q_{ref,3} \\ q_{ref,4} \end{bmatrix} \quad (5.22)$$

The derivative of quaternion error vector is [48]:

$$\dot{q}_{err} = \begin{bmatrix} \dot{q}_{err,1} \\ \dot{q}_{err,2} \\ \dot{q}_{err,3} \\ \dot{q}_{err,4} \end{bmatrix} = \begin{bmatrix} q_{err,4} & -q_{err,3} & q_{err,2} & q_{err,1} \\ q_{err,3} & q_{err,4} & -q_{err,1} & q_{err,2} \\ -q_{err,2} & q_{err,1} & q_{err,4} & -q_{err,3} \\ -q_{err,1} & -q_{err,2} & -q_{err,3} & q_{err,4} \end{bmatrix} \begin{bmatrix} w_{IB_x}^B \\ w_{IB_y}^B \\ w_{IB_z}^B \end{bmatrix} \quad (5.23)$$

5.4.2. PID Controller for Reaction Wheels DC Motor

The goal of attitude controller is to change the rotational speed of reaction wheels to adjust the satellite orientation to meet the desired course. This means that the angular velocities of RWs shall be changed to meet the desired performance specifications.

The chosen controller law for each reaction wheels is PID controller in a cascaded form. The derivative controller is especially set to keep a constant rotation speed until the command torque is received. The fundamental equations of reaction wheel torque dynamics are hereafter:

$$M_M = k_t i = I_{RW} \dot{w}_{RW} + b w_{RW} \quad (5.24)$$

$$M_M(s) = k_t I(s) = (I_{RW}s + b)w_{RW}(s) \quad (5.25)$$

After taking the Laplace transformation for the voltage equation of reaction wheels ($V_A = Ri + L(di/dt) + k_M w_{RW}$), the following equation is obtained:

$$V(s) = (R + Ls)I(s) + k_M w_{RW}(s) ; w_{RW}(s) = \frac{k_t I(s)}{I_{RW}s + b} \quad (5.26)$$

$$V(s) = \frac{(R + Ls)(I_{RW}s + b) + k_M k_t}{I_{RW}s + b} I(s) \quad (5.27)$$

$$\frac{I(s)}{V(s)} = \frac{I_{RW}s + b}{(L I_{RW})s^2 + (R I_{RW} + Lb)s + (Rb + k_M k_t)} \quad (5.28)$$

The cascaded PI controller design arises from the control of two sequential processes where the output of the inner loop supplies the outer process in the sequence. The main objective of cascaded control is to attenuate the effect of internal disturbances on final output measurements.

The data flow is illustrated in the following figure:

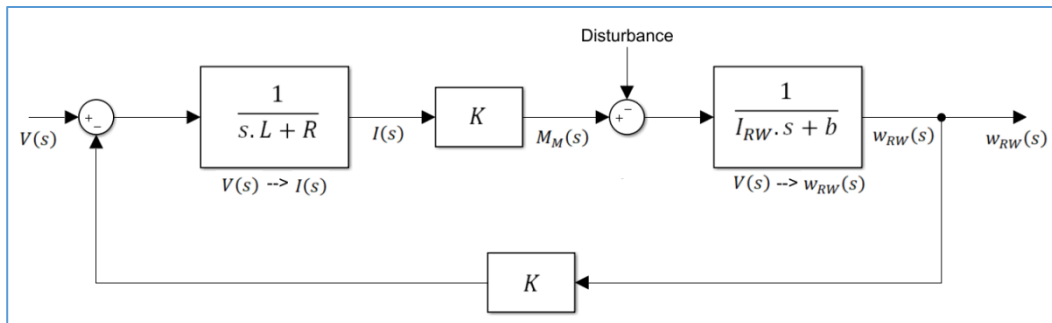


Figure 5-4 The Data Diagram of RW DC Motor

In general, the results of cascaded controller are better than a single loop controller system. The inner loop reduces the gain uncertainty of whole system with the help of inner loop processing. The general diagram of cascaded PID controllers is indicated:

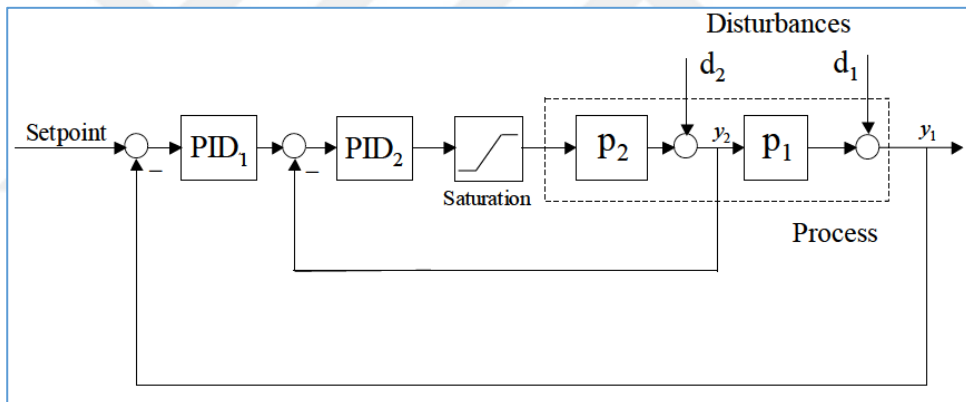


Figure 5-5 Cascade PID Controller General Diagram [85]

It is necessary to implement a couple of saturation blocks into the simulation model to restrict the torque and rotation speed of reaction wheels. The following figure shows a cascaded inner (PI) and outer (PID) controller design for each reaction wheels:

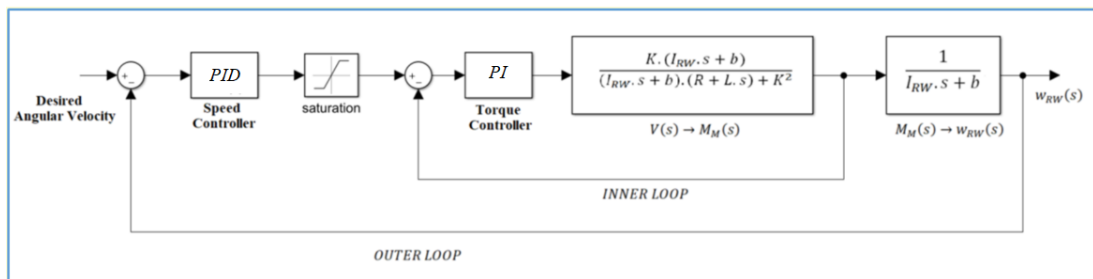


Figure 5-6 Inner and Outer Loop of Cascade PI Controllers for RW-DC motors

For the torque controller loop (inner loop), the last equation can be written in terms of the torque definition specified above:

$$I(s) = \frac{M_M(s)}{k_t}; \quad w_{RW}(s) = \frac{M_M(s)}{I_{RW}s + b} \quad (5.29)$$

$$V(s) = (R + Ls) \left(\frac{M_M(s)}{k_t} \right) + k_M \left(\frac{M_M(s)}{I_{RW}s + b} \right) \quad (5.30)$$

If assumed that the coefficients k_t and k_M have equal values ($k_t = k_M = K$) and the damping ratio (b) is relatively small to be implemented, the transfer function of inner loop will be:

$$\frac{M_M(s)}{V(s)} = \frac{K(I_{RW}s + b)}{(I_{RW}s + b)(R + Ls) + K^2} \quad (5.31)$$

The open-loop plant function which is a transfer function of speed controller loop (outer loop) representing the transition from voltage input to angular speed output is:

$$\frac{w_{RW}(s)}{V(s)} = \frac{M_M(s)}{V(s)} \frac{w_{RW}(s)}{M_M(s)} = \frac{K}{(I_{RW}s + b)(R + Ls) + K^2} \quad (5.32)$$

The following parameters are defined for the modelling of each DC motor:

Table 5-1 Reaction Wheel - DC Motor Parameters

RW- DC Motor Parameters	Values
DC Motor Electromotive Force Constant (k_M)	0.1 V/rad/sec
DC Motor Torque Constant (k_t)	0.1 N.m/Amp
DC Motor Viscous Friction Constant (b)	$1 \times 10^{-5} \text{ Nms}$
Armature Resistance (R)	2 Ohms
Armature Inductance (L)	$5.2 \times 10^{-3} \text{ H}$
Moment of Inertia (I_{RW})	$5.0 \times 10^{-4} \text{ kgm}^2$

The design requirements are listed below for a reference motor speed (1 rad/s step):

- ✓ Settling time shall be less than 3 seconds (< 3 s),
- ✓ Overshoot level shall be less than 5% (< 5%),
- ✓ Steady-state error shall be less than 1% (< 1%).

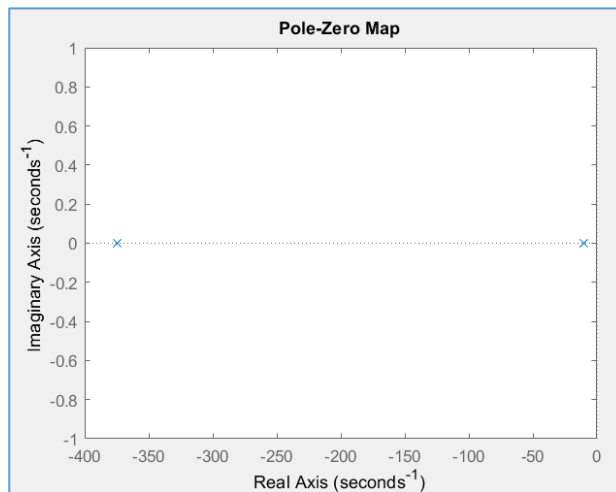


Figure 5-7 The Open Loop Pole-Zero Map of Reaction Wheel DC Motor

According to the pole locations of transfer function (-374.3404, -10.29) in the pole-zero map diagram, there is no overshoot in the step response. The more negative pole dominates the system dynamics in terms of the response speed.

The following Simulink diagrams show all the DC motor models of reaction wheels and the commanded torque distribution for each of them:

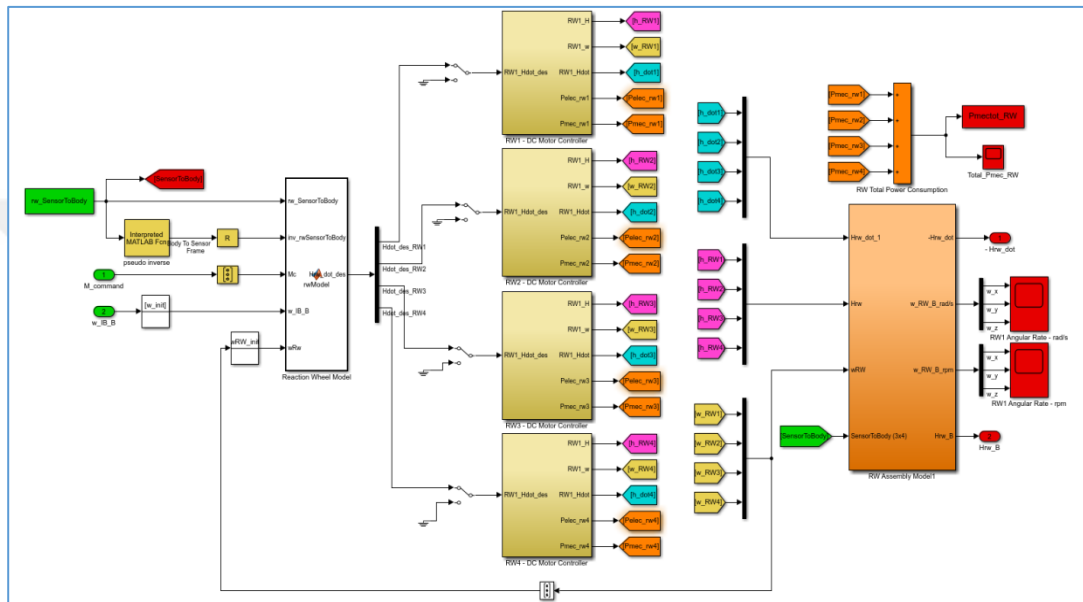


Figure 5-8 Reaction Wheels Model Block Diagram

The DC motor model of each reaction wheel placed in the previous figure is:

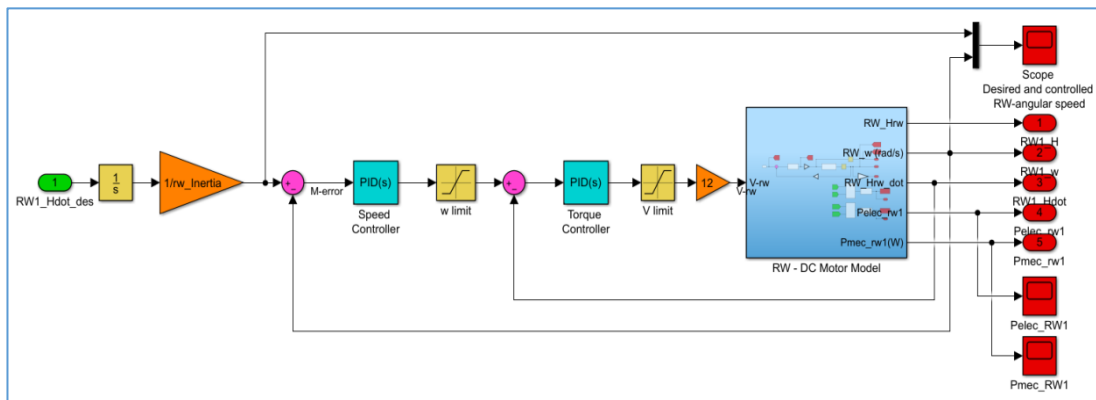


Figure 5-9 The Simulink Diagram of RW – DC Motors

The operating frequency of inner loop shall have larger value than the outer loop's frequency value ($RWf_{in} = 1000 \text{ Hz}$, $RWf_{out} = 100 \text{ Hz}$). The Simulink diagram of DC motors of reaction wheels is defined hereafter:

After applying the automated PID tuning method provided by MATLAB/Simulink software tool, the following gain parameters are obtained by considering the design requirements. The PID torque and speed controller parameters are shown below with some specifications of linear system analyses such as rise time and settling time:

Table 5-2 PID Controller Parameters of Inner Loop

K_P	K_I	K_D	N	Settling Time	Rise Time	Overshoot
2.503e-5	0.022215	0	100	0.99 s	0.0735 s	3.77 %

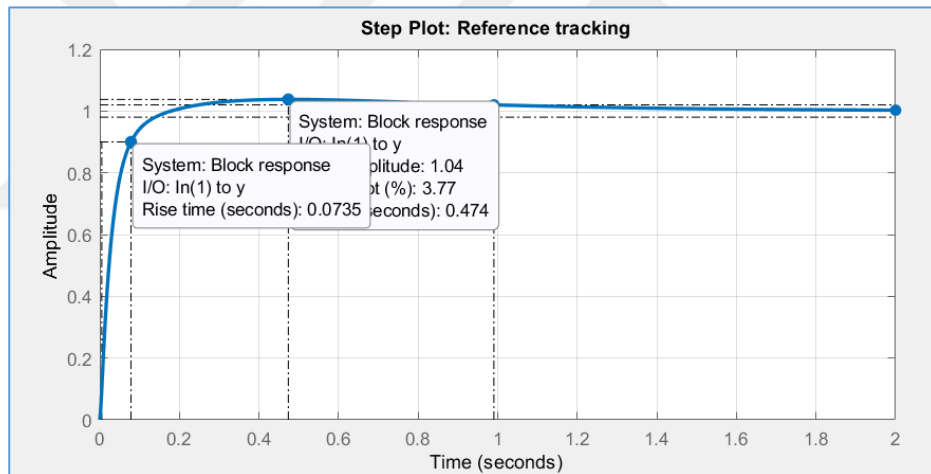


Figure 5-10 The Step Response of Inner Controller Loop

The parameters of outer PID loop and its step diagrams are hereafter:

Table 5-3 PID Controller Parameters of Outer Loop

K_P	K_I	K_D	N	Settling Time	Rise Time	Overshoot
9.5605	13.4366	1.1625	2668.953	1.16 s	0.0948 s	4.88 %

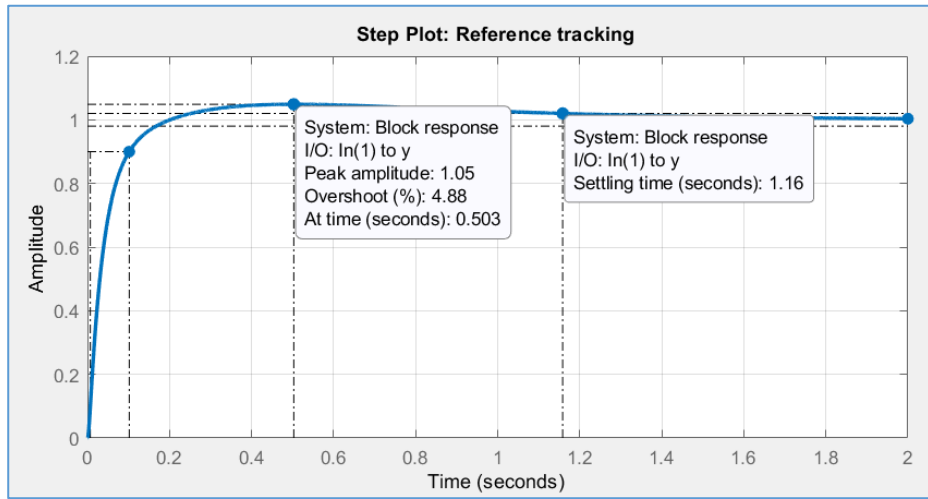


Figure 5-11 The Step Response of Outer Controller Loop

5.5. LQR Control

Linear Quadratic Regulator method is based on linear attitude model. The only negative effects of gravity gradient and aerodynamic drag can be taken into consideration and the disturbance torques of solar radiation and magnetic dipole moment can be ignored for linearization process [52, 71]. The linear quadratic cost function is always positive and defined as the following:

$$J(x, u) = \frac{1}{2} \int_0^{\infty} [x^T Q x + u^T R u] dt \quad (5.33)$$

$$Q = \begin{bmatrix} Q_1 & \dots & 0 \\ \vdots & \ddots & \vdots \\ 0 & \dots & Q_n \end{bmatrix}; \quad x^T Q x \geq 0 \quad (5.34)$$

$$R = \begin{bmatrix} R_1 & \dots & 0 \\ \vdots & \ddots & \vdots \\ 0 & \dots & R_n \end{bmatrix}; \quad u^T R u > 0 \quad (5.35)$$

Q is a constant, real symmetric positive semi-definite matrix and it defines the cost of state error. On the other hand, R is a constant, real symmetric positive definite

matrix and it defines the cost of control effort. State vector (x) represents the error between true and reference states in the cost function.

Solving the optimization problem is based on the minimization of cost function by the help of full state feedback controller definition of $u(t) = -K \cdot x(t)$. When the cost function is minimized, the state vectors reach to zero in infinite time and this situation guarantees system stability [48]:

$$J = \frac{1}{2} \int_0^{\infty} x^T (Q + K^T R K) x \, dt \quad (5.36)$$

K is the optimal gain and computed from the solution to Riccati Equation:

$$A^T S + S A - S B R^{-1} B^T S + Q = 0 \quad (5.37)$$

$$K = R^{-1} B^T S \rightarrow u = -(R^{-1} B^T S)x \quad (5.38)$$

A and B matrices are stabilizable by means of the cost function $J(x, u)$. K matrix is also adjusted by setting Q and R matrices. The selection of these matrices is based on an iterative procedure using a trial and error method. They are commonly selected to be diagonal in engineering problems and their initial values can be unit vectors:

$$Q = [I]_{10 \times 10}; \quad R = [I]_{6 \times 6} \quad (5.39)$$

- ✓ Q matrix shall be bigger than R matrix for an aggressive controller,
- ✓ R matrix shall be bigger than Q matrix for a conservative controller.

The procedure for the implementation of LQR is:

1. Calculation of linearized system matrices (A and B),
2. Calculation of state feedback matrices (Q and R),
3. Finding a solution to Riccati equation for sliding manifold (S),

4. Computation of optimal gain ($K = R^{-1}B^T S$),
5. Selection of K solution to yield a stable system for ($\dot{x} = (A - BK)x$),
The real part of eigenvalues should be negative for a stable system.
6. Calculation of control torque for actuators ($M_{cmd} = -Kx(t)$)

Feedback gain matrix (K_{LQR}), system eigenvalues ($E = eig(A - BK)$) and the solution of algebraic Riccati equation (S) can be obtained using the following MATLAB command in the simulations:

$$[K_{LQR}, S, E] = lqr(A, B, Q, R) \quad (5.40)$$

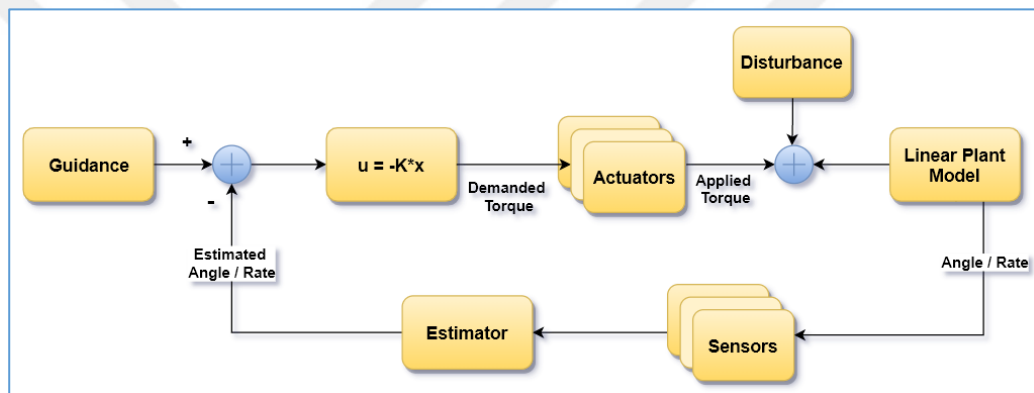


Figure 5-12 LQR Controller Diagram of Satellite Linear Attitude Model

5.6. Sliding Mode Control (SMC)

Sliding mode controller is a kind of nonlinear controller method and shows robust characteristics against parameter changes, uncertainties and external disturbances. In this controller process, there is a predefined sliding line or surface to force state trajectories to lie on it.

When the system is out of a sliding surface, the system dynamics reach this surface and the control torque is also needed to force the system states towards it. When the

system is on the surface, its states provide the system stability and its control torque is needed to keep the system at the surface.

The deviation between the equilibrium and the actual states is defined as the errors, and denoted by w_{err} and q_{err} respectively.

$$\dot{q}_{v,err} = \frac{1}{2} [\Omega(q_{v,err}) + [I_{3x3}]q_4] w_{OB}^B \quad (5.41)$$

$$\dot{q}_{v,err} = \frac{1}{2} \begin{bmatrix} q_{err,4} & -q_{err,3} & q_{err,2} \\ q_{err,3} & q_{err,4} & -q_{err,1} \\ -q_{err,2} & q_{err,1} & q_{err,4} \end{bmatrix} w_{OB}^B = \frac{1}{2} S(q_{v,err}) w_{OB}^B \quad (5.42)$$

A sliding manifold denoted by (s) forces system states towards the manifold and provides them to converge to the desired attitude. When the system is on the manifold ($s = 0$), sliding variable can be rewritten as (K_{SMC} is a positive sliding manifold gain) [75]:

$$s = w_{OB}^B + K_{SMC} q_{v,err} = 0 \rightarrow w_{OB}^B = -K_{SMC} q_{v,err} \quad (5.43)$$

The convergence towards a sliding surface is proven by the Lyapunov function such as ($V(q) = (q_v)^T q_v + (1 - q_4)^2$) and its derivative with the expression of $(q_v)^T q_v + (q_4)^2 = 1$:

$$V(q) = 2(1 - q_4) \quad (5.44)$$

$$\dot{V}(q) = 2\dot{q}_4 \quad (5.45)$$

- ✓ For an error quaternion $q_{err} = [q_{v,err}, q_{4,err}]^T = [0,0,0,1]^T \rightarrow V(0) = 0$
- ✓ $\dot{q}_4 = -\frac{1}{2}(q_v)^T w_{OB}^B \rightarrow \dot{V}(q) = -(q_{v,err})^T K_{SMC} q_{v,err}$

When K_{SMC} is a positive definite weight matrix, then $\dot{V}(q)$ is smaller than zero value. This situation satisfies the stability condition and the preferred sliding manifold function is considered as asymptotically stable.

When the sliding function ($s = 0$) is multiplied by $\frac{1}{2}S(q_{v,err})$:

$$\frac{1}{2}S(q_{v,err})w_{OB}^B + \frac{1}{2}S(q_{v,err})K_{SMC} \cdot q_{v,err} = 0 \quad (5.46)$$

$$\dot{q}_{v,err} + \frac{1}{2}S(q_{v,err})K_{SMC}q_{v,err} = 0 \quad (5.47)$$

The derivative of selected Lyapunov function ($V = \frac{1}{2}s^T s$) is the following:

$$\dot{V} = s^T \dot{s} = s^T (w_{OB}^B + K_{SMC} \dot{q}_{v,err}) \quad (5.48)$$

$$\dot{V} = s^T I_S^{-1} (M_D + M_{cmd} - w_{OB}^B \times (I_S w_{OB}^B + H_{RW}^B) + I_S K_{SMC} \dot{q}_{v,err}) \quad (5.49)$$

The equivalent torque (M_{eq}) versus to control torque (M_{cmd}) can be derived from the previous equation:

$$M_{cmd} = w_{OB}^B \times (I_S w_{OB}^B + H_{RW}^B) - M_D - I_S w_{OB}^B - I_S K_{SMC} \dot{q}_{v,err} - I_S G_{SMC} sign(s) \quad (5.50)$$

The selected control torque in the last equation is replaced in the derivative Lyapunov function:

$$\dot{V} = -s^T (w_{OB}^B + G_{SMC} sign(s)) \quad (5.51)$$

$$sign(s) = \begin{cases} 1, & s > 0 \\ 0, & s = 0 \\ -1, & s < 0 \end{cases} \quad (5.52)$$

G_{SMC} is a positive definite weight matrix, then the relationship between G_{SMC} and \dot{w}_{OB}^B shall be $G_{SMC} > |\dot{w}_{OB}^B|_{max}$ to achieve the stability condition $\dot{V} < 0$.

The function of $sign(s)$ results in chattering problem (high frequency oscillation) in a control torque simulation. There are several solutions in the literature being proposed to eliminate this problem and modify the controller method. One of the possible solutions is to design a switching controller by combining sliding mode controller with PID controller in the same simulation. In this way, sliding mode controller is applied till the attitude error is sufficiently small and then PID controller takes its position to ensure system stabilization [77]. In this study, this problem is removed by using saturation function ($sat(s)$) instead of $sign(s)$ function. “ ε ” is the sliding thickness in the following function:

$$sat(s) = \tanh\left(\frac{s}{\varepsilon}\right) = \begin{cases} 1, & s > \varepsilon \\ \frac{s}{\varepsilon}, & |s| \leq \varepsilon \\ -1, & s < -\varepsilon \end{cases} \quad (5.53)$$

The control torque (M_{cmd}) will be:

$$M_{cmd} = w_{OB}^B \times (I_S w_{OB}^B + H_{RW}^B) - M_D - I_S \dot{w}_{OB}^B - I_S K_{SMC} \dot{q}_{v,err} - I_S G_{SMC} \tanh\left(\frac{s}{\varepsilon}\right) \quad (5.54)$$

The procedure for the implementation of sliding mode controller can be divided into three action steps:

1. Defining a sliding manifold function and its derivative (s, \dot{s}) which satisfy Lyapunov stability analysis,
2. Finding sliding control weight matrices empirically (K_{SMC}, G_{SMC}),
3. Calculating control torque function with respect to Lyapunov candidate function by the help of (\dot{s}).

The weight matrices can be chosen as the magnitude order of satellite inertia matrix [75]. Another solution proposed for torque command function can be found by multiplying with inertia matrix:

$$I_S \dot{s} = I_S \dot{w}_{OB}^B + I_S K_{SMC} \dot{q}_v \quad (5.55)$$

$$\dot{s} = I_S^{-1} M_{eqv} + I_S^{-1} M_{cmd} \quad (5.56)$$

The equivalent torque (M_{eqv}) versus to control torque (M_C^{RW}) can be derived from the previous equation:

$$M_{eqv} = w_{OB}^B \times (I_S w_{OB}^B + H_{RW}^B) - M_D - I_S \dot{w}_{OB}^B - I_S K_{SMC} \dot{q}_{v,err} \quad (5.57)$$

When the controller gain is symbolized by (λ) and it is selected as long as in an appropriate way, the control torque can be determined like the following equation:

$$M_{cmd} = -\lambda sign(s) \quad (5.58)$$

In this case, chattering problem can be removed by using directly sliding function ((s)) instead of $sign(s)$ function:

$$M_{cmd} = -\lambda s \quad (5.59)$$

5.7. Summary

In the first phase (detumbling) a specific controller named B-dot are applied to satellite dynamics and kinematics. PID, LQR and SMC controllers are executed afterwards.

CHAPTER 6

RESULTS and DISCUSSIONS

6.1. Introduction

The simulation test results of attitude controllers with related requirements are explained in this section for different configurations and gain values. Their performance parameters are compared and analyzed based on the related graphical results. The main purpose is to prove that whether the satellite model tracks the reference points indicated as Euler angles or not. The satellite should keep its stable state after reaching a given reference value and keep its power consumption low.

In this section, the simulation sampling time is chosen as 0.1 seconds for all main controllers (PID, LQR, SMC). B-dot controller is implemented to meet the demanded results for satellite initial phase. All these type of controllers are modelled and simulated in MATLAB/Simulink environment with different test cases.

6.2. The Results of Detumbling Control

It is expected that detumbling controller should be capable of damping the tumble motion of a satellite within a few orbits after deployment from a launcher. The aim of detumbling phase is to decrease satellite Euler rates under 0.01 degree per second.

The initial value of satellite tumbling rate is assumed to be around 0.1 radian per second in each axis for the first test case and the reference attitude is not applied in this phase. The following graphics are generated for different test configurations.

Case-1: No RW Failure & PID Controller Design

Table 6-1 The Simulation Parameters of Detumbling Phase (Case-2)

Parameters	Values
Initial Satellite Velocity	$w_0 = [0.1, 0.1, 0.1]$
Sampling Time	$T_s = 0.01$
System Noise Covariance Matrix	$Q_k = 1 \times 10^{-10}$
Measurement Noise Covariance Matrix	$R_{gyro} = 1 \times 10^{-12}; R_{str} = 1 \times 10^{-12}$ $R_{mgm} = R_{sus} = R_{gps} = 1 \times 10^{-7}$
Constant Controller Gain $K_{Bdot} = [I_{S_x} \times 10^4 \quad I_{S_y} \times 10^4 \quad I_{S_z} \times 10^4]$	$K_{Bdot,x} = 7.066197 \times 10^4$ $K_{Bdot,y} = 6.950219 \times 10^4$ $K_{Bdot,z} = 8.555828 \times 10^4$

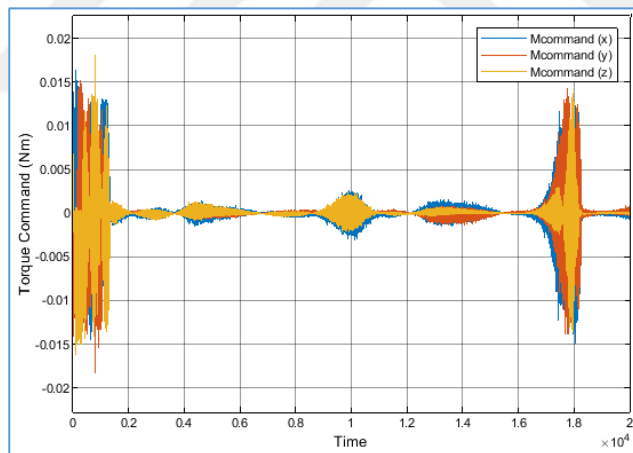


Figure 6-1 MTR Torque Command in Detumbling Phase (Case-1)

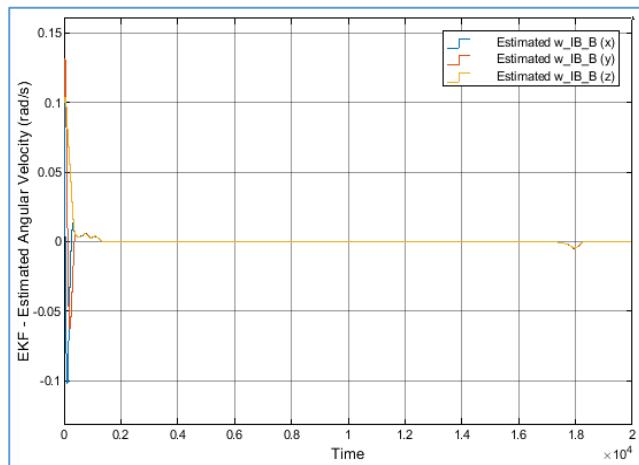


Figure 6-2 Satellite Angular Velocity in Detumbling Phase (Case-1)

This test shows that B-dot controller is capable of reducing the satellite initial angular velocity under 0.01 [rad/s] under 2000 seconds.

Case-2: No RW Failure & PID Controller with the same parameters like as the previous case, but with the more aggressive initial angular velocity of a satellite ($w_0 = [0.5, 0.0, 0.5]$)

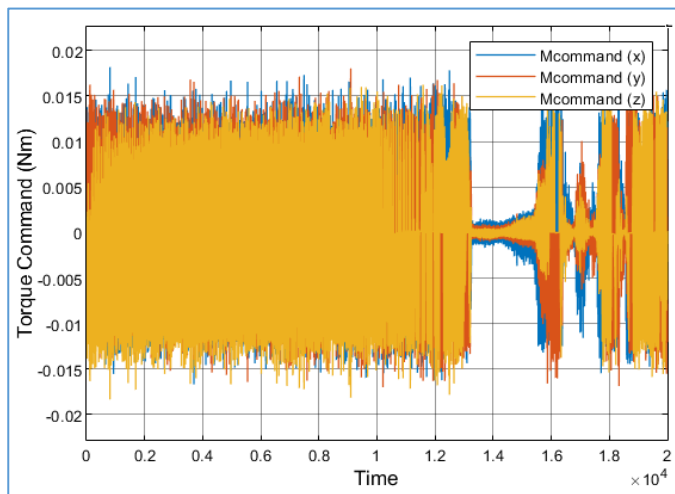


Figure 6-3 MTR Torque Command in Detumbling Phase (Case-2)

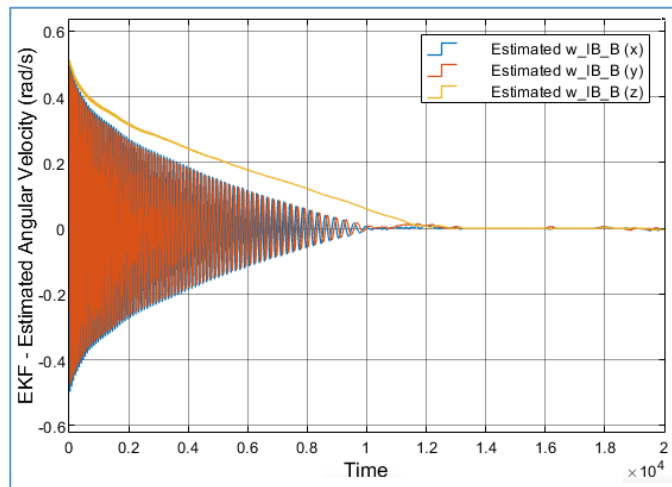


Figure 6-4 Satellite Angular Velocity in Detumbling Phase (Case-2)

In this case, the settling time is about ~ 13250 sec. and angular velocity is between $+0.01$ and -0.01 after providing a stable state. The settling duration is much longer whenever the initial conditions have higher values than the previous case.

Case-3: No RW Failure & PID Controller with the same parameters and initial values like as in Case-1, but implementing lower gain value ($K_{Bdot} = 10$)

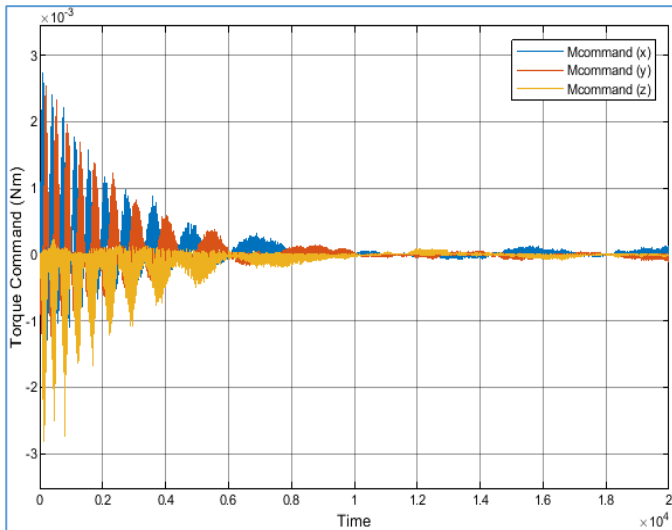


Figure 6-5 MTR Torque Command in Detumbling Phase (Case-3)

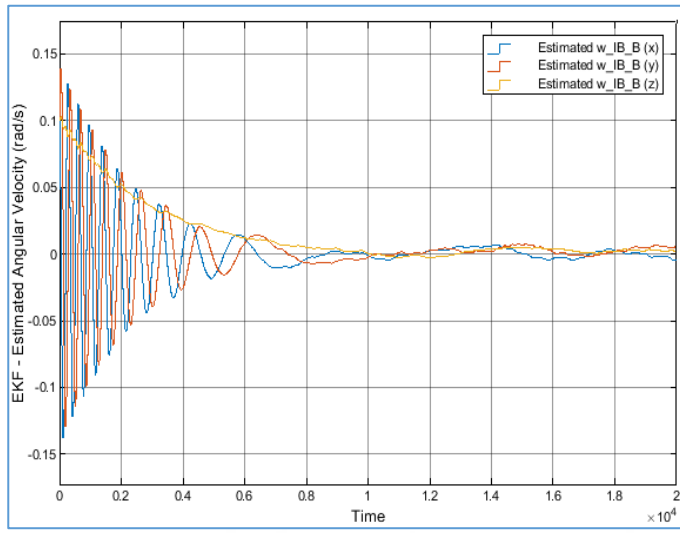


Figure 6-6 Satellite Angular Velocity in Detumbling Phase (Case-3)

In this case, B-dot controller stabilizes the system by reducing its initial angular velocity in the range of ± 0.007 . However, its settling time is much higher than the case of controller gain (K_{Bdot}) has much higher value. The selection of gain value affects the signal stability.

Case-4: No RW Failure & PID Controller with the same parameters like as in Case-1, but performing higher gain value ($K_{Bdot} = [I_{S_x} \times 10^7, I_{S_y} \times 10^7, I_{S_z} \times 10^7]$)

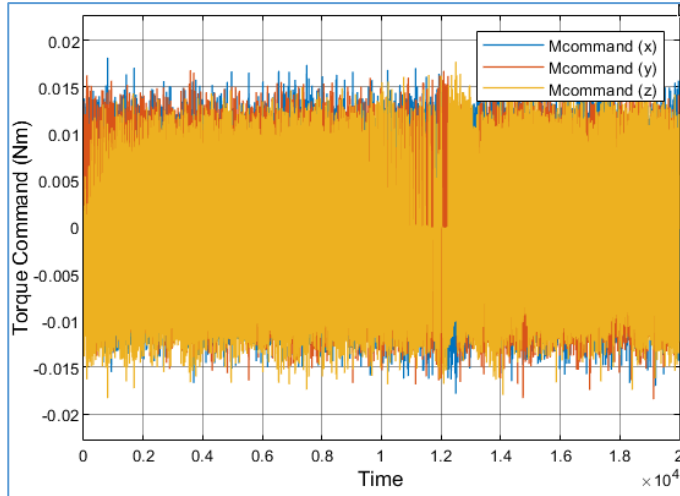


Figure 6-7 MTR Torque Command in Detumbling Phase (Case-4)

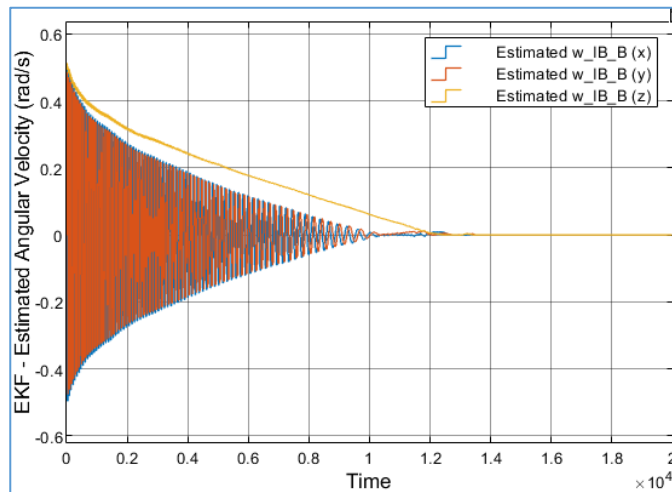


Figure 6-8 Satellite Angular Velocity in Detumbling Phase (Case-4)

This test shows that B-dot controller is capable of reducing the satellite initial angular velocity under 0.01 [rad/s] within almost three orbits. The time needed to meet requirements is approximately ~14000 seconds for this case.

6.3. The Results of Desaturation Control

It can be seen that reaction wheels are desaturated by torque rods each time whenever a new attitude maneuver is applied. The satellite initial conditions of momentum unloading phase are defined in this section for each simulation test case. The main controller can be selected as PID, SMC or LQR to generate the expected graphical results.

Case-1: No RW Failure & PID Controller

Table 6-2 The Simulation Parameters of Desaturation Phase (Case-1)

Parameters	Values
Initial Satellite Velocity	$w_0 = [0.0, 0.0, 0.0]$
Initial / Desired Euler Angels	$[\psi_0, \theta_0, \Phi_0] = [0, 0, 0]$ $[\psi_d, \theta_d, \Phi_d] = [-15, -5, 5]$

Parameters	Values
Constant Controller Gain	$K_{dump} = 10^{-6}$
The Command Torque	$M_{cmd} = -K_p \cdot q_{v,err} \cdot q_{err,4} - K_{PD} \cdot \dot{q}_{err}$

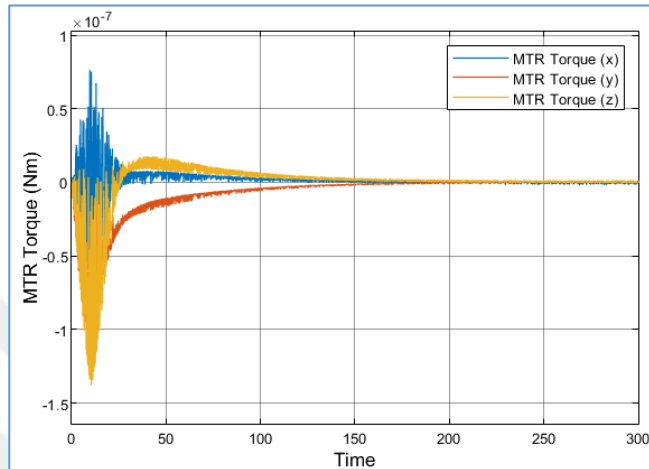


Figure 6-9 MTR Torque in Desaturation Phase of Satellite PID (Case-1)

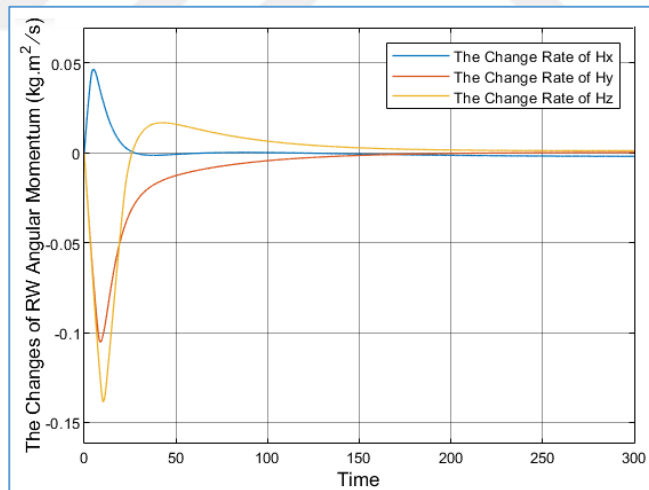


Figure 6-10 RW Angular Momentum Desaturation of PID (Case-1)

In the first test case, the final value of angular momentum in the range of $\pm 0.005 \text{ kgm}^2/\text{sec}$. The settling time is about ~ 200 seconds.

Case-2: No RW Failure & PID Controller with the same parameters like in the previous test case, but using higher gain value ($K_{dump} = 10^6$).

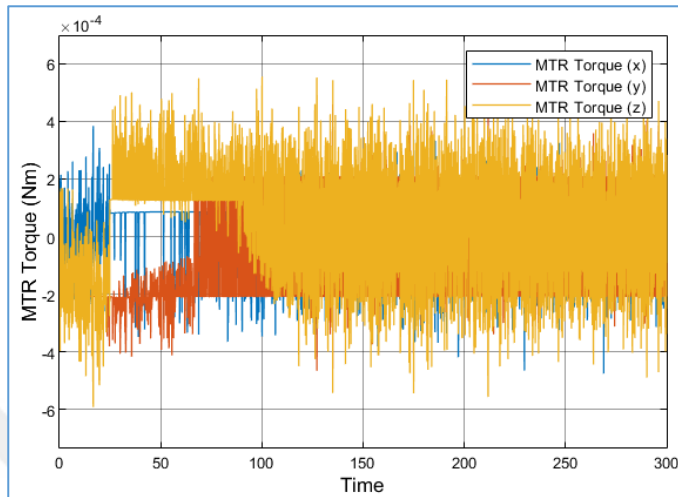


Figure 6-11 MTR Torque in Desaturation Phase of PID (Case-2)

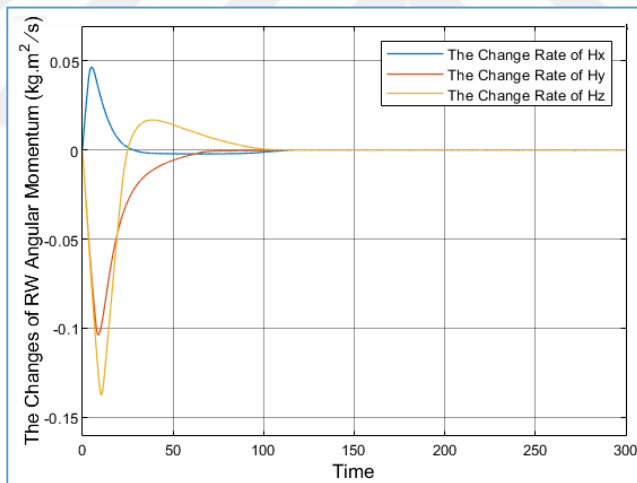


Figure 6-12 RW Angular Momentum Desaturation of PID (Case-2)

The angular momentum changes are stabilized in about 110 seconds and its value is reduced to around $\pm 1 \times 10^{-4} \text{ kgm}^2/\text{sec}$. MTR torque contains much noise while dump gain is larger twelve times than the previous gain value.

Case-3: RW-1 Failure & PID Controller with the same parameters and gain values ($K_{dump} = 10^{-6}$) like in the first test case, but implementing different PID controller law ($M_{cmd} = -K_P \cdot q_{v,err} \cdot q_{err,4} - K_{PD} \cdot w_{OB}^B$).

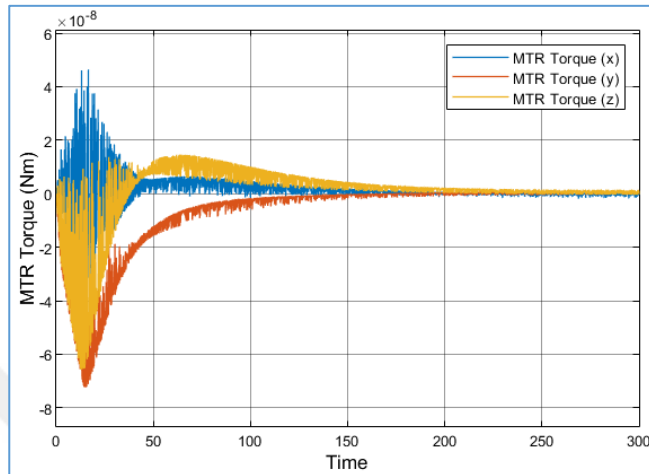


Figure 6-13 MTR Torque in Desaturation Phase of SMC (Case-3)

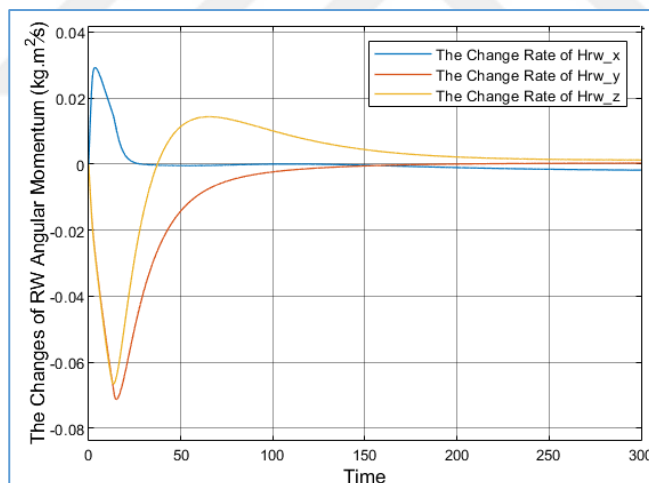


Figure 6-14 RW Angular Momentum Desaturation of PID (Case-3)

This test proves that the selected controller law also affects the results of desaturation controller design. In this case, the settling time is adversely effected by this PID controller law.

Case-4: No RW Failure & SMC Controller without chattering problem with the same gain value ($K_{dump} = 10^{-6}$)

Table 6-3 The Simulation Parameters of Desaturation Phase (Case-4)

Parameters	Values
Initial Satellite Velocity	$w_0 = [0.0, 0.0, 0.0]$
Initial / Desired Euler Angels	$[\psi_0, \theta_0, \Phi_0] = [0, 0, 0]$ $[\psi_d, \theta_d, \Phi_d] = [-15, -5, 5]$
Constant Controller Gains	$K_{SMC} = 0.5 * [I]_{3x3}$ $G_{SMC} = 1 * [I]_{3x3}$
Sliding Manifold	$s = w_{OB}^B + K_{SMC} \cdot q_{v,err}$

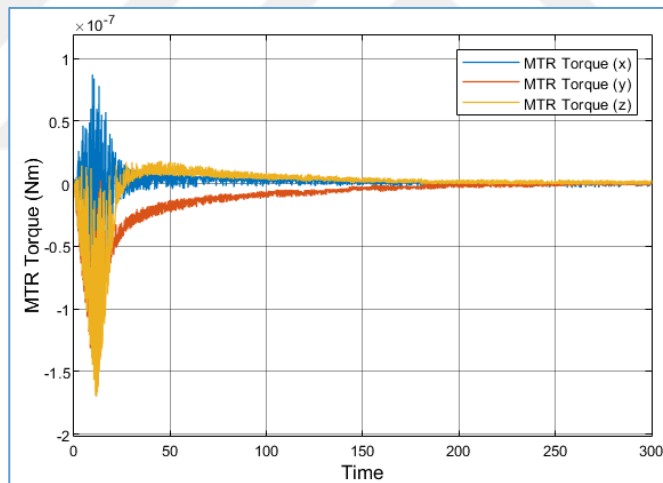


Figure 6-15 MTR Torque in Desaturation Phase of SMC (Case-4)

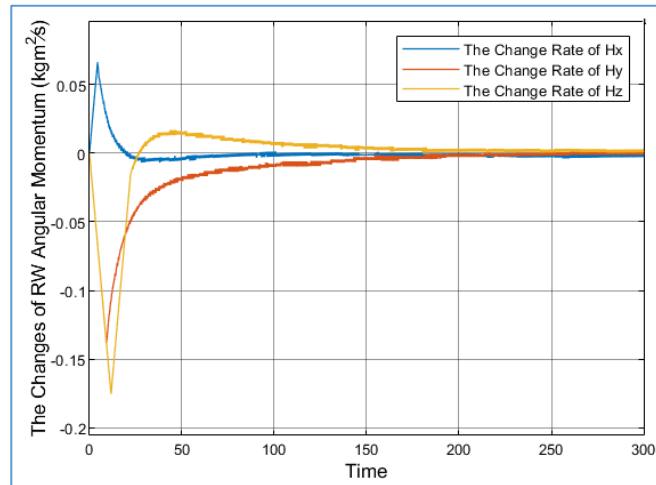


Figure 6-16 RW Angular Momentum Desaturation of SMC (Case-4)

The change rates of RW angular momentum is between $\pm 0.2 \text{ kgm}^2/\text{sec}$. After dumping is completed in about 80 seconds, the angular momentum changes are descended around $\pm 1 \times 10^{-4} \text{ kgm}^2/\text{sec}$.

Case-5: No RW Failure & LQR Controller under the same conditions and gain values used in the section of “The Results of LQR Controller / Case-1”

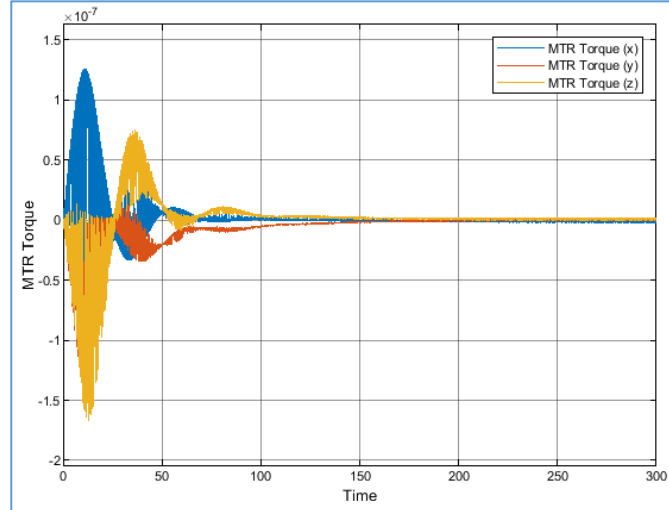


Figure 6-17 MTR Torque in Desaturation Phase of LQR (Case-5)

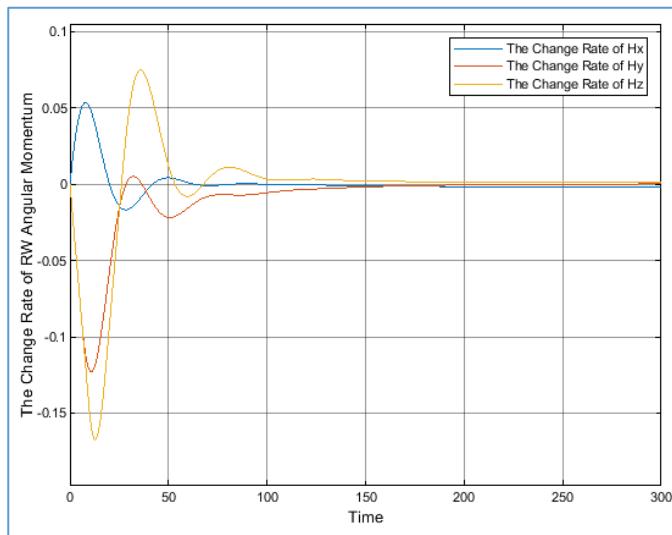


Figure 6-18 RW Angular Momentum Desaturation of LQR (Case-5)

As it can be seen in the graphics, the torque changes of RWs and MTRs and settling times are almost in the same level for each type of main controllers. The only exception is seen in the case of using LQR controller due to the chosen weight matrices. In addition to this, they are not in the same margins for different test cases. It can also be observed that the biggest differences among the angular momentum values are in the SMC test cases.

6.4. The Results of PID Control

For the usage of reaction wheels and magnetic torque rods as torque generators, the matrices of measurement equation for the configuration of using all sensors are specified in the following test cases.

Sensor Configuration: GYRO + STR + MGM + SS + GPS

$$y_{CONF} = [w_{meas} \quad q_{meas} \quad B_{meas} \quad SV_{meas} \quad r_{meas} \quad v_{meas}]^T \quad (6.1)$$

$$y_{CONF} = [H_{CONF}] \Delta x_k + [R_{CONF}] v_k \quad (6.2)$$

$$[H_{CONF}] \Delta x_k = \begin{bmatrix} [I]_{3x3} & 0_{3x4} & 0_{3x3} \\ 0_{4x3} & [I]_{4x4} & 0_{4x3} \\ 0_{3x3} & [H_{MGM}^{non}]_{3x4} & 0_{3x3} \\ 0_{3x3} & [H_{SUS}^{non}]_{3x4} & 0_{3x3} \\ 0_{3x3} & [H_{GPS1}^{non}]_{3x4} & 0_{3x3} \\ 0_{3x3} & [H_{GPS2}^{non}]_{3x4} & 0_{3x3} \end{bmatrix} \begin{bmatrix} \Delta w_{IB}^B \\ \Delta q \\ \Delta H_{RW}^B \end{bmatrix} \quad (6.3)$$

$$[R_{CONF}] =$$

$$\begin{bmatrix} I_{3x3} \cdot R_{GYRO} & 0_{3x4} & 0_{3x3} & 0_{3x3} & 0_{3x3} & 0_{3x3} \\ 0_{4x3} & I_{4x4} \cdot R_{STR} & 0_{4x3} & 0_{4x3} & 0_{4x3} & 0_{4x3} \\ 0_{3x3} & 0_{3x4} & I_{3x3} \cdot R_{MGM} & 0_{3x3} & 0_{3x3} & 0_{3x3} \\ 0_{3x3} & 0_{3x4} & 0_{3x3} & I_{3x3} \cdot R_{SUS} & 0_{3x3} & 0_{3x3} \\ 0_{3x3} & 0_{3x4} & 0_{3x3} & 0_{3x3} & I_{3x3} \cdot R_{GPS1} & 0_{3x3} \\ 0_{3x3} & 0_{3x4} & 0_{3x3} & 0_{3x3} & 0_{3x3} & I_{3x3} \cdot R_{GPS2} \end{bmatrix} \quad (6.4)$$

$$R_{GYRO} = R_{STR} = 1 \times 10^{-12}; R_{MGM} = R_{SUS} = R_{GPS1} = R_{GPS2} = 1 \times 10^{-10}$$

The controller gains are directly proportionate to the components of satellite inertia matrix (I_{S_x} , I_{S_y} , I_{S_z}) according to the following attitude control law [15]:

$$\begin{bmatrix} M_{cmd,x} \\ M_{cmd,y} \\ M_{cmd,z} \end{bmatrix} = \begin{bmatrix} -2 \cdot K_{P_x} q_{err,1} q_{err,4} - K_{PD_x} \dot{q}_{err,1} \\ -2 \cdot K_{P_y} q_{err,2} q_{err,4} - K_{PD_y} \dot{q}_{err,2} \\ -2 \cdot K_{P_z} q_{err,3} q_{err,4} - K_{PD_z} \dot{q}_{err,3} \end{bmatrix} \quad (6.5)$$

Case-1: No RW Failure & PID Controller

Table 6-4 The Simulation Parameters of PID Controller (Case-1)

Parameters	Values
Initial Satellite Velocity	$w_0 = [0.0, 0.0, 0.0]$
Initial / Desired Euler Angels	$[\Psi_0, \theta_0, \Phi_0] = [0, 0, 0]$ $[\Psi_d, \theta_d, \Phi_d] = [-15, -5, 5]$

Parameters	Values
Constant Controller Gains $K_{P_{x,y,z}} = [I_{S_x}/5, I_{S_y}/5, I_{S_z}/5]$ $K_{PD_{x,y,z}} = 10 * K_{P_{x,y,z}}$	$K_{P_{x,y,z}} = [7.0662/5, 6.9502/5, 8.5558/5]$ $K_{PD_{x,y,z}} = [14.1324, 13.9004, 17.1117]$
Dumping Gain (K_{dump})	$K_{dump} = 10^{-6}$

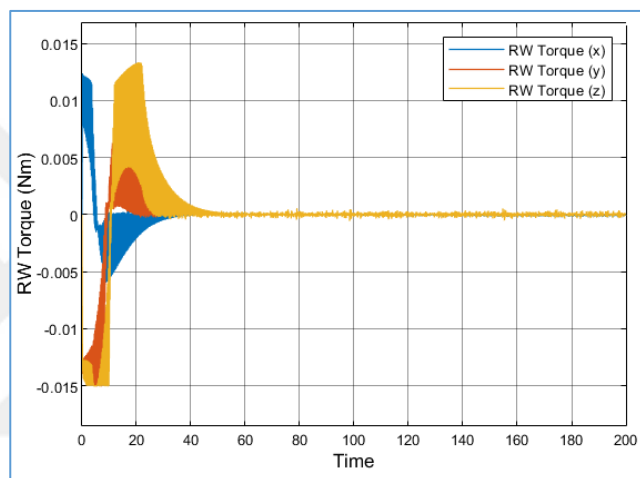


Figure 6-19 RW Commanded Torque (PID / Case-1)

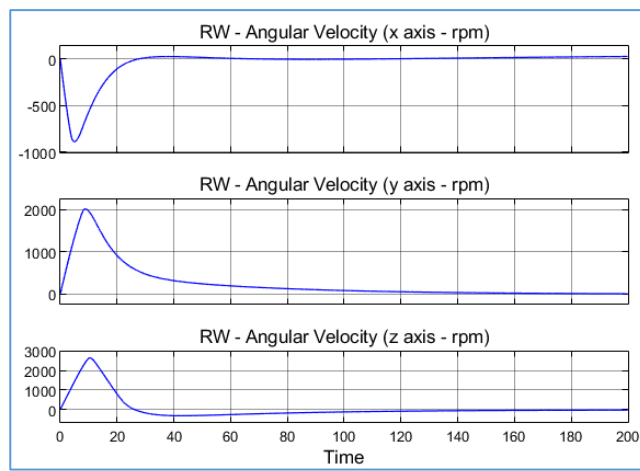


Figure 6-20 RW Angular Velocities (PID/Case-1)

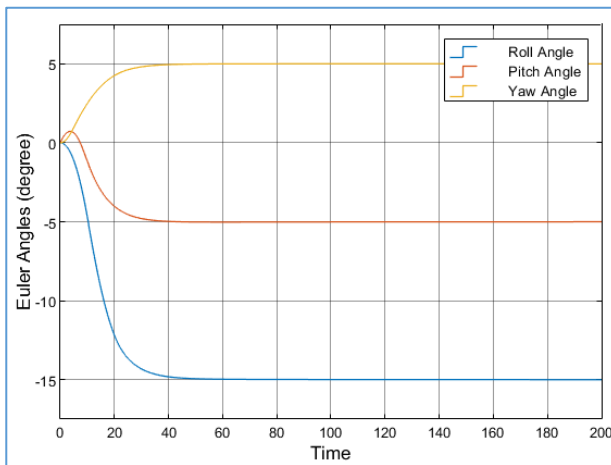


Figure 6-21 Satellite Euler Angles (PID/Case-1)

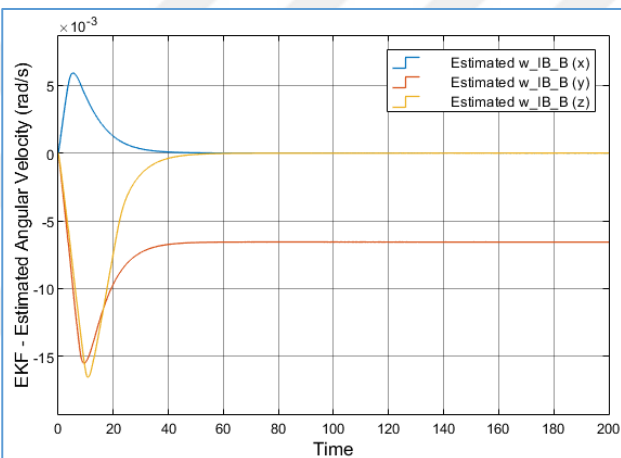


Figure 6-22 Satellite Angular Velocities (PID/Case-1)

The controller parameters obtained from the simulation for this case are hereafter:

Table 6-5 The Simulation Results of PID Controller for Case-1

	Settling Time	Rise/Fall Time	Overshoot
Roll Angle	~50 s	~17.905 s	1.983 %
Pitch Angle	~40 s	~16.485 s	1.994 %
Yaw Angle	~50 s	~19.006 s	0.505 %

The applied command torque equation gives appropriate results for small angular maneuvers in the first test case. Another command equation is applied for high angular maneuvers like in the following and third test case.

Case-2: No RW Failure with the same parameters applied in the previous test case, but using different command torque law ($M_{cmd} = -K_P q_{v,err}q_{err,4} - K_{PD}W_{OB}^B$)

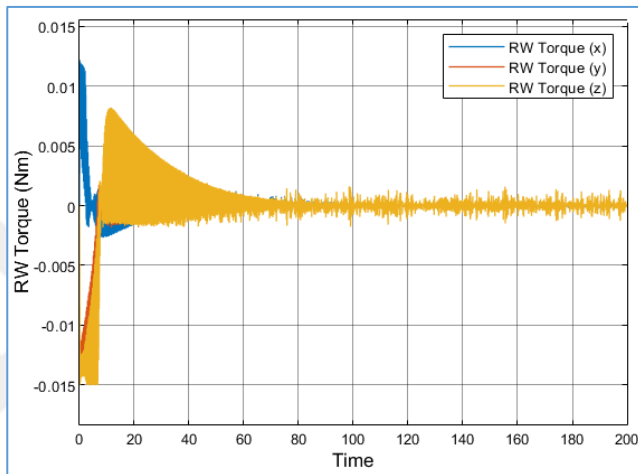


Figure 6-23 RW Commanded Torque (PID/Case-2)

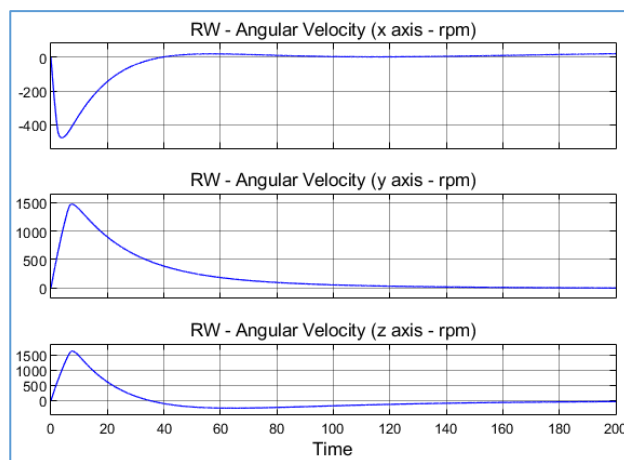


Figure 6-24 RW Angular Velocities (PID/Case-2)

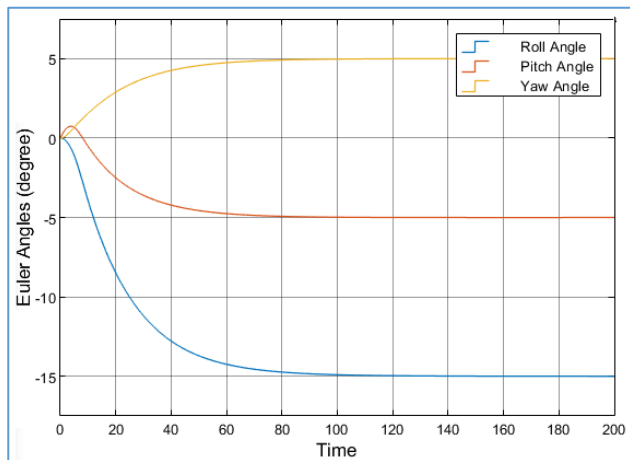


Figure 6-25 Satellite Euler Angles (PID/Case-2)

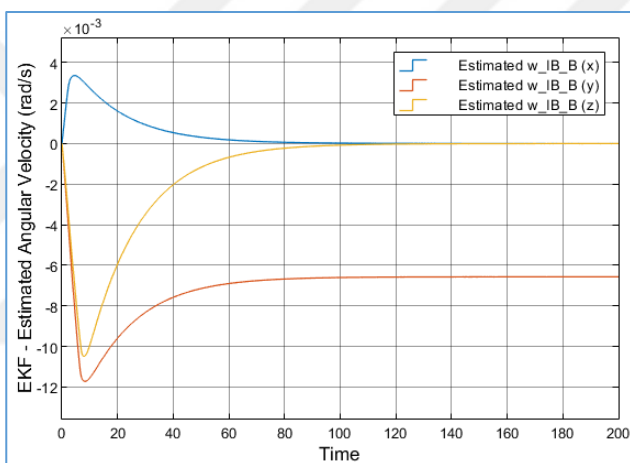


Figure 6-26 Satellite Angular Velocities (PID/Case-2)

The controller parameters obtained from the simulation for this case are hereafter:

Table 6-6 The Simulation Results of PID Controller for Case-2

	Settling Time	Rise/Fall Time	Overshoot
Roll Angle	~120 s	~40.304 s	2.011 %
Pitch Angle	~100 s	~36.407 s	2.010 %
Yaw Angle	~100 s	~44.104 s	0.504 %

The settling time and rise time obtained from the results show that they have higher values as compared with the results of previous test case.

Case-3: No RW Failure under the same conditions in terms of controller gains and torque equations ($M_{cmd} = -K_P q_{v,err} q_{err,4} - K_{PD} w_{OB}^B$), but performing high Euler reference angles ($[\psi_d, \theta_d, \Phi_d] = [120, 50, -30]$) from zero initial angles.

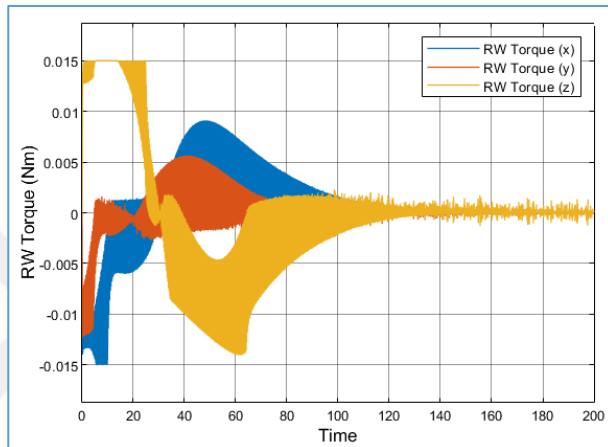


Figure 6-27 RW Commanded Torque (PID/Case-3)

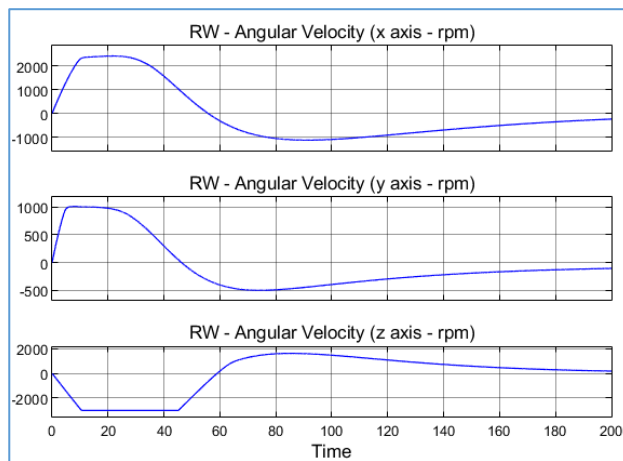


Figure 6-28 RW Angular Velocities (PID/Case-3)

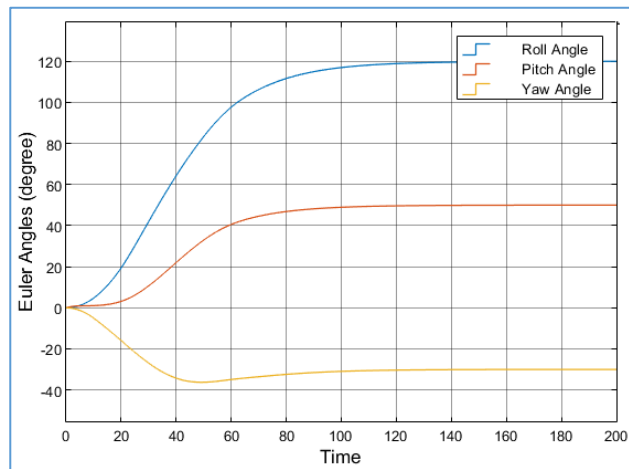


Figure 6-29 Satellite Euler Angles (PID/Case-3)

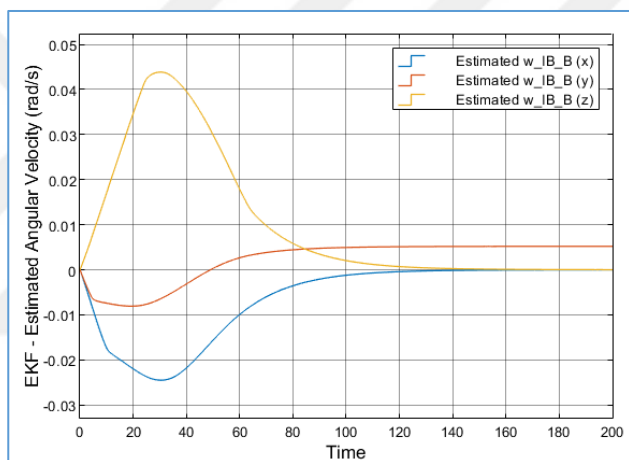


Figure 6-30 Satellite Angular Velocities (PID/Case-3)

The controller parameters obtained from the simulations for this case are hereafter:

Table 6-7 The Simulation Results of PID Controller for Case-3

	Settling Time	Rise/Fall Time	Overshoot
Roll Angle	~120 s	~56.606 s	0.504 %
Pitch Angle	~90 s	~47.902 s	0.509 %
Yaw Angle	~70 s	~21.908 s	2.252 %

It can be concluded that the requested torque is increased than the case of applying low reference angles. Similarly, it is the same situation for the timing properties of this case.

Case-4: RW-1 Failure under the same conditions like in the first case, but with the torque command of ($M_{cmd} = -K_P q_{v,err} q_{err,4} - K_{PD} W_{OB}^B$) and the expected last Euler angular values are $[\psi_d, \theta_d, \Phi_d] = [-15, -5, 5]$ from zero initial values.

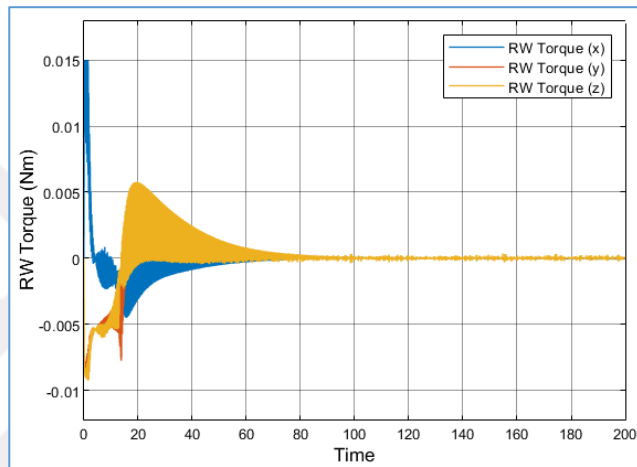


Figure 6-31 RW Commanded Torque (PID/Case-4)

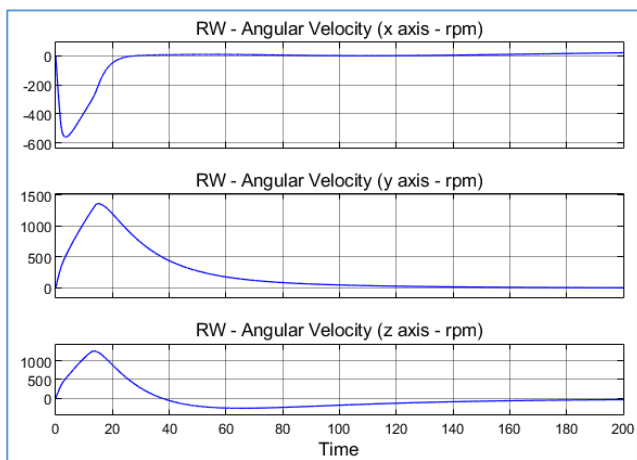


Figure 6-32 RW Angular Velocities (PID/Case-4)

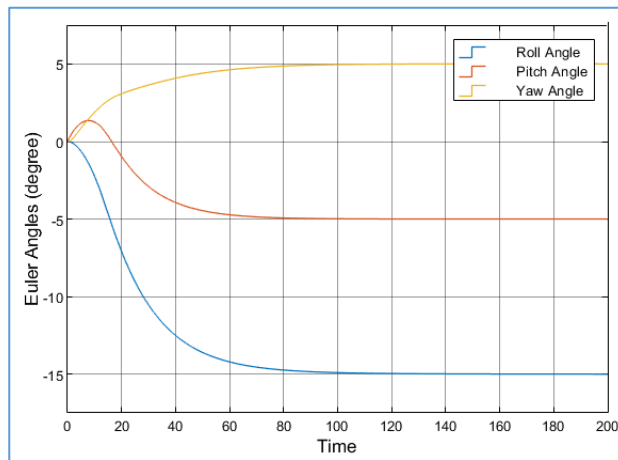


Figure 6-33 Satellite Euler Angles (PID/Case-4)

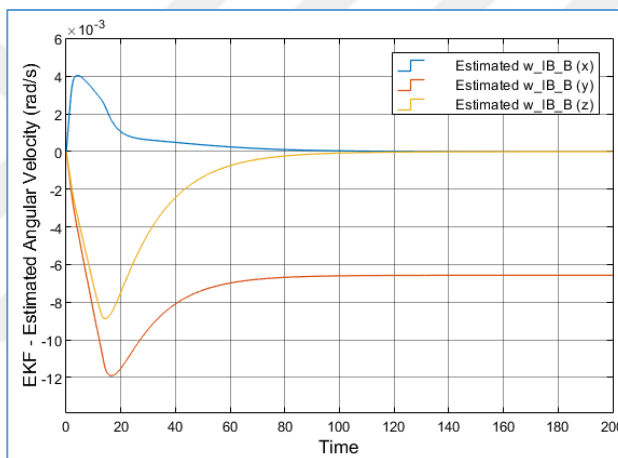


Figure 6-34 Satellite Angular Velocities (PID/Case-4)

The simulation parameters obtained from this case are defined here:

Table 6-8 The Simulation Results of PID Controller for Case-4

	Settling Time	Rise/Fall Time	Overshoot
Roll Angle	~90 s	~39.503 s	2.000 %
Pitch Angle	~90 s	~32.602 s	2.001 %
Yaw Angle	~90 s	~50.405 s	0.493 %

In the case of more than one reaction wheel failure, the expected attitude results are not acquired properly. The power consumptions for both cases of a RW failure and non-failure are also hereafter:

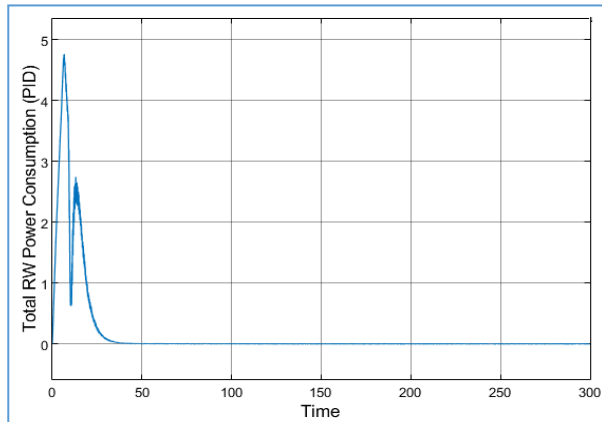


Figure 6-35 RW Power Consumption for a Non-Failure Case (PID)

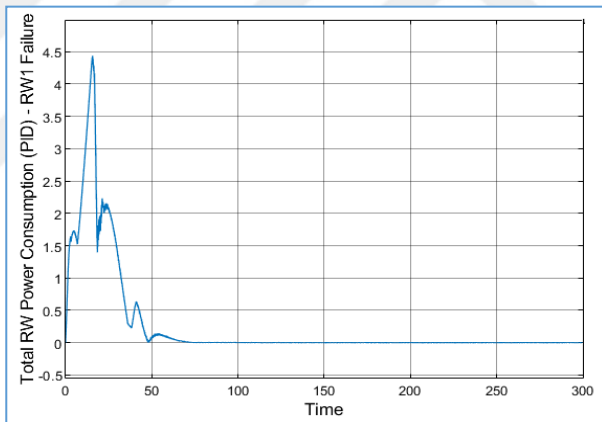


Figure 6-36 RW Power Consumption for a RW Failure Case (PID)

The following equation is used for the calculation of RW power consumption:

$$P = \dot{H}_{RW} w_{RW} \quad (6.1)$$

The calculations of both RW electrical and mechanical power consumption are implemented into DC motor model like in the following figure:

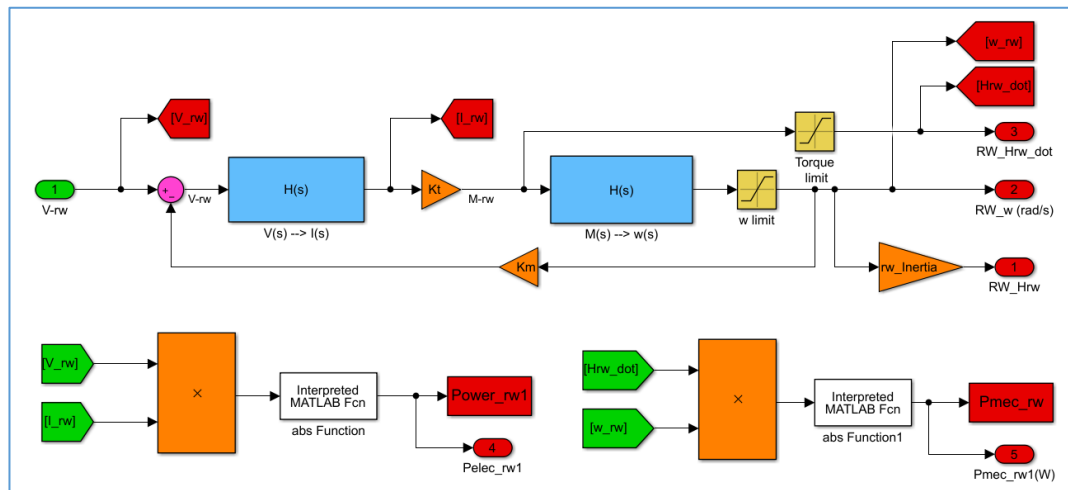


Figure 6-37 The Calculation of Electrical and Mechanical Power Consmp.

6.5. The Results of LQR Control

The main controller consisting of optimal and desaturation controller to keep wheels under their saturation limits in this section. The controlled state is a quaternion vector and it is simulated by handling error rate according to the given reference angles for LQR controller design.

The linearized satellite plant model is the base point for this controller type. H measurement matrix is taken as a unit matrix which is sized suitably with the state vector size. Two different test cases are analyzed taking into consideration the failure situation of one reaction wheel and their graphical results are presented here.

Case-1: No RW Failure & LQR Controller using both RWs and MTRs using as torque generators with the following simulation parameters:

Table 6-9 The Simulation Parameters of LQR Controller (Case-1)

Parameters	Values
Initial Satellite Velocity	$w_0 = [0.0, 0.0, 0.0]$

Parameters	Values
Initial / Desired Euler Angels	$[\psi_0, \theta_0, \Phi_0] = [0, 0, 0]$ $[\psi_d, \theta_d, \Phi_d] = [-15, -5, 5]$
Constant Weight State Matrix	$Q_{RW} = \begin{bmatrix} [I_{3x3}] & 0 & 0 \\ 0 & [I_{3x3}] * (1000) & 0 \\ 0 & 0 & [I_{4x4}] \end{bmatrix}$
Constant Weight Input Matrix	$R_{RW} = [I_{6x6}] * (2500)$
Controller Gain Matrix	$K_{LQR} = [K_w_{LQR}, K_q_{LQR}, K_{hrw_{LQR}}]$

The gain matrix in accordance with the selected weight matrices is obtained like:

$$K_{LQR} =$$

$$\begin{bmatrix} 0.8895 & 0.0000 & -0.0009 & 0.3640 & -0.0000 & 0.0028 & 0.0000 & -0.0164 & -0.0000 & -0.0000 \\ -0.0000 & 0.9046 & -0.0000 & 0.0000 & 0.3819 & -0.0000 & 0.0066 & -0.0000 & -0.0164 & -0.0000 \\ -0.0007 & 0.0000 & 0.9745 & -0.0035 & -0.0000 & 0.3637 & -0.0000 & 0.0000 & -0.0000 & -0.0164 \\ 0.9470 & -0.0000 & -0.0009 & 0.3657 & -0.0000 & 0.0029 & 0.0000 & 0.0081 & 0.0000 & -0.0000 \\ -0.0000 & 0.9612 & -0.0000 & 0.0000 & 0.3836 & -0.0000 & 0.0077 & -0.0000 & 0.0081 & -0.0000 \\ -0.0007 & -0.0000 & 1.0441 & -0.0035 & -0.0000 & 0.3658 & 0.0000 & 0.0000 & 0.0000 & 0.0081 \\ 0.9470 & -0.0000 & -0.0009 & 0.3657 & -0.0000 & 0.0029 & 0.0000 & 0.0081 & 0.0000 & -0.0000 \\ -0.0000 & 0.9612 & -0.0000 & 0.0000 & 0.3836 & -0.0000 & 0.0077 & -0.0000 & 0.0081 & -0.0000 \\ -0.0007 & -0.0000 & 1.0441 & -0.0035 & -0.0000 & 0.3658 & 0.0000 & 0.0000 & 0.0000 & 0.0081 \end{bmatrix}$$

The eigenvalues (E_{LQR}) of linearized plant model are specified here to prove system stability. Their real parts are negative values and system stability is guaranteed by using this specification:

Table 6-10 The Eigenvalues of Linearized Plant Model

Eigenvalues of LQR	Values
$E_{LQR,1}$	$-0.1969 + 0.1968i$
$E_{LQR,2}$	$-0.1969 - 0.1968i$
$E_{LQR,2}$	$-0.1791 + 0.1787i$
$E_{LQR,2}$	$-0.1791 - 0.1787i$
$E_{LQR,2}$	$-0.2034 + 0.2032i$

Eigenvalues of LQR	Values
$E_{LQR,2}$	$-0.2034 - 0.2032i$
$E_{LQR,2}$	$-0.0001 + 0.0000i$
$E_{LQR,2}$	$-0.0163 + 0.0000i$
$E_{LQR,2}$	$-0.0163 - 0.0000i$
$E_{LQR,2}$	$-0.0163 + 0.0000i$

The graphical outputs acquired from this test case are depicted here:

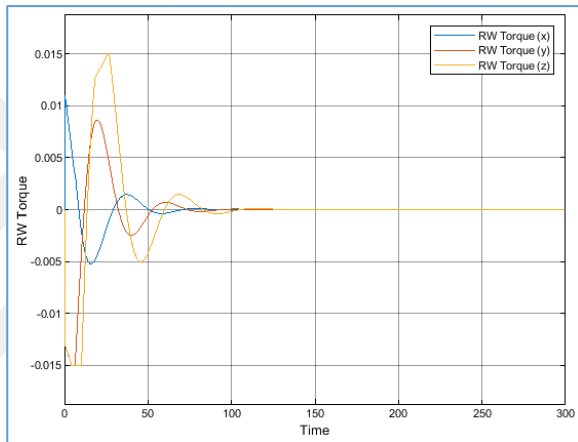


Figure 6-38 RW Commanded Torque (LQR/Case-1)

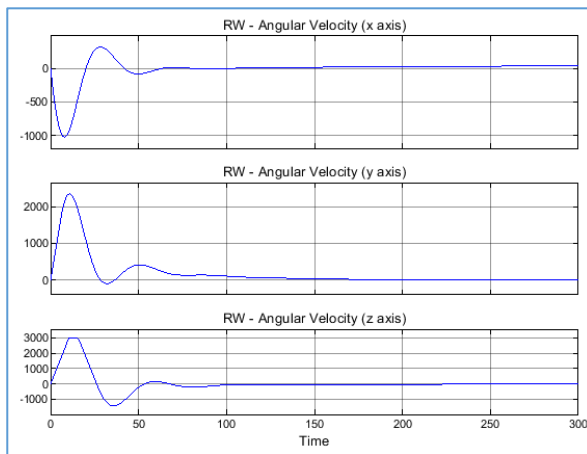


Figure 6-39 RW Angular Velocities (LQR/Case-1)

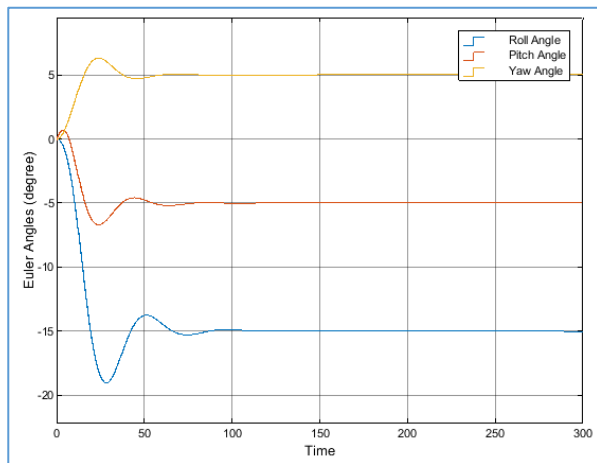


Figure 6-40 Satellite Euler Angles (LQR/Case-1)

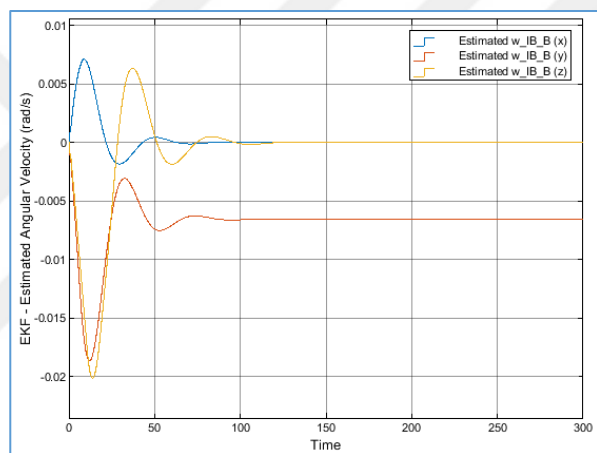


Figure 6-41 Satellite Angular Velocities (LQR/Case-1)

The simulation parameters obtained from this case are defined here:

Table 6-11 The Simulation Results of LQR Controller for Case-1

	Settling Time	Rise/Fall Time	Overshoot
Roll Angle	~100 s	- 11.606 s	8.028 %
Pitch Angle	~75 s	- 8.005 s	4.072 %
Yaw Angle	~60 s	+10.302 s	25.949 %

It is observed that the satellite reaches to a stable state on the average of almost ~80 seconds with tolerable fluctuations in the range of ± 0.05 degrees especially for the measured values taken from Y axis.

The system performances are affected by the changes in weight matrices determined by trial and error method. For the sake of example, the settling time gets smaller whenever R weight matrix has smaller values compared with its previous version.

Case-2: RW1 Failure & LQR Controller with the same parameters handled in the previous test case.

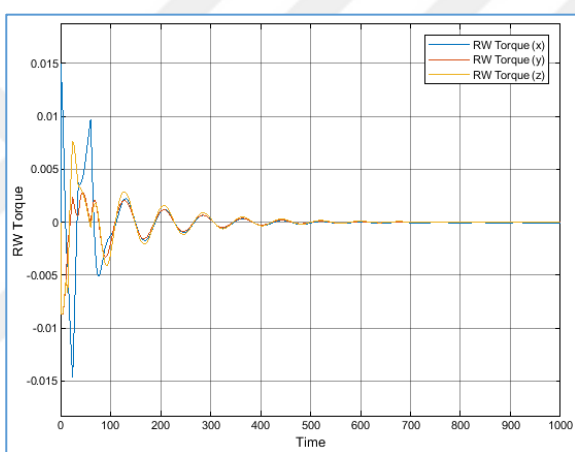


Figure 6-42 RW Commanded Torque (LQR/Case-2)

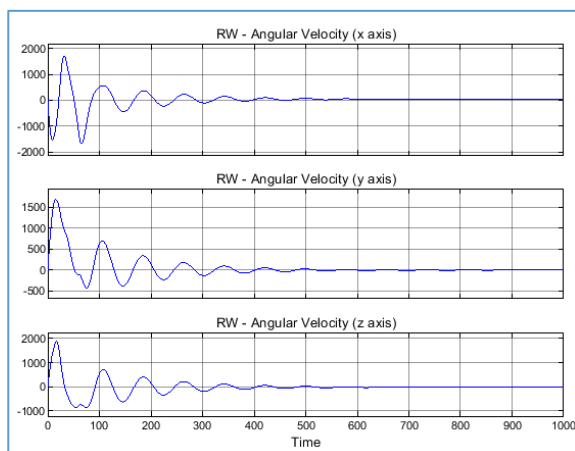


Figure 6-43 RW Angular Velocities (LQR/Case-2)

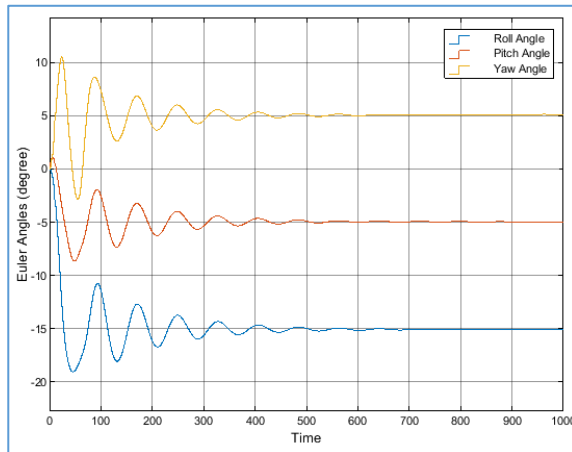


Figure 6-44 Satellite Euler Angles (LQR/Case-2)

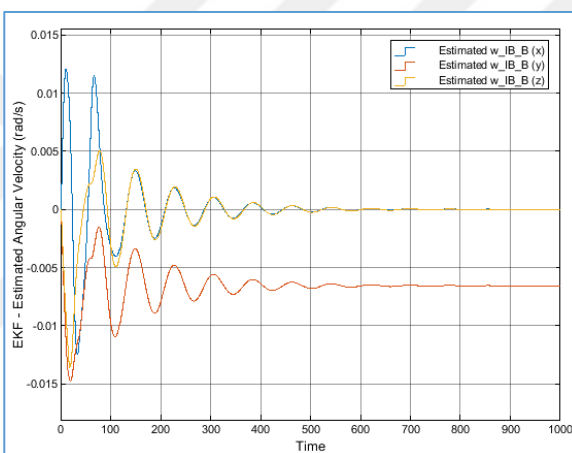


Figure 6-45 Satellite Angular Velocities (LQR/Case-1)

The simulation parameters obtained from this case are defined here:

Table 6-12 The Simulation Results of LQR Controller for Case-2

	Settling Time (s)	Rise/Fall Time (s)	Overshoot (%)
Roll Angle	~ 600	- 16.903	- 7.133
Pitch Angle	~ 600	8.654 / 8.337	38.072 / 6.877
Yaw Angle	~ 600	6.305 / 6.803	137.676 / 3.450

The usage of three RWs instead of four of them effects the system negatively. The power consumptions for both cases of a RW failure and non-failure are here:

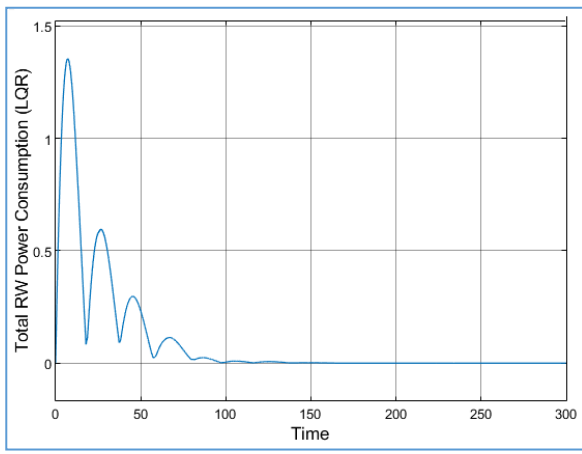


Figure 6-46 RW Power Consumption for a Non-Failure Case (LQR)

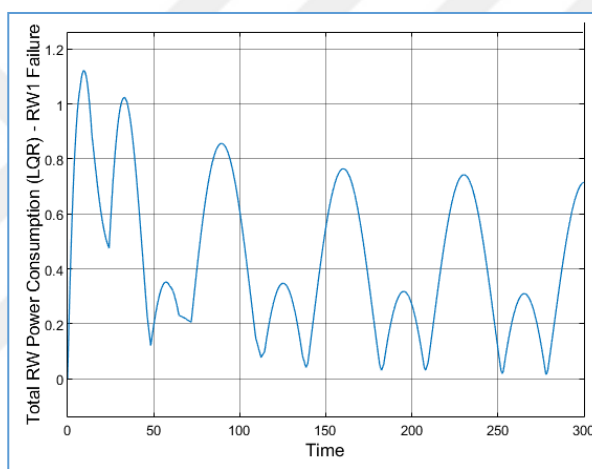


Figure 6-47 RW Power Consumption for a RW Failure Case (LQR)

6.6. The Results of Sliding Mode Control

The graphical evaluation of sliding mode controller design taking into account the chattering problem with different configurations is presented in this section.

Case-1: No RW Failure & Sliding Mode Controller with chattering problem

Table 6-13 The Simulation Parameters of SM Controller (Case-1)

Parameters	Values
Initial Satellite Velocity	$w_0 = [0.0, 0.0, 0.0]$
Initial / Desired Euler Angels	$[\Psi_0, \theta_0, \Phi_0] = [0, 0, 0]$ $[\Psi_d, \theta_d, \Phi_d] = [-15, -5, 5]$
Constant Controller Gains	$K_{SMC} = 0.5 * [I]_{3x3}$; $G_{SMC} = 1 * [I]_{3x3}$
Sliding Thickness	$\varepsilon = 0.02$

The applied control torque definition with chattering problem will be:

$$M_{cmd} = w_{OB}^B \times (I_S w_{OB}^B + H_{RW}^B) - M_D - I_S \dot{w}_{OB}^B - I_S K_{SMC} \dot{q}_{v,err} - I_S G_{SMC} sign(s)$$

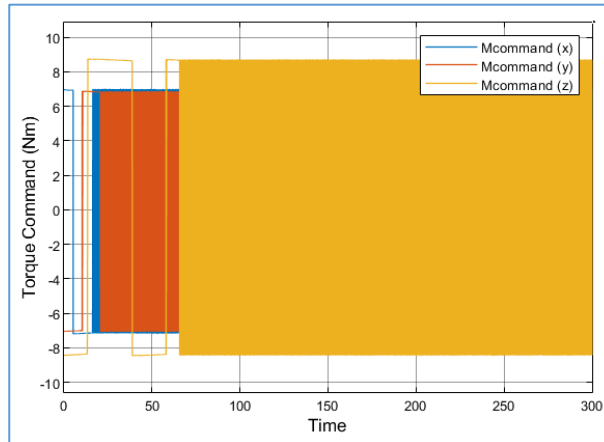


Figure 6-48 Torque Command of SMC with Chattering Problem (Case-1)

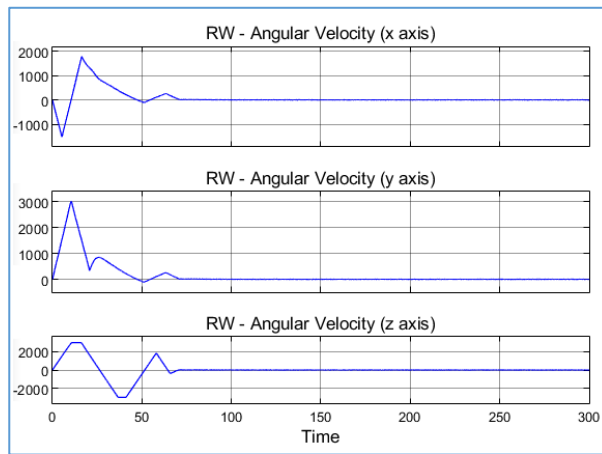


Figure 6-49 RW Angular Velocity of SMC with Chattering Problem (Case-1)

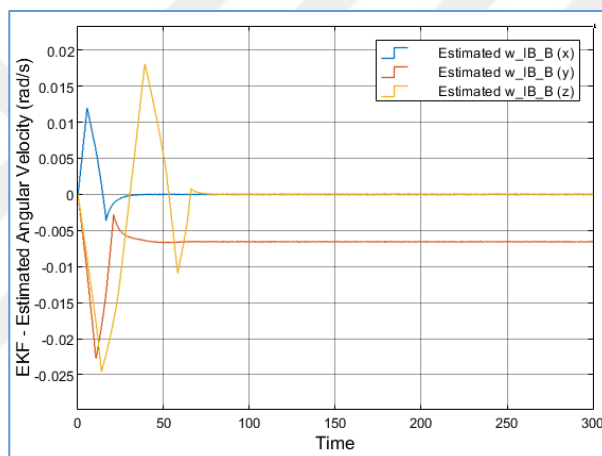


Figure 6-50 Satellite Ang. Vel. of SMC with Chattering Problem (Case-1)

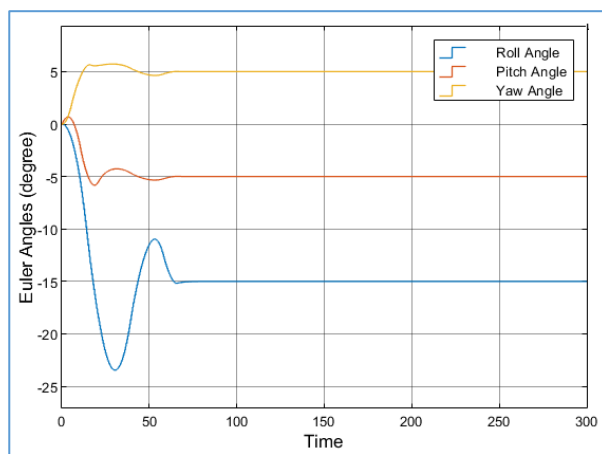


Figure 6-51 Euler Angles of SMC with Chattering Problem (Case-1)

The simulation results of Euler angles for this test case are here:

Table 6-14 The Simulation Results of SMC Controller for Case-1

	Settling Time	Rise/Fall Time	Overshoot
Roll Angle	~75 s	5.703 s	4.479 %
Pitch Angle	~60 s	7.005 s	13.333 %
Yaw Angle	~60 s	7.407 s	14.368 %

Case-2: No RW Failure & Sliding Mode Controller with same parameters applied in the previous test case, but without having chattering problem. The applied control torque can be specified to eliminate the chattering problem:

$$M_{cmd} = w_{OB}^B \times (I_S w_{OB}^B + H_{RW}^B) - M_D - I_S \dot{w}_{OB}^B - I_S K_{SMC} \dot{q}_{v,err} - I_S G_{SMC} \tanh\left(\frac{s}{\varepsilon}\right)$$

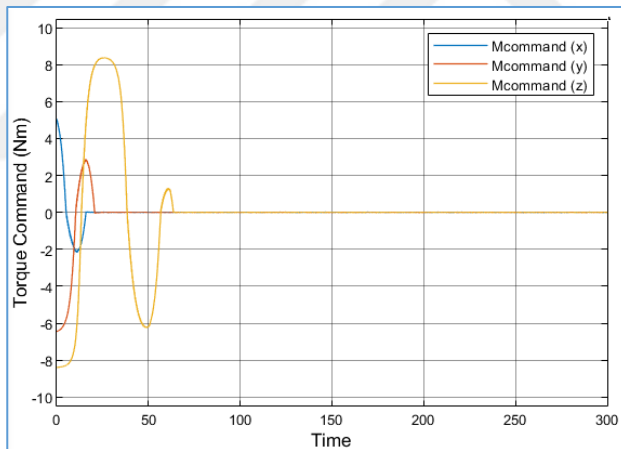


Figure 6-52 Torque Command of SMC without Chattering Problem (Case-2)

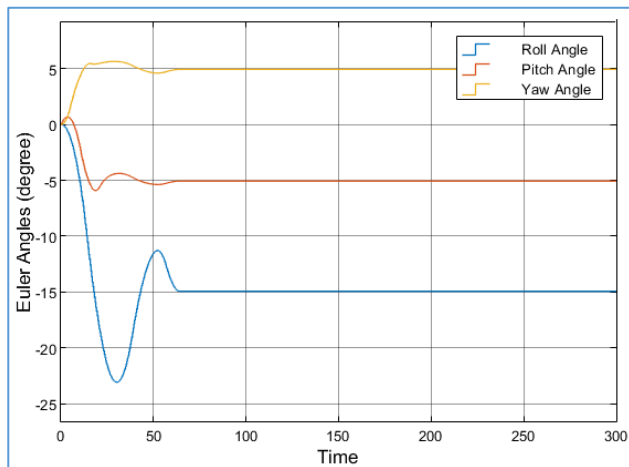


Figure 6-53 Euler Angles of SMC without Chattering Problem (Case-2)

The simulation results of Euler angles for this test case are shown below:

Table 6-15 The Simulation Results of SMC Controller for Case-2

	Settling Time	Rise/Fall Time	Overshoot
Roll Angle	~75 s	5.502 s	4.217 %
Pitch Angle	~60 s	7.006 s	12.459 %
Yaw Angle	~60 s	7.602 s	14.368 %

The angular velocity graphics of both satellite and RWs have almost the same results. After momentum unloading is completed, it can be seen that there is a little attitude error between the desired and estimated orientation angles for each axis in the ratio of ± 0.1 degree for this test case.

Case-3: RW-1 Failure & Sliding Mode Controller with under same conditions applied in the previous case. Controller gains have completely same values too.

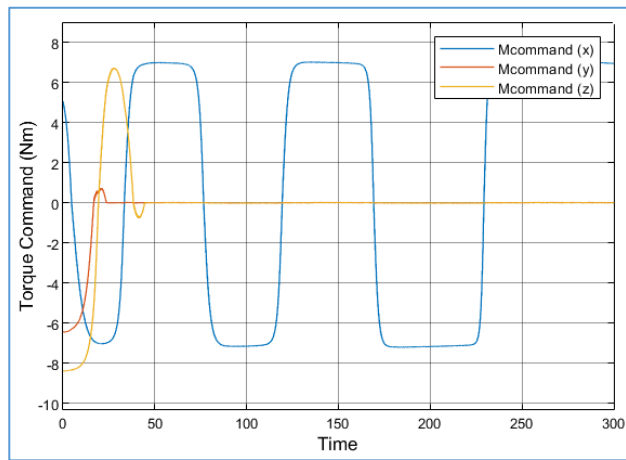


Figure 6-54 Torque Command of SMC without Chattering Problem (Case-3)

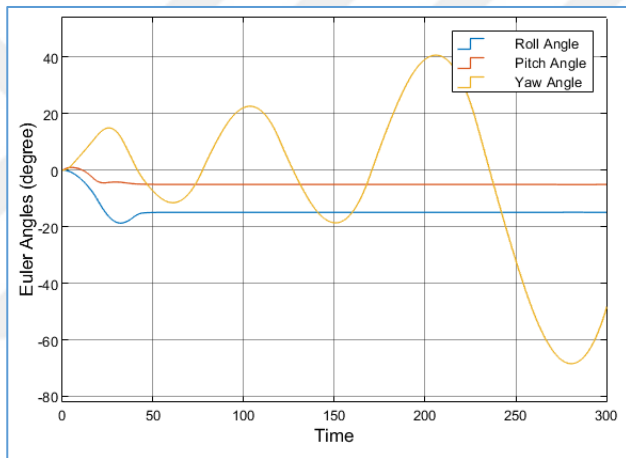


Figure 6-55 Euler Angles of SMC without Chattering Problem (Case-3)

While the roll and pitch angles reach their reference values, the yaw angle has not got successful outputs. It is necessary to change the controller gain (K_{SMC}) to achieve the given reference angles, in the case of a wheel failure.

Case-4: RW-1 Failure & Sliding Mode Controller with under same conditions applied in the previous case, but controller gain is selected like as ($K_{SMC} = 0.25[I]_{3x3}$ and $G_{SMC} = 15[I]_{3x3}$).

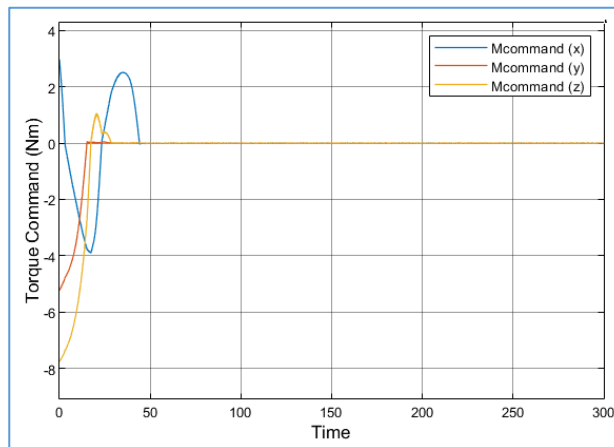


Figure 6-56 Torque Command of SMC without Chattering Problem (Case-4)

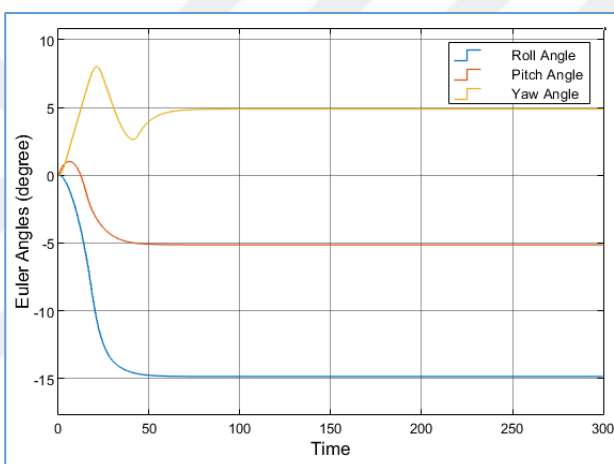


Figure 6-57 Euler Angles of SMC without Chattering Problem (Case-4)

The simulation results of Euler angles for this modified case are listed in the following table:

Table 6-16 The Simulation Results of SMC Controller for Case-2

	Settling Time	Rise/Fall Time	Overshoot
Roll Angle	~100 s	19.907 s	2.008 %
Pitch Angle	~90 s	19.403 s	2.018 %
Yaw Angle	~120 s	10.602 s	70.560 / 2.267 %

It is important to state that there are some deviations for each rotation axis between reference and measured angles in the range of \pm (0.1-0.2) degrees, when G_{SMC} gain is not changed. However, these deviations are reduced by increasing G_{SMC} value. The power consumptions for both cases of a RW failure and non-failure are:

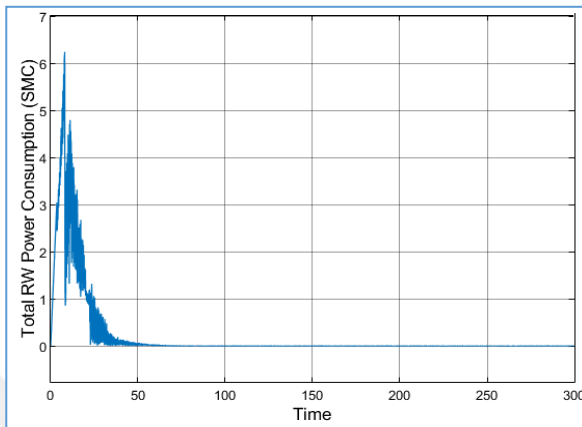


Figure 6-58 RW Power Consumption for a Non-Failure Case (SMC)

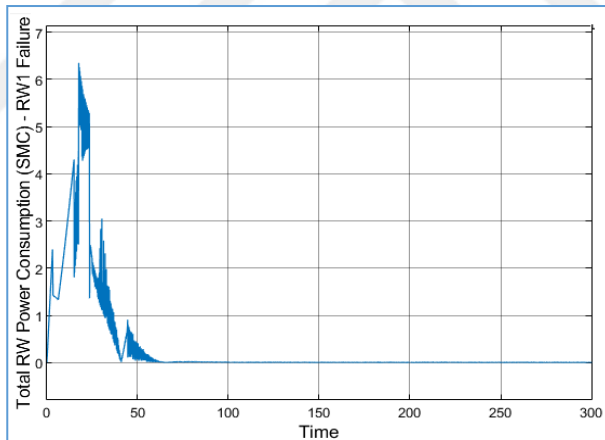


Figure 6-59 RW Power Consumption for a RW Failure Case (SMC)

6.7. Summary

In this chapter, there are five different controller types implemented to satellite system model including both plant model and space environment model. The

simulation graphics of the main controllers called PID, LQR and SMC with several test cases are compared and analyzed.

Even though detumbling and momentum desaturation controllers are supposed to be auxiliary controllers, there is also a great deal of test cases related to demonstrate their impact on attitude stabilization. The simulation results show that they are able to fulfill the expected results and requirements about smooth maneuvering and detumbling.



CHAPTER 7

CONCLUSION

7.1. Summary

The main object of this thesis is to develop and design different types of satellite attitude controllers, which includes four reaction wheels and torque rods under external disturbance torques and sensor noises by integrating the measurements of proper sensor combinations called multi-sensor integration.

Within the scope of this thesis, it will be mostly focused on the implementation of different types of attitude controllers such as PID, LQR and SMC for both initial and nominal satellite phases with multi-sensor integrated navigation systems. The most popular and important sensor combination includes gyroscopes and star trackers. However, the other auxiliary attitude sensors such as sun sensors, magnetometers and GPS receivers were also modelled considering their noise components.

After several investigations on academic dissertations which deal with different design methods of satellite controllers, the controller types required for detumbling and momentum desaturation phases were designed in a software tool called MATLAB/Simulink.

7.2. Conclusion

Microsatellites are not capable of reaching the specified orientation and tracking points unless their initial angular velocities are decreased. In the first phase of satellite life, B-dot controller was preferred to reduce the satellite tumbling rate and stabilize its initial angular velocity. In the nominal phase where a satellite is able to

track a commanded attitude, attitude controller types such as PD, LQR and SMC were used as a main controller in this study. The results obtained from these methods were analyzed and compared eliminating redundant momentum accumulated on wheels by the help of using desaturation function. In the whole process, satellite stability was provided with regard to the standard Lyapunov theorems.

The linear optimal controllers such as LQR controller use satellite linearized dynamic/kinematic equations. This controller type eliminates the fluctuations on output signals in finite time and provides much acceptable responses in terms of attitude stabilization. The comparisons of these responses between linear and nonlinear controllers were carried out by visualizing them on test graphics.

LQR has better performance in terms of the percentage of its signal overshoot and rising time. In addition to the satellite maneuver time is shortened with LQR controller which is more stable and lower settling time than PID controller.

As a result of analysis, it can be shown that the best performance belongs to SMC controller design according to the simulation tests realized under the same conditions. All main controller types (PID, LQR, and SMC) give stable results based on Lyapunov stability theorem in terms of the desired orientation. Reaction wheel detumbling and redundant momentum desaturations are brought under control with satisfied results for each type of attitude controller.

In this study, SMC was also proposed to orient the motion of FLP satellite to its desired trajectory. The recommended control equations and strategies guarantee that there is no chattering issue in the graphics of torque command value. It can be concluded that SMC design has the best results among of all controllers in terms of settling time and robustness.

The Kalman filter provides better stability with low noise measurement and process covariance matrices for roll, pitch and yaw axes like as the referenced study in [84]. The responses time of Kalman filters based controllers are nominally compatible

with the real responses time. The controller performance is highly dependent on the estimated parameters and noise covariance matrices. Since sensor estimation errors can result in angular deviation from the reference attitude.

In any case of one reaction wheel failure, it was necessary to specify controller gains again for all controller designs. This case induces signal distortion, increases the settling time and power consumption.

7.3. Future Works

Different sensor configurations using with different noise covariance matrices can be modeled and their system responses and Kalman filter analysis can be compared for attitude actuators such as torque rods or reaction wheels. Even though there is not any thrusters in the selected satellite to put it back its initial place in orbit, the effects of them can be implemented to all type of controller models.

Multi-sensor integrated navigation process including different integration architectures and different combinations of navigation sensors such as Inertial Navigation System (INS) and GPS receivers can be applied to sensor model [24, 61]. The integration algorithms such as loosely coupled, tightly coupled and deeply coupled integration shall provide the maximum processing accuracy, efficiency and robustness. They shall also minimize the complexity of navigation solution [19].

There are some integration architectures for multi-sensor navigation processing such as the simplest one, the least squares integration, then cascaded, centralized, federated, and hybrid integration architectures. Each of them has different advantages and disadvantages in terms of the selected sensors. The optimum solution of navigation processing model is found out as a federated integration method by applying Kalman Filters.

The results of following methods can be compared and analyzed for all attitude sensors located in the selected satellite [19, 64]:

- ✓ Least Squares Integration
- ✓ Cascaded Integration with EKF and UKF
- ✓ Centralized Integration with EKF and UKF
- ✓ Federated Integration with EKF and UKF

There are also quite a few advanced and robust controller types can be performed for the generated satellite model in this study:

- ✓ H-Infinity Controller (H_{∞})
- ✓ Model Based Predictive Controller (MPC)
- ✓ Fuzzy Logic Controller
- ✓ Neural Networks Controller

MATLAB/Simulink model files (.m and .slx files) can be converted to C or C++ source and header files (.c,.cpp and .h files) using auto code generation tool in order to realize these models in a cross platform environment. This situation provides them to extend their operating scope and integrate with different simulation platforms such as Eurosime that it can be interoperated with real time operating systems.

Machine learning algorithms can be performed for fine tuning on the results of main controllers instead of traditional methods. These trendy algorithms have been hot topics for a long time among the recent technological investigations.

There is one redundant wheel providing angular momentum and causing over actuation for the system. An alternative optimal controller can be introduced for this over-actuated system in order to determine an optimal path in terms of minimum energy or minimum time problem.

REFERENCES

- [1] A. Kutlu, “*Design of Kalman Filter Based Attitude Determination Algorithms for a LEO Satellite and for a Satellite Attitude Control Setup*”, MSc.dissertation, Dept. Aeronautical Eng., Middle East Technical Univ., Ankara, 2008.
- [2] A. Kutlu, “*Alçak Yörünge Uydusunun Yönelme Kontrol Sistem Tasarımı*”, MSc. dissertation, Dept. Aeronautics & Astronautics Eng., İstanbul Technical Univ., İstanbul, 2005.
- [3] C. Kaplan, “*LEO Satellites: Attitude Determination and Control Components; Some Linear Attitude Control Techniques*”, MSc. dissertation, Dept. Electrical & Electronics Eng., Middle East Technical Univ., Ankara, 2006.
- [4] S. Karataş, “*LEO Satellites: Dynamic Modelling, Simulations and Some Nonlinear Attitude Control Techniques*”, MSc. dissertation, Dept. Electrical & Electronics Eng., Middle East Technical Univ., Ankara, 2006.
- [5] H.Ö. Derman, “*3-Axis Attitude Control of a Geostationary Satellite*”, MSc. dissertation, Dept. Aeronautical Eng., Middle East Technical Univ., Ankara, 1999.
- [6] H. Abacı, “*Satellite Orbit Simulation and Orbit Determination*”, MSc. dissertation, Dept. Electrical & Electronics Eng., Hacettepe Univ., Ankara, 2008.
- [7] T.Ç. Elmas, “*Development of Control Allocation Methods for Satellite Attitude Control*”, MSc. dissertation, Dept. Electrical & Electronics Eng., Middle East Technical Univ., Ankara, 2010.
- [8] A.İ. Ak, “*Landing Autopilot Design for an Unmanned Aerial Vehicle*”, MSc. dissertation, Dept. Electrical & Electronics Eng., Middle East Technical Univ., Ankara, 2014.

- [9] M. Yasir, “*Development and Implementation of the Attitude Control Algorithms for the Micro-satellite Flying Laptop*”, Ph.D. dissertation, Dept. Aerospace Eng., University of Stuttgart, Stuttgart, 2010.
- [10] J.R. Wertz and W.J. Larson, “*Space Mission Analysis and Design*”, 3rd. ed. Library of Congress Cataloging-in-Publication Data, 1999.
- [11] D.A. Vallado, “*Fundamentals of Astrodynamics and Applications*”, 1st ed. Space Technology Series, McGraw-Hill Publishers, 1997.
- [12] J.R. Wertz, “*Spacecraft Attitude Determination and Control*”, Kluwer Academic Publishers, Netherlands, 1997.
- [13] V.A. Chobotov, “*Spacecraft Attitude Dynamics and Control*”, Krieger Publishing Co., Florida, 1991.
- [14] B. Wie, “*Space Vehicle Dynamics and Control*”, Arizona State University, Tempe Arizona, 1998.
- [15] M.J. Sidi, “*Spacecraft Dynamics and Control*”, Cambridge University Press, 1997.
- [16] B.P. Gibbs, “*Advanced Kalman Filtering, Least Squares and Modelling*”, 1st ed. Wiley, 2011.
- [17] J. Eickhoff, “*The FLP Microsatellite Platform Flight Operations Manual*”, 1st ed. Springer International Publishing, 2015.
- [18] J. Eickhoff, “*Simulating Spacecraft Systems*”, 1st ed. Springer-Verlag Berlin Heidelberg, 2009.
- [19] P.D. Groves, “*Principles of GNSS, Inertial, and Multisensor Integrated Navigation Systems*”, 1st ed. Artech House, 2008.

- [20] N2YO.com (2019, Dec. 23). Fyling Laptop TLE Data [Online]. Available: <https://www.n2yo.com/satellite/?s=42831#results>
- [21] B. Nelson, “*Flight Stability and Automatic Control*”, 2nd ed. McGrawHill, Inc., 1997, pp. 92-95.
- [22] C. Wilkening, “*Attitude Determination, Control and Stabilization*”, Microsatellite Spartnik Team, San José State Univ., 2001.
- [23] Space.com (2019, Dec. 23). How Far is Earth from the Sun [Online]. Available: <https://www.space.com/17081-how-far-is-earth-from-the-sun.html>
- [24] C. Titterton, D. H., J. L. Weston, “*Strapdown Inertial Navigation Technology*”, 2nd ed. The Institution of Engineering and Technology, 2004.
- [25] M. S. Grewal, L. R. Weill, A. P. Andrews, “*Global Positioning Systems, Inertial Navigation, and Integration*”, 1st ed. Wiley John & Sons Incorporated, 2001.
- [26] J. A. Farrell, M. Barth, “*The Global Positioning System and Inertial Navigation*”, McGraw-Hill, 1999.
- [27] R. L. Greenspan, “*GPS and Inertial Integration in Global Positioning System: Theory and Applications*”, Volume II, B. W. Parkinson and J. J. Spilker, Jr., (eds.), Washington, AIAA, 1996, pp.187–220.
- [28] “*IEEE Standard Specification Format Guide and Test Procedure for Accelerometers and Gyroscopes*”, IEEE Std., 952&1293, 1998.
- [29] “*IEEE Standard for Sensor Performance Parameter Definitions*”, IEEE Std., 2700TM, 2017.
- [30] “*IEEE Standard for Inertial Sensor Terminology*”, IEEE Std., 528-2001.
- [31] M.Lee, P.Crouse, R. Harman, T.Leid, W.Davis, S.Underwood, “*In-Flight Estimation of Gyro Noise on the upper Atmosphere Research Satellite(UARS) and Extreme Ultraviolet Explorer (EUVE) Missions*”, Flight Mechanics / Estimation Theory Symposium, 1994, pp.123-139.

[32] H. Chang, L. Xue, W. Qin, G. Yuan, W. Yuan, “*An Integrated MEMS Gyroscope Array with Higher Accuracy Output*”, Sensors 2008, 2008, pp.2886-2899.

[33] W.S. Flenniken Iv, J.H. Wall, D.M. Bevly, “*Characterization of Various IMU Error Sources and the Effect on Navigation Performance*”, Proceedings of the 18th International Technical Meeting of the Satellite Division of The Institute of Navigation (ION GNSS 2005), Long Beach, CA, 2005, pp. 967-978.

[34] L.Wang, F.Wang, “*Intelligent Calibration Method of Low Cost MEMS Inertial Measurement Unit for an FPGA-Based Navigation System*”, International Journal of Intelligent Engineering & Systems, 2011, pp.32-41.

[35] D.H. Titterton, J.L. Weston, “*Strapdown Inertial Navigation Technology*”, 2nd ed., 2004, pp.126-137.

[36] Northrop Grumman LITEF GmbH, μFORS-3U / -3UC / -6U / -6UC, High Performance Fiber Optic Rate Gyros Datasheet, Germany

[37] VectorNav Embedded Navigation Solutions (2019, Dec. 23) , Available: <https://www.vectornav.com/support/library>

[38] O. Montenbruck, B. Nortier, S. Mostert, “*A Miniature GPS Receiver for Precise Orbit Determination of the Sunsat 2004 Micro-Satellite*”, ION NTM 2004, San Diego, California, 2004.

[39] E. Gill, O. Montenbruck, K. Arichandran, S. H. Tan, T. Bretschneider, “*High Precision Onboard Orbit Determination For Small Satellites the GPS Based XNS on X-SAT*”, 6th Symposium on Small Satellites Systems and Services, La Rochelle, France, 2004.

[40] O. Montenbruck, E. Gill, M. Markgraf, “*Phoenix-XNS a Miniature Real Time Navigation System For a LEO Satellites*”, NAVITEC’2006, Noordwijk, 2006.

[41] DLR (Deutsches Zentrum für Luft- und Raumfahrt), “*Phoenix Spaceborne GPS Receiver Data Sheet*”, Issue 1.1, 2007.

- [42] P.S. Jørgensen, J.L. Jørgensen, T. Denver, P. van den Braembuche,”*The Micro Advanced Stellar Compass For Esa’s Proba 2 Mission*”, Small Satellites for Earth Observation: Selected Proceedings of the 5th International Symposium of the IAA. De Gruyter, 2005, pp. 299-303.
- [43] J.L. Jørgensen, T. Denver, M. Betto, Pieter Van den Braembussche, “*The PROBA Satellite Star Tracker Performance*”, Acta Astronautica 56, 2005, pp.153-159.
- [44] J. Rohac, M. Rerabek, R. Hudec, “*Multi-functional Star Tracker - Future Perspectives*”, Acta Polytechnica, Vol. 51, 2011.
- [45] S.T. El Moussaoui Brembo, “*Sensor Modelling, Attitude Determination and Control for Microsatellite*”, Norwegian University of Science and Technology, Trondheim, 2005.
- [46] C. Maule, A. Pollard, “*Design of the Attitude and Orbit Control System for ESA’s Solar Orbiter*”, Tessella Ltd. MATLAB Expo Benelux, 2017.
- [47] J.E. Smith, “*Attitude Model of a Reaction Wheel/Fixed Thruster Based Satellite Using Telemetry Data*”, Air Force Institute of Technology Air Univ., Captain, USAF, 2005.
- [48] İ. Kök, “*Comparison and Analysis of Attitude Control Systems of a Satellite Using Reaction Wheel Actuators*”, Dept. Electrical and Space Eng., Univ. of Würzburg, Luleå University of Technology, Department of Computer Science, 2012.
- [49] V.A. Chobotov, “*Orbital Mechanics*”, 3rd ed. American Institute of Aeronautics and Astronautics Inc., Reston, Virginia, 2002.
- [50] F.L. Markley, J.L. Crassidis, “*Fundamentals of Spacecraft Attitude Determination and Control*”, Space Technology Library, Springer, 2014.
- [51] M. Blanke, M. B. Larsen, “*Satellite Dynamics and Control in a Quaternion Formulation*”, Lecture Notes for Spacecraft Dynamics and Control Course, Dept. Electrical Eng., Technical Univ. of Denmark, 2010.

- [52] R. Holst, “*Satellite Attitude Control Using Magnetorquers with Magnetic Dipole Moment Cancellation*”, MSc. dissertation, Institute of Electronic Systems Control Eng., Aalborg Univ, Denmark, 2014.
- [53] S.M. Mukut, “*Attitude Controller Design and Simulation for an Artificial Satellite β* ”, MSc. dissertation, Dept. Aerospace Eng., Nanchang Hangkong Univ., 2015.
- [54] T. Lorentzen, “*Attitude Control and Determination System for DTUsat1*”, MSc. dissertation, Dept. of Automation Eng., Technical Univ. of Denmark, 2002.
- [55] I. Reda, A. Andreas, “*Solar Position Algorithm for Solar Radiation Applications*”, NREL National Renewable Energy Laboratory, 2008.
- [56] P. Schlyter, “*How to Compute Planetary Positions*”, Stockholm, Sweden, <http://stjarnhimlen.se/comp/ppcomp.html#5>
- [57] PV Performance Modelling and Collaborative (2019, Dec. 23), Available: <https://pvpmc.sandia.gov/modeling-steps/1-weather-design-inputs/sun-position/>
- [58] M. Mandea, S. Macmillan, “*International Geomagnetic Reference Field - The Eighth Generation*”, Earth Planets Space, 2000, pp.1119–1124.
- [59] J. Tuthill, “*Design and Simulation of a Nano-Satellite Attitude Determination System*”, MSc. dissertation, Naval Postgraduate School, Monterey, California, 2009.
- [60] Q.M. Lam, N. Stamatakos, C. Woodruff, S. Ashton, “*Gyro Modeling and Estimation of Its Random Noise Sources*”, AIAA Guidance, Navigation, and Control Conference and Exhibit, Austin, Texas, 2003.
- [61] R. Juhant, D. Vrecko, J. Knez, S. Blazic, “*Improved Pose Estimation for Vehicle Navigation using Frame Alignment and Forward Smoothing*”, Automatika 56, 2015, pp.120–131.
- [62] NASA Goddard Space Flight Center, DGRF/IGRF Geomagnetic Field Model 1945 - 2020 and Related Parameters (2019, Dec. 23), Available: https://ccmc.gsfc.nasa.gov/modelweb/models/igrf_vitmo.php

- [63] L. Benziane, “*Attitude Estimation & Control of Autonomous Aerial Vehicles*”, Universite de Versailles-Saint Quentin en Yvelines, 2015.
- [64] T. Akça, “*An Adaptive Unscented Kalman Filter for Tightly-Coupled INS/GPS Integration*”, MSc. dissertation, Dept. Electrical and Electronics Eng., Middle East Technical Univ., Ankara, 2012.
- [65] F. Gardosi, “*Development of a MATLAB/ Simulink ®Tool for Coupled Attitude and Orbit Control Using Electric Propulsion for Low-Earth Orbit Satellite*”, MSc. dissertation, Space Engineering Dept. of Aerospace Science and Technology, Politecnico di Milano, Milano, 2016.
- [66] A.R. Catanzaro, “*Design and Simulation Analysis of Attitude and Determination Control System for the CubeSat 12U ATISE*”, Politecnico Di Torino, I Facoltà di Ingegneria, Corso di Laurea in Ingegneria Aerospaziale, 2018.
- [67] A.d.S. Curiel, L. Gomes, J. Harding, S. Eves, D. Purll, M. Cutter, W. Sun, M. Sweeting, “*Small Satellites for Real Operational Missions in Earth Observation*”, Surrey Satellite Technology Ltd., Surrey Space Centre, UK,
- [68] F. Alvenes, “*Satellite Attitude Control System*”, MSc. dissertation, Dept. of Engineering Cybernetics, 2012.
- [69] C.C. Mbaocha, C.U. Eze, I.A. Ezenugu, J.C. Onwumere, “*Satellite Model for Yaw-Axis Determination and Control Using PID Compensator*”, International Journal Of Scientific & Engineering Research, Volume 7, Issue 7, 2016.
- [70] K. Ogata, ”*Modern Control Engineering*”, Pearson Education International, 1995.
- [71] G. Bråthen, “*Design of Attitude Control System of a Double CubeSat*”, MSc. dissertation, Dept. of Engineering Cybernetics, Norwegian Univ. of Science and Technology, Trondheim, 2013.
- [72] N. Jovanovic, “*Aalto-2 Satellite Attitude Control System*”, MSc. dissertation, Dept. of Electrical Engineering and Automation, Aalto Univ., Otaniemi, 2014.

- [73] B.Ø. Andresen, C. Grøn, R.H. Knudsen, C. Nielsen, K.K. Sørensen, D. Taagaard, “*Attitude Control System for AAUSAT-II*”, 8th Semester – Group 834, Project Report, Institute of Electronic Systems, Aalborg Univ., Denmark, 2005.
- [74] F.G. Stray, “*Attitude Control of a Nano Satellite*”, MSc. dissertation, Dept. of Physics, Univ. of Oslo, Kjeller, 2010.
- [75] R.Wisniewski, “*Satellite Attitude Control Using Only Electromagnetic Actuation*”, Ph.D. dissertation, Dept. of Control Eng., Aalborg Univ., Denmark, 1997.
- [76] E.J. Øverby, “*Attitude Control for the Norwegian Student Satellite nCube*”, MSc. dissertation, Dept. of Engineering Cybernetics, Norwegian Univ. of Science and Technology, Trondheim, 2004.
- [77] N.A. Nobari, “*Attitude Dynamics and Control of Satellites with Fluid Ring Actuators*”, MSc. dissertation, Dept. of Mechanical Eng., McGill University, Montreal, 2013.
- [78] Z. Ismail, R. Varatharajoo, “*Satellite Cascade Attitude Control via Fuzzy PD Controller with Active Force Control Under Momentum Dumping*”, Aerotech VI - Innovation in Aerospace Engineering and Technology, IOP Conf. Series: Materials Science and Engineering 152, 2016.
- [79] A. Muksin, R.E. Poetro, R.H. Triharjanto, “*Pico-Satellite Detumbling Simulation Using Magnetic Attitude Actuator*”, Jurnal Teknologi Dirgantara, Vol. 15, No.1, 2017, pp.11-20.
- [80] Y. Yang, “*Spacecraft Attitude and Reaction Wheel Desaturation Combined Control Method*”, IEEE Transactions on Aerospace and Electronic Systems, Vol. 53 , Issue 1 , 2017 , pp.286-295.
- [81] Ö. Kahraman, “*Control Allocation Against Actuator Failures in Overactuated Small Satellites*”, MSc. dissertation, Dept. of Aerospace Eng., Middle East Technical Univ., Ankara, 2007.

- [82] T. Graversen, M.K. Frederiksen, S.V. Vedstesen, “*Attitude Control System for AAU CubeSat*”, MSc. dissertation, Dept. of Control Eng., Aalborg Univ., Denmark, 2002.
- [83] M.C. Mahdi, M.J. AL-Bermani, “*LQR Controller for Kufasat*”, Journal of Kufa Physics, Vol.6, No.1, 2014.
- [84] G.H.J. van Vuuren, “*The Design and Simulation Analysis of an Attitude Determination and Control System for a Small Earth Observation Satellite*”, MSc. dissertation, Dept. of Electrical and Electronic Eng., Stellenbosch Univ., Stellenbosch, 2015.
- [85] B. Joseph, C. Brosilow, “*Techniques of Model-Based Control*”, Chapter 10 Cascade Control, Prentice Hall, 2002.

APPENDICES

A. The Properties of Quaternions

There is a mathematical approach used in modern spacecraft called quaternions that has the capability of quicker computations and less integration steps than direction cosine matrix. This approach also eliminates the singularities of Euler angles. It is vital to have information about the different properties of quaternion vectors to be able to calculate the quaternion vector multiplications accurately.

Quaternion vectors are based upon a special unit vector multiplication [47]:

$$i^2 = j^2 = k^2 = ijk = -1 \quad (A.1)$$

$$ij = k = -jk; \quad jk = i = -kj; \quad ki = j = -ik \quad (A.2)$$

The quaternion vectors including both vector and scalar parts are shown below:

$$q = q_1i + q_2j + q_3k + q_4 = q_v + q_4 \quad (A.3)$$

$$p = p_1i + p_2j + p_3k + p_4 = p_v + p_4 \quad (A.4)$$

Vector elements of q_1, q_2, q_3 and q_4 are real numbers and they have unit lengths:

$$q_1^2 + q_2^2 + q_3^2 + q_4^2 = 1 \quad (A.5)$$

The scalar multiplication of two different quaternion vectors:

$$t = q \odot p = (q_1 i + q_2 j + q_3 k + q_4) \cdot (p_1 i + p_2 j + p_3 k + p_4) \quad (A.6)$$

$$q \odot p = q_4 p_4 - q_v p_v + q_4 p_v + p_4 q_v + q_v \times p_v \quad (A.7)$$

$$q \odot p = \begin{bmatrix} t_1 \\ t_2 \\ t_3 \\ t_4 \end{bmatrix} = \begin{bmatrix} p_4 & p_3 & -p_2 & p_1 \\ -p_3 & p_4 & p_1 & p_2 \\ p_2 & -p_1 & p_4 & p_3 \\ -p_1 & -p_2 & -p_3 & p_4 \end{bmatrix} \begin{bmatrix} q_1 \\ q_2 \\ q_3 \\ q_4 \end{bmatrix} \quad (A.8)$$

$$q \odot p = \begin{bmatrix} t_1 \\ t_2 \\ t_3 \\ t_4 \end{bmatrix} = \begin{bmatrix} q_4 & -q_3 & q_2 & q_1 \\ q_3 & q_4 & -q_1 & q_2 \\ -q_2 & q_1 & q_4 & q_3 \\ -q_1 & -q_2 & -q_3 & q_4 \end{bmatrix} \begin{bmatrix} p_1 \\ p_2 \\ p_3 \\ p_4 \end{bmatrix} \quad (A.8)$$

The cross and dot products of quaternion vectors are defined respectively:

$$q \otimes p = \begin{bmatrix} p_4 q_v + q_4 p_v - q_v \times p_v \\ q_4 p_4 - q_v p_v \end{bmatrix} \quad (A.8)$$

$$q \odot p = \begin{bmatrix} p_4 q_v + q_4 p_v + q_v \times p_v \\ q_4 p_4 - q_v p_v \end{bmatrix} \quad (A.9)$$

The relation between vector product and dot product is:

$$q \otimes p = p \odot q \quad (A.10)$$

The conjugate of a quaternion vector (q^*) is:

$$q = q_4 + q_v \rightarrow q^* = q_4 - q_v \quad (A.11)$$

The norm of a quaternion vector ($N(q)$) is:

$$N(q) = \sqrt{q^* q} = \sqrt{q_1^2 + q_2^2 + q_3^2 + q_4^2} \quad (A.12)$$

The inverse of a quaternion vector (q^{-1}) is:

$$q^{-1} = q^* = q_4 - q_v \quad (A.13)$$

The derivative of a quaternion vector (\dot{q}) is:

$$\frac{dq}{dt} = \begin{bmatrix} \dot{q}_1 \\ \dot{q}_2 \\ \dot{q}_3 \\ \dot{q}_4 \end{bmatrix} = \frac{1}{2} [\Omega(w_{OB}^B)] \begin{bmatrix} q_1 \\ q_2 \\ q_3 \\ q_4 \end{bmatrix} \quad (A.14)$$

The derivative of a quaternion vector (\dot{q}) can be written using the definition of $q = [q_v; q_4]$, where q_v is the first three components of quaternion vector. The scalar part of a quaternion is q_4 and $\Omega(w_{OB}^B)$ is a 3x3 skew-symmetric matrix [47, 51]:

$$\dot{q}_v = -\frac{1}{2} w_{OB}^B \times q_v + \frac{1}{2} w_{OB}^B q_4 = -\frac{1}{2} [\Omega(w_{OB}^B)] q_v + \frac{1}{2} q_4 w_{OB}^B \quad (A.15)$$

$$\dot{q}_v = \frac{1}{2} [\Omega(q_v)] w_{OB}^B + \frac{1}{2} q_4 w_{OB}^B = \frac{1}{2} [\Omega(q_v) + [I_{3x3}] q_4] w_{OB}^B \quad (A.16)$$

$$S(q) = [\Omega(q_v) + [I_{3x3}] q_4] = \begin{bmatrix} q_4 & -q_3 & q_2 \\ q_3 & q_4 & -q_1 \\ -q_2 & q_1 & q_4 \end{bmatrix} \quad (A.17)$$

$$\dot{q}_v = \frac{1}{2} S(q) w_{OB}^B \quad (A.18)$$

$$\dot{q}_4 = -\frac{1}{2} (w_{OB}^B)^T q_v = -\frac{1}{2} (q_v)^T w_{OB}^B \quad (A.19)$$

In more compact forms of a quaternion vector derivation are hereafter [47]:

$$\dot{q} = \frac{1}{2} S(q) w_{OB}^B - \frac{1}{2} [I_{3x3}] (q_v)^T w_{OB}^B \quad (A.20)$$

$$\dot{q} = -\frac{1}{2} \begin{bmatrix} [\Omega(w_{OB}^B)] \\ (w_{OB}^B)^T \end{bmatrix} q_v + \frac{1}{2} [I_{3x3}] w_{OB}^B q_4 \quad (A.21)$$

B. Transfer Functions

The transfer functions of the following satellite plant model are explained in this chapter:

$$\dot{x}_k = \begin{bmatrix} \dot{w}_{IB}^B \\ \dot{q} \\ \dot{H}_{RW}^B \end{bmatrix} = A_k \begin{bmatrix} w_{IB}^B \\ q \\ H_{RW}^B \end{bmatrix} + B_k \begin{bmatrix} M_C^{RW} \\ M_C^{MTR} \\ M_D \end{bmatrix} + Q_k \begin{bmatrix} M_C^{RW} \\ M_C^{MTR} \\ M_D \end{bmatrix}$$

In the case of $M_{C,x}^{RW}$ is an input, the related transfer functions are:

$$\frac{w_{IB,x}^B(s)}{M_{C,x}^{RW}(s)} = \frac{0.1415}{s} \quad (B.1)$$

$$\frac{q_1(s)}{M_{C,x}^{RW}(s)} = \frac{0.07075 s}{s^3 + 1.089 \times 10^{-6} s} \quad (B.2)$$

$$\frac{q_3(s)}{M_{C,x}^{RW}(s)} = \frac{-0.0002335}{s^3 + 1.089 \times 10^{-5} s} \quad (B.3)$$

$$\frac{H_{RW,x}^B(s)}{M_{C,x}^{RW}(s)} = \frac{-1}{s} \quad (B.4)$$

In the case of $M_{C,y}^{RW}$ is an input, the related transfer functions are:

$$\frac{w_{IB,y}^B(s)}{M_{C,y}^{RW}(s)} = \frac{0.1439}{s} \quad (B.5)$$

$$\frac{q_2(s)}{M_{C,y}^{RW}(s)} = \frac{0.07195 s}{s^3 + 3.3 \times 10^{-5} s} \quad (B.6)$$

$$\frac{q_4(s)}{M_{C,y}^{RW}(s)} = \frac{-0.0002374}{s^3 + 3.3x10^{-5}s} \quad (B.7)$$

$$\frac{H_{RW,y}^B(s)}{M_{C,y}^{RW}(s)} = \frac{-1}{s} \quad (B.8)$$

In the case of $M_{C,z}^{RW}$ is an input, the related transfer functions are:

$$\frac{w_{IB,z}^B(s)}{M_{C,z}^{RW}(s)} = \frac{0.1169}{s} \quad (B.9)$$

$$\frac{q_1(s)}{M_{C,z}^{RW}(s)} = \frac{0.0001929}{s^3 + 1.089x10^{-5}s} \quad (B.10)$$

$$\frac{q_3(s)}{M_{C,z}^{RW}(s)} = \frac{0.05845 s}{s^3 + 1.089x10^{-5}s} \quad (B.11)$$

$$\frac{H_{RW,z}^B(s)}{M_{C,z}^{RW}(s)} = \frac{-1}{s} \quad (B.12)$$

In the case of $M_{C,x}^{MTR}$ is an input, the related transfer functions are:

$$\frac{w_{IB,x}^B(s)}{M_{C,x}^{MTR}(s)} = \frac{0.1415}{s} \quad (B.13)$$

$$\frac{q_1(s)}{M_{C,x}^{MTR}(s)} = \frac{0.07075 s}{s^3 + 1.089x10^{-5}s} \quad (B.14)$$

$$\frac{q_3(s)}{M_{C,x}^{MTR}(s)} = \frac{-0.0002335}{s^3 + 1.089x10^{-5}s} \quad (B.15)$$

In the case of $M_{C,y}^{MTR}$ is an input, the related transfer functions are:

$$\frac{w_{IB,y}^B(s)}{M_{C,y}^{MTR}(s)} = \frac{0.1439}{s} \quad (B.16)$$

$$\frac{q_2(s)}{M_{C,y}^{MTR}(s)} = \frac{0.07195 s}{s^3 + 3.3 \times 10^{-5} s} \quad (B.17)$$

$$\frac{q_4(s)}{M_{C,y}^{MTR}(s)} = \frac{0.0002374}{s^3 + 3.3 \times 10^{-5} s} \quad (B.18)$$

In the case of $M_{C,z}^{MTR}$ is an input, the related transfer functions are:

$$\frac{w_{IB,z}^B(s)}{M_{C,z}^{MTR}(s)} = \frac{0.1169}{s} \quad (B.19)$$

$$\frac{q_1(s)}{M_{C,z}^{MTR}(s)} = \frac{0.0001929}{s^3 + 1.089 \times 10^{-5} s} \quad (B.20)$$

$$\frac{q_3(s)}{M_{C,z}^{MTR}(s)} = \frac{0.05845 s}{s^3 + 1.089 \times 10^{-5} s} \quad (B.21)$$

In the case of $M_{D,x}$ is an input, the related transfer functions are:

$$\frac{w_{IB,x}^B(s)}{M_{D,x}(s)} = \frac{0.1415}{s} \quad (B.22)$$

$$\frac{q_1(s)}{M_{D,x}(s)} = \frac{0.07075 s}{s^3 + 1.089 \times 10^{-5} s} \quad (B.23)$$

$$\frac{q_3(s)}{M_{D,x}(s)} = \frac{-0.0002335}{s^3 + 1.089 \times 10^{-5} s} \quad (B.24)$$

In the case of $M_{D,y}$ is an input, the related transfer functions are:

$$\frac{w_{IB,y}^B(s)}{M_{D,y}(s)} = \frac{0.1439}{s} \quad (B.25)$$

$$\frac{q_2(s)}{M_{D,y}(s)} = \frac{0.07195 s}{s^3 + 3.3 \times 10^{-5} s} \quad (B.26)$$

$$\frac{q_4(s)}{M_{D,y}(s)} = \frac{-0.0002374}{s^3 + 3.3 \times 10^{-5} s} \quad (B.27)$$

In the case of $M_{D,z}$ is an input, the related transfer functions are:

$$\frac{w_{IB,z}^B(s)}{M_{D,z}(s)} = \frac{0.1169}{s} \quad (B.28)$$

$$\frac{q_1(s)}{M_{D,z}(s)} = \frac{0.0001929}{s^3 + 1.089 \times 10^{-5} s} \quad (B.29)$$

$$\frac{q_3(s)}{M_{D,z}(s)} = \frac{0.05845 s}{s^3 + 1.089 \times 10^{-5} s} \quad (B.30)$$

The transfer functions of reaction wheel model:

$$\frac{w_{RW}(s)}{M_M(s)} = \frac{1}{0.0005s + 10^{-6}} \quad (B.31)$$

$$\frac{w_{RW}(s)}{V(s)} = \frac{0.1}{2.6 \times 10^{-6}s^2 + 0.001s + 0.1} \quad (B.32)$$

$$\frac{M_M(s)}{V(s)} = \frac{5 \times 10^{-5} + 10^{-6}}{2.6 \times 10^{-6}s^2 + 0.001s + 0.1} \quad (B.33)$$

$$\frac{I(s)}{V(s)} = \frac{5 \times 10^{-4} + 10^{-5}}{2.6 \times 10^{-6}s^2 + 0.001s + 0.1} \quad (B.34)$$

C. MATLAB / Simulink Functions and Model Files

MATLAB has some commands utilized in this study and helping to analyze the properties of linear models, state space definitions and system stabilization.

Table 7-1 Useful MATLAB Functions

Func.	Example	Definition
tf()	sys = tf(numerator, denominator)	tf() function is used to create transfer function model represented in continuous time.
ssdata()	[A,B,C,D] = ssdata(tf) [A,B,C,D] = ssdata(sys)	ssdata() function extracts matrix definitions from state space model or transfer functions.
ss()	sys = ss(A,B,C,D)	ss() function is used to create state space model represented in continuous time.
damp()	[wn,z,p] = damp(sys)	damp() function gives the natural frequency, damping ratio and poles of a LTI model.
pole()	p = pole(sys)	pole() function computes the system poles to evaluate the stability.
pzmap()	pzmap(sys)	pzmap() function computes both the system poles and zeros, plots them in a complex plane.

D. MATLAB / Simulink Model Blocks

The Simulink implementation for Detumbling Control (B-dot Control) of satellite attitude model:

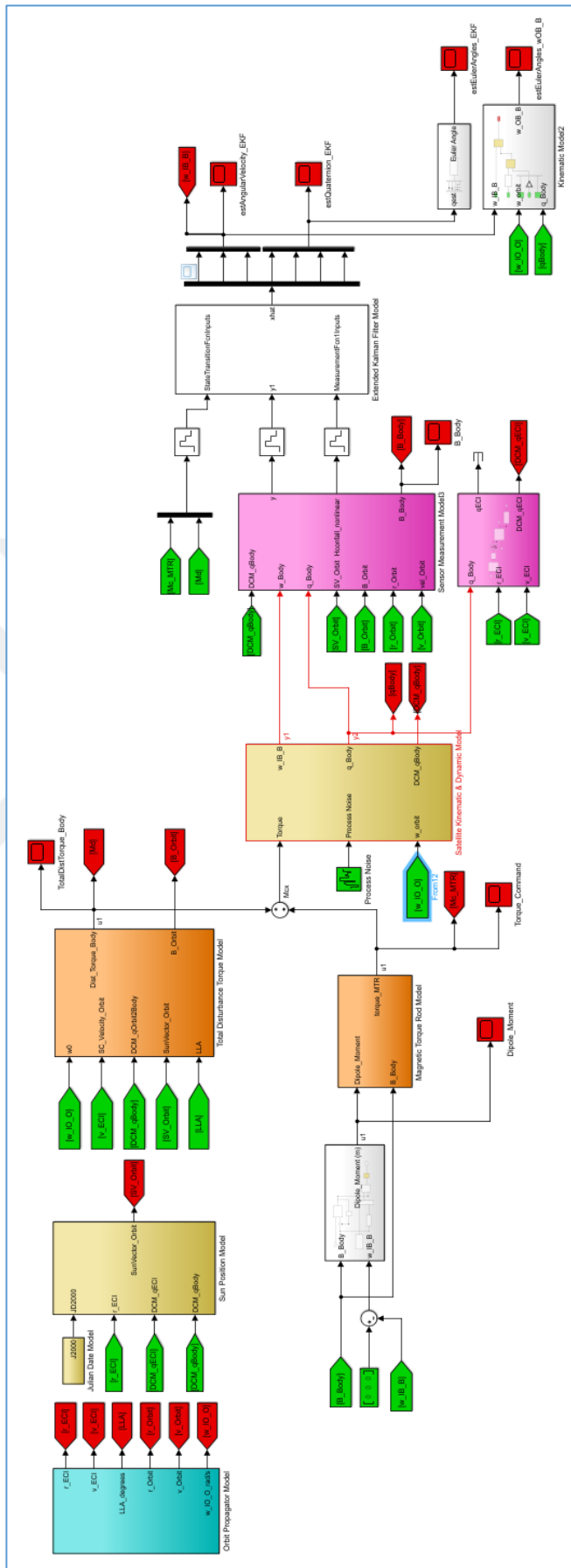


Figure 8-1 B-dot Controller Design for Satellite Detumbling

The Simulink implementation for PID Control of satellite attitude model:

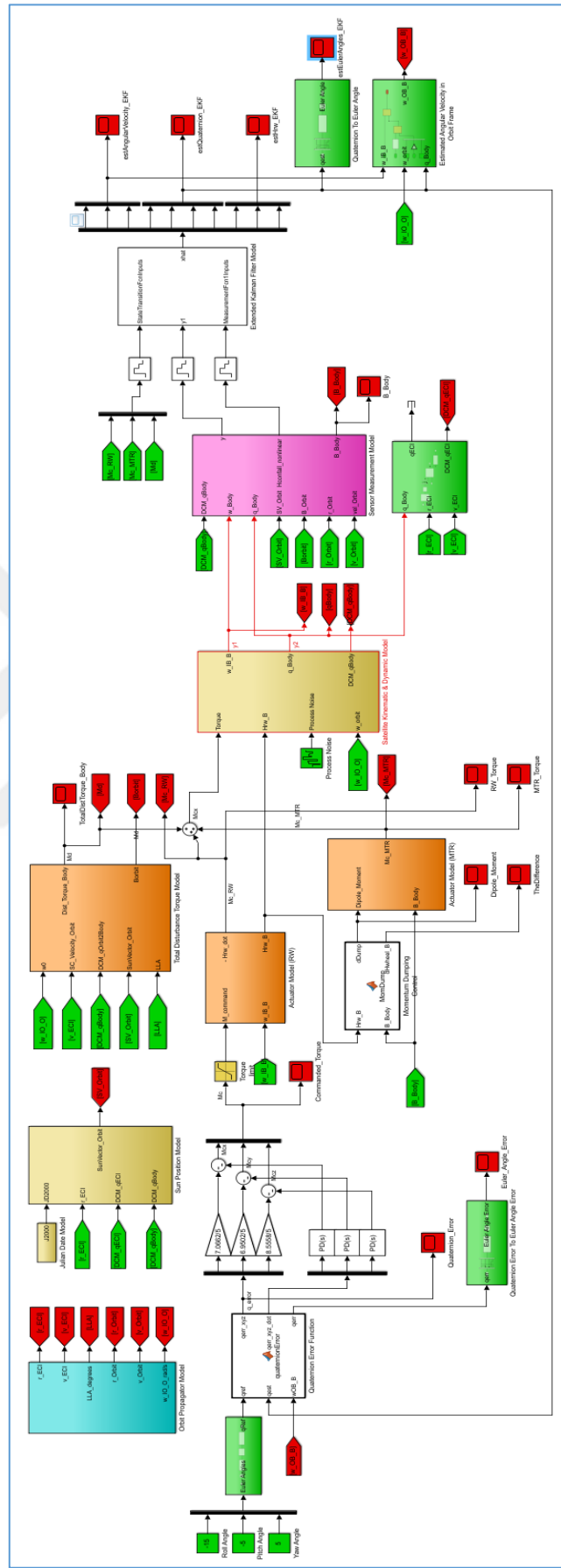


Figure 8-2 PID Controller Design with Desaturation for Satellite Attitude

The Simulink implementation for LQR Control of satellite attitude model:

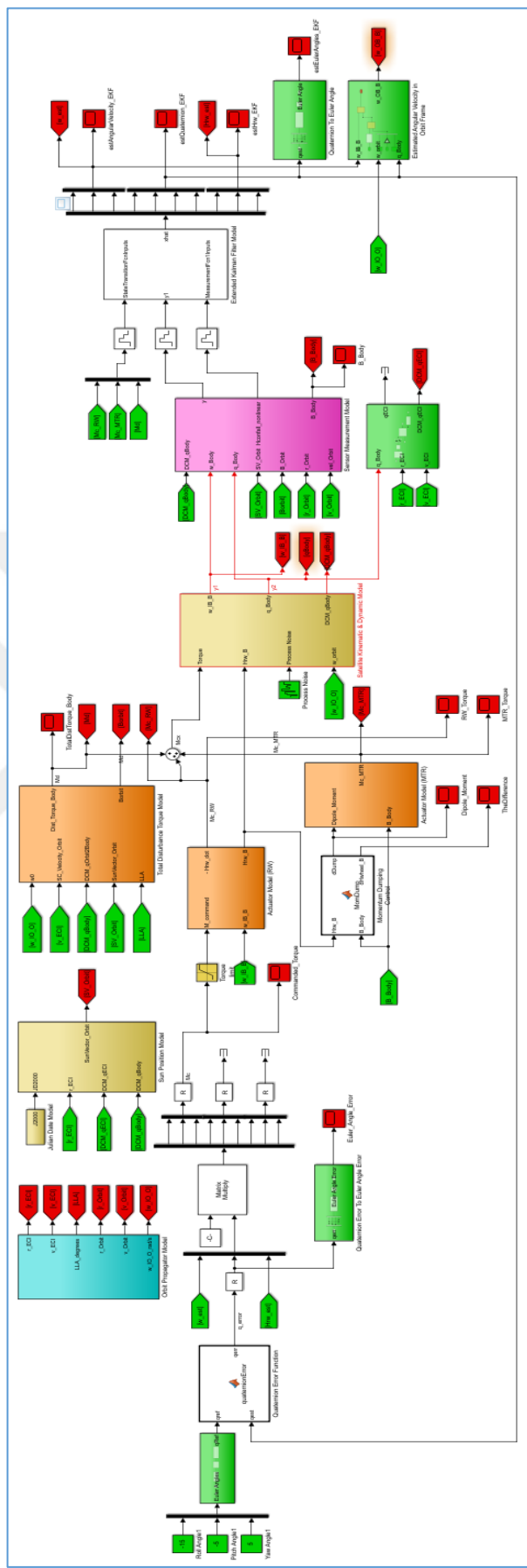


Figure 8-3 LQR Controller Design with Desaturation for Satellite Attitude

The Simulink implementation for SMC Control of satellite attitude model:

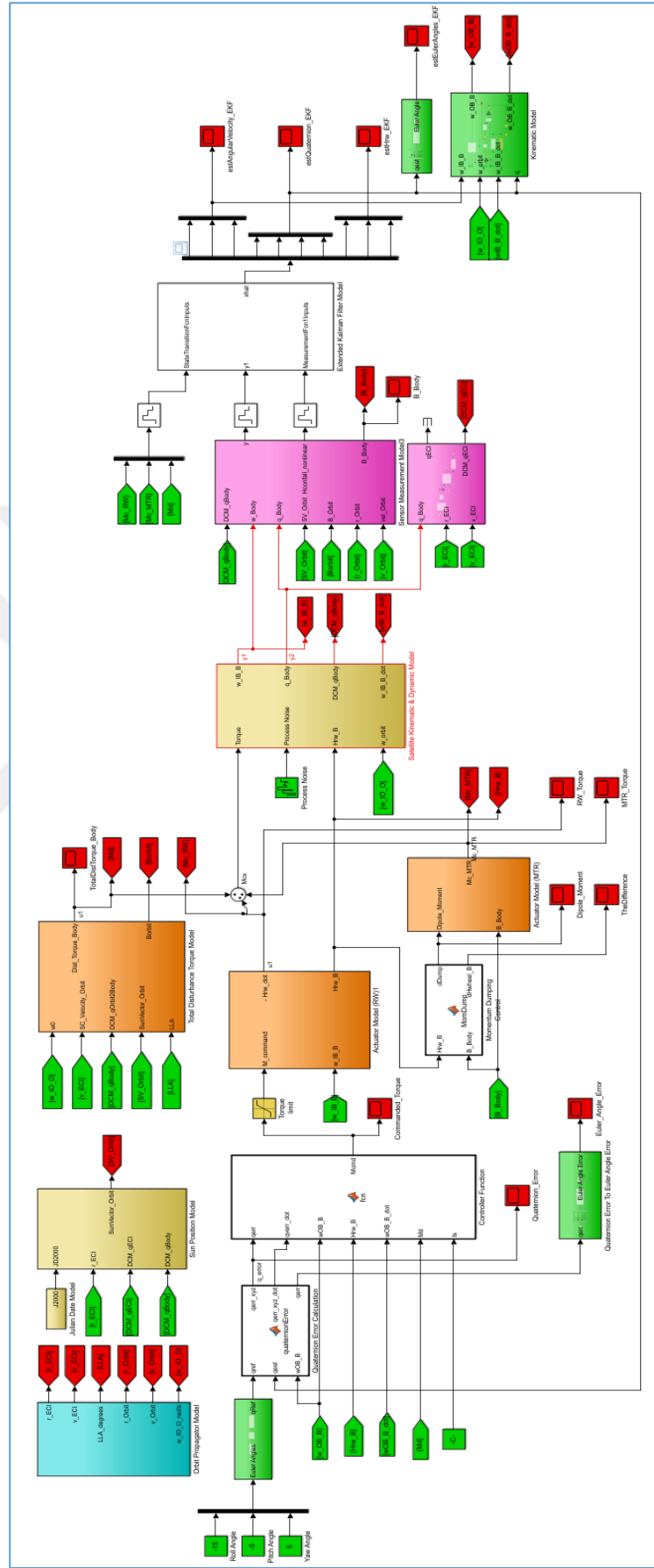


Figure 8-4 SMC Controller Design with Desaturation for Satellite Attitude